TECHNOLOGICAL STUDIES OF MULTIDIMENSIONAL MAGNETOHYDRODYNAMICS AND LIQUID METALS: GALLIUM-INDIUM-TIN

by
Kenan Şentürk

Submitted to the Institute of Graduate Studies in
Science and Engineering in partial fulfillment
of the requirements for the degree of
Doctor of Philosophy
in
Physics

Yeditepe University
2011

TECHNOLOGICAL STUDIES OF MULTIDIMENSIONAL MAGNETOHYDRODYNAMICS AND LIQUID METALS: GALLIUM-INDIUM-TIN

APPROVED BY:

Prof. Dr. Necdet Aslan
(Thesis Supervisor) .....

Assoc. Prof. Dr. Ertan Akşahin .....

Assoc. Prof. Dr. Şahin Aktaş .....

Prof. Dr. Uğur Yahşi .....

Assist. Prof. Dr. Vildan Üstoğlu Ünal .....

DATE OF APPROVAL: 22.02.2011

ACKNOWLEDGEMENTS

This work is finished after the meaningful education in physics at Yeditepe University, Physics Department, with the guidance of my advisor Prof. Dr. Necdet Aslan, who supported me in both theoretical and experimental physics together, especially in computational fluid dynamics and liquid metal experiments and applications. By the help and guidance of him I could overcome the problems I encountered at different times and in different areas such as computer programming, experimental setup preparation etc.

I owe special thanks to the members of my Ph. D. Examining Committee, Prof. Dr. Uğur Yahşi, Assoc. Prof. Dr. Ertan Akşahin, Assoc. Prof. Dr. Şahin Aktaş, Assist. Prof. Dr. Vildan Üstoğlu Ünal.

I owe my deepest gratitude to my precious family, my mother, my sister, my mother in law, my father in law, my cousins. Especially my mother Vasviye and my sister Figen deserve more than a thank because of their continuous support from the beginning to the end of the thesis. They were always with me with their patience, love and understanding. I will never forget their devotions.

This thesis would not have been possible without the encouragements, patience, enduring moral support of my wife, Elif, who devoted too much during the troubled, annoying and difficult days of this work. Their support together with my son Hasan Ömer deserves more than a thank.

I also thank TUBITAK for support done by COST P17 Project with Grant Number TBAG-U/166 (105T547), ICTP-Italy, University of Trieste and Prof Dr. Massimo Tessarotto from Department of Mathematics and Informatics, Trieste University, Italy.

Finally I thank Dr. İpek Karaaslan, Eylem Çoker, Melda Patan Alper, Tuba Şen, Mehmet Torun, Michael Feeney, Gülhan Yalçınkaya, Turgay Çoruhlu because of their support during the intensive works in Physics Department of Yeditepe University and special thanks to Dr. Ercüment Akat for final corrections.

ABSTRACT

TECHNOLOGICAL STUDIES OF MULTIDIMENSIONAL MAGNETOHYDRODYNAMICS AND LIQUID METALS: GALLIUM-INDIUM-TIN

Plasma phenomenon was described in detail and the derivation of momentum and energy equations for magnetohydrodynamic applications is done.

The effects of externally applied electric and magnetic field on the conducting fluids such as liquid metals or alloys were numerically investigated. Since the code used in these numerical studies was in two dimensions a new original three dimensional mesh generating programme was developed. The adaptation to the old code was left as a future work. Not only benchmark problems but also different numerical problems related to liquid metals were solved. The problems such as liquid metal flow past a circular cylinder in open channels exposed to external magnetic fields and electromagnetic braking of liquid metals in a vertical channel and levitation were solved numerically and the effects of externally applied magnetic and electric fields were seen. The effects of externally applied fields on flow pattern were very important especially for metalurgical applications. The spatial discretization scheme used in this thesis was matrix distribution scheme. Dual time stepping was used for time discretization.

In experimental works GaInSn alloy was used as a conducting medium on which different external effects were applied. The behaviour of GaInSn versus oxidation was studied, the expansion due to the heat addition was also studied in order to know how the surface will change under the increasing temperature and how this will affect the reflectivity from the surface. Under different conditions the reflectivity of GaInSn was studied. The reflection change because of the external heat addition, external current application, external magnetic field application were studied separately. As a final experiemntal study the current and magnetic field were applied together and again the reflectivity of GaInSn was studied. The effect of induced Lorentz force on reflectivity is seen. A hint which showed the

correlation between Lorentz force induced from the externally applied current and magnetic field together with normalized reflection intensity was found.

ÖZET

ÇOK BOYUTLU MANYETOHİDRODİNAMİK DENKLEMLERİN ÇÖZÜMÜ VE SIVI METALLERİN TEKNOLOJİK İNCELENMESİ: GALYUM-İNDİYUM-KALAY

Plazma konusu incelenip manyetohidrodinamik denklemlerden momentum ve enerji denklemlerinin türetilmesi yapıldı.

Akışkan metal ve alaşımlar gibi iletken akışkanlara dışarıdan uygulanan manyetik ve elektrik alanların etkileri sayısal olarak incelendi. Sayısal çalışmada kullanılan kodun iki boyuttan üç boyuta çıkarılabilmesi için ağ örgüsünün yeni ve ilk çalışması olarak bilgisayar programı yazıldı. Bu ek programın iki boyutlu gerçek programa uyarlanması doktora sonrası çalışma olarak bırakıldı. Geleneksel sayısal problemlerin dışında akışkan metaller konusunda özgün problemler tasarlandı ve onların da sayısal çözümleri yapıldı. Akışkan metallerde elektromanyetik frenleme ve yine bu metallerin açık kanalda dairesel silindir çevresindeki akışlarının dışarıdan uygulanan elektrik ve manyetik alanlardan nasıl etkilendikleri incelendi.

Galyum İndiyum Kalay alaşımının çeşitli dış etkilere karşı verdiği tepkiler, özellikle yüzeyine düşen ışığı yansıtma özellikleri incelendi. Bu deneylerde kullanılan ışık kaynağı görünür bölgede ışık veren bir halojen lamba idi. Bu alaşımın yüzeyinin oksitlenmesi, ısıtılarak sıcaklığının arttırılması, üzerinden akım geçirilmesi, manyetik alan uygulanılması ve hem akım hem de manyetik alanın aynı anda dışarıdan uygulanılması ile yüzeyinden meydana gelen ışık yansımasının nasıl değiştiği incelendi. Galyum İndiyum Kalay alaşımında dışarıdan aynı anda uygulanan elektrik akımı ve manyetik alanın etkileri ile oluşan Lorentz kuvvetinin yansıtmaya ne gibi bir etkide bulunduğu incelendi. Bu etkilerden ötürü Lorentz kuvveti ile normalize edilmiş ışık şiddeti arasında bir ilişki olabileceği görüldü.

TABLE OF CONTENTS

LIST OF FIGURES

LIST OF TABLES

LIST OF SYMBOLS AND ABBREVIATIONS

A , B	Jacobian matrices
A_{ch}	Characteristic constants for liquid
A_n	Normalization constant
A_p, B_p, C_p	Polynomial coefficients
$\vec{A}_z$	Vector potential
B	The magnitude of the applied magnetic field
$\vec{B}$	Magnetic field
B_{ch}	Characteristic constants for liquid
$\vec{B}^{ext}$	External magnetic field
B_l	The distribution matrix
B_i^{GAL}	The distribution matrix for Galerkin scheme
B_i^N	The distribution matrix for N- Scheme
B_i^{LDA}	The distribution matrix for low diffusion A method
B_i^{LW}	The distribution matrix for Lax-Wendroff – Scheme
B_i^{PSI}	The distribution matrix for positive streamwise invariant method
B_i^{SUPG}	The distribution matrix for streamline upwind Petrov Galerkin method
$\vec{B}^T$	Total magnetic field
C_v	The specific heat under constant volume
C_p	Heat capacity under constant pressure
D	Number of dimensions
E^*	Electric field in a moving reference frame
$\vec{E}$	Electric field
$\vec{E}^{ext}$	External electric field
E_k	Kinetic energy perpendicular to magnetic field

E_{kin}	Kinetic energy for moving fluid element
$E_{neutron}$	Neutron excess energy
$\vec{E}^T$	Total (external+internal) electric field
E_{TOT}	Total energy
E_{α_p}	α particle energy
$F_{BNET,x}$	Net body force actintg to the fluid element in x direction
$F_i(U(\vec{r},t))$	The flux vector in the r_i direction
$\vec{F}_L$	Lorentz force
$F_{net,x}$	The net force acting in x direction
$F_{S,X}$	The surface force acting in x direction
Ha	Hartmann number
H_1	Hamiltonian of a single system
$\vec{H}_1$	The magnetic field strength in medium 1
I	The identity matrix
I_m^*	The modified diagonal matrix
I_0	Initial intensity of light
$\vec{I}_{tang}$	Tangential component of the volume current
$\vec{J}$	Current density
$\vec{J}_m$	Mass current density
$\vec{J}_p$	Particle current density
$\vec{J}_{qs}$	Quasi-surface current
$\vec{J}^T$	Total current density
K_i	The flux matrix
L_0	Characteristic length
M	Molecular weight
N	Interaction parameter
N_D	Number of particles in Debye sphere

$N_i(\vec{r})$	The nodal basis functions
N_s	The total number of systems
P	Scalar pressure
$\widetilde{P}$	The pressure tensor
P_e	Pressure produced by plasma
P_k	Kinetic pressure of plasma
P_m	The preconditioning matrix
Pr	Prandtl number
$\dot{Q}_T$	Total heat transfer rate to the fluid element by thermal conduction
$\dot{Q}_{TOT}$	The total heat rate
$\dot{Q}_{V,M}$	Volumetric heat addition rate per unit mass
$\dot{Q}_V$	Volumetric heat addition rate
$\dot{Q}_x$	Net heat flux in x direction
R	Gas constant
$R(q_z)$	Reflectivity
R_e	Total number of events per second and per cubic centimeter
Re	Reynold's number
Re_m	Magnetic Reynold's number
Res_T	Cell residual
$Rf(q_z)$	Frensel reflectivity
S	Control surface
$S(U(\vec{r},t))$	The source term
$\vec{S}_{MAG}$	Source term driving the magnetic field
$\vec{S}_v$	The viscous term
T	Temperature in Kelvin
$T(x,t)$	Temperature as a function of both displacement x and time t
T_a	Ambient temperature
T_c	Cold wall's temperature

T_e	Electron's temperature
T_h	Hot wall's temperature
T_i	Ion temperature
U_i	The ionization energy of a gas
$U(\vec{r},t)$	A vector of conserved variables
V	Volume
V_g	Glass chamber's volume
V_t	Volume of tubing
$\dot{W}_b$	The work rate due to the body force
$\dot{W}_{NET}$	The net rate of work which is done by both surface and body forces on the fluid element
$\dot{W}_{S,NET_x}$	Net work rate due to shear in x direction
$\dot{W}_{S,P}$	Work rate due to the pressure
a_L	Larmor radius
c	The speed of light
$c(p)$	Function depending to the geometrical position of the source point in the domain
d	Molecular size
d^3v	Volume element in velocity space
dS	Surface element
dV	Volume element
$d\vee$	Elemental volume in phase space
e	The electron charge
f	The distribution function
f_L	Flux function
$f_{In}(z),\ f_{Ga}(z)$	The electron density distributions for atomic In and Ga respectievely
$f(E)$	Energy distribution function
$f(\vec{r},\vec{v},t)$	The distribution function in phase space
$f(v)$	The velocity distribution function

$f'(\vec{r},\vec{v},t)$	The normalized distribution function
f_x	Body force per unit mass, acting on the x coordinate
$\vec{g}$	Gravitational acceleration
g_p	Plasma parameter
$g(v)$	Speed distribution
h	Planck constant
h_t	The time step
k	Boltzmann's constant
k_i	Scalar inflow parameter
k_{max} , k_{min}	Short and long wavelengths
k_T	Thermal conductivity
l_{mfp}	Mean free path
$\dot{m}_{dec}$	The mass decrease rate in the control volume
m_e	The mass of electron
m_{FE}	The mass of fluid element
$\dot{m}_{inc}$	The mass increase rate in the control volume
$\dot{m}_{out}$	The net mass flow out of the entire control volume
m_T	Mass inside the control volume
n	The particle density
$\vec{n}_1, \vec{n}_2, \vec{n}_3$	The inward normals
$n[\langle\delta\rangle]$	The rate at which particles are lost or gain due to the inelastic collissions
n_e	The number of electrons per volume
n_i	The number of ionized atoms per volume
n_i^{ext}	The component of the unit outward vector in direction
n_n	The number of neutral atoms per volume
n_β	The density of beta particles
p_k	Generalized momentum coordinate

p_m	Order of moment
q	Electrical charge
q_f, q_f^*	Net fluxes flowing through the boundary in the direction of the normal vector for u_f, u_f^* functions respectively
q_k	Generalized position coordinate
$\dot{q}_X$	Heat flux in x direction
q_z	Wave vector
$\vec{r}$	The position vector
u_f, u_f^*	Arbitrary functions used in boundary element method
$\vec{v}_{DEB}$	The velocity caused by the electric and magnetic fields
$\vec{v}_{DGB}$	The velocity caused by the gravitational and magnetic fields
$v_{D,Grad}$	Drift motion velocity due to the gradient of magnetic field
v_β	Mean velocity of beta particles
w_i	Weight function
$\vec{w}_r$	Peculiar velocity or random velocity
Δm	Finite mass
ΔV	Finite volume
Φ_p	Potential of charge in rest located in plasma
$\Psi(\vec{r},\vec{v},t)$	An arbitrary function
ψ_m	Artificial magnetic relaxation function
Ω	Solution domain
Ω_i	Veroni area
Ω_T	The area of triangle T
Ω_V	Collision integral
α_R	Recombination coefficient
α_t	Thermal diffusivity

α^k	Constant numbers changing between 0 and 1
β_{pl}	Plasma beta
β_T	Coefficient of volume expansion
β^2	Artificial compressibility parameter
γ	Surface tension
δm	Mass element
δ_{ij}	Kronecker delta function
δ^2	Magnetic relaxiation constant
ε^*	Thermal energy
ε_m	Internal energy per mass
ε_n	Energy used in distribution function for Maxwell-Boltzmann statistics
η	Electrical resistivity
θ_t	Dimensionless temperature
λ	Wavelength
$\vec{\lambda}$	Constant speed vector
λ_D	Debye length
λ_f	Free parameter
λ_s	Second viscosity coefficient
μ	Viscosity
μ_0	The magnetic permeability
μ_m	Molecular viscosity coefficient
ν_C	The collision frequency
ν_i	The ionization frequency
ρ	Density
ρ_{Bulk}	The bulk electron density
ρ_E	Electric charge density
ρ_m	Mass density

ρ_p	Density with which the particles are scattered in phase space
$\rho(z)$	The electron density in z direction
σ	Electrical conductivity
σ_C	Coulomb cross section
σ_{cs}	The collision cross section
σ_{cw}	Capillary width
σ_d	Collision diameter
τ	Pseudo-time
τ_{ij}	Shear stress
τ_{mft}	Mean free time
τ_t	The positive parameter
υ	Kinematic viscosity
ω_p	Plasma ferquency
ω_c	Cyclotron frequency

a. u.	Arbitrary unit
BAKI	Bilimsel araştırmalarla kollektif icat
BEM	Boundary element method
CFD	Computational fluid dynamics
CPU	Central processing units
FEM	Finite element method
FDM	Finite difference method
FVM	Finite volume method
GaInSn	Gallium Indium Tin ternary alloy
GUI	Graphical user interface
MHD	Magnetohydrodynamics
PPPL	Princeton Plasma Physics Laboratory
UCLA	University of California, Los Angeles
UV-Vis	Ultra violet and visible range

1. INTRODUCTION

The simple word energy has a very deep meaning in daily life for our living planet. Since it is a very important phenomenon all the countries have their own plans and objectives about energy. Because of the fact that the consumption and demand for energy are increasing day by day nowadays, the most outstanding subject is the production of energy. The main sources for energy production are fossil fuels like petroleum, coal, natural gas etc. However, some different energy sources are also available such as nuclear energy, alternative energy sources like wind, solar, biomass, geothermal and hydroelectric energies. Energy supply and demand play a very vital role in national security and the economic output of every nation. Since the importance of the energy is increasing day by day all around the world, a lot of researchers are working to find out new reliable and sustainable energy sources.

One of the most important energy sources is nuclear energy. Nowadays nuclear power reactors produce energy by taking the advantage of the physical phenomenon called fission, splitting up heavy nuclei such as Uranium (U) or Plutonium (Pu). Fusion, which has a different mechanism than fission is based on composition of some lighter nuclei. In order to overcome the Coulomb repulsion force between the light nuclei the ambient temperature must be extremely high such as $10^6 - 10^8\ K$ to make these nuclei stick to each other. Resources for fusion reaction are thought to be infinite since oceans are the main sources for these light nuclei which are Hydrogen (H), Deuterium (^{2}H) and Tritium (^{3}H). However controlled fusion is a very difficult task and has some technological inabilities at least for now. Together with fusion, fuel cycle and vacuum systems, microwave heating, blanket and divertor design, superconducting magnet and material development, plasma wall interactions are also being investigated. The main problem for these new fusion power reactors is to control the plasma. Basically, plasma which is described as the fourth state of matter will be discussed in detail in the next chapter. Actually it is a gas which is assumed to be neutral as a whole but has electrons and ions travelling freely in it. Since the ambient temperature for fusion is very high, the normal outcome will be the ionization process. The plasma can be obtained in different ways but

in every way energy supply is the essential precondition. Being an ionized gas, the plasma is strongly affected by the electromagnetic fields because it contains positively charged ions and negatively charged electrons. Plasma simulation research together with fluid mechanics is one of the most important fields for understanding and describing the particle motion under the effects of electromagnetic fields.

In this thesis, firstly the concept of plasma will be discussed briefly. Some important definitions such as magnetic pressure, distribution function, plasma frequency, Debye length, plasma parameter, etc. will be mentioned. The link between the plasma and magnetohydrodynamics equations will be discussed. After some assumptions the resulting momentum and energy equations will be derived. This will be done in a systematical way.

Since the particles in the plasma are assumed to be moving as in the way that the particles behave like fluid, the fluid properties will be studied. Since the problems which will be studied in this thesis are not related with the motion of the individual particles or molecules, some of the macroscopic properties of fluids which are relatively more important in studying the dynamics of fluids such as viscosity, pressure, density, temperature will be mentioned. Because of the fact that the fluid is assumed as a continuum the properties can be obtained as a result of the statistical average of the particles in volume under consideration. Since the dimensions of the volume under consideration are much more bigger than those of the individual particles the statistical approach is applicable. Differential and integral forms for continuity equations will be studied basically. Navier-Stokes equations which are governing the mathematical model for fluid dynamics and energy equations will also be discussed. The expressions for different geometries such as cylindrical and spherical cases will be given directly without any derivation.

Both experimental and theoretical physics nowadays are trying together to describe this particle motion better and better. In order to prevent very high expenses of the experimental works scientists started to use computers instead. Over the last two or three decades especially the speed and capacities of computers increased dramatically. Fluid dynamics is used as a tool for describing the particles' motion and it has a very important role in industrial processes. Since the power of computers increased nowadays scientists

make the calculations of fluid dynamics by using these computers. The 'Computational Fluid Dynamics' which is presented with the universally accepted acronym CFD is the most used research tool nowadays in science and industry related with the fluid dynamics. It is used in a very wide range of engineering applications such as hydrodynamic problems of ships, submarines, etc. (for naval engineering) design and optimizations of aircrafts, cars and trucks by reducing both expensive and time consuming wind tunnel tests, heating and air conditioning processes for the houses, blood circulation in the body, fusion plasma research etc. However, CFD nowadays can be thought as a mathematically sophisticated discipline. Previously fluid dynamics was divided into two branches, theoretical and experimental. However, nowadays CFD is the third and equal branch of fluid dynamics. CFD tries to solve the governing equations by using the numerical methods instead of analytical ones. In this thesis CFD and its philosophy will be studied. The space discretization methods such as finite difference, finite element, finite volume, boundary element and matrix distribution scheme will be described. The space discretization processes in the numerical works in this thesis are done by using matrix distribution scheme. The detailed description for matrix distribution sheme will be given. Dual time stepping method which will be used in this thesis as a time discretization procedure will also be studied in detail.

Simulations done in this thesis will be performed by using a homemade computer code which will be discussed in detail here. It is desired to be expanded to three dimensions in the future. Actually only the mesh generation procedure for three dimensional studies will be presented here. The mesh which is containing three dimensional coordinates for every node and the formula which will be used in this process will be studied in detail. This will be a novel approach in which the code will be developed and this code is planned to be embedded in the previous original two dimensional code.

Numerical simulations of some benchmark problems and originally designed problems will be solved in the numerical results part and the obtained outcomes will be discussed. Some of the benchmark problems which are planned to be solved here are the steady state lid driven cavity test, the unsteady lid driven cavity test, the unsteady oscillatory lid driven cavity test etc. The relatively new designed problems such as vertical obstructed flow through the square channels, liquid metal flow past a circular cylinder in

open channels exposed to external magnetic field, and so on. The fluids in the problems solved in this thesis will be considered to be incompressible. The flow pattern will be assumed to be laminar except for some simulations for steady-state lid driven cavity test problem.

As previously mentioned the energy production is a very important phenomenon. After the energy is extracted as heat from the reactions such as fission or fusion it is desired to be converted to electrical energy which is materialized by using the turbines. One of the most important agents during this energy conversion process is the matter which is used as a cooler. In some reactors instead of water the liquid metals are used as a cooling agent. They are chosen because of the fact that they have bigger thermal conductivity coefficients than that of water. However, the application areas of liquid metals are not restricted only to cooling. Here in this thesis, the technological applications for liquid metals will be mentioned and experiments will be presented in which the GaInSn alloy will be used. Some light reflection properties of the free surface of this alloy will be studied in more detail under different external effects such as temperature increase, current application, magnetic field application etc. The reflection dependence of Lorentz force induced by current and perpendicularly applied magnetic field through GaInSn alloy will be studied.

2. CONCEPT OF PLASMA AND MAGNETOHYDRODYNAMIC EQUATIONS

2.1. The Definition

As a very simple definition, plasma is an ionized gas and a collection of charged particles. In some sources in the literature it is also called as a fourth state of matter. However, its main importance comes from the fact that more than 99.9 per cent of the matter or the apparent universe is in this fourth state, plasma. There is an important formula proposed by Saha

$$\frac{n_i}{n_n} \approx 2.4 \times 10^{21} \frac{T^{\frac{3}{2}}}{n_i} e^{-U_i / kT} \tag{2.1}$$

where n_i is the number of ionized atoms per volume $(number/m^3)$ and n_n represents the number of neutral atoms per volume, T is the gas temperature in Kelvin (K), k is the Boltzmann constant and U_i is the ionization energy of the gas. This equation explains the ionization expected for a gas in thermal equilibrium at temperature T. Actually this equation is obtained by rearranging the momentum equation for electron under certain assumptions. It provides a simplification to determine the number of electrons per volume n_e without solving the momentum equations. As an example for the air in the ordinary room temperature for Nitrogen, the ratio given in Equation 2.1 turns out to be

$$\frac{n_i}{n_n} \approx 10^{-122}$$

where $n_n = 3 \times 10^{25} m^{-3}$, $T = 300\,K$ and $U_i = 14.5\,eV$ are used [1]. In order to have a plasma from a gas the heat addition method can be used. If enough energy is added to the solid by heating it up, the atoms which form the crystal lattice start to go through thermal motions [2] which is ended up by a phase transition such that the solid becomes liquid. If

the heat addition continues the atoms start to vapourize and the gas phase is formed. The addition of more energy to the gas causes the gas atoms to collide with each other and this collective motion causes ionization of some atoms. This is a new formed state which is called the fourth state of matter, namely plasma. After the temperature is increased sufficiently then the number of neutral atoms becomes fewer than the number of the ionized atoms and plasma becomes fully ionized. This shows that fully ionized plasma is only formed at extremely high temperatures. Collective behaviour is very important in plasmas. Since it is composed of the charged particles, their motion can generate not only the current and subsequently magnetic field but also the local concentrations of positive and negative charges which can generate internal electric fields. These fields affect the motion of the other charged particles. The force which has long range and affecting the particles in the plasma, is the force named Coulomb Force. At the temperatures above $100\,000\ K$ most of the matters are in an ionized state. However, by using some other ionization mechanisms, the plasma can be formed also under $100\,000\ K$. In this mechanism the density must be low enough in order to prevent from the recombination process as much as possible [3]. The name plasma, which means 'jelly' or 'moldable substance' in Greek, is given by the Nobel laureate Irving Langmuir [2]. In the laboratories, the plasma is simply obtained by passing the electric current through the small amount of gas. The previously mentioned method which is based on heating the matter is not so much preferable because the container in which the process occurs may not withstand the temperatures at which the plasma is formed. Additionally, during the heating process the container itself can vapourize and become a plasma as well. Another way of forming the plasma is to send the radio waves through the gas. Since the electrons absorb the radio waves, the ionization occurs and subsequently the plasma is formed.

When protons and electrons coexist together at a sufficiently low density, this collection is thought to exist in equilibrium state, which is described by equilibrium statistical mechanics. Classical mechanics and nonrelativistic statistical mechanics, electromagnetism are the main areas inolved with plasma physics. The problems in controlled fusion reactors, astrophysics, molecular physics, magnetohydrodynamics power generation, contemporary physics and an atomic physics are related directly to the plasma physics. As an example, in thermonuclear fusion process, Deuterium and Tritium ions which collide with the energy in the range of tens of keV can fuse and produce α

particles and neutrons with total excess energy of 17.6 MeV ($E_{neutron} \approx 14.1\,\text{MeV}$ and $E_{\alpha_p} \approx 3.5$ MeV). The energy needed for this fusion process can be obtained from the plasma which has the density in the range of $10^{20} m^{-3}$.

High density of the Earth and its atmosphere, prevents the existence of plasma. However, the plasma exists in the ionosphere. In dailylifes of people the plasma is seen as the conducting gas inside the fluorescent tubes, as the rocket exhausts and as the flash of lightning bolt.

Because of the fact that there are charged particles such as ions and electrons, the separation between them provides an electric field and the flow of these charged particles produces currents and magnetic fields. The electric and magnetic fields produced by the moving charged particles in plasma affect the other charged particles. The forces between the elements of plasma act on each other even at large distances. Many plasma properties result from the long range Coulomb interaction, such that particles may interact simultaneously. Table 2.1 shows some properties for different plasmas.

2.2. The Terminology for Plasma

Brief introduction for the terms mostly used in plasma physics is given below. Since the subject of this study was not only about 'plasma', there is only brief description of plasma terminology given in this thesis. Figure 2.1 gives the electron temperature dependence of plasma density.

2.2.1. Meta-Equilibrium

It would be better to describe the term equilibrium before metaequilibrium. If the particles in plasma are not colliding with each other and the small perturbations are neglected, the system can be assumed to be in equilibrium. From the thermodynamical point of view the electrons and ions forming the plasma system can be described with the Maxwellian distribution which is only related to temperature. Here the system is in

equilibrium with its surroundings. If the situation that was described as an equilibrium is altered by the binary collisions a new state is obtained and it is named as meta-equilibrium.

Table 2.1. The parameters for natural and artificial plasmas [2]

	Length scale (m)	Particle density (m^{-3})	Electron temperature (eV)	Magnetic field (T)
Interstellar gas	10^{16}	10^{6}	1	10^{-10}
Solar wind	10^{10}	10^{7}	10	10^{-8}
Van Allen belts	10^{6}	10^{9}	10^{2}	10^{-6}
Earth's ionosphre	10^{5}	10^{11}	10^{-1}	3×10^{-5}
Solar corona	10^{8}	10^{13}	10^{2}	10^{-9}
Gas discharges	10^{-2}	10^{18}	2	-
Process plasmas	10^{-1}	10^{18}	10^{2}	10^{-1}
Fusion experiment	1	$10^{19}-10^{20}$	$10^{3}-10^{4}$	5
Fusion reactor	2	10^{20}	10^{4}	5

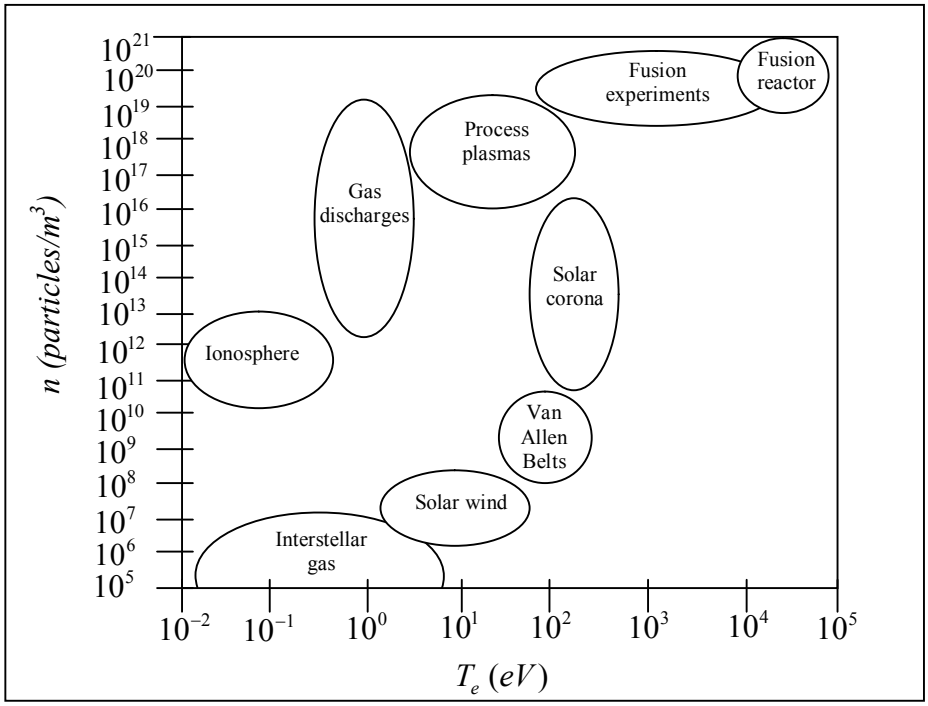

Figure 2.1. Plasma density versus electron temperature graph [2]

2.2.2. Drifts Acting on the Particles in Plasma

The electrons and ions have collective behaviour in the plasma. However, sometimes it is needed to consider the motion of individual charge or charges under the gravitational, magnetic and electric fields. These fields can be either time varying or static. Under uniform magnetic fields and if the collisions are ignored, the movement of the charged particle is helical in nature.

Larmor radius (a_L) is the radius at which the particle rotates at the cyclotron frequency which is given as, ω_c

$$\omega_c = \frac{eB}{m_e c} \tag{2.2}$$

where e is the electron charge, B is the magnitude of the applied magnetic field, m_e is the mass of electron and c is the speed of light. The rotation mentioned above is perpendicular to the applied magnetic field. When there are some other fields, the hellical motion of the charged particle can change. If the steady electric and magnetic fields are applied to the charged particles together, they cause a drift motion perpendicular not only to the magnetic field but also to electric field. The velocity expression for this drift motion caused by the electric and magnetic fields is given as:

$$\vec{v}_{DEB} = c\frac{\vec{E} \times \vec{B}}{B^2} \tag{2.3}$$

where $\vec{E}, \vec{B}$ are electric and magnetic fields respectively.

If there is neither an electric field nor a gravitiational field, another drift velocity which is given as:

$$\vec{v}_{DGB} = \frac{mc}{q}\frac{\vec{g} \times \vec{B}}{B^2} \tag{2.4}$$

must be taken into account.

If the applied magnetic field is not homogeneous, another drift motion arises because of the gradient of $\vec{B}$, $\vec{\nabla}\vec{B}$

$$v_{D,Grad} = \frac{E_k c}{qB^2}\vec{\nabla}\vec{B} \tag{2.5}$$

where E_k is kinetic energy perpendicular to $\vec{B}$, q is electrical charge and c is the speed of light [3].

2.2.3. Magnetic Pressure

The confinement of plasma in most of the cases is done by using externally applied magnetic field. Actually plasma has a diamagnetic nature magnetically. It tries to exclude the magnetic field applied to its boundary. If the static magnetic field is applied it produces an opposite pressure force given as

$$P_e = \frac{B^2}{8\pi} \quad \left[\frac{dyns}{cm^2}\right] \tag{2.6}$$

across a surface tangent to the magnetic flux surface. This magnetic pressure force must be balanced in order to confine the plasma. This balance can be done by the kinetic pressure of the plasma which can be expressed as

$$P_k = nkT \tag{2.7}$$

where P_k is the kinetic pressure, n is the particle density, k is Boltzmann's constant and T is the absolute temperature. This balance is described in the boundary between plasma and magnetic field. By increasing the value of magnetic pressure force by adjusting the magnetic field B, the plasma can be compressed and its density and temperature will increase.

Another important quantity in plasma physcics is plasma beta which is the ratio of plasma pressure to magnetic pressure, and it is expressed as:

$$\beta_{pl} = \frac{Internal\ Plasma\ Pressure}{Externally\ Applied\ Pressure} = \frac{n_i kT_i + n_e kT_e}{B^2/8\pi} \ . \tag{2.8}$$

Pressure balance in the interface requires the condition given as :

$$\vec{\nabla}\left(nkT + \frac{B^2}{8\pi} \right) = 0 \, . \tag{2.9}$$

It means that the pressure gradient at the boundary of the plasma must be zero, otherwise it can not be confined [3].

2.2.4. The Distribution Function

The distribution function f which will be used intensively later in this chapter of the thesis is used to describe the plasma. Basically, it is the number of particles per unit volume in six dimensional velocity configuration phase space $(dx\,dy\,dz\,dv_x dv_y dv_z)$.

Since, unfortunately it is not possible to know everything such as position and velocity of any individual particle in plasma, a distribution function is used as a statistical function in order to describe the plasma properties mentioned above.

In the most detailed plasma descriptions it is desired to know the velocity and the location of each particle. However, it is impossible to individually follow a lot of ions and electrons and know their locations and velocities instantaneously even with super computers. The laboratory plasmas almost always obey the Maxwellian distribution, actually a plasma can never achieve the exact distribution but it is very close. It is usually necessary to define different distribution functions for each charge species, let's say β, so that $n_\beta f_\beta(\vec{r},\vec{v})d\vec{r}d\vec{v}$ is the number of β particles, in the volume element expressed as

$d\vec{r}d\vec{v}$. If the normalization is done, then total number of β particles in the system is found. The unit of the distribution function is $[f] = m^{-3}(m/s)^{-3} = [s^3/m^6]$.

For a Maxwell-Boltzmann distribution, the distribution function, f needs appropriate normalization. By taking the moments of distribution function some macroscopic parameters of plasma system such as density, mean velocity, pressure etc. can be found. The expressions for density and mean velocity are given respectively below.

$$n_\beta = \int f_\beta d\vec{v} \tag{2.10}$$

$$v_\beta = \frac{\int v f_\beta d\vec{v}}{\int f_\beta d\vec{v}}. \tag{2.11}$$

The distribution function can be used to find the value of some quantities averaged over the distribution. For any quantity Q, the local velocity-space average of Q, $\langle Q \rangle_v$ is given as:

$$\langle Q \rangle_v = \frac{\int f Q d^3v}{\int f d^3v}. \tag{2.12}$$

It is useful to relate the experimental distribution function to the Maxwellian distribution that can fit the data better. This can be done by describing the system which is a plasma having the temperature T. Otherwise if the distribution function has no relation with Maxwellian distribution it is purely described by only specifying the temperature [2].

2.2.5. The Plasma Frequency

Some interesting behaviours of plasma can be observed because of the fact that the particles affect each other with the long range forces. Actually the plasma can behave as a system of coupled oscillators. The frequency of the plasma ω_p is the one basic oscillator's frequency which is given as :

$$\omega_p = 2\pi f_p = \left(\frac{4\pi n e^2}{m_e} \right)^{\frac{1}{2}} \text{ with the unit } \left[\frac{rad}{s} \right]. \quad (2.13)$$

In Equation 2.13, $f_p \approx 10^4 \sqrt{n}$ Hz for electrons where n is the particle number in cubic centimeter, m_e is the mass of electron. ω_p is the frequency of the plasma giving the information about how electrons fluctuate in the plasma, and it also gives the information about the time which is required for an electron or an ion moving with thermal speed to cover a Debye length which will be discussed later [3].

2.2.6. Debye Length

One of the important features of plasma is that it has an ability to shield the electric potentials applied externally. Plasma has a fundamental property which states that if any additional charged particle or particles are added (immersed) to plasma, the new additional electric field due to the newly added particle is shielded by plasma. In order to screen the plasma from penetration of a new electric field caused by the newly added particle all the other particles in the plasma go through new arrangements. The Debye length λ_D which is the measure of the shielding distance, is one of the important criteria for an ionised gas to be a plasma or not.

Debye sphere, another term, is the sphere with the radius which is equal to the Debye length. In order to say the ionized gas is a 'plasma' it must have the dimensions such as 'L ' which must satisfy $L >> \lambda_D$ and also the number of particles in the Debye sphere, N_D, must satisfy $N_D >> 1$. If the frequency of a typical plasma is ω_p and the mean free time which is the time taken between two successive collisions with neutral atoms is τ_{mft}, then the plasma must also satisfy the criterion which is $\omega_p \tau_{mft} >> 1$ otherwise the gas will be said to be a neutral gas instead of plasma [1, 2].

By using a little mathematical interpretation a little different definition for Debye length can be given as follows. The potential of a charge at rest located in a plasma can be solved as follows:

$$\Phi_p = \left(\frac{q}{r}\right) exp\left(-\frac{r}{\lambda_D}\right) \tag{2.14}$$

where λ_D is Debye length which is a kind of measure of the sphere of influence of the given test particle in plasma. Actually λ_D depends on the speed of the test charge with respect to the plasma. As a brief example for electron-proton plasma, Debye length is given as :

$$\lambda_D = \left(\frac{kT}{8\pi ne^2}\right)^{\frac{1}{2}} = 4.9\left(\frac{T}{n}\right)^{\frac{1}{2}} \tag{2.15}$$

where n is again the density of electrons (or ions) in cm^3, T is temperature in K and k is Boltzmann's constant with the value of $1.38\times10^{-16}\, ergs/K$.

2.2.7. Plasma Parameter

The plasma parameter, is the parameter which gives an idea about the number of particles in Debye sphere. The mathematical representation of the plasma parameter is:

$$g_p = \frac{1}{n\lambda_D{}^3}. \tag{2.16}$$

If the plasma description is required to be statistically correct then the Debye sphere must be larger and subsequently the plasma parameter, g_p must be smaller. The assumption for g_p is called the 'plasma approximation'. This parameter is one of the most important dimensionless parameters related to the plasma.

2.2.8. Stability of a Plasma and Controlled Thermonuclear Fusion

One of the aims of the fusion plasma research is to be able to confine the plasma at a sufficient density and sufficient time period to make the thermonuclear fusion possible .

However, the energy spent in order to maintain this confinement is wanted to be less than the energy which is recovered from the fusion process. The main drawbacks for this process are plasma instabilities. Stability theory is the most interesting part of plasma research. The problem is not solved totally up to now but a very intensive research is directed to this phenomenon. The instability actually can be defined as a small perturbation in plasma which is in equilibrium and the effect of this small perturbation can grow with time. One of the important instabilities of plasma is configuration-space instability which is due to the spatial localization of particularly used devices during the confinement of plasma. Velocity-space instability is another important instability of plasma. When a beam of monoenergetic electrons is injected into a cold plasma this kind of instability occurs.

2.2.9. Collisions in Plasma

Not only elastic but also inelastic collisions occur among the particles in the plasma. Mostly the collisions in the partially ionized gas are electron-electron, electron-ion, and electron-neutral collisions. The cross section term is usually used to describe the collisions in plasma. It gives an idea about the probability of interaction of the particles. Since the value of some cross sections are changed by the plasma, Coulomb cross section is defined σ_C. Coulomb cross section is obtained by changing the upper limit of total cross section integral to Debye length [3].

The mean free path, l_{mfp} is another important parameter in plasma physics. It is defined as a path length travelled by the particle before collision process occurs. Mathematically it is given as :

$$l_{mfp} = \frac{1}{n\sigma_{cs}} \tag{2.17}$$

where σ_{cs} is the collision cross section. The collision frequency, ν_C, is given as

$$\nu_C = n\sigma_{cs}v \tag{2.18}$$

where v is the velocity with which the incoming particle is travelling relatively to the target particle. The incoming particle will travel the l_{mfp} mean free path in time τ_{mft} before collision.

The reciprocal of this time is defined as collision frequency. Since in most cases the cross section is the function of velocity so the effective collision frequency is the average value of the product of cross section and velocity. Velocities of target particles are thermally distributed. The effective collision frequency is given as :

$$\nu_C = n\langle\sigma_{cs}(v)v\rangle . \tag{2.19}$$

For incident particles the total number of events per second and per cubic centimeter is expressed as :

$$R_e = n_1 n_2 \left\langle \sigma_{cs} v \right\rangle_{1,2} . \tag{2.20}$$

There are many important terms and parameters for plasma such as Landau damping, waves in plasma (e.q. ion-sound waves, plasma waves etc.), shock waves, solitary waves, plasma radiation (e.q. Bremstrahlung, Blackbody radiation, Impurity radiation, Synchrotron or Cyclotron radiation, Cherenkov radiation, diffusion and Bohm diffusion etc. which will not be mentioned in detail in this thesis since they are out of our scope of discussion.

Another important process for plasma is its production. Since it does not exist as a normal state on the Earth it is produced depending on the aims of the researcher and customers. It can be produced having different densities, different temperatures, stable or unstable and etc. Some of the main plasma production techniques are the low pressure cold cathode discharge, the thermionic arc discharge, rf produced plasmas, alkali metal vapour plasmas, the Solar plasma, laser produced plasma etc.

The measurements are also very important events for plasma technology. The properties of plasma such as density, temperature, thermal conductivity, radiation rate,

collision frequency, stability or instability are desired to be known. Actually measuring one of these properties can help in calculation of the other parameters. Mostly measurement of the current and voltage in plasma helps in understanding the other properties. There are some probes such as electrostatic or Langmuir probes and magnetic probes. Some other methods also exist in measuring such as fast photography and atomic spectroscopy, radiation measurements, single particle measurements etc. The measurement techniques used are classified as active and passive techniques. The active technique disturbs the plasma and produces a perturbation after and during the measurement process. In active technique the plasma is directly involved in measurement. The contribution to errors is highly probable. In passive technique plasma is not disturbed and the measurements are taken without producing any perturbation in plasma.

2.3. From Plasma Definion to Magnetohydrodynamics Equations

The typical plasma density can be about 10^{12} ion-electron pair per cm^3. Similarly to the fluids the individual particles containing the plasma can be neglected. Instead of looking at an individual particle it is better to take account of the motion of the fluid elements. In an ordinary fluid the collisions between the particles keep the particles moving together. Plasma, as a fluid contains charged particles in frequent collisions . The collective particle movements in plasma occure are similar to the movements in fluids. When the fluid assumption is taken into account the plasma can be thought as it is formed from two or more interpenetrating fluids. This theory or assumption is the simplest one and sometimes it is not enough for some high level researches. In that point another theory comes to the help of the scientists. The name of this theory is 'Kinetic Theory' and it describes the plasma statistically. Therefore kinetic theory forces to define a distribution function which is called 'the velocity distribution function' and which is denoted as $f(v)$. Differently from the ordinary fluid theory which has only four independent variables which are x, y, z *and* t , additionally three more variables which are velocities such as v_x, v_y and v_z will be taken into account. Most of the plasmas obey the Maxwellian distribution since the plasmas are in thermal equilibrium which can not be changed easily. Actually the density $n = n(\vec{r},t)$ is a function of four scalar variables, however considering the velocity distributions, the number of variables increase to seven independent variables. In phase

space the distribution function $f = f(\vec{r},\vec{v},t)$ has seven independent variables which are $x,\ y,\ z,\ v_x,\ v_y,\ v_z,\ t$. The function $f(\vec{r},\vec{v},t)dv_x dv_y dv_z$ gives the number of particles which are located at x, y, z space point in time t with velocity limits which are between v_x and $v_x + dv_x$, v_y and $v_y + dv_y$, v_z and $v_z + dv_z$. Basically it gives an idea about the particle distribution not only in physical space but also in velocity space together. $f = f(\vec{r},\vec{v},t)$ represents the same particles per volume $d^3v = dv_x dv_y dv_z$. Note that the velocity dependence is removed by taking the moment of distribution function.

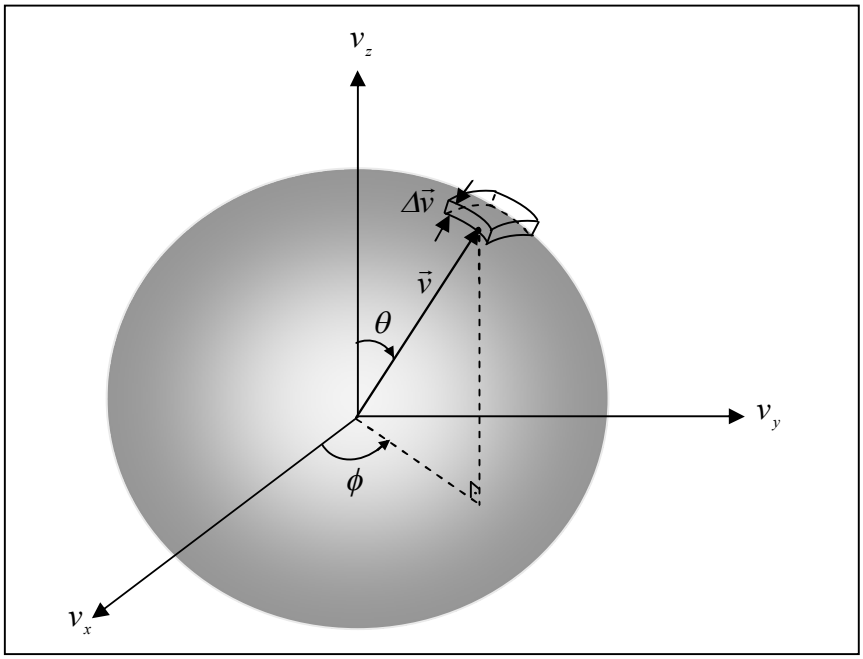

Figure 2.2. Velocity space in three dimensions [1]

The phase space can be defined as:

$$Phase\ Space = 3\ \ Dimensional\ \ Velocity\ \ Space + 3\ \ Dimensional\ \ Coordinate\ \ System$$

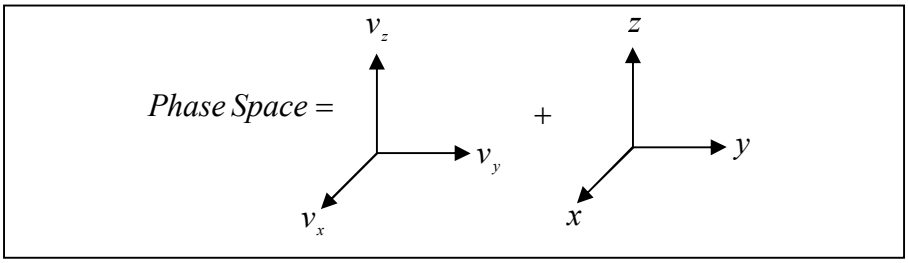

Figure 2.3. Phase space description

Actually phase space has six dimensions which are x, y, z, v_x, v_y, v_z. The volume element is given as $dV = d\vec{v}d\vec{r}$ in Figure 2.4. The geometrical meaning is that phase space occupied consists of the sum of all the individual phase space volume elements. Under the effect of the forces the volume of the fluid element can deform. However the magnitude of the volume after the deformations can be constant which leads to the fact called particle conservation. If no particles are lost and no particles are added to the plasma the exact phase space density will be conserved.

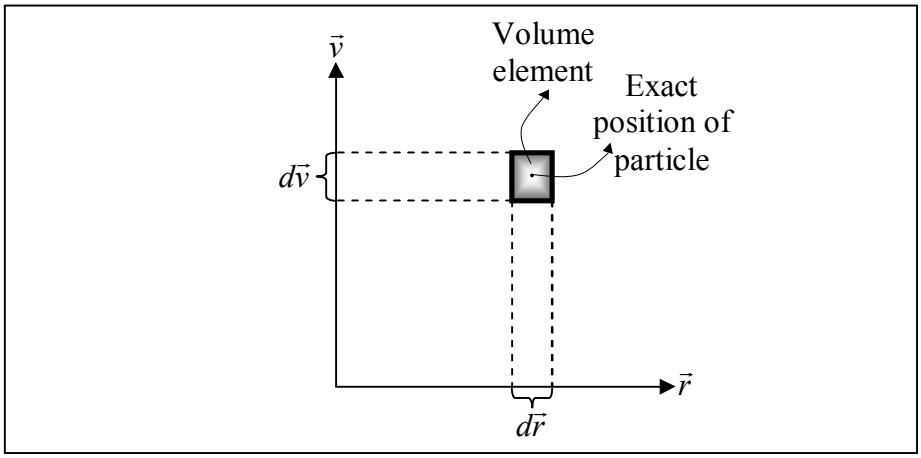

Figure 2.4. Six dimensional phase space

A number of particles in a unit volume of phase space mentioned previously is specified by a distribution function.

$$dn = f(\vec{r},\vec{v},t)d^3rd^3v \tag{2.21}$$

where

$$d^3r = dxdydz \text{ and } d^3v = dv_x dv_y dv_z$$

then

$$n(\vec{r},t) = \int_{-\infty}^{\infty} f(\vec{r},\vec{v},t)d^3v = \int_{-\infty}^{\infty} dv_x \int_{-\infty}^{\infty} dv_y \int_{-\infty}^{\infty} dv_z f(\vec{r},\vec{v},t) \tag{2.22}$$

is obtained. The distribution function can be normalized as given in Equation 2.23:

$$\int_{-\infty}^{\infty} f'(\vec{r},\vec{v},t)d^3v = 1. \tag{2.23}$$

The unit of normalized distribution function $f'(\vec{r},\vec{v},t)$ will be $\left[s^3/m^3\right]$. Consequently the previously known unit for distribution function

$$f(\vec{r},\vec{v},t) = \underbrace{n(\vec{r},t)}_{\left[1/m^3\right]}\underbrace{f'(\vec{r},\vec{v},t)}_{\left[s^3/m^3\right]} \tag{2.24}$$

was obtained as $\left[s^3/m^6\right]$. By using different velocity integrals of the distribution function any quantity can be expressed in $(\vec{r},t)$ space. The average velocity, average kinetic energy and collision frequency expressions with the help of distribution function are given respectively as :

$$\langle\vec{v}\rangle = \frac{\int_{-\infty}^{\infty}\vec{v}f(\vec{r},\vec{v},t)d^3v}{\int_{-\infty}^{\infty}f(\vec{r},\vec{v},t)d^3v} = \frac{1}{n(\vec{r},t)}\int_{-\infty}^{\infty}\vec{v}f(\vec{r},\vec{v},t)d^3v \tag{2.25}$$

$$\langle KE\rangle = \frac{1}{n(\vec{r},t)}\int_{-\infty}^{\infty}(\frac{1}{2}mv^2)f(\vec{r},\vec{v},t)d^3v \tag{2.26}$$

$$\nu_C = n\langle\sigma_{cs}(v)v\rangle = \frac{n}{n(\vec{r},t)}\int_{-\infty}^{\infty}\sigma\vec{v}f(\vec{r},\vec{v},t)d^3v. \tag{2.27}$$

The system of particles gives rise to equilibrium distribution if the system is not subject to external forces and if the system is in thermodynamic equilibrium. The equilibrium requires the temperature of heavy particles to be the same $(T_n = T_i)$;

however, electrons temperature T_e is usually higher since they are much smaller than heavy particles.

In Maxwell-Boltzmann statistics, the distribution function is given as $f(\varepsilon_n) = A_n e^{-\varepsilon_n \beta}$ where ε_n is energy, A_n is a normalization constant and $\beta = 1/kT$. For an ideal gas system (not at very high temperatures) the velocity distribution function is given as

$$f(v) = A_n e^{\left(-\frac{1}{2}mv^2/kT\right)} \tag{2.28}$$

and

$$dn = f(v)d^3v. \tag{2.29}$$

By integrating Equation 2.28 in velocity space one gets the number density as

$$n_0 = \int_{-\infty}^{\infty}\int_{-\infty}^{\infty}\int_{-\infty}^{\infty} f(v_x, v_y, v_z)dv_x dv_y dv_z \tag{2.30}$$

$$= \int_{-\infty}^{\infty}\int_{-\infty}^{\infty}\int_{-\infty}^{\infty} A_n e^{-\left[\frac{1}{2}mv_x^2/kT + \frac{1}{2}mv_y^2/kT + \frac{1}{2}mv_z^2/kT\right]} dv_x dv_y dv_z$$

$$= A_n \int_{-\infty}^{\infty} e^{-K_x/kT} dv_x \int_{-\infty}^{\infty} e^{-K_Y/kT} dv_y \int_{-\infty}^{\infty} e^{-K_z/kT} dv_z \tag{2.31}$$

where temperature is assumed to be homogeneous in space. Note that the Cartesian coordinate system is assumed to perform the calculations. Thus the velocity can be given as:

$$v^2 = v_x^{\,2} + v_y^{\,2} + v_z^{\,2} \tag{2.32}$$

so that

$$v = (v_x^2 + v_y^2 + v_z^2)^{1/2} \tag{2.33}$$

and K_x, K_y, K_z in Equation 2.31 are kinetic energies for x, y and z directions respectively. Since

$$\int_{-\infty}^{\infty} e^{-\alpha x^2} = \sqrt{\pi/\alpha} \tag{2.34}$$

, Equation 2.31 can be written as:

$$n_0 = A_n \sqrt{\frac{2\pi kT}{m}} \sqrt{\frac{2\pi kT}{m}} \sqrt{\frac{2\pi kT}{m}} \tag{2.35}$$

so one gets

$$A_n = n_0 \left(\frac{2\pi kT}{m} \right)^{-\frac{3}{2}}. \tag{2.36}$$

As a result, Maxwell-Boltzmann velocity distribution function becomes

$$f(\vec{v}) = n_0 \left(\frac{m}{2\pi kT} \right)^{\frac{3}{2}} e^{\left(-\frac{1}{2} m v^2 / kT \right)}. \tag{2.37}$$

By using the distribution function one can obtain different average quantities. For example average velocity in x direction can be found by using the velocity distribution function.

$$\langle v_x \rangle = \frac{1}{n_0} A_n \int_{-\infty}^{\infty} \int_{-\infty}^{\infty} \int_{-\infty}^{\infty} v_x f(\vec{v}) d^3 v =$$

$$= \frac{A_n}{n_0} \int_{-\infty}^{\infty} v_x e^{-\frac{K_x}{kT}} dv_x \int_{-\infty}^{\infty} e^{-\frac{K_y}{kT}} dv_y \int_{-\infty}^{\infty} e^{-\frac{K_z}{kT}} dv_z$$

$$= \frac{A_n}{n_0} \left(\frac{2\pi kT}{m} \right)^{\frac{1}{2}} \left(\frac{2\pi kT}{m} \right)^{\frac{1}{2}} . \left[\frac{kT}{m} e^{-\frac{1}{2} m v_x^2 / kT} \right]_{-\infty}^{\infty} = 0 \qquad (2.38)$$

It is obvious from symmetry that the average velocities in $x, y,$ and z directions are zero.

$$\langle v_x \rangle = \langle v_y \rangle = \langle v_z \rangle = 0 . \qquad (2.39)$$

Velocity and speed are two different physical quantities. First of all velocity is a vectoral quantity and speed which is a scalar quantity is the magnitude of the velocity. One of the important aspects is that the average velocity for different spaces can have different values (Figure 2.5). Since there is no preferred direction of notation the volume element in velocity space is $d^3v = dv_x dv_y dv_z$. For the spherical coordinate system the volume element in velocity space (v, θ, ϕ) can be given as:

$$d^3v = v^2 (Sin\theta d\theta d\phi) dv . \qquad (2.40)$$

By taking into account the volume element given in Figure 2.2, v can take the values between the limits $[0, \infty]$, θ can take the values between $[0, \pi]$ and finally ϕ can have the values between the limits $[0, 2\pi]$, [2]. Since the velocity distribution is assumed to be isotropic the expression given in paranthesis in Equation 2.40 will have the value of 4π . Then the volume element in speed space will be

$$d^3v = 4\pi v^2 dv . \qquad (2.41)$$

Let us consider two distribution functions $g(v)$ and $f(v)$ defined respectively as: $g(v) = f(\vec{r}, v, t) \equiv$ speed distribution, $f(\vec{v}) = f(\vec{r}, \vec{v}, t) \equiv$ velocity distribution. The relation between these functions is $g(v) = 4\pi v^2 f(\vec{r}, \vec{v}, t)$.

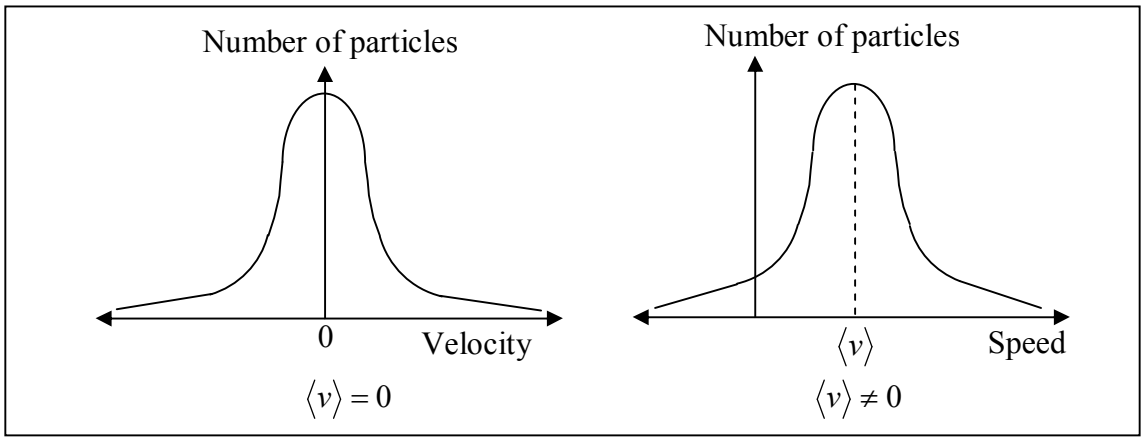

Figure 2.5. The distribution functions for different spaces

By using these distribution functions the particle density can be expressed in speed space as:

$$n(\vec{r},t) = \int_0^\infty 4\pi v^2 f(\vec{r},\vec{v},t)dv = \int_0^\infty f(\vec{r},v,t)dv = \int_0^\infty g(v)dv\,. \tag{2.42}$$

Here the limits of integral are taken as the limits of the radius of sphere (Figure 2.2) in velocity space. The speed distribution function is thus given by

$$f(\vec{r},v,t) = 4\pi v^2 \left(\frac{m}{2\pi kT}\right)^{\frac{3}{2}} e^{\left(-\frac{1}{2}mv^2/kT\right)}\,. \tag{2.43}$$

By using the speed distribution one can get averages of scalar quantities such as kinetic energy, collision frequency etc. and by using the velocity distribution the averages for vector quantities such as velocity, momentum, angular momentum, etc. can be found.
As an example, the average kinetic energy will be

$$\langle KE \rangle = \frac{1}{n_0}\int_0^\infty 4\pi v^2 \left(\frac{m}{2\pi kT}\right)^{\frac{3}{2}} \left(\frac{1}{2}mv^2\right) e^{\left(-\frac{1}{2}mv^2/kT\right)} dv \tag{2.44}$$

after some simplifications the equation becomes

$$\langle KE \rangle = \frac{2\pi m^{5/2}}{(2\pi kT)^{3/2}} \int_0^\infty v^4 e^{\left(-\frac{1}{2}mv^2/kT\right)} dv \,. \tag{2.45}$$

In order to get the integral from Equation 2.45, Gamma function: $\Gamma(n)$ is used. This function is defined as

$$\Gamma(n+1) = n! \text{ for } n = 0,1,2,... \tag{2.46}$$

and

$$\Gamma(n) = \frac{\Gamma(n+1)}{n} \text{ for } n < 0 \,. \tag{2.47}$$

The solution for the integrals in the form of

$$\int_0^\infty x^n e^{-ax^2} dx \tag{2.48}$$

is obtained by using Gamma function:

$$\int_0^\infty x^n e^{-ax^2} dx = \frac{\Gamma[(n+1)/2]}{2a^{(n+1)/2}} \,. \tag{2.49}$$

As a result, Equation 2.45 can be written as

$$\langle KE \rangle = \frac{2\pi m^{5/2}}{(2\pi kT)^{3/2}} \frac{\Gamma(5/2)}{2(m/2kT)^{5/2}} \tag{2.50}$$

$$\Gamma\left(\frac{5}{2}\right) = \Gamma\left(2+\frac{1}{2}\right) = \frac{1.3}{2^2}\sqrt{\pi} = \frac{3}{4}\sqrt{\pi} \tag{2.51}$$

$$\langle KE \rangle = \frac{2\pi m^{5/2}}{(2\pi)^{3/2}(kT)^{3/2}} \frac{3/4\sqrt{\pi}}{2m^{5/2}/(2kT)^{5/2}} \tag{2.52}$$

so that one gets

$$\langle KE \rangle = \frac{3}{2} kT \,. \tag{2.53}$$

Another distribution function, $f(E)$ which is the energy distribution function can be obtained by using the kinetic energy equation $E = mv^2/2$. The velocity expression can be written as $v = (2E/m)^{1/2}$. The differential of energy is $dE = mvdv$ so that one can write $dv = dE/mv$ and energy distribution function can be written as:

$$f(E) = n_0 \left(\frac{1}{\pi kT} \right)^{3/2} e^{(-E/kT)} 2\pi \sqrt{E} dE \,. \tag{2.54}$$

One of the main theorems in kinetic theory is Liouville's theorem. This theorem basically expresses the conservation of phase space density. The volume element in phase space can evolve under the effect of the forces in time but the volume itself and the number of the particles in it can remain unchanged.

Liouville's theorem actually describes the time evolution of the distribution function in phase space. It states that the distribution function is constant along any trajectory in phase space. As a result it can be easily said that the number of particles in the chosen system is constant in time when the system is travelling and deforming through the phase space (Figure 2.6). At this point some definitions which will be used in derivations later, will be given.

ρ_p : Density with which the particles are scattered in phase space,

q_k : Generalized position coordinate, $q_1 = x,\ q_2 = y,\ q_3 = z$ (in Cartesian geometry),

p_k : Generalized momentum coordinate, $p_1 = mv_x, p_2 = mv_y, p_3 = mv_z$

D : Number of dimensions,

$d\vee$: Elemental volume in phase space.

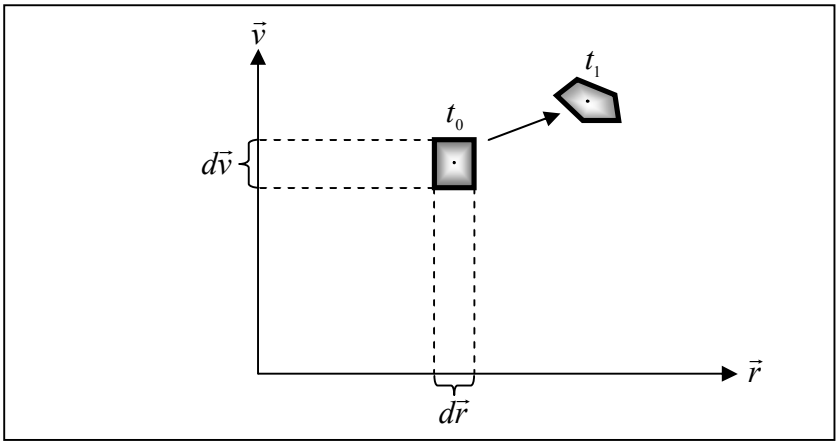

Figure 2.6. The time evolution for the volume element in phase space

The expression for the elemental volume in phase space can be given by using the generalized coordinates.

$$d\vee = dp_1 dp_2 ... dp_D dq_1 dq_2 ... dq_D \tag{2.55}$$

Since the incremental volume in phase space is defined as:

$$\Delta\vee = \Delta q_1 \Delta q_2 ... \Delta q_D \Delta p_1 \Delta p_2 ... \Delta p_D , \tag{2.56}$$

the number of systems in this volume is then $\rho_p \Delta q_1 \Delta q_2 ... \Delta q_D \Delta p_1 \Delta p_2 ... \Delta p_D$.

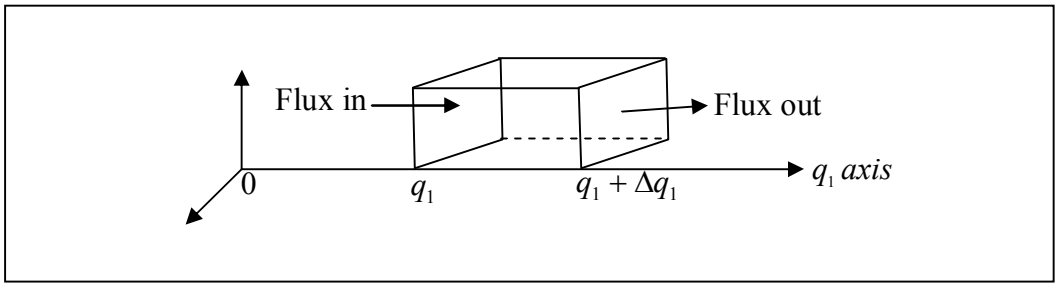

Figure 2.7. The particle fluxes entering and leaving the incremental volume

The number of particles that enters the incremental volume per unit time is $\rho_p \dot{q}_1 \Delta q_2 ... \Delta q_D \Delta p_1 \Delta p_2 ... \Delta p_D$. By using Taylor series expansion, the number of particles leaving the face at $q_1 + \Delta q_1$ (by neglecting other terms) is

$$\left[\left(\rho_p + \frac{\partial \rho_p}{\partial q_1}\Delta q_1\right) + \left(\dot{q}_1 + \frac{\partial \dot{q}_1}{\partial q_1}\Delta q_1\right)\right]\Delta q_2 \Delta q_3 ... \Delta q_D \Delta p_1 \Delta p_2 ... \Delta p_D \tag{2.57}$$

so the difference between the entering and leaving numbers is (by neglecting $\Theta(\Delta q_1^{\,2})$)

$$-\left(\rho_p \frac{\partial \dot{q}_1}{\partial q_1} + \dot{q}_1 \frac{\partial \rho_p}{\partial q_1}\right)\Delta q_1 \Delta q_2 \Delta q_3 ... \Delta q_D \Delta p_1 \Delta p_2 ... \Delta p_D . \tag{2.58}$$

The net rate of accumulation inside the incremental volume can be found by extending and adding up the result obtained in Equation 2.58 over all $2D$ coordinates and momenta so that

$$\frac{\partial(\Delta \vee)}{\partial t} = -\sum_1^D \left[\rho_P \left(\frac{\partial \dot{q}_i}{\partial q_i} + \frac{\partial \dot{p}_i}{\partial p_i}\right) + \left(\frac{\partial \rho_p}{\partial q_i}\dot{q}_i + \frac{\partial \rho_p}{\partial p_i}\dot{p}_i\right)\right]\Delta q_1 \Delta q_2 \Delta q_3 .. \Delta q_D \Delta p_1 \Delta p_2 \Delta p_3 ... \Delta p_D \tag{2.59}$$

is obtained.

It is very well known that $\dot{q}_i = \partial H / \partial p_i$ and $\dot{p}_i = \partial H / \partial q_i$, where H is the Hamiltonian operator. Then $\partial \dot{q}_i / \partial q_i = -\partial \dot{p}_i / \partial p_i$ so that $\sum_{i=1}^{D} \partial \dot{q}_i / \partial q_i + \partial \dot{p}_i / \partial p_i = 0$ and if the density is given as $\rho_p = \Delta \forall / \Delta p_1 \Delta p_2 ... \Delta p_D$ then by dividing Equation 2.59 by $\Delta q_1 \Delta q_2 \Delta q_3 ... \Delta q_D \Delta p_1 \Delta p_2 \Delta p_3 ... \Delta p_D$ one can obtain

$$\frac{\partial(\rho_p)}{\partial t} = -\sum_1^D \left[\left(\frac{\partial \rho_p}{\partial q_i}\dot{q}_i + \frac{\partial \rho_p}{\partial p_i}\dot{p}_i\right)\right] \tag{2.60}$$

and eventually Liouville equations is obtained as

$$\frac{\partial(\rho_p)}{\partial t} = -\sum_{1}^{D}\left[\left(\frac{\partial \rho_p}{\partial q_i}\frac{\partial H}{\partial p_i} - \frac{\partial \rho_p}{\partial p_i}\frac{\partial H}{\partial q_i}\right)\right] = -[\rho, H]. \tag{2.61}$$

In terms of total derivative the same Liouville equations will be written as:

$$\frac{D\rho_p}{Dt} = \frac{\partial \rho_p}{\partial t} + [\rho, H] = 0\,. \tag{2.62}$$

Equation 2.62 is the expression for conservation of phase space points. This equation states that the density of representative points in phase space corresponding to the motion of the system of particles remains constant during the motion. It means that ρ_p is conserved. The complete rate of change with time, considering the explicit and implicit variations at a given point in phase space of a density function ρ_p for an ensemble of systems is given by an expression involving the explicit rate of change with time and additional function of the coordinates and momenta.

If N_s is the total number of systems which is expressed as $N_D = \int \rho_p(p,q,t)d\vee$, ρ_p / N_D is the probability that a system of particles will be in a region of phase space.

Let us assume that the distribution function is given as follows:

$$f_N = f_n[(q_1 q_2 \ldots q_s p_1 p_2 \ldots p_D)_1 (q_1 q_2 \ldots q_s p_1 p_2 \ldots p_D)_2 (q_1 q_2 \ldots q_s p_1 p_2 \ldots p_D)_3 \ldots]. \tag{2.63}$$

This expression gives the number of particles per unit volume of phase space. If f is a single particle distribution,

$$\frac{Df}{Dt} = \frac{\partial f}{\partial t} + [f, H_1] = 0 \tag{2.64}$$

where H_1 is the Hamiltonian of a single system. This equation is known as Vlasov equation or collisionless Boltzmann equation. This result states that there is no interaction among the particles. However, the Boltzmann equation which includes collisions is given as

$$\frac{Df}{Dt} = \left(\frac{\delta f}{\delta t}\right)_{collisions}. \tag{2.65}$$

Because of the fact that most space plasmas are collisonless, the right hand side of the Equation 2.65 is neglected and 'Vlasov equation' is obtained. Vlasov equation conserves particles which means that time rate of change of the total number of particles is zero [3].

By considering the collection of charged particles of one species the evolution of the particle distribution function can be expressed as :

$$\frac{Df}{Dt} = \frac{\partial f}{\partial t} + \frac{\partial f}{\partial x}\frac{\partial x}{\partial t} + \frac{\partial f}{\partial y}\frac{\partial y}{\partial t} + \frac{\partial f}{\partial z}\frac{\partial z}{\partial t} + \frac{\partial f}{\partial v_x}\frac{\partial v_x}{\partial t} + \frac{\partial f}{\partial v_y}\frac{\partial v_y}{\partial t} + \frac{\partial f}{\partial v_z}\frac{\partial v_z}{\partial t} = 0 \tag{2.66}$$

where $\partial f/\partial t$ is the explicit dependence on time and, for example, $\partial x/\partial t = v_x$, $\partial v_x/\partial t = F_x/m$. Then Equation 2.66 becomes

$$\frac{\partial f}{\partial t} + \frac{\partial f}{\partial x}v_x + \frac{\partial f}{\partial y}v_y + \frac{\partial f}{\partial z}v_z + \frac{\partial f}{\partial v_x}\frac{F_x}{m} + \frac{\partial f}{\partial v_y}\frac{F_y}{m} + \frac{\partial f}{\partial v_z}\frac{F_z}{m} = 0 \tag{2.67}$$

if one takes the following gradients into consideration

$$\vec{\nabla}_r = \frac{\partial}{\partial x}\hat{i} + \frac{\partial}{\partial y}\hat{j} + \frac{\partial}{\partial z}\hat{k} = \frac{\partial}{\partial \vec{r}}$$

$$\vec{\nabla}_v = \frac{\partial}{\partial v_x}\hat{i} + \frac{\partial}{\partial v_y}\hat{j} + \frac{\partial}{\partial v_z}\hat{k} = \frac{\partial}{\partial \vec{v}}$$

the Vlasov equation is obtained

$$\frac{Df}{Dt} = \frac{\partial f}{\partial t} + \vec{v}.\vec{\nabla}_r f + \frac{\vec{F}}{m}.\vec{\nabla}_v f = 0 . \tag{2.68}$$

If collisions exist, i.e., $Df/Dt \neq 0$ then

$$\frac{Df}{Dt} = \left(\frac{\delta f}{\delta t}\right)_{collisions} \tag{2.69}$$

Boltzmann equation is obtained.

It is important to note that if the force which is acting on plasma particles is given as:

$$\vec{F} = q(\vec{E} + \vec{v} \times \vec{B}) + m\vec{g} \tag{2.70}$$

where $\vec{E}$ is the electric field, $\vec{B}$ is the magnetic field, $\vec{g}$ is gravitational acceleration then Vlasov equation given in Equation 2.68 will have the form

$$\frac{Df}{Dt} = \frac{\partial f}{\partial t} + \vec{v}.\vec{\nabla}_r f + \frac{q}{m}\left[(\vec{E} + \vec{v} \times \vec{B}) + m\vec{g}\right]\vec{\nabla}_v f = 0 . \tag{2.71}$$

The macroscopic equations of plasma are transport equations which describe the flow of mass, momentum and energy. The transport phenomena are frequently used to identify plasma properties associated with collisional effects. Electrical conductivity, thermal conductivity and some other physical properties are associated with transport phenomena. There are two aspects for the problem in plasma transport phenomenon which are statistical and macroscopical approaches.

Mass, momentum and energy conservations are very important physical principles which can be derived from the transport equations.

Assume that the distribution function, $f(\vec{r},\vec{v},t)$ for single particle species which are identical but indistinguishable, satisfies the Boltzmann equation. An arbitrary function $\Psi(\vec{r},\vec{v},t)$ is also defined to give the arbitrary properties such as mass, momentum, energy, etc. of the particles. The Boltzmann equation is given as:

$$\frac{\partial f}{\partial t} + \vec{v}.\vec{\nabla}_r f + \vec{a}.\vec{\nabla}_v f = \left(\frac{\delta f}{\delta t}\right)_{collisions}. \tag{2.72}$$

Multiplying Boltzmann equation by $\Psi(\vec{r},\vec{v},t)$ and integrate over velocity space one gets:

$$\underbrace{\int \Psi \frac{\partial f}{\partial t} d^3v}_{(I)} + \underbrace{\int \Psi \vec{v}.\vec{\nabla}_r f d^3v}_{(II)} + \underbrace{\int \Psi \vec{a}.\vec{\nabla}_v f d^3v}_{(III)} = \underbrace{\int \Psi \left(\frac{\delta f}{\delta t}\right) d^3v}_{(IV)}. \tag{2.73}$$

Each term can be studied separately. Let us start from terms number (IV) and (I).

$$(IV) = \int \Psi \left(\frac{\delta f}{\delta t}\right) d^3v = n(\vec{r},t)\langle \delta\Psi \rangle \tag{2.74}$$

$$(I) = \int \Psi \frac{\partial f}{\partial t} d^3v = \frac{d}{dt}\int (\Psi f) d^3v - \int \frac{d\Psi}{dt} f d^3v = \frac{\partial}{\partial t}(n\langle \Psi \rangle) - n\left\langle \frac{\partial \Psi}{\partial t} \right\rangle. \tag{2.75}$$

Note that the following is used in these modifications: $\int f(\vec{r},\vec{v},t)d^3v = n$ and $\int \Psi f(\vec{r},\vec{v},t)d^3v = n\langle \Psi \rangle$. Term (II) can be written as

$$(II) = \int \Psi \vec{v}.\vec{\nabla}_r f d^3v = \vec{\nabla}_r . \int \Psi \vec{v} f d^3v - n\left\langle \vec{\nabla}_r \Psi \vec{v} \right\rangle \tag{2.76}$$

The gradient term in Equation 2.76 can be written as

$$\vec{v}.\vec{\nabla}_r f = v_x \frac{\partial f}{\partial x} + v_y \frac{\partial f}{\partial y} + v_z \frac{\partial f}{\partial z}$$

$$\int \Psi v_x \frac{\partial f}{\partial x} d^3v = \frac{\partial}{\partial x}\int \Psi v_x f d^3v - \int \frac{\partial \Psi}{\partial x} v_x f d^3v - \int \frac{\partial v_x}{\partial x} \Psi f d^3v$$

The last term vanishes since v_x is independent of x and its derivative is 0. Since

$$\int \Psi v_x \frac{\partial f}{\partial x} d^3v = \frac{\partial}{\partial x}\left[n\left(\Psi v_x\right)\right] - n\left\langle \frac{\partial \Psi}{\partial x} v_x \right\rangle \tag{2.77}$$

and similarly for v_y and v_z

$$\int \Psi v_y \frac{\partial f}{\partial y} d^3v = \frac{\partial}{\partial y}\left[n\left(\Psi v_y\right)\right] - n\left\langle \frac{\partial \Psi}{\partial y} v_y \right\rangle \tag{2.78}$$

$$\int \Psi v_z \frac{\partial f}{\partial z} d^3v = \frac{\partial}{\partial z}\left[n\left(\Psi v_z\right)\right] - n\left\langle \frac{\partial \Psi}{\partial z} v_z \right\rangle \tag{2.79}$$

are obtained. The gradient term can be written as

$$\int \Psi \vec{v}.\vec{\nabla}_r f d^3v = \int \Psi \left(v_x \frac{\partial f}{\partial x} + v_y \frac{\partial f}{\partial y} + v_z \frac{\partial f}{\partial z} \right) d^3v$$

$$= \frac{\partial}{\partial x}\left[n\left(\Psi v_x\right)\right] - n\left\langle \frac{\partial \Psi}{\partial x} v_x \right\rangle + \frac{\partial}{\partial y}\left[n\left(\Psi v_y\right)\right] - n\left\langle \frac{\partial \Psi}{\partial y} v_y \right\rangle + \frac{\partial}{\partial z}\left[n\left(\Psi v_z\right)\right] - n\left\langle \frac{\partial \Psi}{\partial z} v_z \right\rangle \tag{2.80}$$

or

$$\int \Psi \vec{v}.\vec{\nabla}_r f d^3v = \frac{\partial}{\partial x}\int \Psi v_x d^3v + \frac{\partial}{\partial y}\int \Psi v_y d^3v + \frac{\partial}{\partial z}\int \Psi v_z d^3v - n\left\langle \frac{\partial \Psi}{\partial x} v_x + \frac{\partial \Psi}{\partial y} v_y + \frac{\partial \Psi}{\partial z} v_z \right\rangle \tag{2.81}$$

then

$$\int \Psi \vec{v}.\vec{\nabla}_r f d^3v = \vec{\nabla}_r . \int \Psi \vec{v} f d^3v - n\left\langle \vec{\nabla}_r \Psi . \vec{v} \right\rangle \tag{2.82}$$

is found. Term *(III)* in Equation 2.73 becomes

$$(III) = \vec{a}.\vec{\nabla}_v f = a_x \frac{\partial f}{\partial v_x} + a_y \frac{\partial f}{\partial v_y} + a_z \frac{\partial f}{\partial v_z} \tag{2.83}$$

then

$$\int \Psi \vec{a}.\vec{\nabla}_v f d^3v = \int \Psi \left(a_x \frac{\partial f}{\partial v_x} + a_y \frac{\partial f}{\partial v_y} + a_z \frac{\partial f}{\partial v_z} \right) d^3v \tag{2.84}$$

$$\int_{-\infty}^{\infty} \Psi a_x \frac{\partial f}{\partial v_x} dv_x = \int_{-\infty}^{\infty} \frac{\partial}{\partial v_x} \left[\Psi a_x f \right] dv_x - \int_{-\infty}^{\infty} f \frac{\partial}{\partial v_x} (\Psi a_x) dv_x \tag{2.85}$$

can be written.

In that case the first term on the right hand side of Equation 2.84 becomes

$$\int \Psi a_x \frac{\partial f}{\partial v_x} d^3v = -\int f \frac{\partial}{\partial v_x} (\Psi a_x) d^3v = -n \left\langle \frac{\partial}{\partial v_x} (\Psi a_x) \right\rangle = -n \left\langle \Psi \frac{\partial a_x}{\partial v_x} + a_x \frac{\partial \Psi}{\partial v_x} \right\rangle \tag{2.86}$$

The acceleration is given from Lorentz force as : $\vec{a} = q\left[\vec{E} + \vec{v} \times \vec{B}\right] / m$ then a

$$a_x = \frac{q}{m} \left[E_x + \left(B_z v_y - B_y v_z \right) \right] \tag{2.87}$$

$$a_y = \frac{q}{m} \left[E_y + \left(B_x v_z - B_z v_x \right) \right] \tag{2.88}$$

$$a_z = \frac{q}{m} \left[E_z + \left(B_y v_x - B_x v_y \right) \right] \tag{2.89}$$

$\vec{E}$ is an electric field and it does not depend on v_x, v_y, v_z so $\partial E/\partial v_x = 0$, $\partial E/\partial v_y = 0$ and $\partial E/\partial v_z = 0$. One gets

$$\int \Psi a_x \frac{\partial f}{\partial v_x} d^3v = -n\left\langle a_x \frac{\partial \Psi}{\partial v_x} \right\rangle \tag{2.90}$$

$$\int \Psi a_y \frac{\partial f}{\partial v_y} d^3v = -n\left\langle a_y \frac{\partial \Psi}{\partial v_y} \right\rangle \tag{2.91}$$

$$\int \Psi a_z \frac{\partial f}{\partial v_z} d^3v = -n\left\langle a_z \frac{\partial \Psi}{\partial v_z} \right\rangle. \tag{2.92}$$

Finally the term (III) in Equation 2.73 is obtained as:

$$(III) = \int \Psi \vec{a}.\vec{\nabla}_v f d^3v = -n\left\langle \vec{a}\vec{\nabla}_v \Psi \right\rangle. \tag{2.93}$$

After all the terms of Equation 2.73 are derived and this equation becomes:

$$n(\vec{r},t)\langle \delta\Psi \rangle = \frac{\partial}{\partial t}(n\langle \Psi \rangle) - n\left\langle \frac{\partial \Psi}{\partial t} \right\rangle + \vec{\nabla}_r\left(n\langle \Psi\vec{v} \rangle\right) - n\left\langle \vec{\nabla}_r \Psi\vec{v} \right\rangle - n\left\langle \vec{a}\vec{\nabla}_v \Psi \right\rangle. \tag{2.94}$$

However, if Equation 2.94 is rearranged one gets the moment equation:

$$\frac{\partial}{\partial t}(n\langle \Psi \rangle) - n\left[\left\langle \frac{\partial \Psi}{\partial t} \right\rangle + \left\langle \vec{\nabla}_r \Psi\vec{v} \right\rangle + \left\langle \vec{a}\vec{\nabla}_v \Psi \right\rangle + \langle \delta\Psi \rangle\right] + \vec{\nabla}_r\left(n\langle \Psi\vec{v} \rangle\right) = 0. \tag{2.95}$$

Although the microscopic distribution depends on $\vec{r}$, $\vec{v}$ and t i.e., $f(\vec{r},\vec{v},t)$ the macroscopic physical parameters depend on only $\vec{r}$ and t. Therefore they are obtained by integration over the entire velocity space so-called moments. Let us look at the moments and their results.

Since $\Psi \propto v^p$ then there will be three different cases given as below.

Case 1: $p_m = 0$ this is the 0^{th} moment of equation and it gives the conservation of mass,

Case 2: $p_m = 1$ this is the 1^{st} moment of equation gives the conservation of momentum,

Case 3: $p_m = 2$ this is the 2^{nd} moment of equation gives the conservation of energy.

2.3.1. The 0^{th} Moment ($p_m = 0$, $\Psi = 1$)

If $\Psi = 1$ is used into Equation 2.95

$$\frac{\partial}{\partial t}(n\langle 1\rangle) - n\left[\left\langle\frac{\partial 1}{\partial t}\right\rangle + \left\langle\vec{\nabla}_r 1\vec{v}\right\rangle + \left\langle\vec{a}.\vec{\nabla}_v 1\right\rangle + \langle\delta 1\rangle\right] + \vec{\nabla}_r\left(n\langle 1\vec{v}\rangle\right) = 0 \tag{2.96}$$

is found. Since $\langle 1\rangle = 1$, $\partial 1/\partial t = 0$ and $\vec{\nabla}_v 1 = 0$

$$\frac{\partial n}{\partial t} + \vec{\nabla}_r\left(\langle n\vec{v}\rangle\right) = n\left[\langle\delta\rangle\right] \tag{2.97}$$

is obtained.

The term $n\left[\langle\delta\rangle\right]$ is described as the rate at which particles are lost or gained due to the inelastic collisions in volume element d^3r. Elastic collisions do not involve a particle loss or gain in volume element d^3r, rather a loss or gain in velocity space. The particle loss or gain depends on the ionization, electron-ion recombination, electron attachment processes.

2.3.1.1. Ionization

The expression for a single ionization process can be given as : $e^- + A \rightarrow A^+ + 2e^-$. Here the ionization frequency ν_i, depends on the temperature of electrons and ions $\nu_i = \nu_i(T_e, T_i)$ where T_i and T_e are ion and electron temperatures respectively. Ionization serves as a gain term and $\nu_i n_i$ is the number of ions produced per second and per unit volume while $\nu_e n_e$ is the number of electrons produced per second and per unit volume.

2.3.1.2. Electron-Ion Recombintion

The term from the electron-ion recombination is a loss term. The expression for this process is $e^- + A^+ \rightarrow A + h\nu$ where h is the Planck's constant and ν is frequency. The rate of this process is directly proportional to number of electrons and ions. Mathematically it can be written as $Rate \propto n_e n_i$ where $n_e \cong n_i$ and it means that $Rate \propto n_e^2$. Then formally the rate is given as $Rate = \alpha_R n_e^2$ where α_R is a recombination coefficient.

2.3.1.3. Electron Attachment

Since the expression for this process is $e^- + A \rightarrow A^-$. The rate for electron-ion recombination $Rate \propto n_N n_i$ where subscript N is the number of neutrals in the system. This process can also be expressed as $Rate = \nu_A n_e$ where ν_A is the attachment frequency. Using these processes, Equation 2.97 can be written as:

$$\frac{dn_e}{dt} + \vec{\nabla}_r\left(\langle n_e \vec{v}_e \rangle\right) = n_e(\nu_i - \nu_A) - \alpha_R n_e^2 \tag{2.98}$$

where dn_e/dt is time rate of change of the density of electrons in a small volume. $\vec{\nabla}_r\left(\langle n_e \vec{v}_e \rangle\right)$ is the term representing the flow in or out of the particles of a small volume and the right hand side represents the generation or loss of electrons in a small volume due to the elastic collisions in the system. If there is no loss and generation of particles in the volume considered the equation is simplified as:

$$\frac{dn_e}{dt} + \vec{\nabla}_r \left(\langle n_e \vec{v}_e \rangle \right) = 0 \tag{2.99}$$

which is nothing but the same form for conservation of mass in fluid dynamics.

2.3.2. The 1st Moment ($p_m = 1$, $\Psi = m\vec{v}$)

This moment will give us the momentum transfer equation in fluid dynamics. The main expression which is Equation 2.95 now will have a different form given as:

$$\frac{\partial}{\partial t}(n\langle m\vec{v}\rangle) - n\left[\left\langle \frac{\partial(m\vec{v})}{\partial t}\right\rangle + \left\langle \vec{\nabla}_r.(m\vec{v}\vec{v})\right\rangle + \left\langle \vec{a}.\vec{\nabla}_v(m\vec{v})\right\rangle + \left\langle \delta(m\vec{v})\right\rangle\right] + \vec{\nabla}_r.\left(n\langle m\vec{v}\vec{v}\rangle\right) = 0 \tag{2.100}$$

Here $\vec{v}$ is assumed to be the particle velocity in laboratory frame (instantaneous velocity) and it is given by

$$\vec{v} = \langle \vec{v} \rangle + Random\ \ Velocity \tag{2.101}$$

where $\langle \vec{v} \rangle = \vec{u}(\vec{r},t)$ defined as average velocity. If $\vec{w}_r$ is defined as peculiar velocity or random velocity

$$\vec{w}_r = \vec{v} - \langle \vec{v} \rangle = \vec{v} - \vec{u} \tag{2.102}$$

Random average velocity $= 0$. One can show this as follows:

$$\langle \vec{w}_r \rangle = \frac{1}{n}\int (\vec{v} - \langle \vec{v} \rangle) f(\vec{r},\vec{v},t) d^3v = \frac{1}{n}\left[\int \vec{v} f(\vec{r},\vec{v},t) d^3v - \int \langle \vec{v} \rangle f(\vec{r},\vec{v},t) d^3v\right] = \langle \vec{v} \rangle - \langle \vec{v} \rangle = 0 . \tag{2.103}$$

It is important to note that the thermal energy of the system kT is proportional to scalar pressure, $P = nkT$. By using the definition for velocity given above the third term in Equation 2.100 can be expressed as :

$$\left\langle \vec{\nabla}_r .(m\vec{v}\vec{v}) \right\rangle = \vec{\nabla}_r .\langle m\vec{u}\vec{u} \rangle + \vec{\nabla}_r \langle m\vec{w}_r \vec{w}_r \rangle + 2\vec{\nabla}_r \langle m\vec{u}\vec{w}_r \rangle \tag{2.104}$$

by relating the velocity in laboratory frame to the random and average velocities. Random energy $m\vec{w}_r \vec{w}_r$ is related to kT and $nm\langle \vec{w}_r \vec{w}_r \rangle \equiv \tilde{P}$ where $\tilde{P}$ is the pressure tensor.

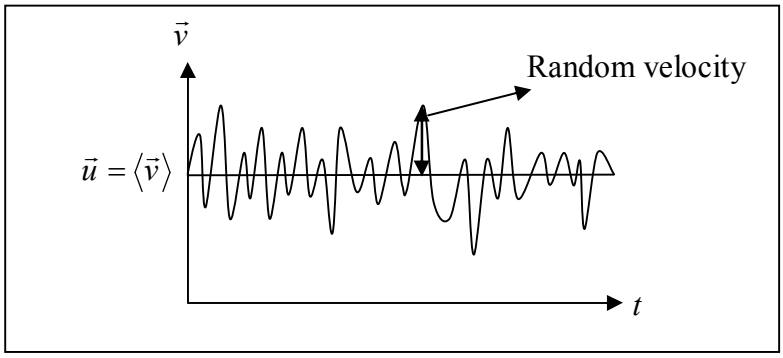

Figure 2.8. The random and the average velocity plots

The pressure tensor, $\tilde{P}$, contains a kinetic contribution and contribution from n-body interactions. Another name of the pressure tensor is stress tensor and its components specify both the direction of motion and component of momentum involved.

$$\tilde{P} = nm\langle \vec{w}_r \vec{w}_r \rangle = \begin{pmatrix} P_{xx} & P_{xy} & P_{xz} \\ P_{yx} & P_{yy} & P_{yz} \\ P_{zx} & P_{zy} & P_{zz} \end{pmatrix} \tag{2.105}$$

where the diagonal terms

$$P_{xx} = P_{yy} = P_{zz}$$

are scalar pressures.

The off-diagonal elements in pressure tensor are related to the viscosity. Shear stress is given as: $\tau_{yx} = -\mu(\partial v_x / \partial y)$.

The divergence of the pressure tensor is a vector given by

$$\vec{\nabla}_r.\widetilde{P} = \left(\frac{\partial}{\partial x}\hat{x} + \frac{\partial}{\partial y}\hat{y} + \frac{\partial}{\partial z}\hat{z}\right).\begin{pmatrix} \hat{x}w_x w_x\hat{x} & \hat{x}w_x w_y\hat{y} & \hat{x}w_x w_z\hat{z} \\ \hat{y}w_y w_x\hat{x} & \hat{y}w_y w_y\hat{y} & \hat{y}w_y w_z\hat{z} \\ \hat{z}w_z w_x\hat{x} & \hat{z}w_z w_y\hat{y} & \hat{z}w_z w_z\hat{z} \end{pmatrix}. \tag{2.106}$$

This equation becomes

$$\begin{aligned} \vec{\nabla}_r.\widetilde{P} = &\left(\frac{\partial}{\partial x}w_x w_x\hat{x} + \frac{\partial}{\partial y}w_y w_x\hat{x} + \frac{\partial}{\partial z}w_z w_x\hat{x}\right) + \\ &\left(\frac{\partial}{\partial x}w_x w_y\hat{y} + \frac{\partial}{\partial y}w_y w_y\hat{y} + \frac{\partial}{\partial z}w_z w_y\hat{y}\right) + \\ &\left(\frac{\partial}{\partial x}w_x w_z\hat{z} + \frac{\partial}{\partial y}w_y w_z\hat{z} + \frac{\partial}{\partial z}\hat{z}w_z w_z\hat{z}\right) \end{aligned}. \tag{2.107}$$

In that case Equation 2.100 is rearranged as:

$$\frac{\partial}{\partial t}(n\langle m\vec{v}\rangle) = n\Bigg[\underbrace{\left\langle\frac{\partial(m\vec{v})}{\partial t}\right\rangle}_{(I)} + \underbrace{\left\langle\vec{\nabla}_r(m\vec{v}\vec{v})\right\rangle}_{(II)} + \left\langle\vec{a}\vec{\nabla}_v(m\vec{v})\right\rangle + \left\langle\delta(m\vec{v})\right\rangle\Bigg] - \vec{\nabla}_r\left(n\langle m\vec{v}\vec{v}\rangle\right). \tag{2.108}$$

The term *(I)* is equal to zero since $\vec{v}$ is independent from t and similarly term *(II)* is also zero because $\vec{v}$ is again independent of space variables. Then

$$\frac{\partial}{\partial t}(n\langle m\vec{v}\rangle) = n\left[\left\langle\vec{a}\vec{\nabla}_v(m\vec{v})\right\rangle + \left\langle\delta(m\vec{v})\right\rangle\right] - \vec{\nabla}_r\left(n\langle m\vec{v}\vec{v}\rangle\right) \tag{2.109}$$

is obtained. By rearranging one gets

$$\frac{\partial}{\partial t}(n\langle m\vec{v}\rangle) + \vec{\nabla}_r\left(n\langle m\vec{v}\vec{v}\rangle\right) = n\left[\left\langle\vec{F}\right\rangle + \left\langle\delta(m\vec{v})\right\rangle\right]. \tag{2.110}$$

Note that since $\langle\vec{v}\rangle = (1/n)\int \vec{v} f d^3v = \vec{u}(\vec{r},t)$ then $\partial\langle\vec{v}\rangle/\partial v = 0$, so that 1st term on the right hand side of Equation 2.109 vanishes.

By using no source continuity equation (i. e., $\partial n/\partial t + \vec{\nabla}.(n\vec{v}) = 0$ one can write

$$\frac{\partial}{\partial t} nm\langle\vec{v}\rangle = mn\frac{\partial}{\partial t}\langle\vec{v}\rangle\left(\vec{\nabla}_r\langle n\langle\vec{v}\rangle\rangle\right). \tag{2.111}$$

Using this Equation 2.100 can be written as:

$$mn\frac{\partial\langle\vec{v}\rangle}{\partial t} - m\langle\vec{v}\rangle\left(\vec{\nabla}_r\langle n\langle\vec{v}\rangle\rangle\right) = n\left[\langle\vec{F}\rangle + \langle\delta(m\vec{v})\rangle\right] - \vec{\nabla}_r\left(nm\langle\vec{v}\vec{v}\rangle\right). \tag{2.112}$$

The last term in Equation 2.112 can be studied separately as:

$$-\vec{\nabla}_r\left(nm\langle\vec{v}\vec{v}\rangle\right) = -\vec{\nabla}_r\underbrace{\left[nm\left(\vec{w}_r + \langle\vec{v}\rangle\right)\left(\vec{w}_r + \langle\vec{v}\rangle\right)\right]}_{(I)} \tag{2.113}$$

and the term (I) can be written in a different form as

$$(I) = (\vec{w}_r\vec{w}_r) + \langle\langle\vec{v}\rangle\langle\vec{v}\rangle\rangle + \langle\langle\vec{v}\rangle\vec{w}_r\rangle + \langle\vec{w}_r\langle\vec{v}\rangle\rangle$$

where the last two terms are zero. Now let us put these results in Equation 2.113 to get

$$-\vec{\nabla}_r\left[nm\left((\vec{w}_r\vec{w}_r) + \langle\vec{v}\rangle\langle\vec{v}\rangle\right)\right] = -\vec{\nabla}_r\tilde{P} - \left(nm\langle\vec{v}\rangle\vec{\nabla}_r\right)\langle\vec{v}\rangle - \langle\vec{v}\rangle\left(\vec{\nabla}_r nm\langle\vec{v}\rangle\right).$$

Using this expression in Equation 2.112

$$mn\frac{\partial\langle\vec{v}\rangle}{\partial t} - m\langle\vec{v}\rangle\left(\vec{\nabla}_r\langle n\langle\vec{v}\rangle\rangle\right) = n\left[\langle\vec{F}\rangle + \langle\delta(m\vec{v})\rangle\right] - \vec{\nabla}_r\tilde{P} - \left(nm\langle\vec{v}\rangle\vec{\nabla}_r\right)\langle\vec{v}\rangle - \langle\vec{v}\rangle\left(\vec{\nabla}_r nm\langle\vec{v}\rangle\right) \tag{2.114}$$

is obtained and after cancellation is done for the second term on the left hand side and the last term on right hand side the simplified form is found to be:

$$mn\frac{\partial \vec{u}}{\partial t} + nm\left(\vec{u}\vec{\nabla}_r\right) = n\left[\left\langle \vec{F}\right\rangle + \left\langle \delta(m\vec{v})\right\rangle\right] - \vec{\nabla}_r \tilde{P} \tag{2.115}$$

where $\vec{u}(\vec{r},t) = \langle \vec{v}(\vec{r},t)\rangle$ is the average velocity. Equation 2.115 is the momentum conservation equation.

Now the last moment of Vlasov equation will be studied in the same manner.

2.3.3. The 2nd Moment($p_m = 2$, $\Psi = mv^2/2$)

If $\Psi = mv^2/2$ is inserted into Equation 2.95 one gets

$$\frac{\partial}{\partial t}(n\langle\Psi\rangle) - n\left[\left\langle\frac{\partial\Psi}{\partial t}\right\rangle + \left\langle\vec{\nabla}_r\Psi\vec{v}\right\rangle + \left\langle\vec{a}\vec{\nabla}_v\Psi\right\rangle\right] + \vec{\nabla}_r\left(n\langle\Psi\vec{v}\rangle\right) = 0 \tag{2.116}$$

then the equation will have the form given as: (using $v^2 = \vec{v}.\vec{v}$)

$$\underbrace{\frac{\partial}{\partial t}(n\left\langle\frac{1}{2}mv^2\right\rangle)}_{(I)} + n\left[\left\langle\frac{\partial(mv^2/2)}{\partial t}\right\rangle + \left\langle\vec{\nabla}_r\left(\frac{1}{2}mv^2\right)\right\rangle + \left\langle\vec{a}\vec{\nabla}_v\left(\frac{1}{2}mv^2\right)\right\rangle\right] + \underbrace{\vec{\nabla}_r\left(n\left\langle\left(\frac{1}{2}mv^2\right)\vec{v}\right\rangle\right)}_{(II)} = 0 \tag{2.117}$$

Again the terms will be studied separately. Let us start from term (I). Here v, r *and* t are independent variables and mass m is assumed to be constant and $\langle v\rangle = u$. Then

$$\frac{nm}{2}\langle\vec{v}.\vec{v}\rangle = \frac{nm}{2}\langle(\vec{u}+\vec{w}_r).(\vec{u}+\vec{w}_r)\rangle$$

$$\frac{nm}{2}\left(\langle \vec{w}_r.\vec{w}_r \rangle + \langle \vec{u}.\vec{u} \rangle + \langle \vec{w}_r.\vec{u} \rangle + \langle \vec{u}.\vec{w}_r \rangle\right) \tag{2.118}$$

is found. It must be remembered that the last two terms are equal to zero. The term $nm\langle \vec{w}_r.\vec{w}_r \rangle$ gives the scalar pressure

$$nm\left\langle w_x^2 + w_y^2 + w_z^2 \right\rangle = P_x + P_y + P_z = 3P \tag{2.119}$$

so

$$n\left\langle \frac{1}{2}mv^2 \right\rangle = nm\frac{u^2}{2} + \frac{3}{2}P \tag{2.120}$$

is obtained. The first term on the right hand side is directed energy and the second term is the thermal energy.

Let us analyze term *(II)*. Notice that

$$\left\langle v^2\vec{v} \right\rangle = \left\langle (\vec{u} + \vec{w}_r)(\vec{u} + \vec{w}_r)(\vec{u} + \vec{w}_r) \right\rangle =$$

$$\left\langle w_r^2\vec{w}_r + w_r^2\vec{u} + u^2\vec{w}_r + u^2\vec{u} + 2(\vec{w}_r.\vec{u})\vec{w}_r + 2(\vec{w}_r.\vec{u})\vec{u} \right\rangle . \tag{2.121}$$

In Equation 2.121 $\langle u^2\vec{w}_r \rangle = 0$ and $\langle 2(\vec{w}_r\vec{u})\vec{u} \rangle = 0$ since $\langle \vec{w}_r \rangle = 0$. The term $2(\vec{w}_r.\vec{u})\vec{w}_r$ can be written as $\tilde{P}\vec{u}$. Here it is just the time to define a heat flux term which is the flux of random (thermal) energy across a surface element moving with mean velocity u.

$$\vec{q}_h = \left\langle \frac{1}{2}nw_r^2\vec{w}_r \right\rangle \tag{2.122}$$

So that Equation 2.120 will have the form such as given in Equation 2.123 below.

$$\frac{\partial}{\partial t}\left(nm\frac{u^2}{2}+\frac{3}{2}P \right)+n\left\langle \vec{a}.\vec{\nabla}_v\left(\frac{1}{2}mv^2 \right) \right\rangle+\vec{\nabla}_r.\left(\vec{q}_h+\frac{3}{2}P\vec{u}+\frac{nmu^2\vec{u}}{2}+\tilde{P}\vec{u} \right)=0\,. \quad (2.123)$$

Since $d/dv\left(mv^2/2\right)=mv$ and energy ε^* is defined as:

$$\varepsilon^*=nm\frac{u^2}{2}+\frac{3}{2}P\,.$$

So Equation 2.123 becomes as:

$$\frac{\partial\varepsilon^*}{\partial t}+n\left\langle \vec{a}\left(mv\right) \right\rangle+\vec{\nabla}_r\left(\varepsilon^*\vec{u}\right)+\vec{\nabla}_r\vec{q}_h+\vec{\nabla}_r\left(\tilde{P}\vec{u}\right)=0\,. \quad (2.124)$$

Using the Lorentz force, then the acceleration will have the form as given in Equation 2.125.

$$\vec{a}=\frac{q}{m}\left(\vec{E}+\vec{v}\times\vec{B}\right) \quad (2.125)$$

Let us change the velocity in Equation 2.125 by $\left(\vec{w}_r+\vec{u}\right)$ to get

$$\vec{a}=\frac{q}{m}\left[\vec{E}+\left(\vec{w}_r+\vec{u}\right)\times\vec{B}\right]\,. \quad (2.126)$$

Then the second term on the right hand side of Equation 2.126 can be written as

$$n\left\langle \vec{a}\left(mv\right) \right\rangle=nm\left\langle \left[\frac{q}{m}\left[\vec{E}+\left(\vec{w}_r+\vec{u}\right)\times\vec{B}\right]\right]\left(\vec{w}_r+\vec{u}\right) \right\rangle \quad (2.127)$$

so that

$$n\left\langle \vec{a}\left(mv\right) \right\rangle=nm\left\langle \frac{q}{m}\left[\vec{E}\vec{u}+\left(\vec{u}\times\vec{B}\right)\vec{u}\right] \right\rangle \quad (2.128)$$

is obtained. If the electric field in a moving reference frame, E^*, is given as :

$$E^* = \vec{E} + \left(\vec{u} \times \vec{B}\right) \tag{2.129}$$

and by using the definition for total derivative given by

$$\frac{d}{dt} = \frac{\partial}{\partial t} + \vec{v}.\vec{\nabla}_r \tag{2.130}$$

one gets

$$\frac{d\varepsilon^*}{dt} + \varepsilon^* \vec{\nabla}_r \vec{u} + \vec{\nabla}_r \vec{q}_h + \vec{\nabla}_r \left(\tilde{P}\vec{u}\right) = \vec{J}.\vec{E}^* \tag{2.131}$$

where $\vec{J}$ is the average current density given as $\vec{J} = nq\vec{u}$.

In Equation 2.131 the first term on the left hand side is the total rate of change of thermal energy of the gas in a volume element moving with mean velocity, the second term is the energy carried into (or out to) the moving volume element by thermal flow of atoms, the third term is the change of energy due to the heat flow, fourth term is the work done in the moving element (control volume) by the pressures on its surface. The term on the right hand side of equation is called Joule heating term.

- If some definition such as:
- Mass density $\rho_m = n_e m_e + n_i m_i$
- Particle current density $\vec{J}_p = n_e \langle \vec{v}_e \rangle + n_i \langle \vec{v}_i \rangle$
- Mass current density $\vec{J}_m = n_e m_e \langle \vec{v}_e \rangle + n_i m_i \langle \vec{v}_i \rangle$
- Electric charge density $\rho_E = n_e q_e + n_i q_i$
- Electric current density $\vec{J}_E = n_e q_e \langle \vec{v}_e \rangle + n_i q_i \langle \vec{v}_i \rangle$ are assumed and heat flux term is assumed to be $\vec{q}_k = 0$ together with $\vec{J}.\vec{E}^* = 0$.

Then the centre of mass velocity of the system is taken $\vec{v}$ and new peculiar velocity $\left\langle w_e^* \right\rangle \neq 0$ and $\left\langle w_i^* \right\rangle \neq 0$ but $n_e m_e \left\langle w_i^* \right\rangle + n_i m_i \left\langle w_e^* \right\rangle \neq 0$ are assumed. As an addition to the above assumptions $\widetilde{P}_e = n_e m_e \left\langle w_e^* w_e^* \right\rangle$ and $\vec{v}_e = w_e^* - \vec{v}$, $\vec{v}_i = w_i^* - \vec{v}$ are taken into account one gets momentum equation in the form given as:

$$\rho_m \frac{d\vec{v}}{dt} = -\vec{\nabla}.\widetilde{P} + \vec{J} \times \vec{B} + \rho_e \vec{E} \quad . \tag{2.132}$$

Here the momentum equation was obtained by using some assumptions described above. This is a relatively different derivation of momentum equation which is one the most important equations which were used in this thesis. During the theoretical study given in this chapter especially references [1-3] were used intensively.

3. FLUIDS AND FLUID PROPERTIES

The matter can exist in three different states which are solid, liquid and gas. The liquid and gas states together form the fluids. Typically gases are considered as compressible fluids and liquids as noncompressible, that means they have fixed volumes under the conditions of constant temperature and pressure. Actually a fluid is a continuum material which can not resist the shear stress. Under the effect of some shear stress the fluid is deformed. The fluids are deformed continuously under the tangential (shear) stresses no matter how small the magnitude of the stres is. A solid, in contrary, deforms by the amount proportional to the stress applied, after which a static equilibrium will result. The magnitude of the shear stress depends on the magnitude of angular deformation [4].

Table 3.1. The states of matter and some properties [5]

State	Intermolecular Forces	Molecular Arrangement	Type of statistics required
Solid	Strong	Ordered	Quantum
Liquid	Medium	Partially Ordered	Quantum+Classical
Gas	Weak	Disordered	Classical

The molecules composing a fluid are free to move and past each other. The behaviours of a fluid is defined by the set of partial differential equations called Navier-Stokes Equations. A fluid is considered as a continuum material. The continuum mechanics is the science interested in continuum materials. In continuum mechanics the discrete nature of fluid is ignored and the idea which says that the materials are not composed of discrete particles is accepted. After ignoring the atomic structure of the matter the modelling for large scales, which are very much greater than the interatomic distances, is very accurate. The physical properties which enter the interested area of continuum mechanics are independent from the particular coordinate system in which they are observed. Mathematical objects called tensors which are independent from the coordinate systems are mostly used for representing these physical properties.

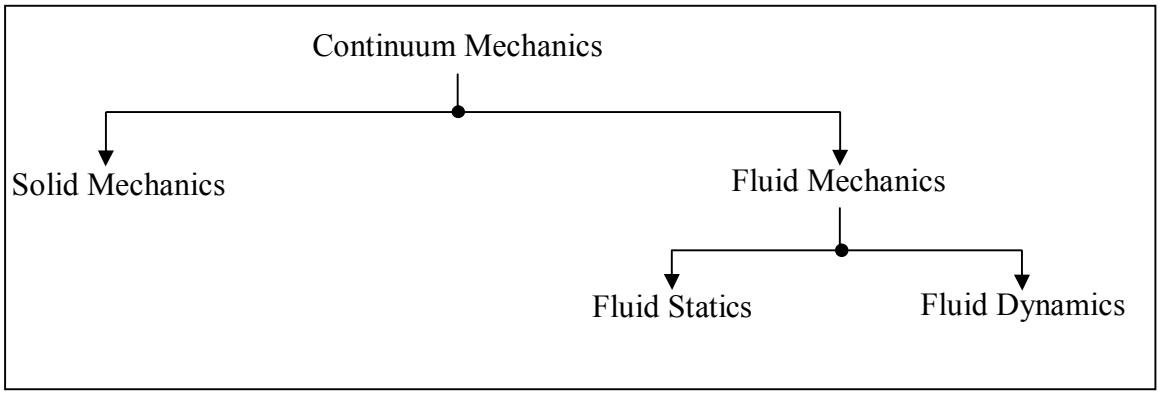

Figure 3.1. The subdivisions of continuum mechanics

Since the problems of interest of this thesis are particularly related to the fluid dynamics, the study of fluid in motion, our interest will not be focused on the motion of individual molecules, instead it would be on describing the fluid and its motion in very large spaces. These spaces are very much larger than the distances between atoms and molecules. Not only the distances but also the number of particles in the scope of interest are very large, the statistical average is very meaningful in these cases. Actually the fluid mechanics is mathematically very complex in some cases. In order to avoid from this complexity a relatively modern discipline called computational fluid dynamics is used by the scientists and engineers. Computational fluid dynamics (CFD) is the subject of the next chapter . By using the mathematical models the properties of materials are calculated by using the statistical averages which are necessary after the material is assumed as a continuum. There are approximately 2.5×10^{25} molecules in a cubic meter of air at room temperature at sea-level, which corresponds to about 2.5×10^{10} molecules in a cube which has a side of $0.01\,\text{mm}$ and the mean free path is about $6.6\times10^{-8}\,\text{m}$ [6]. As a conclusion the consideration of a fluid as a continuum is rather a highly accurate assumption.

3.1. Macroscopic Properties of Fluids

Since gas and liquid states of matter form together it is very important to classify the meaning of the word fluid. From rheological point of view fluids can be classified as liquids and gases. If the spatial dimensionality is under consideration they can be one dimenisonal, two dimensional and three dimensional. From the temporal variation point of view fluids can be divided into steady and unsteady fluids. The classifications depend on

the properties of the fluids. The most important properties of the fluids can be considered as pressure, temperature, density, velocity, viscosity etc.

3.1.1. Viscosity

One of the most important properties of the fluid is viscosity which is basically the willingness of fluid to flow. However, more scientifically the viscosity can be described as the resistance of fluid to deformation under the effect of shear stress. Since it can be thought as the resistance to flow, viscosity is related to the internal structure of the fluid under consideration. Qualitatively viscosity is a material property related to the resistance of fluid or alternatively is a measure of stresses exerted by a fluid on the surrounding media when the fluid is undergoing the deformation [7]. Since it is a scalar transport property, viscosity is related to the transport of momentum. Formally it gives the ratio of the shearing stress to the velocity gradient in the fluid. Mathematically it is given by

$$\mu = \frac{Shear\ Stress}{Shear\ Rate} \tag{3.1}$$

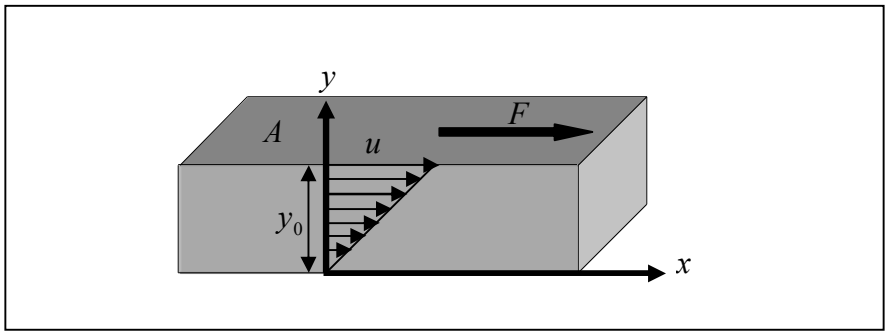

Figure 3.2. The velocity profile for the fluid element on which the force acts on the upper part

$$\mu = \frac{F/A}{u/y_0} \tag{3.2}$$

The shear stress, τ , is the stress applied tangentially to the face of material. The unit for shear stress is Pascal (Pa). Shear rate is the velocity gradient applied to the fluid and it

gives an idea about the rate at which the adjacent layers of fluids move with respect to each other. The unit for shear rate is s^{-1} $(1/second)$. The unit for viscosity is Pascal second $(Pa.s)$ or $(kg/m.s)$.

Materials are classified as Newtonian and non-Newtonian depending on their viscosity profiles. Newtonian fluids are fluids in which the shearing stress is linearly related to the rate of shearing strain (Figure 3.3).

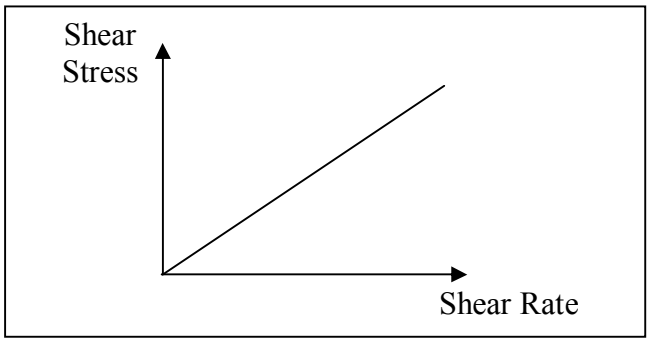

Figure 3.3. The plot of shear stress versus shear rate for Newtonian fluids

In non-Newtonian fluids the relation between shear stress and shear rate is nonlinear and can be time-dependent. Water, milk, gasoline, sugar solutions, minearal oils are examples of Newtonian fluids. The molten polymers, blood, soap, grease and paint are non-Newtonian fluids.

The viscosity of the fluids can be studied under two parts, viscosity of liquids and viscosity of gases. Especially the liquids have an enourmously wide range of values of viscosity. The temperature is the main exterior agent which affects the viscosity in liquids. The increase in temperature causes the decrease in viscosity of liquids. The temperature dependence of viscosity for many liquids is given as

$$\mu = A_l e^{B_l / T} \tag{3.3}$$

where A_l and B_l are characteristic constants for liquid and T is absolute temperature in Kelvins [7]. This shows that viscosity reduces very fast as temperature increases. The

viscosities of pure gases at low temperature and far away from the critical points can be found from so called Chapman-Enskog theory. The gas viscosity is given by

$$\mu = 2.67 \times 10^{-6} \frac{(MT)^{1/2}}{{\sigma_d}^2 \Omega_V} \tag{3.4}$$

where M is the molecular weight, T is the absolute temperature in Kelvins, σ_d is the collision diameter sometimes referred to as molecular diameter in angstroms $(1^\circ A = 10^{-10} m)$, Ω_V is collision integral. From Equation 3.3 and Equation 3.4 it is seen that the temperature dependences of liquids and gases are different. Actually when the air is considered for temperatures below $3000\ K$, the viscosity of air is independent of the pressure and for this range Sutherland's Formula can be used.

$$\mu = 1.458 \times 10^{-6} \frac{T^{3/2}}{T + 110.4} \tag{3.5}$$

Table 3.2. Temperature dependence of the viscosity calculated from Equation 3.5 for air [6]

$T(K)$	$\mu \times 10^5 (kg/m.s)$
20	1.329
40	2.285
60	3.016
80	3.624
100	4.152
120	4.625
140	5.057
160	5.456
180	5.828
200	6.179
220	6.512
240	6.829

The viscosity has two different parts: dynamic viscosity and kinematic viscosity. In the literature the word viscosity is used instead of the dynamical viscosity. When the word viscosity is used it is related to dynamical viscosity unless otherwise is specified. Because of the fact that in fluid dynamics area, the density is a mostly used property for fluids instead of mass, and the ratio μ/ρ frequently appears in the equations. This ratio has its own name called kinematic viscosity. The unit of kinematic viscosity is cm^2/s. It should also be noted that the temperatures given in Table 3.2 and Table 3.3 are Kelvins and Centigrade respectively.

Table 3.3. Temperature dependence of the kinematic viscosity for different materials [8]

Material	$T(^\circ C)$	*Kinematic Viscosity* $\left(cm^2/s\right)$
Mercury	0	0.00125
	10	0.00123
	20	0.00117
Air	0	0.133
	10	0.140
	20	0.143
Water	0	0.0178
	10	0.0130
	20	0.0101
Machine Oil	0	7.34
	20	3.82

3.1.2. Pressure

The definition of pressure simply is the force per unit area. The pressure of fluids, both liquids and gases, are due to the random motion of the particles which are atoms and molecules forming them. If the fluids are heated their pressures increase. The SI unit for pressure is N/m^2 or simply Pascal.

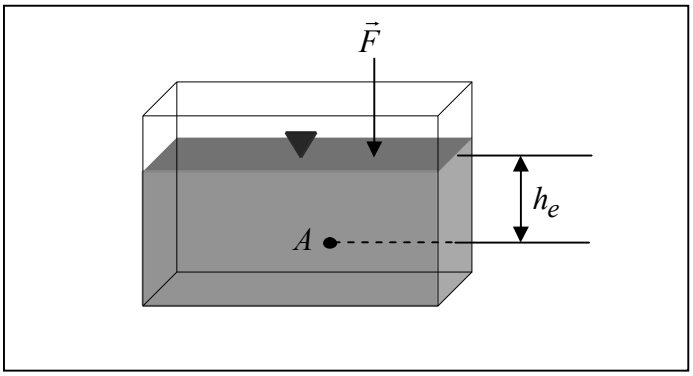

Figure 3.4. The pressure definiton for the container filled with liquid

The pressure for point A (Figure 3.4) which is located in the liquid with the density ρ is expressed as:

$$P_A = \rho g h_e + P_{atm} \tag{3.6}$$

where g is the gravitational acceleration, h_e is the vertical height measured from the surface of the liquid and P_{atm} is the atmospheric pressure. The pressure in the liquid increases in a directly proportional manner with the depth. P_{atm} is the pressure due to the weight of the column of air above any point in the Earth's atmosphere. The value for the standard atmospheric pressure is 101.325 kPa. Manometers, elastic-type pressure gauges, electric type pressure gauges are devices which are used to measure the pressure. At any cross section the pressure generates a force which can cause the fluid particles to flow. For the liquids under critical point the pressure does not affect the volume too much, as a numerical example the change of water pressure by 1000 per cent, change the volume is less than 1 per cent. However, for the gases any change in pressure directly affects the volume [9]. The pressure has two characteristics: the pressure of the fluid acts perpendicularly to the wall in contact with the fluid, the pressure applied to the fluid in the closed vessel is transmitted to all parts at the same value with the applied pressure regardless of its direction [10].

3.1.3. Density

The definition for density is the ratio between the mass and the volume of material or the mass per unit volume. For the liquids the density is a property which is assumed to be constant. It is considered to be indepenedent of the sample size. Actually the density can change as a function of time and location $\rho = \rho(x, y, z, t)$ but it must be a continuous property. As a mathematical definition it is given as:

$$\rho = \lim_{\Delta V \to \varepsilon} \frac{\Delta m}{\Delta V} \tag{3.7}$$

where Δm and ΔV are finite mass and finite volume amounts of matter. ε must be chosen so as not to break the continuity assumption. Otherwise, the principles of the statistical mechanics must be utilized [9].

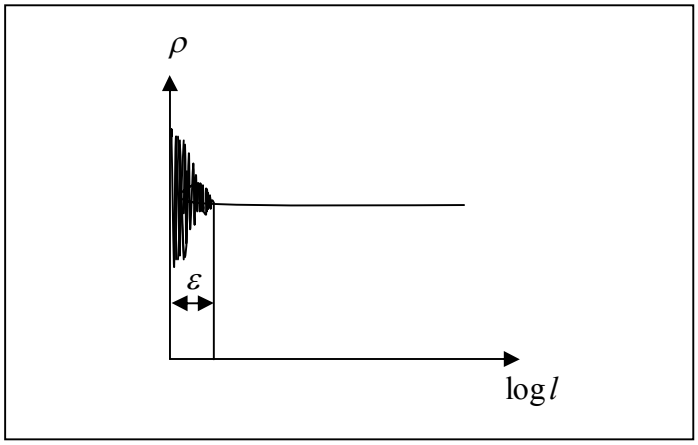

Figure 3.5. The density as a function of the size of sample

SI units for the density is kg/m^3 . The equation of state for gas phase relates the density to its pressure and temperature as:

$$P = \rho RT \tag{3.8}$$

where T is the temperature in Kelvins, P is the pressure, R is the gas constant which has a specific value for each gas and ρ is the density of the gas. The density is assumed to be

constant in the numerical simulations presented in this thesis, since the flows are incompressible.

3.1.4. Temperature

As a definition temperature is the measure of the average kinetic energy of the atoms or molecules in the substance. Actually it can be thought as a property which gives the clue about the degree of freedom in the view of statistical physics. Temperature is related directly to the heat or the thermal energy of the system. Temperature gives an idea about the energy of the atoms forming the system. If the heat is added to the system the random movement of the atoms and molecules will become more vigorous in the microscopic scale. Temperature is an intrinsic property of the system so it is independent of the amount of matter in the system or the size of the system. The temperature affects a lot of physical properties of the matter such as electrical conductivity, density, phase etc. It is measured directly by using a thermometer, a thermopile, a termistor etc. It affects the viscosity of the fluids since the viscosity of the gases increases while the viscosity of the liquids decreases with the increasing temperature. In gases, the increasing temperature makes the molecules' movements faster and this results in the increase in viscosity. In contrast with liquids the molecular separation increases and this results in the decrease of the attraction between them. This results in the decrease in viscosity [10]. The SI unit for temperature is Kelvin (K). Other temperature units which are mostly in use today are Celsius $\left(^{\circ}C\right)$ and Fahrenheit $\left(^{\circ}F\right)$. In order to convert the Celsius to Kelvin

$$T(K) = T(^{\circ}C) + 273.15 \tag{3.9}$$

and from Fahrenheit to Celsius

$$T(^{\circ}C) = \frac{5}{9}\left[T\left(^{\circ}F\right) - 32\right] \tag{3.10}$$

expressions are used.

Since the fluids obey the laws of physics such as conservation of mass, conservation of momentum and conservation of energy, the properties of the fluids can be calculated and understood better from these equations.

3.2. Mass Conservation: The Continuity Equation

Basically conservation of mass states that the mass cannot be created or destroyed by the flow of the fluid under the condition of ignoring conversion of mass to energy. Therefore the mass can move without being destroyed by the fluid flow. The equation which describes this physical principle is called the mass conservation and is also named as 'continuity equation'. This is the one of the most important equations in the subject of fluid flows. During the derivation of this equation some mathematical models must be used. The same equation can be written in integral and differential forms. But not only these two expressions are available but also the equation can be written in conservative and in nonconservative forms. In order to derive the equation in integral form the finite control volume must be used. This finite control volume can be fixed in space or it can move together with the flow. Therefore two different expressions for the same equation will be obtained. The surface bounding the control volume is called the control surface, these terms are very important and are used intensively during the derivation process.

3.2.1. Integral Form of Continuity Equation Obtained by Using the Stationary Finite Control Volume

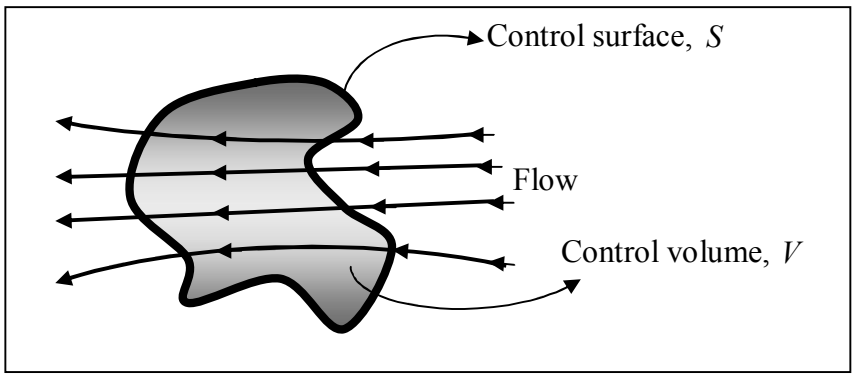

Figure 3.6. The arbitrary shape for the control volume with finite dimensions and stationary nature

In this study the control body which is under investigation has finite dimensions and is fixed in space. It has an arbitrary shape and arbitrary surface. The physical principle which is conservation of mass for this control volume can state that [11]

$$\begin{array}{l} \textit{The decrese rate} \\ \textit{of mass inside the} \\ \textit{control volume} \end{array} \quad \underline{\qquad} \quad \begin{array}{l} \textit{Net mass flow out of} \\ \textit{the control volume by} \\ \textit{crossing the surface} \end{array} \tag{3.11}$$

The elemental mass flow crossing the surface dS is given as:

$$\rho v dS = \rho \vec{v}.d\vec{S} \tag{3.12}$$

where ρ is the density, v is the velocity component perpendicular to the surface and dS is the surface element [11].

The multiplication $\vec{v}.d\vec{S}$ can be either positive or negative depending on the direction of velocity. Since $d\vec{S}$ is always pointing outwards from the control volume the sign of multiplication depends on the velocity direction. If the velocity $\vec{v}$ points inward, which means that the flow is entering the control volume, the result is negative and when the flow is leaving the control volume which mens that the velocity $\vec{v}$ points outwards from the control volume and the result of product mentioned above is positive.

If the control volume is divided into volume elements which have the elemental volume as dV, the mass inside the control volume can be given as:

$$m_T = \iiint_V \rho \, dV \, . \tag{3.13}$$

The rate of increase of mass in the control volume can be expressed as:

$$\dot{m}_{inc} = \frac{\partial}{\partial t} \iiint_V \rho \, dV \, . \tag{3.14}$$

The rate of decrease of mass in the control volume can be expressed as:

$$\dot{m}_{dec} = -\frac{\partial}{\partial t}\iiint_V \rho \, dV \,. \tag{3.15}$$

The net mass flow out of the entire control volume through the surface S is given as:

$$\dot{m}_{out} = \iint_S \rho \vec{v}.d\vec{S} \,. \tag{3.16}$$

By inserting Equations 3.14, 3.15 and 3.16 into Equation 3.11

$$-\frac{\partial}{\partial t}\iiint_V \rho \, dV = \iint_S \rho \vec{v}.d\vec{S} \tag{3.17}$$

or

$$\frac{\partial}{\partial t}\iiint_V \rho \, dV + \iint_S \rho \vec{v}.d\vec{S} = 0 \,. \tag{3.18}$$

The last equation is the continuity equation written in integral and in conservation form. Since the control volume was chosen stationary and fixed in space, the equation obtained is in conservation form otherwise it would be in nonconservation form.

3.2.2. Integral Form of Continuity Equation Obtained by Using the Moving Finite Control Volume

In this study the control volume with finite dimensions is moving together with the flow. The condition for this case is that the mass elements are staying in the control volume and the number of them does not change. This means that the mass of control volume does not change. As it is seen in Figure 3.7 the volume and shape of the control volume can change.

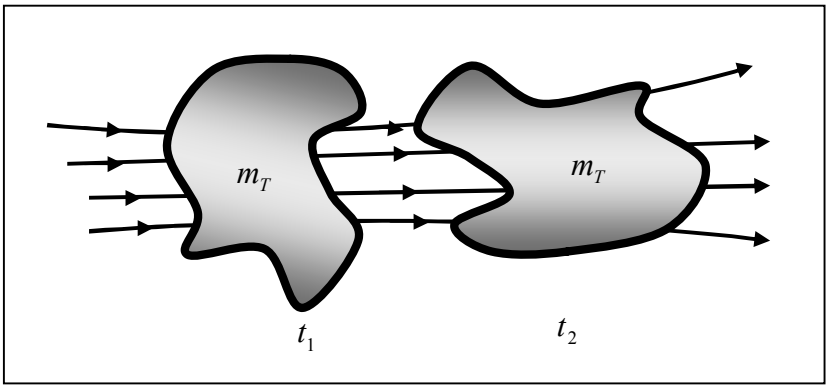

Figure 3.7. The arbitrary shape for the control volume moving together with the flow and finite dimensions

The particles inside the control volume are fixed and have unchanging masses. This means that the mass is constant as the control volume is moving together with the flow. Therefore substantial derivatives of these unchanging masses is equal to zero. Mathematically this can be expressed as:

$$\frac{D}{Dt}\iiint_V \rho\, dV = 0\,. \tag{3.19}$$

This is another equation which is again the integral form of the continuity equation but in nonconservative form. Since the control volume is moving with the flow the equation obtained from this control volume is directly in nonconservative form [11].

3.2.3. Differential Form of the Continuity Equation Obtained by Using the Stationary Infinitesimal Small Element Model

In this model, the infinitesimally small element is under consideration. This element does not move with the fluid, it is stationary. In order to take the continuum assumption into account made previously the number of the elements inside the control volume is considered to be sufficiently high.

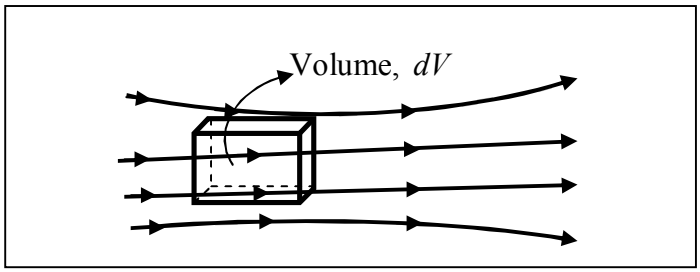

Figure 3.8. The shape of infinitesimal small element fixed in space and the flow through it

For a detailed study the shape of the infinitesimally small element is considered as given in Figure 3.8. Both the density and the velocity are functions of coordinates (x, y, z) and time, t. In order to simplify the derivation the Cartesian coordiate system is under consideration. ($u = u(x, y, z, t)$, $v = v(x, y, z, t)$, $w = w(x, y, z, t)$, $\rho = \rho(x, y, z, t)$)

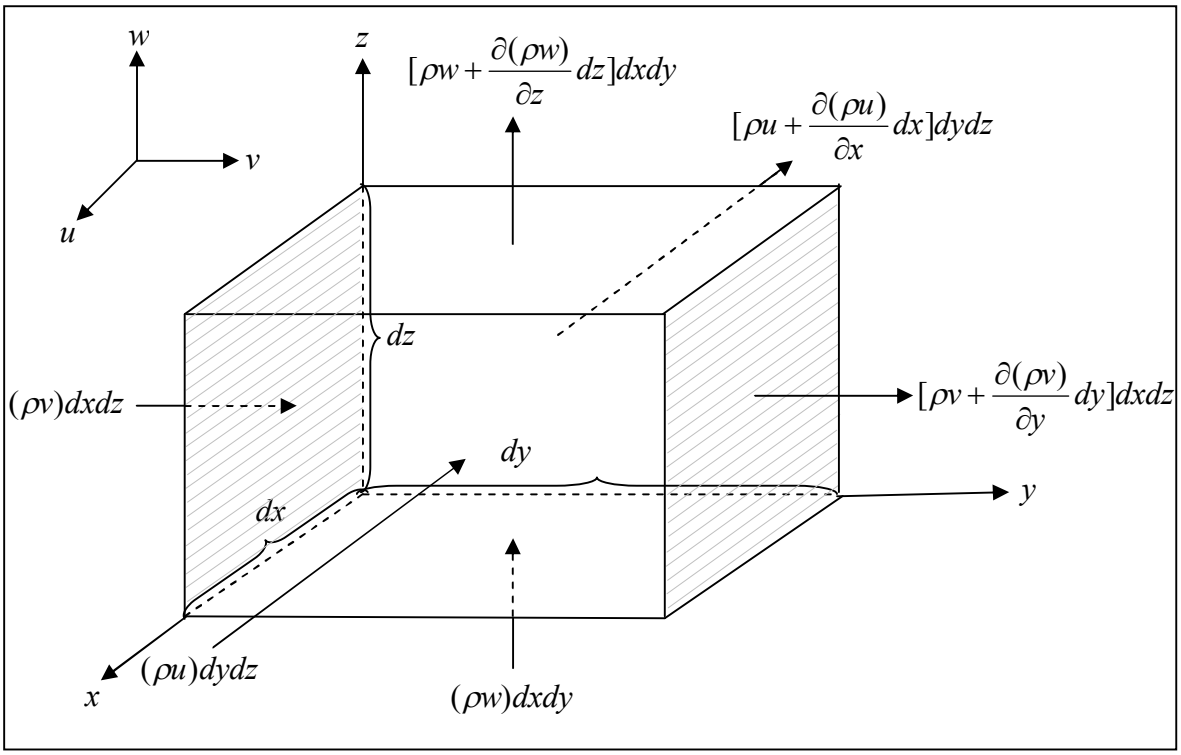

Figure 3.9. The plot of mass flow in and out of an infinitesimally small control element

The mass flow through the left face with the surface area $dxdz$ is $(\rho v)dxdz$. Since the density and velocity depend on the spatial coordinates, the mass flow through the right

face is $[\rho v + (\partial(\rho v)/\partial y)dy]dxdz$. The same work is done for y and z axes. As a result of this study with the help of the shape in Figure 3.9 *net outflows* for each coordinate is written as:

for direction x

$$[\rho u + \frac{\partial(\rho u)}{\partial x}dx]dydz - (\rho u)dydz = \frac{\partial(\rho u)}{\partial x}dxdydz \tag{3.20}$$

for direction y

$$[\rho v + \frac{\partial(\rho v)}{\partial y}dy]dxdz - (\rho v)dxdz = \frac{\partial(\rho v)}{\partial y}dxdydz \tag{3.21}$$

for direction z

$$[\rho w + \frac{\partial(\rho w)}{\partial z}dz]dxdy - (\rho w)dxdy = \frac{\partial(\rho w)}{\partial y}dxdydz\,. \tag{3.22}$$

The total mass inside the infinitesimally small volume element is $\rho dxdydz$. The rate of increase of the mass inside the element is

$$\dot{m}_{inc} = \frac{\partial\rho}{\partial t}dxdydz \tag{3.23}$$

and that of decrease inside the element is

$$\dot{m}_{dec} = -\frac{\partial\rho}{\partial t}dxdydz\,. \tag{3.24}$$

The physical principle of conservation of mass states that the time rate of decrease inside the fixed element must be equal to the net mass flow out of the element which is given as :

$$Net\ mass\ flow = \left[\frac{\partial(\rho u)}{\partial x} + \frac{\partial(\rho v)}{\partial y} + \frac{\partial(\rho w)}{\partial z} \right] dxdydz \tag{3.25}$$

after the equations are written properly one gets

$$\left[\frac{\partial(\rho u)}{\partial x} + \frac{\partial(\rho v)}{\partial y} + \frac{\partial(\rho w)}{\partial z} \right] dxdydz = -\frac{\partial \rho}{\partial t} dxdydz . \tag{3.26}$$

Then by rewriting Equation 3.26, the continuity equation is obtained:

$$\frac{\partial \rho}{\partial t} + \vec{\nabla}.(\rho \vec{v}) = 0 . \tag{3.27}$$

Equation 3.27 is a partial differential equation which is in conservative form. Since the control volume is infinitesimally small, the equation is directly obtained in differential form.

3.2.4. Differential Form of the Continuity Equation Obtained by Using the Infinitesimal Small Element Moving with the Flow

In this model there is a infinitesimally small element which is not stationary and is moving together with the flow. Differently from the previous model, the fluid element has constant mass. The shape and the volume of the element naturally can change while moving with the flow.

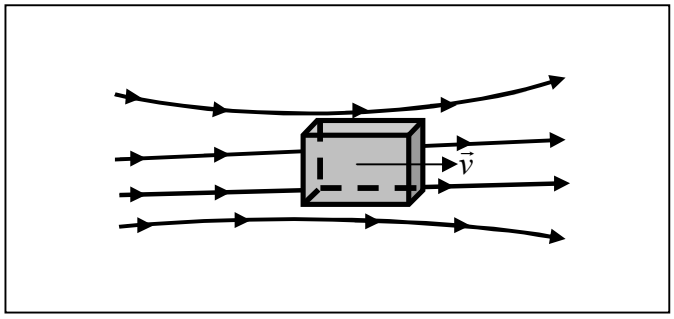

Figure 3.10. The shape of infinitesimal small element moving together with the flow

The mass element for this model can be given as:

$$\delta m = \rho \delta V \,. \tag{3.28}$$

Because of the fact that the mass is not changing inside the fluid element during the movement the rate of mass change is obviously zero. Then

$$\frac{D(\delta m)}{Dt} = 0 \tag{3.29}$$

and by using the expression in Equation 3.28 the new form of Equation 3.29 becomes

$$\frac{D(\rho \delta V)}{Dt} = 0$$

$$\frac{D(\rho \delta V)}{Dt} = \delta V \frac{D\rho}{Dt} + \rho \frac{D(\delta V)}{Dt}$$

$$\frac{D\rho}{Dt} + \rho \underbrace{\left[\frac{1}{\delta V} \frac{D(\delta V)}{Dt} \right]}_{\vec{\nabla}.\vec{v}} = 0$$

$$\frac{D\rho}{Dt} + \rho \vec{\nabla}.\vec{v} = 0 \,. \tag{3.30}$$

The Equation 3.30 is the same as the continuity equation but in noncoservative form. There are four different types for continuity equation obtained above.

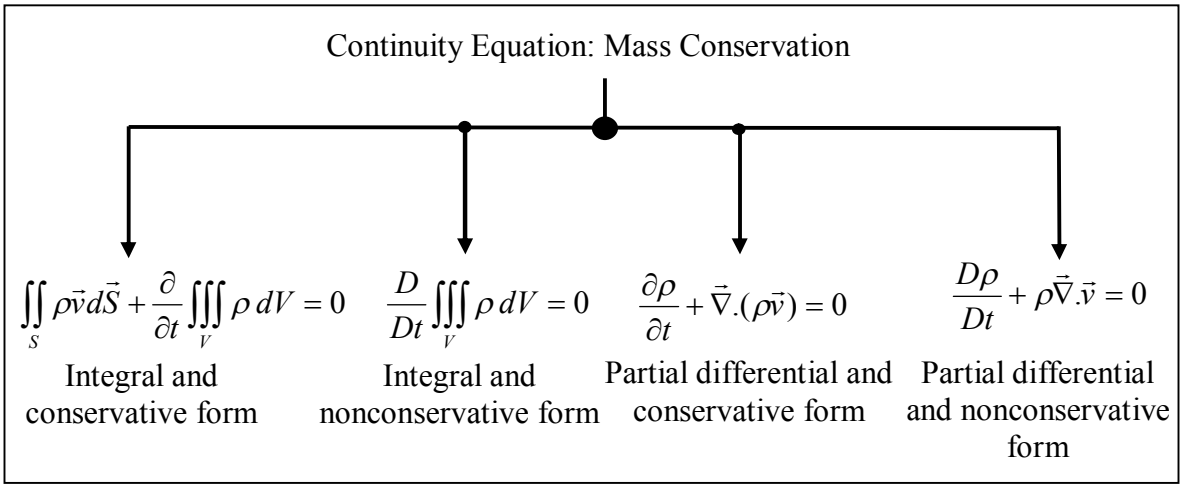

Figure 3.11. Different types of equations for continuity

Actually these equations all represent the same equation with different forms. They can be derived from each other after some manipulations [11].

3.3. Momentum Conservation: Navier-Stokes Equations

The physical principle conservation of momentum is one of the most important principles used in fluid dynamics. By regarding this physical principle the set of equations which are called Navier-Stokes equations are obtained. These equations are named after French scientist Louis Marie Henry Navier and Irish George Gabriel Stokes . Navier, who actively worked in bridge engineering analyzed the fluid flow assuming the force by repulsion and absorption between the neighbouring molecules. Navier derived the equations in 1822 but he did not introduce the viscosity in his derivations. Stokes who is the mathematician and physicist derived the same equation in 1845 by explicitly introducing the viscosity in his works. By taking the Newton's second law in mind the net force acting on the fluid element is given as the product of the mass of fluid element and its acceleration. The sources for the force acting on the fluid element are also important.

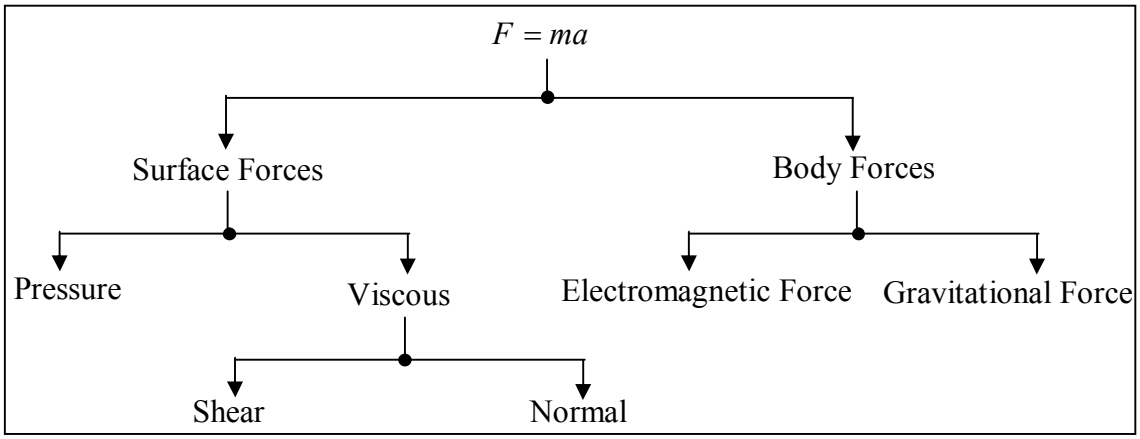

Figure 3.12. The forces acting on the fluid element

The body forces act directly on the whole volume of the fluid element. However the surface forces are acting only on the surfaces where they exist. In this study the fluid element is assumed to move together with the flow. For a detailed investigation the fluid element's shape is assumed to be as in Figure (3.13). In order to simplify the analysis, the derivation will be done only for the x component of forces.

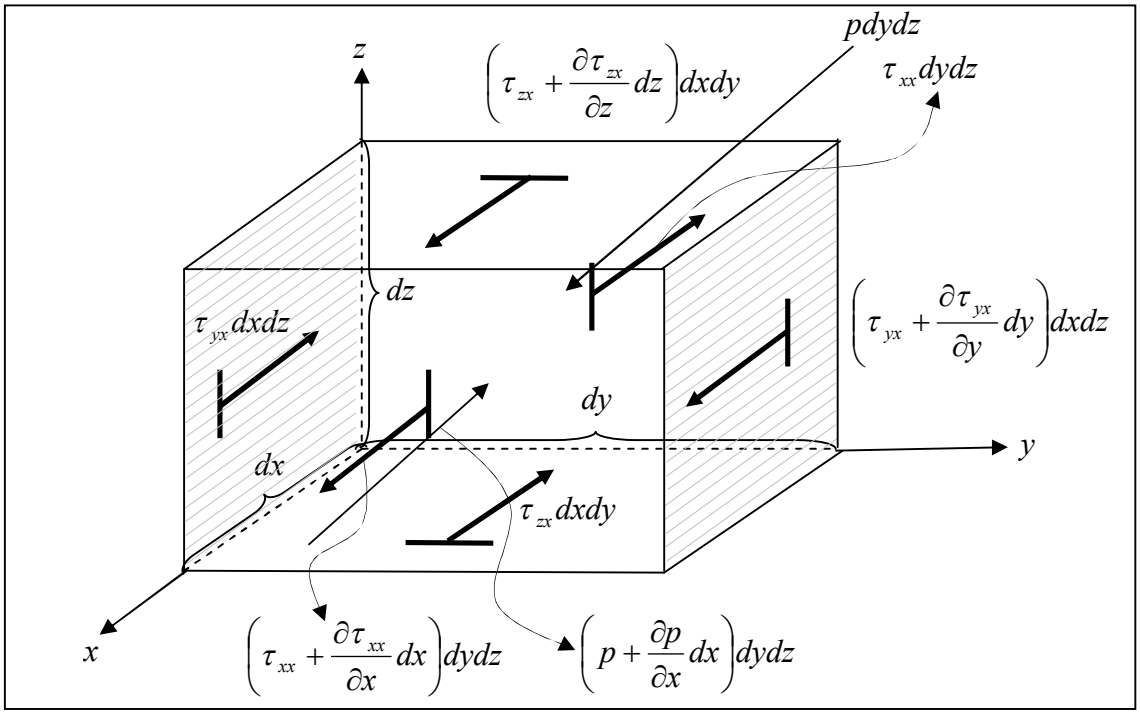

Figure 3.13. The surface forces acting on the fluid element

Actually both the body forces and surface forces are acting on the fluid element and this is taken into account later in the thesis. If the body force per unit mass, acting on the x coordinate is f_x then the net body force acting on the fluid element in x direction is given as:

$$F_{BNET,x} = \rho f_x dxdydz \,. \tag{3.31}$$

The shear stresses such as τ_{xy}, τ_{xz} are related to the time rate of change of the shearing deformation of fluid element. A normal stress which is τ_{xx} is related to the time rate of change of volume of the fluid element. The shear stresses in most of the viscous fluids are much greater than the normal stresses. Therefore normal stresses are neglected generally. In Figure 3.11, the stresses in the positive directions are assumed to be greater for convenience. The pressure forces acting in x directions always point through the fluid element. By using the shape in Figure 3.11 and forces acting on it, the surface force equations can be written as:
for direction x

$$F_{S,X} = \left[p - \left(p + \frac{\partial p}{\partial x} dx \right) \right] dydz + \left[\left(\tau_{xx} + \frac{\partial \tau_{xx}}{\partial x} dx \right) - \tau_{xx} \right] dydz + \left[\left(\tau_{yx} + \frac{\partial \tau_{yx}}{\partial y} dy \right) - \tau_{yx} \right] dxdz + \left[\left(\tau_{zx} + \frac{\partial \tau_{zx}}{\partial z} dz \right) - \tau_{zx} \right] dxdy \,. \tag{3.32}$$

Since there are not only the surface forces acting on the fluid element but also the body forces existing, the net force acting in x direction is the sum of them and the resulting form was given below.

$$F_{net,x} = F_{S,X} + F_{BNET,x} \tag{3.33}$$

$$F_{net,x} = \left[-\frac{\partial p}{\partial x} + \frac{\partial \tau_{XX}}{\partial x} + \frac{\partial \tau_{YX}}{\partial y} + \frac{\partial \tau_{ZX}}{\partial z} \right] dxdydz + \rho f_x dxdydz \,. \tag{3.34}$$

By considering the main expression for Newton's second law $F = ma$ and the x component for this expression is

$$F_X = ma_X . \tag{3.35}$$

The mass in the fluid element can be expressed as

$$m = \rho dxdydz \tag{3.36}$$

and the accelaration in x direction is

$$a_X = \frac{Du}{Dt} . \tag{3.37}$$

By combining Equations 3.34, 3.35, 3.36 and 3.37

$$\left[-\frac{\partial p}{\partial x} + \frac{\partial \tau_{XX}}{\partial x} + \frac{\partial \tau_{YX}}{\partial y} + \frac{\partial \tau_{ZX}}{\partial z} \right] dxdydz + \rho f_x dxdydz = \rho dxdydz \frac{Du}{Dt}$$

and writing in a convenient way, after simplifications

$$\rho \frac{Du}{Dt} = \left[-\frac{\partial p}{\partial x} + \frac{\partial \tau_{XX}}{\partial x} + \frac{\partial \tau_{YX}}{\partial y} + \frac{\partial \tau_{ZX}}{\partial z} \right] + \rho f_x \tag{3.38}$$

is obtained. However this is the expression only for the x component of the momentum and y and z components are needed. By using the same method, one gets y and z components as:

y component of momentum

$$\rho \frac{Dv}{Dt} = \left[-\frac{\partial p}{\partial y} + \frac{\partial \tau_{YY}}{\partial y} + \frac{\partial \tau_{XY}}{\partial x} + \frac{\partial \tau_{ZY}}{\partial z} \right] + \rho f_y \tag{3.39}$$

and z component

$$\rho \frac{Dw}{Dt} = \left[-\frac{\partial p}{\partial z} + \frac{\partial \tau_{ZZ}}{\partial z} + \frac{\partial \tau_{XZ}}{\partial x} + \frac{\partial \tau_{YZ}}{\partial y} \right] + \rho f_z \ . \tag{3.40}$$

Equations 3.38, 3.39 and 3.40 are all partial differential equations. Because of the fact that the fluid element was chosen as moving element, the form of these equations is non-conservative. As a result the very well known expressions in fluid dynamics called the Navier-Stokes equations are obtained.

If the conservation form of the Navier-Stokes equation is desired to be written, the procedure shown below can be used. Again the derivations is done firstly for the x component of the momentum. From the definition for substantial derivative

$$\rho \frac{Du}{Dt} = \rho \frac{\partial u}{\partial t} + \rho \vec{v}.\vec{\nabla} u \tag{3.41}$$

is obtained. By using the rule for derivative of a product

$$\frac{\partial (\rho u)}{\partial t} = \rho \frac{\partial u}{\partial t} + u \frac{\partial \rho}{\partial t}$$

and rearranging one gets

$$\rho \frac{\partial u}{\partial t} = \frac{\partial (\rho u)}{\partial t} - u \frac{\partial \rho}{\partial t} \tag{3.42}$$

which is the new expression for the first term on the right hand side of Equation 3.41. From the definition of divergence of the product of vector and scalar

$$\vec{\nabla}.(\rho u \vec{v}) = u \vec{\nabla}.(\rho \vec{v}) + (\rho \vec{v}).\vec{\nabla} u \tag{3.43}$$

again after rearrangement

$$(\rho\vec{v}).\vec{\nabla}u = \vec{\nabla}.(\rho u\vec{v}) - u\vec{\nabla}.(\rho\vec{v}) \tag{3.44}$$

is obtained. By using Equations 3.42 and 3.44 in Equation 3.41

$$\rho\frac{Du}{Dt} = \frac{\partial(\rho u)}{\partial t} - u\frac{\partial\rho}{\partial t} + \vec{\nabla}.(\rho u\vec{v}) - u\vec{\nabla}.(\rho\vec{v}) \tag{3.45}$$

is found. By doing some rearrangements in Equation 3.45

$$\rho\frac{Du}{Dt} = \frac{\partial(\rho u)}{\partial t} - u\left[\frac{\partial\rho}{\partial t} + \vec{\nabla}.(\rho\vec{v})\right] + \vec{\nabla}.(\rho u\vec{v}) \tag{3.46}$$

is found. Note that the sum in the paranthesis vanishes since it defines the continuity equation. As a result , Equation 3.46 is reduced to

$$\rho\frac{Du}{Dt} = \frac{\partial(\rho u)}{\partial t} + \vec{\nabla}.(\rho u\vec{v}) \tag{3.47}$$

Equation 3.47 is another form of Equation 3.38 and by equating them

$$\frac{\partial(\rho u)}{\partial t} + \vec{\nabla}.(\rho u\vec{v}) = \left[-\frac{\partial p}{\partial x} + \frac{\partial\tau_{XX}}{\partial x} + \frac{\partial\tau_{YX}}{\partial y} + \frac{\partial\tau_{ZX}}{\partial z}\right] + \rho f_x \tag{3.48}$$

is obtained. This expression is for the x component and similarly for the y component

$$\frac{\partial(\rho v)}{\partial t} + \vec{\nabla}.(\rho v\vec{v}) = \left[-\frac{\partial p}{\partial y} + \frac{\partial\tau_{YY}}{\partial y} + \frac{\partial\tau_{XY}}{\partial x} + \frac{\partial\tau_{ZY}}{\partial z}\right] + \rho f_y \tag{3.49}$$

and for the z component

$$\frac{\partial(\rho w)}{\partial t} + \vec{\nabla}.(\rho w\vec{v}) = \left[-\frac{\partial p}{\partial z} + \frac{\partial\tau_{ZZ}}{\partial z} + \frac{\partial\tau_{XZ}}{\partial x} + \frac{\partial\tau_{YZ}}{\partial y}\right] + \rho f_z \tag{3.50}$$

can be written.

The last three Equations 3.48, 3.49 and 3.50 are Navier-Stokes equations written in conservative form. These equations also define the conservation of momentum.

For Newtonian fluids in which the shear stress is proportional to the time rate of strain, Stokes proposed to use

$$\tau_{XX} = \lambda_s(\vec{\nabla}.\vec{v}) + 2\mu_m \frac{\partial u}{\partial x} \tag{3.51}$$

$$\tau_{YY} = \lambda_s(\vec{\nabla}.\vec{v}) + 2\mu_m \frac{\partial v}{\partial y} \tag{3.52}$$

$$\tau_{ZZ} = \lambda_s(\vec{\nabla}.\vec{v}) + 2\mu_m \frac{\partial w}{\partial z} \tag{3.53}$$

$$\tau_{XY} = \tau_{YX} = \mu_m\left(\frac{\partial v}{\partial x} + \frac{\partial u}{\partial y}\right) \tag{3.54}$$

$$\tau_{XZ} = \tau_{ZX} = \mu_m\left(\frac{\partial u}{\partial z} + \frac{\partial w}{\partial x}\right) \tag{3.55}$$

$$\tau_{YZ} = \tau_{ZY} = \mu_m\left(\frac{\partial w}{\partial y} + \frac{\partial v}{\partial z}\right) \tag{3.56}$$

where the coefficients μ_m and λ_s are molecular viscosity coefficient and second viscosity coefficient respectively.

Then by using the definitions given in Equations 3.51-3.56, the Navier-Stokes equations in conservative form can be given as below.

$$\frac{\partial(\rho u)}{\partial t}+\frac{\partial(\rho u^2)}{\partial x}+\frac{\partial(\rho uv)}{\partial y}+\frac{\partial(\rho uw)}{\partial z}=-\frac{\partial p}{\partial x}+\frac{\partial}{\partial x}\left(\lambda\vec{\nabla}\vec{v}+2\mu\frac{\partial u}{\partial x}\right)+\frac{\partial}{\partial y}\left[\mu\left(\frac{\partial v}{\partial x}+\frac{\partial u}{\partial y}\right)\right]+\frac{\partial}{\partial z}\left[\mu\left(\frac{\partial u}{\partial z}+\frac{\partial w}{\partial x}\right)\right]+\rho f_x \tag{3.57}$$

$$\frac{\partial(\rho v)}{\partial t}+\frac{\partial(\rho uv)}{\partial x}+\frac{\partial(\rho v^2)}{\partial y}+\frac{\partial(\rho vw)}{\partial z}=-\frac{\partial p}{\partial y}+\frac{\partial}{\partial x}\left[\mu\left(\frac{\partial v}{\partial x}+\frac{\partial u}{\partial y}\right)\right]+\frac{\partial}{\partial y}\left(\lambda\vec{\nabla}\vec{v}+2\mu\frac{\partial v}{\partial y}\right)+\frac{\partial}{\partial z}\left[\mu\left(\frac{\partial w}{\partial y}+\frac{\partial v}{\partial z}\right)\right]+\rho f_y \tag{3.58}$$

$$\frac{\partial(\rho w)}{\partial t}+\frac{\partial(\rho uw)}{\partial x}+\frac{\partial(\rho vw)}{\partial y}+\frac{\partial(\rho w^2)}{\partial z}=-\frac{\partial p}{\partial z}+\frac{\partial}{\partial x}\left[\mu\left(\frac{\partial u}{\partial z}+\frac{\partial w}{\partial x}\right)\right]+\frac{\partial}{\partial y}\left[\mu\left(\frac{\partial w}{\partial y}+\frac{\partial v}{\partial z}\right)\right]+\frac{\partial}{\partial z}\left(\lambda\vec{\nabla}\vec{v}+2\mu\frac{\partial w}{\partial z}\right)+\rho f_z \tag{3.59}$$

These expressions are given in Cartesian coordinate system [11]. It is useful to express these equations in the cylindrical (r,θ,z) or spherical (r,θ,ϕ) coordinates. Navier-Stokes equations in cylindrical cordinate system (r,θ,z) which are given in reference [7] are:

for component r

$$\rho\left(\frac{\partial v_r}{\partial t}+v_r\frac{\partial v_r}{\partial r}+\frac{v_\theta}{r}\frac{\partial v_r}{\partial\theta}-\frac{{v_\theta}^2}{r}+v_z\frac{\partial v_r}{\partial z}\right)=-\frac{\partial p}{\partial r}+\mu\left[\frac{\partial}{\partial r}\left(\frac{1}{r}\frac{\partial}{\partial r}(rv_r)\right)+\frac{1}{r^2}\frac{\partial^2 v_r}{\partial\theta^2}-\frac{2}{r^2}\frac{\partial v_\theta}{\partial\theta}+\frac{\partial^2 v_r}{\partial z^2}\right]+\rho g_r \tag{3.60}$$

for component θ

$$\rho\left(\frac{\partial v_\theta}{\partial t}+v_r\frac{\partial v_\theta}{\partial r}+\frac{v_\theta}{r}\frac{\partial v_r}{\partial\theta}-\frac{v_r v_\theta}{r}+v_z\frac{\partial v_\theta}{\partial z}\right)=-\frac{1}{r}\frac{\partial p}{\partial\theta}+\mu\left[\frac{\partial}{\partial r}\left(\frac{1}{r}\frac{\partial}{\partial r}(rv_\theta)\right)+\frac{1}{r^2}\frac{\partial^2 v_\theta}{\partial\theta^2}-\frac{2}{r^2}\frac{\partial v_r}{\partial\theta}+\frac{\partial^2 v_\theta}{\partial z^2}\right]+\rho g_\theta \tag{3.61}$$

for component z

$$\rho\left(\frac{\partial v_z}{\partial t}+v_r\frac{\partial v_z}{\partial r}+\frac{v_\theta}{r}\frac{\partial v_z}{\partial \theta}+v_z\frac{\partial v_z}{\partial z}\right)=-\frac{\partial p}{\partial z}+ \mu\left[\frac{1}{r}\frac{\partial}{\partial r}\left(r\frac{\partial v_z}{\partial r}\right)+\frac{1}{r^2}\frac{\partial^2 v_z}{\partial \theta^2}+\frac{\partial^2 v_z}{\partial z^2}\right]+\rho g_z . \tag{3.62}$$

Navier-Stokes equations in spherical cordinate system (r,θ,ϕ) are:

for component r

$$\rho\left(\frac{\partial v_r}{\partial t}+v_r\frac{\partial v_r}{\partial r}+\frac{v_\theta}{r}\frac{\partial v_r}{\partial \theta}+\frac{v_\phi}{rSin\theta}\frac{\partial v_r}{\partial \phi}-\frac{{v_\theta}^2+{v_\phi}^2}{r}\right)=-\frac{\partial p}{\partial r}+ \mu\left[\frac{\partial}{\partial r}\left(\frac{1}{r^2}\frac{\partial^2}{\partial r^2}(r^2 v_r)\right)+\frac{1}{r^2 Sin\theta}\frac{\partial}{\partial \theta}\left(Sin\theta\frac{\partial v_r}{\partial \theta}\right)-\frac{1}{r^2 Sin^2\theta}\frac{\partial^2 v_r}{\partial \phi^2}\right]+\rho g_r \tag{3.63}$$

for component θ

$$\rho\left(\frac{\partial v_\theta}{\partial t}+v_r\frac{\partial v_\theta}{\partial r}+\frac{v_\theta}{r}\frac{\partial v_\theta}{\partial \theta}+\frac{v_\phi}{rSin\theta}\frac{\partial v_\theta}{\partial \phi}+\frac{v_r v_\theta}{r}-\frac{{v_\phi}^2 Cot\theta}{r}\right)=-\frac{1}{r}\frac{\partial p}{\partial \theta}+ \mu\left[\frac{1}{r^2}\frac{\partial}{\partial r}\left(r^2\frac{\partial v_\theta}{\partial r}\right)+\frac{1}{r^2}\frac{\partial}{\partial \theta}\left(\frac{1}{Sin\theta}\frac{\partial}{\partial \theta}(v_\theta Sin\theta)\right)+ \frac{1}{r^2 Sin^2\theta}\frac{\partial^2 v_\theta}{\partial \phi^2}+\frac{2}{r^2}\frac{\partial v_r}{\partial \theta}-\frac{2Cos\theta}{r^2 Sin^2\theta}\frac{\partial v_\phi}{\partial \phi}\right]+\rho g_\theta \tag{3.64}$$

for component ϕ

$$\rho\left(\frac{\partial v_\phi}{\partial t}+v_r\frac{\partial v_\phi}{\partial r}+\frac{v_\theta}{r}\frac{\partial v_\phi}{\partial \theta}+\frac{v_\phi}{rSin\theta}\frac{\partial v_\phi}{\partial \phi}+\frac{v_r v_\phi}{r}+\frac{v_\theta v_\phi Cot\theta}{r}\right)=-\frac{1}{rSin\theta}\frac{\partial p}{\partial \phi}+ \mu\left[\frac{1}{r^2}\frac{\partial}{\partial r}\left(r^2\frac{\partial v_\phi}{\partial r}\right)+\frac{1}{r^2}\frac{\partial}{\partial \theta}\left(\frac{1}{Sin\theta}\frac{\partial}{\partial \theta}(v_\phi Sin\theta)\right)+ \frac{1}{r^2 Sin^2\theta}\frac{\partial^2 v_\phi}{\partial \phi^2}+\frac{2}{r^2 Sin\theta}\frac{\partial v_r}{\partial \phi}+\frac{2Cos\theta}{r^2 Sin^2\theta}\frac{\partial v_\theta}{\partial \phi}\right]+\rho g_\phi . \tag{3.65}$$

The derivation of Navier-Stokes equations which were given previously starts with Newton's second law which is the conservation of momentum. These are nonlinear partial differential equations. By using these equations the liquid flow in pipes, the ocean currents, weather modelling, design of aircrafts and automobile surfaces and shapes can be done. By coupling these equations with Maxwell's equations magnetohydrodynamic equations are obtained. Magnetohydrodynamics (MHD) is the simplified model of a magnetized plasma in which the plasma is assumed as a single fluid which can cary current. The MHD model is the same with the ordinary fluid with the addition of the force caused by the magnetic field. MHD is interested in the fluids such as plasma, liquid metals, salt water etc. Together with suitable equations and boundary conditions Navier-Stokes equations can model the fluids accurately.

3.4. Energy Conservation

The infinitesimally small volume element moving with the fluid is again under consideration. The energy balance for this element can be stated as [11]:

$$\begin{array}{l}\textit{Energy change}\\ \textit{rate inside the}\\ \textit{fluid element}\end{array} = \begin{array}{l}\textit{The net flux of}\\ \textit{heat which}\\ \textit{enters the}\\ \textit{fluid element}\end{array} + \begin{array}{l}\textit{The net rate of work}\\ \textit{which is done by both}\\ \textit{surface and body forces}\\ \textit{on the fluid element}\end{array}. \tag{3.66}$$

There are basically two kinds of forces acting on the fluid element, one of them is body force and the other one is the net surface force as was mentioned previously. Both of them do work on the fluid element separately. Physically the work rate which is expressed in units of $joule/second$ (J/s) can also be described as the product of the force and the velocity acting on the direction of the force. By taking this definition into account the work rate due to the body force is

$$\dot{W}_b = \rho\vec{F}.\vec{v}dxdydz\,. \tag{3.67}$$

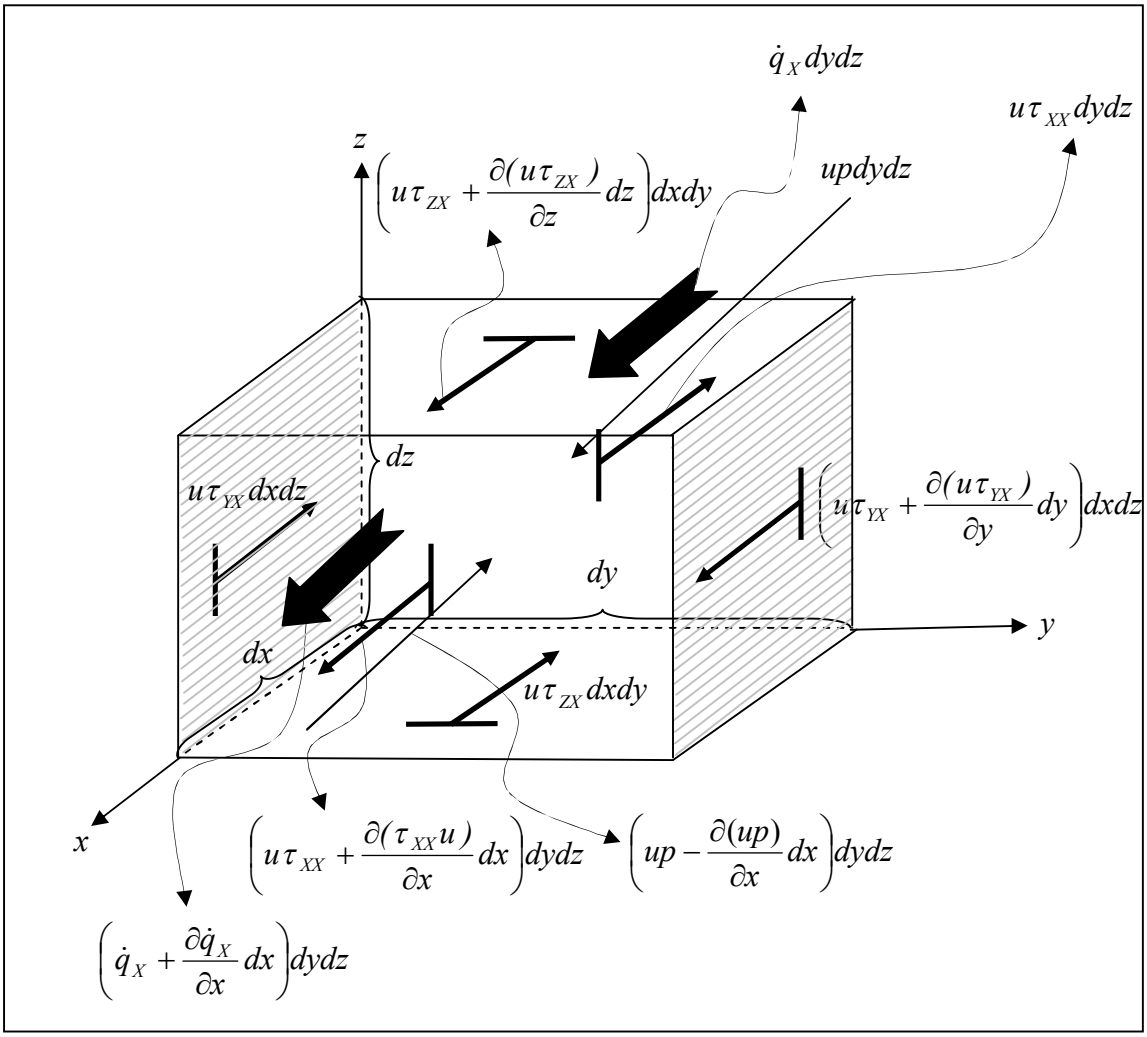

Figure 3.14. The sketch for energy flows in and out of the fluid element

The work rate due to the pressure, shear and normal stresses which are composing the surface forces also have an impact role on the energy balance. By taking into account these forces again only for particularly chosen x direction the rate of work expression will be calculated by multiplying the x component of the velocity which is u with the surface forces acting on the fluid element. First of all the net work rate due to the pressure for x direction is

$$\dot{W}_{S,P} = \left[up - \left(up + \frac{\partial(up)}{\partial x}\right)\right] dxdydz \tag{3.68}$$

$$\dot{W}_{S,P} = -\frac{\partial(up)}{\partial x} dxdydz \,. \tag{3.69}$$

When every shear force acting on the x direction is taken into account one can write

$$\dot{W}_{S,XX} = \left[\left(u\tau_{XX} + \frac{\partial(\tau_{XX} u)}{\partial x} \right) - u\tau_{XX} \right] dxdydz \tag{3.70}$$

$$\dot{W}_{S,XX} = \frac{\partial(\tau_{XX} u)}{\partial x} dxdydz \tag{3.71}$$

$$\dot{W}_{S,YX} = \left[\left(u\tau_{YX} + \frac{\partial(u\tau_{YX})}{\partial y} \right) - u\tau_{YX} \right] dydxdz \tag{3.72}$$

$$\dot{W}_{S,YX} = \frac{\partial(\tau_{YX} u)}{\partial y} dxdydz \tag{3.73}$$

$$\dot{W}_{S,ZX} = \left[\left(u\tau_{ZX} + \frac{\partial(u\tau_{ZX})}{\partial z} \right) - u\tau_{ZX} \right] dzdxdy \tag{3.74}$$

$$\dot{W}_{S,ZX} = \frac{\partial(\tau_{ZX} u)}{\partial z} dxdydz \,. \tag{3.75}$$

By using Equations 3.69, 3.71, 3.73 and 3.75 the net work rate, $\dot{W}_{S,NET_x}$ can be written as:

$$\dot{W}_{S,NET_X} = \dot{W}_{S,P} + \dot{W}_{S,XX} + \dot{W}_{S,YX} + \dot{W}_{S,ZX} \tag{3.76}$$

$$\dot{W}_{S,NET_X} = -\frac{\partial(up)}{\partial x} dxdydz + \frac{\partial(\tau_{XX} u)}{\partial x} dxdydz + \frac{\partial(\tau_{YX} u)}{\partial y} dxdydz + \frac{\partial(\tau_{ZX} u)}{\partial z} dxdydz \,. \tag{3.77}$$

By rearranging Equations 3.77

$$\dot{W}_{S,NET_X} = \left[-\frac{\partial(up)}{\partial x} + \frac{\partial(\tau_{XX}u)}{\partial x} + \frac{\partial(\tau_{YX}u)}{\partial y} + \frac{\partial(\tau_{ZX}u)}{\partial z} \right] dxdydz \tag{3.78}$$

is obtained. Similar expressions for y and z directions can be written.

For y direction

$$\dot{W}_{S,NET_Y} = \left[-\frac{\partial(vp)}{\partial y} + \frac{\partial(\tau_{XY}v)}{\partial x} + \frac{\partial(\tau_{YY}v)}{\partial y} + \frac{\partial(\tau_{ZY}v)}{\partial z} \right] dxdydz \tag{3.79}$$

for z direction

$$\dot{W}_{S,NET_Z} = \left[-\frac{\partial(wp)}{\partial z} + \frac{\partial(\tau_{XZ}w)}{\partial x} + \frac{\partial(\tau_{YZ}w)}{\partial y} + \frac{\partial(\tau_{ZZ}w)}{\partial z} \right] dxdydz\,. \tag{3.80}$$

Then, in that case

$$\dot{W}_{S,NET} = \dot{W}_{S,NET_X} + \dot{W}_{S,NET_Y} + \dot{W}_{S,NET_Z} \tag{3.81}$$

$$\begin{aligned} \dot{W}_{S,NET} = \Bigg\{ & \left[-\frac{\partial(up)}{\partial x} + \frac{\partial(\tau_{xx}u)}{\partial x} + \frac{\partial(\tau_{YX}u)}{\partial y} + \frac{\partial(\tau_{ZX}u)}{\partial z} \right] + \\ & \left[-\frac{\partial(vp)}{\partial y} + \frac{\partial(\tau_{XY}v)}{\partial x} + \frac{\partial(\tau_{YY}v)}{\partial y} + \frac{\partial(\tau_{ZY}v)}{\partial z} \right] + \\ & \left[-\frac{\partial(wp)}{\partial z} + \frac{\partial(\tau_{XZ}w)}{\partial x} + \frac{\partial(\tau_{YZ}w)}{\partial y} + \frac{\partial(\tau_{ZZ}w)}{\partial z} \right] \Bigg\} dxdydz \end{aligned} \tag{3.82}$$

is obtained. The Equations 3.82 is only for surface forces and also body force effect must be included. Then

$$\dot{W}_{NET} = +\dot{W}_{S,NET} + \dot{W}_b \tag{3.83}$$

finally ‘the net rate of work which is done by both surface and body forces on the fluid element is

$$\dot{W}_{NET} = \left\{ \left[-\frac{\partial(up)}{\partial x} + \frac{\partial(\tau_{xx}u)}{\partial x} + \frac{\partial(\tau_{YX}u)}{\partial y} + \frac{\partial(\tau_{ZX}u)}{\partial z} \right] + \left[-\frac{\partial(vp)}{\partial y} + \frac{\partial(\tau_{XY}v)}{\partial x} + \frac{\partial(\tau_{YY}v)}{\partial y} + \frac{\partial(\tau_{ZY}v)}{\partial z} \right] + \left[-\frac{\partial(wp)}{\partial z} + \frac{\partial(\tau_{XZ}w)}{\partial x} + \frac{\partial(\tau_{YZ}w)}{\partial y} + \frac{\partial(\tau_{ZZ}w)}{\partial z} \right] \right\} dxdydz + \rho\vec{F}.\vec{v}dxdydz. \quad (3.84)$$

After the expression for work rate is obtained it is useful to take ‘the net flux of heat which enters the fluid element’ into account. The heat flux in any direciton, as a definition, is the energy per unit area which is perpendicular to the direction and per unit time. For this study the heat flux in x direction is shown as $\dot{q}_X$. For the fluid element considered in the Figure 3.14 the net heat which is transferred into the fluid element is given as:

$$\dot{Q}_X = \dot{q}_X dydz - \left(\dot{q}_X + \frac{\partial \dot{q}_X}{\partial x} dx \right) dydz \quad (3.85)$$

$$\dot{Q}_X = -\frac{\partial \dot{q}_X}{\partial x} dxdydz. \quad (3.86)$$

Equation 3.86 gives only the net heat which is transferred to the fluid element from the x direction, similarly for y direction

$$\dot{Q}_Y = -\frac{\partial \dot{q}_Y}{\partial y} dxdydz \quad (3.87)$$

and for z direction

$$\dot{Q}_Z = -\frac{\partial \dot{q}_Z}{\partial z} dxdydz. \quad (3.88)$$

Total heat transfer rate to the fluid element by thermal conduction is given as:

$$\dot{Q}_T = \dot{Q}_X + \dot{Q}_Y + \dot{Q}_Z \tag{3.89}$$

$$\dot{Q}_T = -\frac{\partial \dot{q}_X}{\partial x} dxdydz - \frac{\partial \dot{q}_Y}{\partial y} dxdydz - \frac{\partial \dot{q}_Z}{\partial z} dxdydz \tag{3.90}$$

$$\dot{Q}_T = \left(-\frac{\partial \dot{q}_X}{\partial x} - \frac{\partial \dot{q}_Y}{\partial y} - \frac{\partial \dot{q}_Z}{\partial z} \right) dxdydz . \tag{3.91}$$

By using the Fourier's law for conduction heat transfer, which states that the heat flux is proportional to the temperature gradient, the heat fluxes can be written as:

$$\dot{q}_X = -k \frac{\partial T}{\partial x} \tag{3.92}$$

$$\dot{q}_Y = -k \frac{\partial T}{\partial y} \tag{3.93}$$

$$\dot{q}_Z = -k \frac{\partial T}{\partial z} . \tag{3.94}$$

After these new definitions Equation 3.91 can be written as:

$$\dot{Q}_T = \left[\frac{\partial}{\partial x} \left(k \frac{\partial T}{\partial x} \right) + \left[\frac{\partial}{\partial y} \left(k \frac{\partial T}{\partial y} \right) \right] + \left[\frac{\partial}{\partial z} \left(k \frac{\partial T}{\partial z} \right) \right] \right] dxdydz . \tag{3.95}$$

Volumetric heat addition rate per unit mass, $\dot{Q}_{V,M}$ is given as ,

$$\dot{Q}_V = \dot{Q}_{V,M} \rho dxdydz \tag{3.96}$$

where $\dot{Q}_V$ is the volumetric heat addition rate. By taking the volumetric heat addition and conduction heats the total heat rate, $\dot{Q}_{TOT}$ will be written as:

$$\dot{Q}_{TOT} = \dot{Q}_V - \dot{Q}_T \tag{3.97}$$

$$\dot{Q}_{TOT} = \dot{Q}_{V,M}\ \rho dxdydz + \left[\frac{\partial}{\partial x}\left(k\frac{\partial T}{\partial x}\right) + \left[\frac{\partial}{\partial y}\left(k\frac{\partial T}{\partial y}\right)\right] + \left[\frac{\partial}{\partial z}\left(k\frac{\partial T}{\partial z}\right)\right]\right]dxdydz\ . \tag{3.98}$$

Since we are interested in the fluid element which is moving and having a kinetic energy, this kinetic energy can be given as

$$E_{kin} = \frac{1}{2}m_{FE}v^2 \tag{3.99}$$

where m_{FE} is the mass of fluid element into consideration. Therefore the word energy which is mentioned in 'the rate of energy change inside the fluid element' expression in Equation 3.66 represents the total energy. The kinetic energy expression by using the the density, ρ, of fluid element,

$$E_{kin} = \frac{1}{2}\rho dxdydzv^2 \tag{3.100}$$

can be written.

The fluid element contains molecules which have their own energies. The sum of all the molecules' energies is the internal energy of the fluid element. This energy arises from the random motions of the molecules inside the fluid element. Let us give this internal energy per mass as ε_m. By taking into account both the kinetic and internal energies of the molecules the total energy E_{TOT} of the fluid element can be written as :

$$E_{TOT} = \left(\varepsilon_m + \frac{1}{2}v^2\right)\rho dxdydz\ . \tag{3.101}$$

The rate of change of the total energy will be

$$\frac{D}{Dt}E_{TOT}=\frac{D}{Dt}\left(\varepsilon_m+\frac{1}{2}v^2\right)\rho dxdydz\,. \tag{3.102}$$

By rearranging Equations 3.102, 3.98 and 3.84

$$\begin{aligned}
&\frac{D}{Dt}\left(\varepsilon_m+\frac{1}{2}\vec{v}^{\,2}\right)\rho dxdydz\;=\dot{Q}_{V,M}\;\rho dxdydz\;+\\
&\left[\frac{\partial}{\partial x}\left(k\frac{\partial T}{\partial x}\right)+\left[\frac{\partial}{\partial y}\left(k\frac{\partial T}{\partial y}\right)\right]+\left[\frac{\partial}{\partial z}\left(k\frac{\partial T}{\partial z}\right)\right]\right]dxdydz\;+\\
&\left\{\left[-\frac{\partial(up)}{\partial x}+\frac{\partial(\tau_{XX}u)}{\partial x}+\frac{\partial(\tau_{YX}u)}{\partial y}+\frac{\partial(\tau_{ZX}u)}{\partial z}\right]+\right.\\
&\left[-\frac{\partial(vp)}{\partial y}+\frac{\partial(\tau_{XY}v)}{\partial x}+\frac{\partial(\tau_{YY}v)}{\partial y}+\frac{\partial(\tau_{ZY}v)}{\partial z}\right]+\\
&\left.\left[-\frac{\partial(wp)}{\partial z}+\frac{\partial(\tau_{XZ}w)}{\partial x}+\frac{\partial(\tau_{YZ}w)}{\partial y}+\frac{\partial(\tau_{ZZ}w)}{\partial z}\right]\right\}dxdydz\;+\\
&\rho\vec{F}.\vec{v}\,dxdydz
\end{aligned} \tag{3.103}$$

is obtained.

This last Equation 3.103 is the defined expression of Equation 3.66. If Equation 3.103 is written for unit volume one gets

$$\begin{aligned}
\frac{D}{Dt}\left(\varepsilon_m+\frac{1}{2}\vec{v}^{\,2}\right)=\dot{Q}_{V,M}\;\rho&+\left[\frac{\partial}{\partial x}\left(k\frac{\partial T}{\partial x}\right)+\left[\frac{\partial}{\partial y}\left(k\frac{\partial T}{\partial y}\right)\right]+\left[\frac{\partial}{\partial z}\left(k\frac{\partial T}{\partial z}\right)\right]\right]+\\
&\left\{\left[-\frac{\partial(up)}{\partial x}+\frac{\partial(\tau_{XX}u)}{\partial x}+\frac{\partial(\tau_{YX}u)}{\partial y}+\frac{\partial(\tau_{ZX}u)}{\partial z}\right]+\right.\\
&\left[-\frac{\partial(vp)}{\partial y}+\frac{\partial(\tau_{XY}v)}{\partial x}+\frac{\partial(\tau_{YY}v)}{\partial y}+\frac{\partial(\tau_{ZY}v)}{\partial z}\right]+\\
&\left.\left[-\frac{\partial(wp)}{\partial z}+\frac{\partial(\tau_{XZ}w)}{\partial x}+\frac{\partial(\tau_{YZ}w)}{\partial y}+\frac{\partial(\tau_{ZZ}w)}{\partial z}\right]\right\}+\rho\vec{F}.\vec{v}\;.
\end{aligned} \tag{3.104}$$

Equation 3.104 found is in nonconservative form. The conservative form of the same equation can be written as

$$\frac{\partial}{\partial t}\left[\rho\left(\varepsilon_m+\frac{1}{2}\vec{v}^2\right)\right]+\vec{\nabla}.\left[\rho\left(\varepsilon+\frac{1}{2}\vec{v}^2\right)\vec{v}\right]=\dot{Q}_{V,M}\ \rho+$$
$$\left[\frac{\partial}{\partial x}\left(k\frac{\partial T}{\partial x}\right)+\left[\frac{\partial}{\partial y}\left(k\frac{\partial T}{\partial y}\right)\right]+\left[\frac{\partial}{\partial z}\left(k\frac{\partial T}{\partial z}\right)\right]\right]+$$
$$\left\{\left[-\frac{\partial(up)}{\partial x}+\frac{\partial(\tau_{XX}u)}{\partial x}+\frac{\partial(\tau_{YX}u)}{\partial y}+\frac{\partial(\tau_{ZX}u)}{\partial z}\right]+\right. \tag{3.105}$$
$$\left[-\frac{\partial(vp)}{\partial y}+\frac{\partial(\tau_{XY}v)}{\partial x}+\frac{\partial(\tau_{YY}v)}{\partial y}+\frac{\partial(\tau_{ZY}v)}{\partial z}\right]+$$
$$\left.\left[-\frac{\partial(wp)}{\partial z}+\frac{\partial(\tau_{XZ}w)}{\partial x}+\frac{\partial(\tau_{YZ}w)}{\partial y}+\frac{\partial(\tau_{ZZ}w)}{\partial z}\right]\right\}+\rho\vec{F}.\vec{v}.$$

This equation is also called conservation of energy [11]. The equations shown in this chapter are the main governing equations for fluid dynamics. The numerical simulations are usually done in the scope of these equations. Numerical methods which can be used for simulations are discussed in the subsequent chapters of this thesis.

4. PHILOSOPHY OF COMPUTATIONAL FLUID DYNAMICS

The advancements in fluid dynamics started with experimental works and theoretical studies in the 17th century. A few centuries later another equal partner to experimental and theoretical fluid dynamics appeared. The name of this third approach is called 'computational fluid dynamics (CFD)'. Fluid dynamics had already been divided into two parts which are theoretical and experimental parts before the invention of the computational fluid dynamics. Fluid dynamics is not only used in industrial processes such as steel production and metal coatings but also in transportation by cars, trains, aircrafts and ships. Since the fluid dynamics plays an important role in science and technology the solutions for governing equations are very important. CFD (computational fluid dynamics) utilizes the numerical methods and solves codes in order to understand solutions to the governing equations. By the invention of high speed computers the numerical accuracy increased and the numerical results began to be used heavily before performing experiments. Since the experiments are very expensive and time consuming nowadays sometimes the results obtained from numerical calculations on high speed computers are used. After a lot of advancement in numerical methods and computer program codes, CFD became an equal partner to the experimental and theoretical fluid dynamics. CFD can not only replace either of pure theory and pure experiment but it can also balance them. Historically the early developments of CFD started by the needs of aerodynamics studies but it is now being used in naval architecture applications, in environmental engineering applications such as heating, air conditioning, in industrial manufactoring applications such as in manufactoring in ceramic composite materials, in civil engineering problems involving the rheology of rivers, lakes etc., and in automobile and engine applications [11]. Bio-mechanical engineering also uses the CFD codes in simulating the blood pump which is taking the the role of the heart in process of open heart surgery. Nowadays, CFD is not only used as a research tool but it is also used as a design tool. Instead of doing real experiments one can obtain identical results needed by using the computer codes. There is no need to carry this code together with someone and he/she can communicate with it from very very long distances by using the internet to do calculations remotely. Therefore CFD can be thought as a tool which replaces the money and time expenditure for real experiments with the numerical experiments.

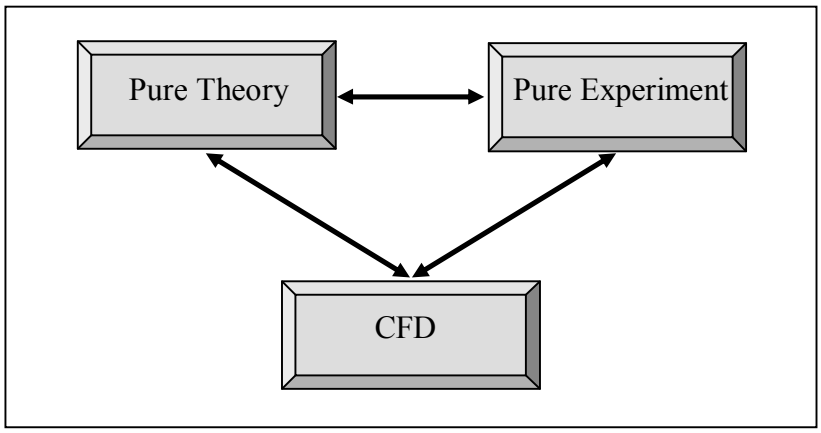

Figure 4.1. Three branches of fluid dynamics

In order to make calculations in CFD there are some processes which must be done previously.

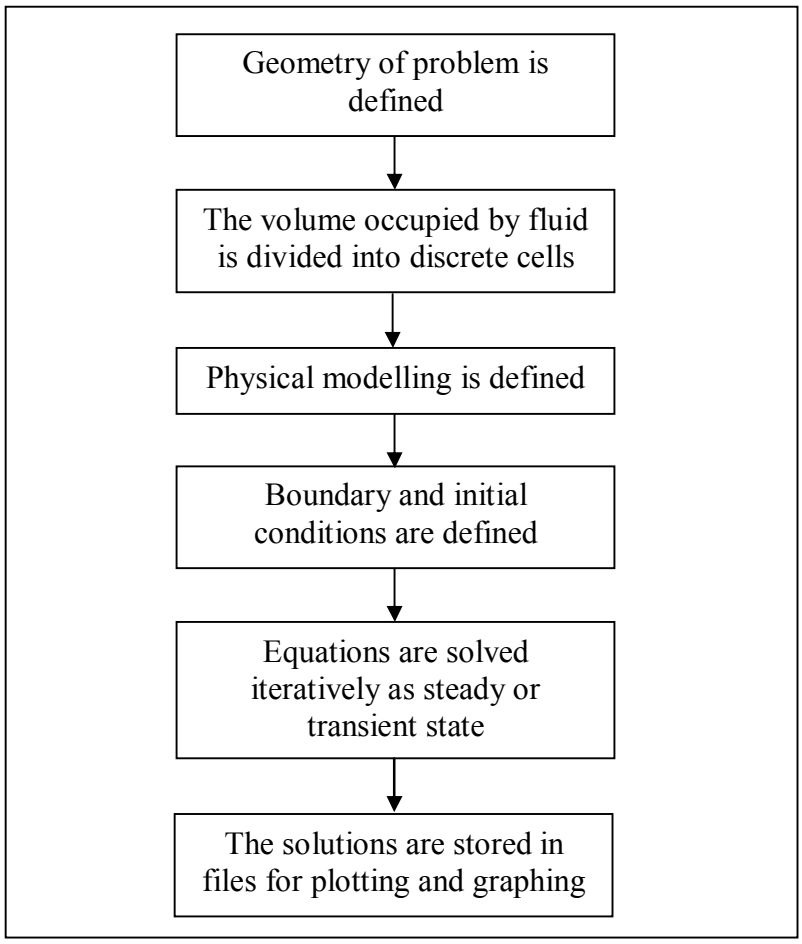

Figure 4.2. The order of CFD processes

The order is shown in Figure 4.2. Initially, the computational domain must be discretized by some space discretization methods such as finite difference, finite element, finite volume, boundary element method, and matrix distribution method.

Figure 4.3 shows the main steps taken before the CFD process.

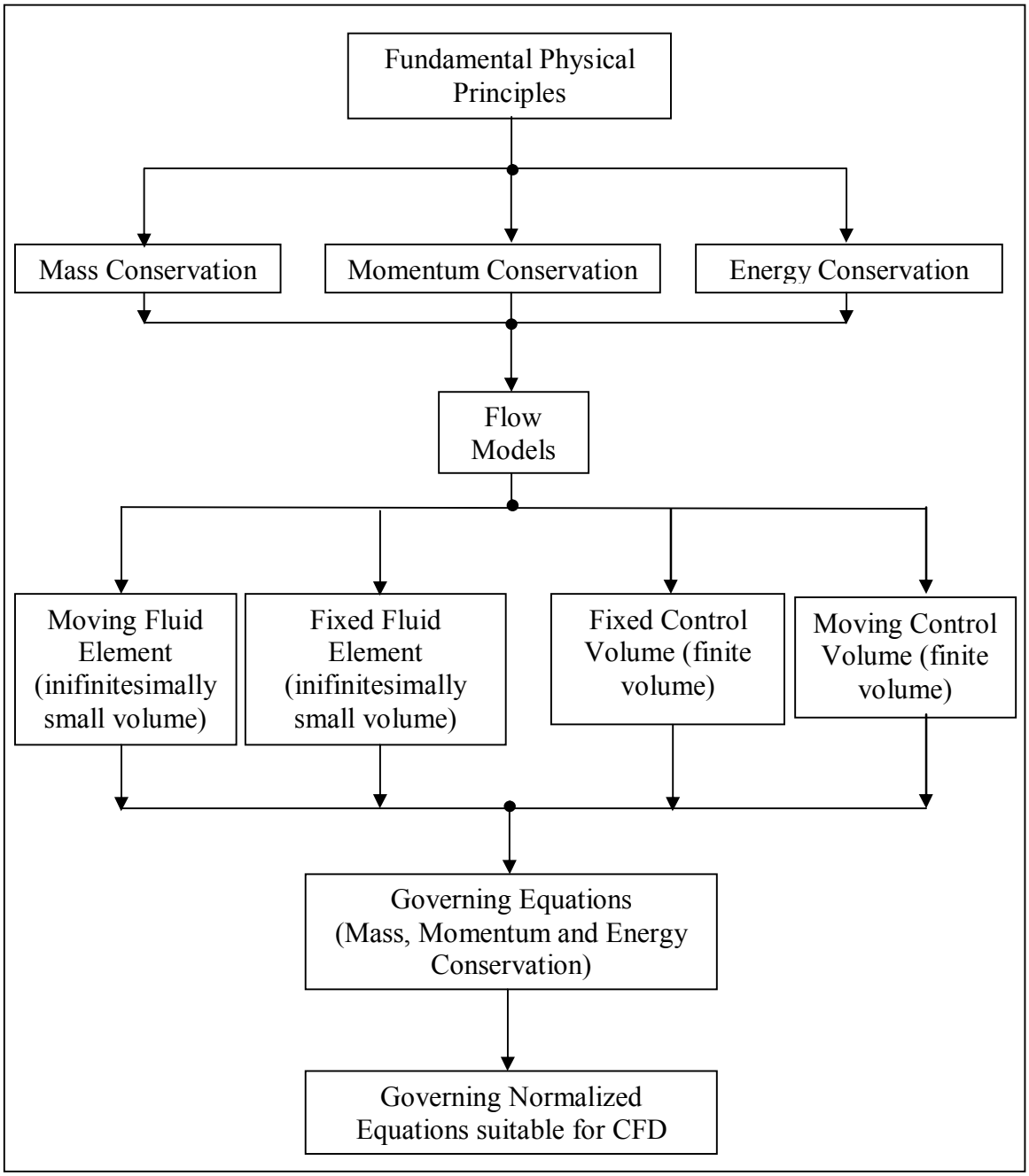

Figure 4.3. The map showing the processes taken before the CFD calculations [11]

As a result, as previously mentioned CFD has a very broaden application area including the aerodynamics of automobiles and aircrafts, hydrodynamics of ships, turbomachinery, pumps and turbines, heat transfer systems like heating and cooling systems, combustion, building ventilations, transport of pollutants, pipe networks, reservoirs, channels, flow of rivers, ocean currents, tidal flows, numerical weather forecasting, plasma flows, blood flow in heart and veins, circuitry cooling, etc.

4.1. The Main Properties of Numerical Solution Methods

Since numerical methods are used to solve some physical problems as good as possible they must have some properties such as accuracy, consistency, stability, realizability, boundedness, etc.

4.1.1. Accuracy

The word accuracy roughly shows how close the results to the real ones are. During the numerical solutions to the problems there are always some errors such as modelling errors, which arise from the difference between the real problem and its mathematical representation, discretization errors, which arise from the difference between exact solution of algebraic equations and solutions after discretizing them and iteration errors, which are due to the fact that the numerical solutions are obtained after some iterations which may have some mathematical errors. Some of these errors are systematic and unavoidable in nature.

The one who does the numerical solutions must be aware of the existence of these errors. In order to decrease the errors coming from disctretization it is better to use finer grids. The order of the approximation is a real measure of accuracy. The errors arising from the iteration processes and from rounf-off are easy to control. The main objective of the code developers is to have better accuracy with less effort [12].

4.1.2. Consistency

The 'truncation error' as a definition is an error which arises from the difference between the exact equation and the discretized one. For a method to be consistent the truncation error must be zero when the mesh spacing $\Delta x_i \to 0$ and $\Delta t \to 0$. Even though the consistency is achieved it does not mean that the solution of discretized equations is the same as the exact solutions to the differential equations.

4.1.3. Stability

If the errors are not increasing during the numerical solution process the numerical solution is said to be stable. If an iterative solution is stable there is no divergence from the correct solution.

4.1.4. Convergence

For convergence, as the grid spacing goes to zero, the discretized equations should tend to the exact solutions of the differential equations. The consistency is useless without the convergence of the method. For small grids the rate of convergence is dominated by the order of truncation error.

4.1.5. Conservation

The numerical schemes must obey the conservation laws because of the fact that the governing equations solved with these methods are real conservation laws in nature.

4.1.6. Boundedness

Every solution must be physically meaningful after numerical discretizations. For example physical properties such as density, kinetic energy, etc. must always be positive in solutions. Boundedness is a difficult condition to guarantee, however there exist some techniques to check the physical bounds.

4.1.7. Realizability

The numerical solutions dealing with complex problems must be designed in a way that they can guarantee physically realistic solutions.

4.2. Space Discretization Techniques

The task of the discretization technique is to transform the differential equations in the following form:

$$\frac{\partial U(\vec{r},t)}{\partial t} + \frac{\partial F_i(U(\vec{r},t))}{\partial r_i} = S(U(\vec{r},t)) \tag{4.1}$$

where $U(\vec{r},t)$ is a vector of conserved variables, $F_i(U(\vec{r},t))$ is the flux vector in the r_i direction, and $S(U(\vec{r},t))$ is the source term. To solve Equation 4.1 one needs to convert coresponding boundary conditions into a set of algebraic equations which can be solved numerically. A lot of physical problems deal with the equations such as in Equation 4.1. These equations are modelled by different conservation laws. Since everything is solved on discrete points during the disctretization, some discretization errors are automatically introduced to the solutions [13].

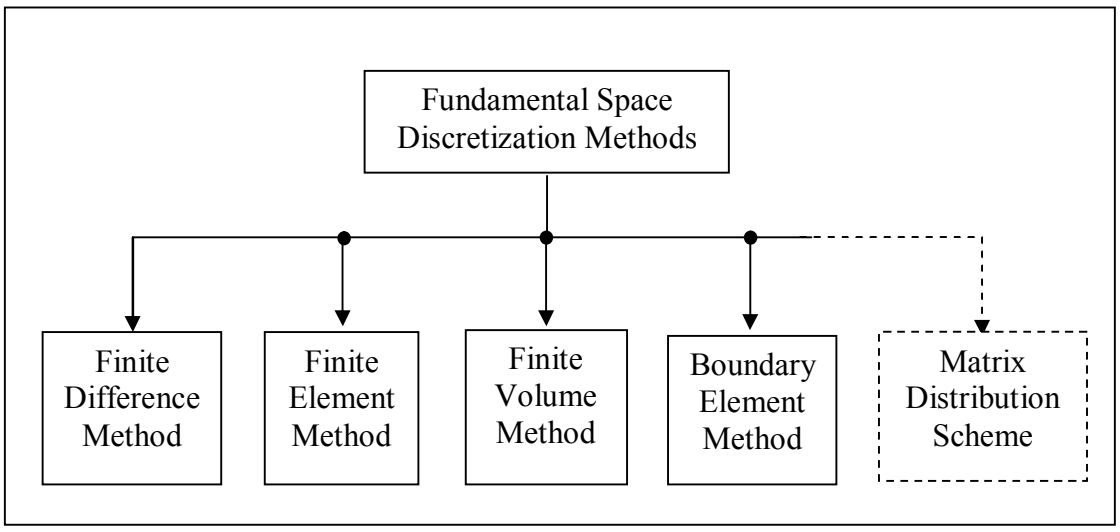

Figure 4.4. The mostly used space discretization methods

Differently from the analytical methods which give the solutions correctly and accurately through the whole domain, the numerical solutions are obtained only on discrete points called the grid points.

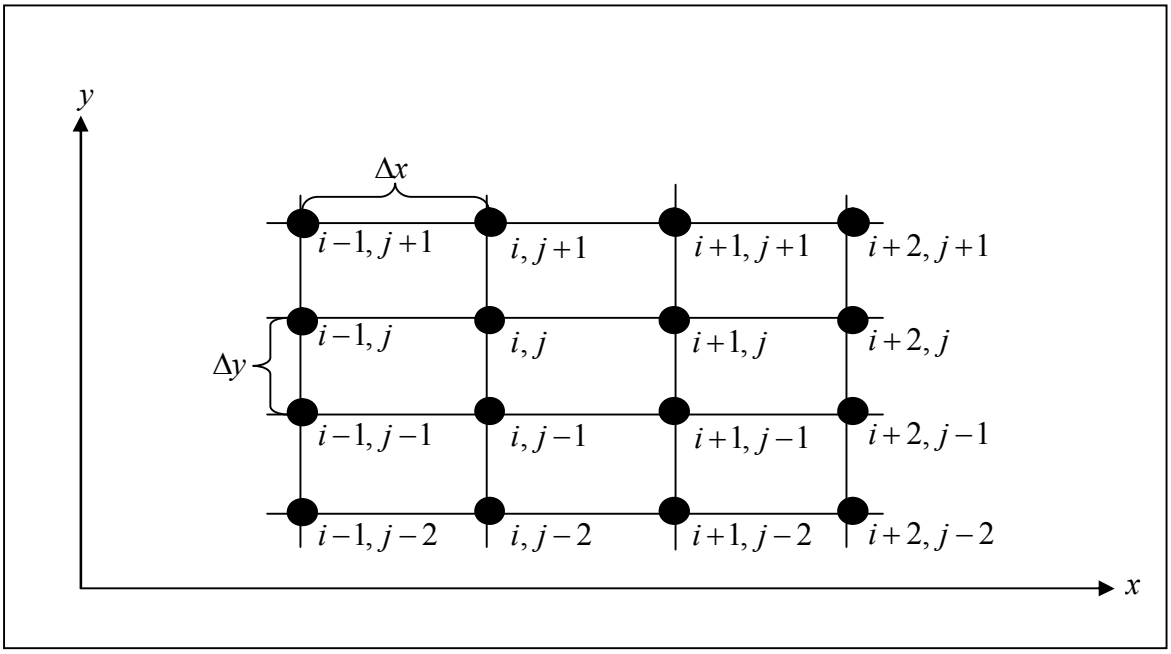

Figure 4.5. Two dimensional discretized solution domain

A domain chosen for solution of governing differential equations is shown in Figure 4.5, where a rectangular domain is divided into subdomains by discrete points called nodes. For convenience spacings Δx and Δy are taken as constant for simplicity. However sometimes it may be necessary to take them varying. The grid shown in Figure 4.5 is called the 'structured grid'. In structured grids the nodes are placed regularly (i.e., Δx and Δy are constant). In 'unstructured' grids the nodes are placed in an irregular fashion to cope with domains with complicated boundaries.

The space discretization is done by using mostly five different techniques which are finite element, finite difference, finite volume, boundary element and recently developed matrix distribution methods. These techniques will be mentioned briefly in chronological order of invention of technique.

4.2.1. Finite Difference Method

In 1910 at the Royal Society of London, Richardson presented a paper on the first 'finite difference method' which is simply presented by the abbrevation FDM. Earlier applications of FDM in CFD started with Courant, Friedrichs, and Lewy in 1928, Evans and Harlow in 1957, Godunov in 1959, Lax and Wendroff in 1960, among others up to date [14].

Historically FDM has dominated the CFD community in early studies about discretization techniques.

The finite difference method is actually based on Taylor's series expansion which is basically given as (in 1 dimension in Cartesian geometry):

$$f(x+\Delta x) = f(x) + \frac{\partial f}{\partial x}\Delta x + \frac{\partial^2 f}{\partial x^2}\frac{(\Delta x)^2}{2} + \frac{\partial^3 f}{\partial x^3}\frac{(\Delta x)^3}{6} + \ldots + \frac{\partial^n f}{\partial x^n}\frac{(\Delta x)^n}{n!}. \qquad (4.2)$$

The Taylor's series given in Equation 4.2 is used to discretize equation on the grid shown in Figure 4.6.

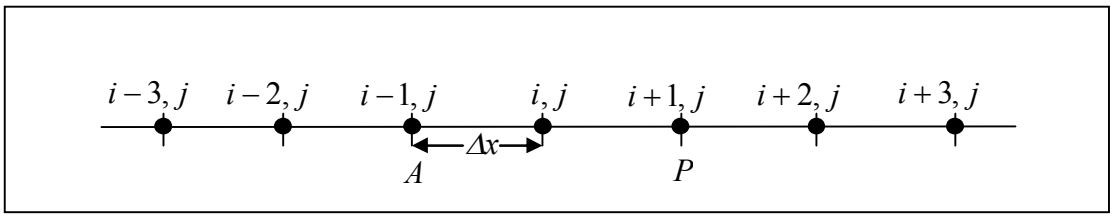

Figure 4.6. One dimensional finite difference grid in Cartesian coordinate system

By using Taylor's expansion and the grid shown in Figure 4.6, any function at point P with the coordinates $(i+1, j)$ can be expressed around point (i, j) as :

$$u_{i+1,j} = u_{i,j} + \left(\frac{\partial u}{\partial x}\right)_{i,j}.\Delta x + \left(\frac{\partial^2 u}{\partial x^2}\right)_{i,j}.\frac{(\Delta x)^2}{2} + \left(\frac{\partial^3 u}{\partial x^3}\right)_{i,j}.\frac{(\Delta x)^3}{6} + \ldots + \left(\frac{\partial^n u}{\partial x^n}\right)_{i,j}.\frac{(\Delta x)^n}{n!}. \qquad (4.3)$$

Again by using Taylor's expansion any quantity of point A with the coordinates $(i-1, j)$ can be around point (i, j) expressed as :

$$u_{i-1,j} = u_{i,j} - \left(\frac{\partial u}{\partial x}\right)_{i,j} .\Delta x + \left(\frac{\partial^2 u}{\partial x^2}\right)_{i,j} .\frac{(\Delta x)^2}{2} - \left(\frac{\partial^3 u}{\partial x^3}\right)_{i,j} .\frac{(\Delta x)^3}{6} + \ldots + \left(\frac{\partial^n u}{\partial x^n}\right)_{i,j} .\frac{(\Delta x)^n}{n!} . \quad (4.4)$$

By taking the Equation 4.3 into account the first derivative is expressed as follows:

$$\left(\frac{\partial u}{\partial x}\right)_{i,j} = \frac{u_{i+1,j} - u_{i,j}}{\Delta x} - \left(\frac{\partial^2 u}{\partial x^2}\right)_{i,j} .\frac{(\Delta x)}{2} - \left(\frac{\partial^3 u}{\partial x^3}\right)_{i,j} .\frac{(\Delta x)^2}{6} - \ldots - \left(\frac{\partial^n u}{\partial x^n}\right)_{i,j} .\frac{(\Delta x)^{n-1}}{n!} . \quad (4.5)$$

The first term on the right hand side of Equation 4.5 is the forward finite difference representation of the actual derivative $(\partial u/\partial x)_{i,j}$. The residual part of the right hand side of the equation (except the first term) is called as 'truncation error'. By using the Equation 4.4 one can write

$$\left(\frac{\partial u}{\partial x}\right)_{i,j} = \frac{u_{i,j} - u_{i-1,j}}{\Delta x} + \left(\frac{\partial^2 u}{\partial x^2}\right)_{i,j} .\frac{(\Delta x)}{2} - \left(\frac{\partial^3 u}{\partial x^3}\right)_{i,j} .\frac{(\Delta x)^2}{6} + \ldots - \left(\frac{\partial^n u}{\partial x^n}\right)_{i,j} .\frac{(\Delta x)^{n-1}}{n!} \quad (4.6)$$

showing a similar derivative which is backward.

The derivatives from Equation 4.5 and Equation 4.6 can be written with first order accuracy as follows:

$$\left(\frac{\partial u}{\partial x}\right)_{i,j} = \frac{u_{i+1,j} - u_{i,j}}{\Delta x} + \Theta(\Delta x) \quad (4.7)$$

$$\left(\frac{\partial u}{\partial x}\right)_{i,j} = \frac{u_{i,j} - u_{i+1,j}}{\Delta x} + \Theta(\Delta x). \quad (4.8)$$

The method shown as Equation 4.7 is called 'forward difference' and the method shown as Equation 4.8 is called 'backward difference' method. There is one more method

obtained from the subtraction of Equation 4.4 from Equation 4.3. This method is called the 'central difference' which is of second order accurate is obtained as follows:

$$u_{i+1,j} - u_{i-1,j} =$$
$$\left[u_{i,j} + \left(\frac{\partial u}{\partial x}\right)_{i,j} \Delta x + \left(\frac{\partial^2 u}{\partial x^2}\right)_{i,j} \frac{(\Delta x)^2}{2} + \left(\frac{\partial^3 u}{\partial x^3}\right)_{i,j} \frac{(\Delta x)^3}{6} + \ldots + \left(\frac{\partial^n u}{\partial x^n}\right)_{i,j} \frac{(\Delta x)^n}{n!} \right] -$$
$$\left[u_{i,j} - \left(\frac{\partial u}{\partial x}\right)_{i,j} \Delta x + \left(\frac{\partial^2 u}{\partial x^2}\right)_{i,j} \frac{(\Delta x)^2}{2} - \left(\frac{\partial^3 u}{\partial x^3}\right)_{i,j} \frac{(\Delta x)^3}{6} + \ldots + \left(\frac{\partial^n u}{\partial x^n}\right)_{i,j} \frac{(\Delta x)^n}{n!} \right] \quad (4.9)$$

$$u_{i+1,j} - u_{i-1,j} = \left[2\left(\frac{\partial u}{\partial x}\right)_{i,j} \Delta x + 2\left(\frac{\partial^3 u}{\partial x^3}\right)_{i,j} \frac{(\Delta x)^3}{6} + \ldots \right] \quad (4.10)$$

$$\left(\frac{\partial u}{\partial x}\right)_{i,j} = \frac{u_{i+1,j} - u_{i-1,j}}{2\Delta x} + \Theta(\Delta x)^2 . \quad (4.11)$$

The central representation given in Equation 4.11 is called 'the second order central difference' formulation. The word 'order ' provides some information about the truncation error or the part of expansion which is neglected in the differential approximation.

In order to solve Navier-Stokes equations not only the first derivative but also the second order derivatives are needed. By adding Equation 4.3 and Equation 4.4 the representation in Equation 4.12 is obtained and it is called 'second order central second derivative'.

$$\left(\frac{\partial^2 u}{\partial x^2}\right)_{i,j} = \frac{u_{i+1,j} - 2u_{i,j} + u_{i-1,j}}{(\Delta x)^2} + \Theta(\Delta x)^2 . \quad (4.12)$$

The equations above are written for variable x in one dimension, the same representation can be used for another variable (say y) in the same fashion. Equation 4.12 can be written for y in the following manner

$$\left(\frac{\partial^2 u}{\partial y^2}\right)_{i,j} = \frac{u_{i,j+1} - 2u_{i,j} + u_{i,j-1}}{(\Delta y)^2} + \Theta(\Delta y)^2 \tag{4.13}$$

where $\Theta(\Delta y)^2$ represents the terms having $(\Delta y)^2$ or higher order.

In addition to the equations derived the mixed derivative representations are also needed (for viscosity etc.) during the numerical solution processes. The derivation for the mixed derivative representation is relatively difficult.

In order to have numerical representatıon for mixed derivatives the extra differentiation technique is used. By differentiating Equation 4.3 with respect to the variable y one gets

$$\frac{\partial}{\partial y}\left[u_{i+1,j} = u_{i,j} + \left(\frac{\partial u}{\partial x}\right)_{i,j}\Delta x + \left(\frac{\partial^2 u}{\partial x^2}\right)_{i,j}\frac{(\Delta x)^2}{2} + \left(\frac{\partial^3 u}{\partial x^3}\right)_{i,j}\frac{(\Delta x)^3}{6} + \ldots + \left(\frac{\partial^n u}{\partial x^n}\right)_{i,j}\frac{(\Delta x)^n}{n!}\right] \tag{4.14}$$

$$\left(\frac{\partial u}{\partial y}\right)_{i+1,j} = \left(\frac{\partial u}{\partial y}\right)_{i,j} + \left(\frac{\partial^2 u}{\partial y \partial x}\right)_{i,j}\Delta x + \left(\frac{\partial^3 u}{\partial y \partial x^2}\right)_{i,j}\frac{(\Delta x)^2}{2} + \left(\frac{\partial^4 u}{\partial y \partial x^3}\right)_{i,j}\frac{(\Delta x)^3}{6} + \ldots . \tag{4.15}$$

If the same differentiation is done for the Equation 4.4

$$\left(\frac{\partial u}{\partial y}\right)_{i-1,j} = \left(\frac{\partial u}{\partial y}\right)_{i,j} - \left(\frac{\partial^2 u}{\partial y \partial x}\right)_{i,j}\Delta x + \left(\frac{\partial^3 u}{\partial y \partial x^2}\right)_{i,j}\frac{(\Delta x)^2}{2} + \left(\frac{\partial^4 u}{\partial y \partial x^3}\right)_{i,j}\frac{(\Delta x)^3}{6} + \ldots \tag{4.16}$$

is obtained. When Equation 4.16 is subtracted from Equation 4.15 one gets

$$\left(\frac{\partial u}{\partial y}\right)_{i+1,j} - \left(\frac{\partial u}{\partial y}\right)_{i-1,j} =$$

$$\left[\left(\frac{\partial u}{\partial y}\right)_{i,j} + \left(\frac{\partial^2 u}{\partial y \partial x}\right)_{i,j} \Delta x + \left(\frac{\partial^3 u}{\partial y \partial x^2}\right)_{i,j} \frac{(\Delta x)^2}{2} + \left(\frac{\partial^4 u}{\partial y \partial x^3}\right)_{i,j} \frac{(\Delta x)^3}{6} + \ldots\right] - \tag{4.17}$$

$$\left[\left(\frac{\partial u}{\partial y}\right)_{i,j} - \left(\frac{\partial^2 u}{\partial y \partial x}\right)_{i,j} \Delta x + \left(\frac{\partial^3 u}{\partial y \partial x^2}\right)_{i,j} \frac{(\Delta x)^2}{2} + \left(\frac{\partial^4 u}{\partial y \partial x^3}\right)_{i,j} \frac{(\Delta x)^3}{6} + \ldots\right]$$

which leads to

$$\left(\frac{\partial u}{\partial y}\right)_{i+1,j} - \left(\frac{\partial u}{\partial y}\right)_{i-1,j} = 2\left(\frac{\partial^2 u}{\partial y \partial x}\right)_{i,j} \Delta x + \left(\frac{\partial^4 u}{\partial y \partial x^3}\right)_{i,j} \frac{(\Delta x)^3}{6} + \ldots \tag{4.18}$$

is derived.

By taking out the mixed derivative which is the first term on the right hand side of the Equation 4.18

$$\left(\frac{\partial^2 u}{\partial y \partial x}\right)_{i,j} = \frac{\left(\frac{\partial u}{\partial y}\right)_{i+1,j} - \left(\frac{\partial u}{\partial y}\right)_{i-1,j}}{2\Delta x} - \left(\frac{\partial^4 u}{\partial y \partial x^3}\right)_{i,j} \frac{(\Delta x)^3}{12} + \ldots \tag{4.19}$$

is found. In order to find the final numerical representation for mixed derivative one can use the following

$$\left(\frac{\partial u}{\partial y}\right)_{i+1,j} = \frac{u_{i+1,j+1} - u_{i+1,j-1}}{2\Delta y} + \Theta(\Delta y)^2 \tag{4.20}$$

$$\left(\frac{\partial u}{\partial y}\right)_{i-1,j} = \frac{u_{i-1,j+1} - u_{i-1,j-1}}{2\Delta y} + \Theta(\Delta y)^2 . \tag{4.21}$$

In that case, one obtains

$$\left(\frac{\partial^2 u}{\partial y \partial x}\right)_{i,j} = \frac{u_{i+1,j+1} - u_{i+1,j-1} - (u_{i-1,j+1} - u_{i-1,j-1})}{2\Delta x.2\Delta y} + \Theta(\Delta x, \Delta y)^2 . \qquad (4.22)$$

The representation given in Equation 4.22 is called the 'second order central difference for mixed derivative'.

These expressions are relatively easy in comparing the numerical representations for derivatives in the boundaries.

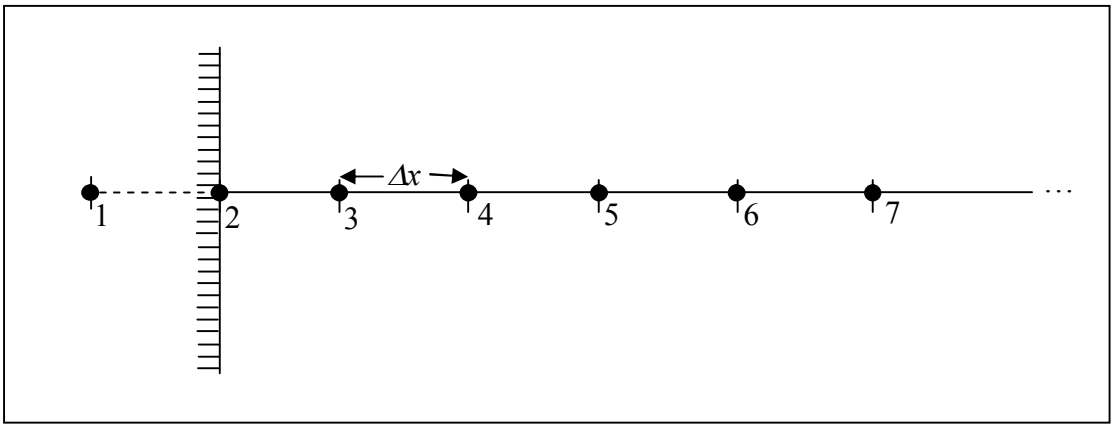

Figure 4.7. One dimensional Cartesian mesh with the boundary on the left

The first derivative representation for finite difference method as forward difference on point $i = 2$ shown in Figure 4.7 is easily written as:

$$\left(\frac{\partial u}{\partial x}\right)_2 = \frac{u_3 - u_2}{\Delta x} + \Theta(\Delta x) . \qquad (4.23)$$

The central difference which is of second order accurate formula for point 2 can not be written since the point 1 which is outside the solution domain is needed. The information about node number 1 is generally known from the domain which surrounds the left side of node 2. It is easily seen that Taylor series expansion does not provide the solution for second order accurate finite difference representation. In order to have the

solutions for boundaries the polynomial approach can be used. The second order polynomial representation of u is given similar to [11] as:

$$u = A_p + B_p x + C_p x^2 + \Theta(\Delta x^3). \tag{4.24}$$

Taking $x = 0$ for node number 2, $x = \Delta x$ for node number 3, $x = 2\Delta x$ for node number 4, $x = 3\Delta x$ for node number 5…. By taking these values into account one can write :

$$u_2 = A_p \tag{4.25}$$

$$u_3 = A_p + B_p \Delta x + C_p (\Delta x)^2 \tag{4.26}$$

$$u_4 = A_p + B_p (2\Delta x) + C_p (2\Delta x)^2. \tag{4.27}$$

Using Equations 4.25-4.27 one can find

$$B_p = \frac{-3u_2 + 4u_3 - u_4}{2\Delta x}. \tag{4.28}$$

By taking the derivative of Equation 4.24 at node number 2 with respect to x,

$$\left(\frac{\partial u}{\partial x}\right)_2 = B_p + 2C_p x\Big|_{x=0}^{\Theta(\Delta x^3)} = B_p + \Theta(\Delta x^3) \tag{4.29}$$

is obtained since $x = 0$ for node number 2. Using these results in Equation 4.28 one gets:

$$\left(\frac{\partial u}{\partial x}\right)_2 = \frac{-3u_2 + 4u_3 - u_4}{2\Delta x} + \Theta(\Delta x^3) \tag{4.30}$$

which shows that the second derivative can be defined as in Equation 4.30 with second order accuracy if two more nodes are used within the domain.

Since the node points, which were used during the derivation of the expression given as Equation 4.30, are only on one side of the boundary, these kinds of representations are called 'one sided differences'. The similar equations are not only used for the boundaries but also they can be used in the internal nodes.

During the derivation of Equation 4.30 only three nodes were used. However more nodes can be used for the same derivations and mostly more accurate results can be obtained. However, the order of accuracies in the interior and in the boundaries must be the same.

Using the definitions so far one can solve one dimensional heat conduction given in as in Equation 4.31 [11].

$$\frac{\partial T}{\partial t} = \alpha_t \frac{\partial^2 T}{\partial x^2} \tag{4.31}$$

Here $T(x,t)$ represents the temperature and it is a function of both displacement x and time t. In addition, α_t is the thermal diffusivity coefficient which is assumed to be constant for simplification. Also the displacements between the nodes for x and for t are chosen to be equal, see Figure 4.8.

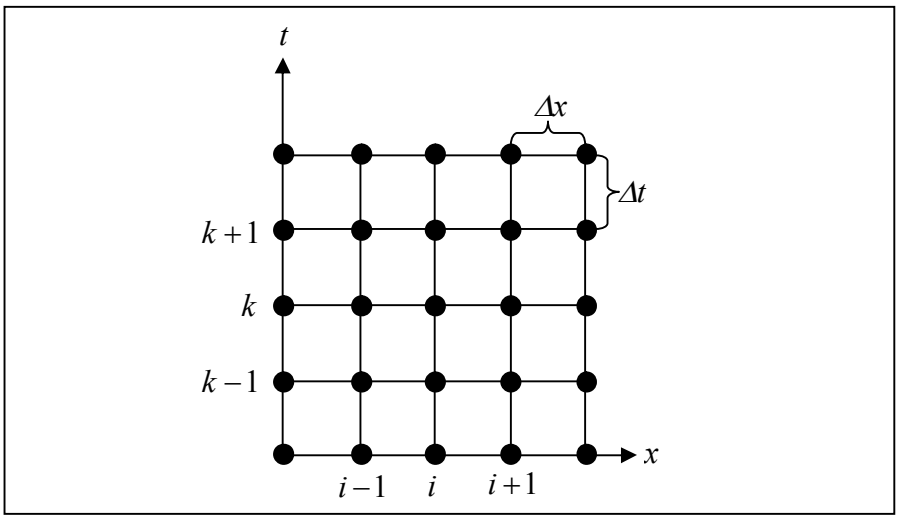

Figure 4.8. Two dimensional solution domain which can represent the example given as Equation 4.31

Left hand side of Equation 4.31 can be represented as

$$\left(\frac{\partial T}{\partial t}\right)_i^k = \frac{T_i^{k+1} - T_i^k}{\Delta t} + \left(\frac{\partial^2 T}{\partial t^2}\right)_i^k \frac{\Delta t}{2} + \left(\frac{\partial^3 T}{\partial t^3}\right)_i^k \frac{\Delta t^2}{6} + \ldots \tag{4.32}$$

and right hand side as

$$\left(\frac{\partial^2 T}{\partial x^2}\right)_i^k = \frac{T_{i+1}^k - 2T_i^k + T_{i-1}^k}{\Delta x^2} + \left(\frac{\partial^4 T}{\partial x^4}\right)_i^k \frac{\Delta x^2}{12} + \ldots \quad . \tag{4.33}$$

Inserting Equation 4.32 and Equation 4.33 into Equation 4.31 one gets

$$\frac{T_i^{k+1} - T_i^k}{\Delta t} + \left(\frac{\partial^2 T}{\partial t^2}\right)_i^k \frac{\Delta t}{2} + \left(\frac{\partial^3 T}{\partial t^3}\right)_i^k \frac{\Delta t^2}{6} + \ldots = \frac{T_{i+1}^k - 2T_i^k + T_{i-1}^k}{\Delta x^2} + \left(\frac{\partial^4 T}{\partial x^4}\right)_i^k \frac{\Delta x^2}{12} + \ldots \quad . \tag{4.34}$$

After some rearrangements, Equation 4.34 turns into

$$\frac{T_i^{k+1} - T_i^k}{\Delta t} - \frac{\alpha_t \left(T_{i+1}^k - 2T_i^k + T_{i-1}^k\right)}{\Delta x^2} + \left[\left(\frac{\partial^2 T}{\partial t^2}\right)_i^k \frac{\Delta t}{2} + \left(\frac{\partial^3 T}{\partial t^3}\right)_i^k \frac{\Delta t^2}{6} . + \ldots\right] - \left[\left(\frac{\partial^4 T}{\partial x^4}\right)_i^k \frac{\Delta x^2}{12} + \ldots\right] = 0 \tag{4.35}$$

where time discretization is 1st order accurate and space discretization is of 2nd order accurate. Finite difference method is not only the oldest but also is the easiest method used for simple geometries for solutions of partial differential equations. The main disavantage of the method is the unapplicability to the complex geometries since indexing becomes extremely difficult.

4.2.2. Finite Element Method

One of the most important discretization techniques is finite element method (with abbrevation FEM). This method is based on the idea which breaks the domain into a set of discrete elements that are generally unstructured. In two dimensions they are usually triangles or quadrilaterals, in three dimensions they are tetrahedra or hexahedra. The most important feature of the technique is that the equations are multiplied by a basis functions before they are integrated over the entire domain [12]. In 1956 in the Aeronautical Science Journal the first FEM studies were published by Turner, Glough, Topp and Martin. This work was done for the applications to aircraft stress analysis. The first one of the main advantages of finite element method is the applicability to any arbitrary shape and dimensions. The shape can be made of different materials and their properties can be nonhomogeneous (depending on location) or anisotropic (depending on the direction). Finite element method converts the governing equations to the matrix equations which can be solved numerically. FEM solves a set of related equations by approximating continuous field variables as a set of field variables at discrete points previously named as nodes. FEM solutions are achieved by either eliminating the differential equation completely (steady state problems), or rendering the partial differential equations PDE, into an equivalent ordinary differential equations which is then solved using standard techniques such as finite differences.

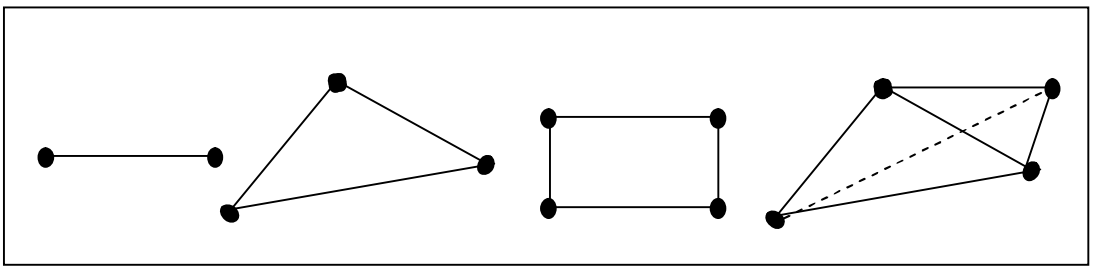

Figure 4.9. Different shapes for finite elements with corner nodes

One of the biggest advantages of finite element method is the applicability to the problems with very great complexity and unusual geometry. The solution for the problem given in Equation 4.1 is considered in the form given below.

$$U(\vec{r},t)=\sum_{i=1}^{n}N_i(\vec{r})U_i(t) \tag{4.36}$$

where $\vec{r}$ is the position vector, U_i is the value of U in the node i, n is the number of the nodes and finally $N_i(\vec{r})$ are the nodal basis functions which have the propery given as in Equation (4.37).

$$N_i(\vec{r}_j)=\delta_{ij} \tag{4.37}$$

where δ_{ij} is Kronecker delta function. $N_i(\vec{r})$ is the function whose geometrical shape is given in Figure 4.9. The expression given in Equation 4.1 is transformed to the equivalent integral formulation by the help of the definition given in Equation 4.36. Then expression is found by replacing U by Equation 4.36 and integrating Equation 4.31 over the solution domain, Ω, after being multiplied by weight function w_i.

$$\iint_{\Omega}\frac{\partial}{\partial t}(\sum_{i=1}^{n}N_iU_i)w_j d\Omega+\iint_{\Omega}\frac{\partial F_k}{\partial r_k}w_j d\Omega=\iint_{\Omega}Sw_j d\Omega\,. \tag{4.38}$$

In Equation 4.38 the index, i, changes from 1 to the number of nodes. Every node has its own value related to the Equation 4.38. The two equations, Equation 4.1 and Equation 4.38 are equivalent if and only if Equation 4.38 holds for all possible choises of the weight function [13]**.** The weight function w_j and its first order derivatives must be integrable [15].

If the weight function w_j are identical with the basis functions $N_i(\vec{r})$ then the classical Galerkin finite element method is obtained. If the functions, $N_i(\vec{r})$ and $w_j(\vec{r})$, are not identical the Petrov-Galerkin finite element method is obtained.

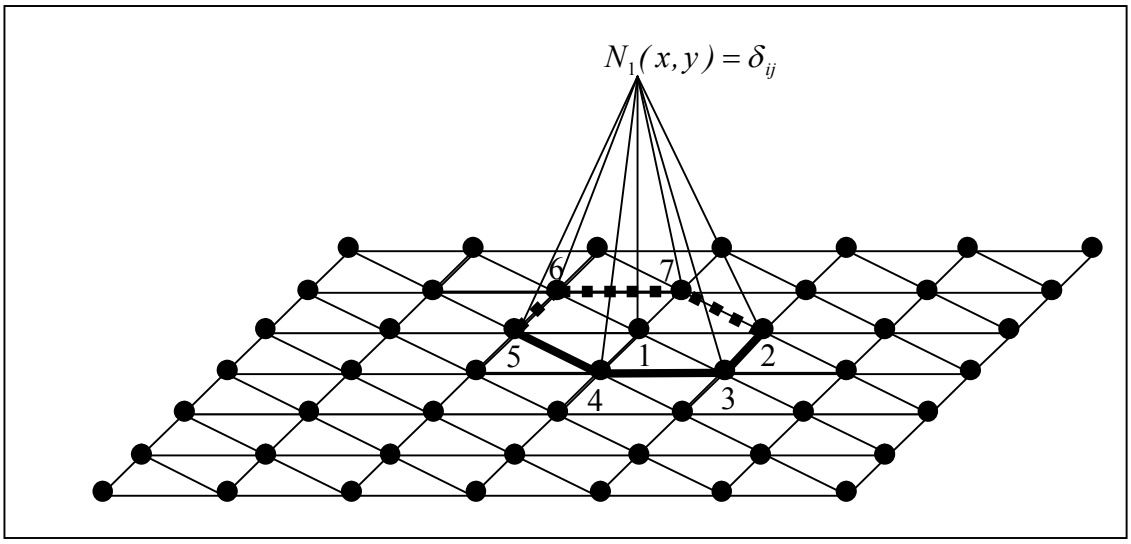

Figure 4.10. The shape of linear nodal basis function

The solution domain in two dimensions given in Figure 4.10 is divided to finite elements which are triangles in this example. The steady advection equation given by

$$u\frac{d\phi}{dx}=0 \tag{4.39}$$

is considered and its FEM representation is desired to be written in one dimensional Cartesian grid shown in Figure 4.6. Multiplying Equation (4.39) by $w_i(x)$ and taking $\phi(x)=\sum_{j=1}^{n}N_j(x)\phi_i(x)$ one gets

$$\int_{\Omega} w_i(x)u\sum_{j=1}^{n}\frac{dN_j(x)}{dx}\phi_i d\Omega=0\,. \tag{4.40}$$

If Galerkin method (i. e., $w_i(x)=N_i(x)$) is used on a structured grid, Equation 4.40 for the node i becomes

$$\frac{u(\phi_{i+1}-\phi_{i-1})}{2}=0\,. \tag{4.41}$$

The result obtained in Equation 4.41 is similar to the result obtained by using Finite Difference Method in Equation 4.11.

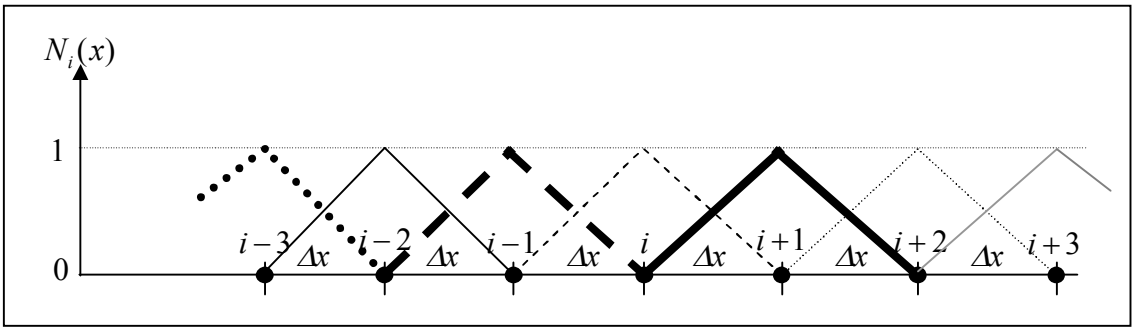

Figure 4.11. Basis functions (piecewise linear and tent shaped) for the nodes with numbers betweeen $i-3$ and $i+3$

There is one dimensional solution domain in Figure 4.11 in which the finite elements are placed between two neighbouring nodes.

Actually the applications of finite element methods are divided into three main categories. The first part which mostly uses the finite element method is based on the problems called 'equilibrium problems' which are also called as 'time-independent problems'. The second part of the problems are eigenvalue problems dealing with the solid mechanics and mostly fluid mechanics. The third category is time dependent or propagation problems in continuum mechanics. Considering all categories one finds out that finite element method is mostly used in the areas such as fluid mechanics, heat transfer, solid mechanics, electromagnetism, etc.

Comparing with finite difference method, finite element method contains more complex algebra but this property makes finite element method more useful for the multidimensional and arbitrary geometries.

4.2.3. Finite Volume Method

Finite volume method (FVM) basically utilizes the integral form of governing equations. The solution domain in this method is divided into the control volumes in finite

numbers. Then the conservation equations are applied to each control volume . The computational node is located at the centre of the control volume and the computations are done at that point. The need for knowing the variable values at the surface of the control volumes to get fluxes is established by using the interpolation in terms of the nodes located in the centres [12].

The finite volume approach is mostly the simplest one for programming but requires several neighbouring cells for defining higher order fluxes at the interfaces between cells.

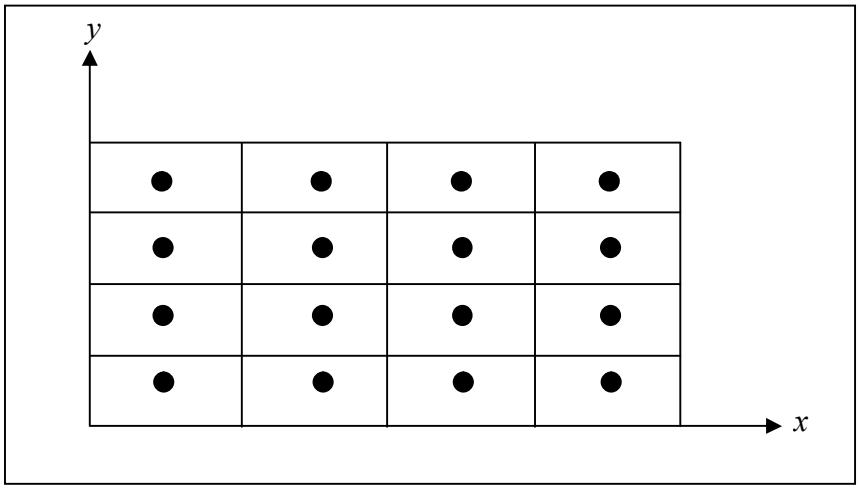

Figure 4.12. The typical rectangular control volumes in a Cartesian grid

In order to understand the method better it is useful to take the Equation 4.1 into account again. The basis of finite volume method is that the differential form of conservation law is integrated after the equation is transformed to integral form. The integration is done over the control volume. Integrating Equation 4.1 within control volume one gets:

$$\int_V \frac{\partial U}{\partial t} dV + \oint_{\partial V} F_i . n_i^{ext} d\partial V = \int_V S_i dV \tag{4.42}$$

by taking the advantage of Gauss' theorem for flux integration.

In Equation 4.43 n_i^{ext} is the component of the unit outward vector in direction i, $\vec{U}$ is the vector containing the conserved variables, $\vec{F}_i$ is the flux vector and $\vec{S}$ is the source vector.

The conservative form of Equation 4.39 can be written as :

$$\frac{du\phi}{dx} = \frac{df_L}{dx} = 0 \tag{4.43}$$

which gives

$$\oint_{\partial V} f_L n_x d\partial V = 0 \tag{4.44}$$

after finite volume integral is taken.

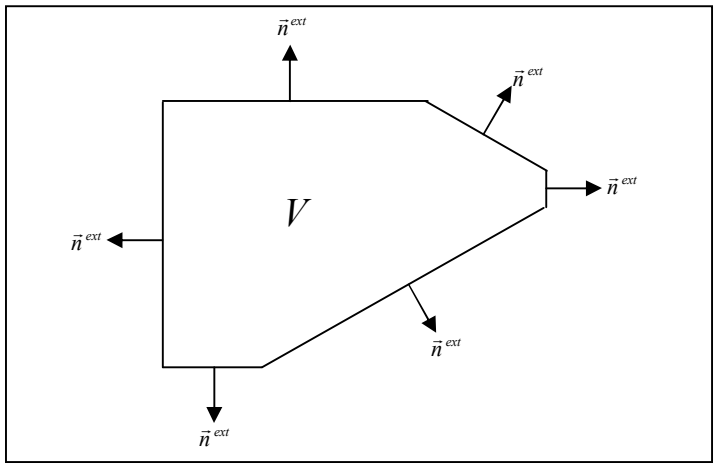

Figure 4.13. Control volume and its unit outward normals

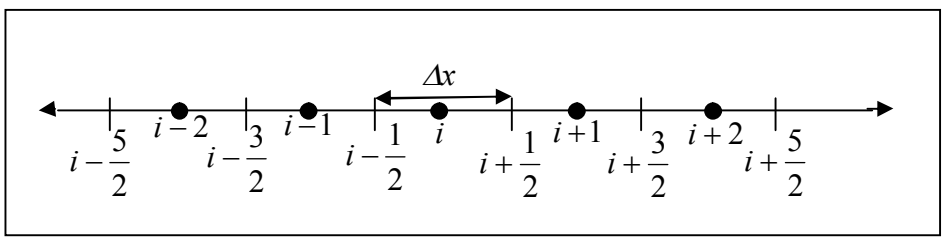

Figure 4.14. Finite volume grid in one dimension

For the grid shown in Figure 4.14, the flux function, $f_L = u\phi$ for the grid point i leads to :

$$f_{L(i+\frac{1}{2})} - f_{L(i-\frac{1}{2})} = 0 . \tag{4.45}$$

Since the physical quantities are defined in nodes $i-2, i-1, i, i+1, i+2$ the flux at the boundary between i and $i+1$ can be taken as

$$f_{L(i+\frac{1}{2})} = \frac{f_{L(i+1)} + f_{L(i)}}{2} + \Theta(\Delta x)^2 \tag{4.46}$$

and similarly

$$f_{L(i-\frac{1}{2})} = \frac{f_{L(i)} + f_{L(i-1)}}{2} + \Theta(\Delta x)^2 \tag{4.47}$$

which concludes that they are the second order accurate discretizations.

The accuracy of discretization not only depends on the definition of the flux function but also it depends on the numerical integration used [13].

Using the finite difference method is very difficult when the coefficients of equations have discontinuities. However, for finite volume method these discontinuities will not be a very big problem if the solution domain is divided in such a way that the discontinuities are on the boundaries of the control volumes. From the industrial point of view, finite volume method is known as the cheap and robust discretization method. Actually for high order polynomials finite element is better [16]. The main disadvantage of finite volume method against finite difference method is that the orders higher than second order are more difficult to develop in three dimensions. This is the result of the need for three levels of approximations which are interpolation, differentiation and integration.

4.2.4. Boundary Element Method

The numerical discretization of boundary integral equations are called the boundary element method. The boundary element method (BEM) is a numerical analysis technique used to obtain solutions to the partial differential equations of a variety of physical problems with well defined boundary conditions. The first prominent development in boundary element method is done in 1963 by the Jaswon and Symm [17]. In their study the linear, uniform elements and constant potentials were chosen. The integral equations that are based on the Laplace equation are solved by using Simpsons algorithm [18]. In 1963 Jaswon and Ponter in 1967 Hess and Smith have also worked hardly on the boundary element method for different physical problems [19, 20].

The formulation of boundary element method is based on the boundary integral equations. In this method, the boundaries are reduced by one which leads to the reduction of the number of space dimensions by one. The differential equation defined over the entire domain is transformed into a surface integral over the surface domain that enclosed entirely the solution domain. The surface itself is then divided into the elements called the boundary elements. The major advantage of this method over the finite element method is that the discretization is done only on the surfaces. Therefore the number of the elements are much less than that of the finite element method. The major disadvantage is the difficulty in dividing the surface into elements for nonuniformly shaped domains [21]. One of the advantages over the other techniques is that it works well on the geometries with voids and holes [22].

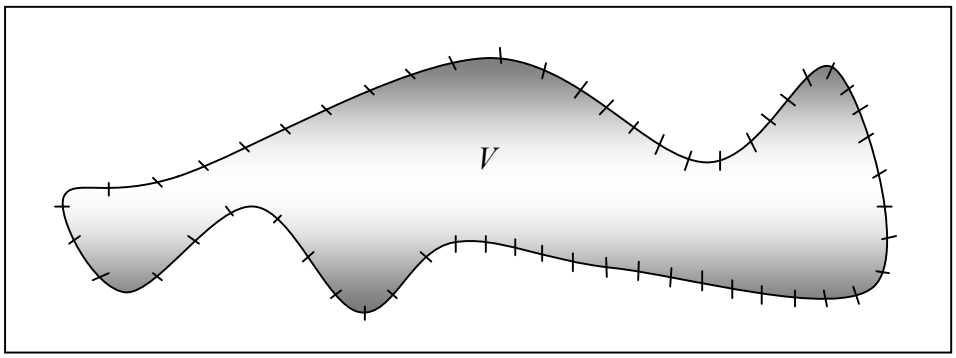

Figure 4.15. The solution domain with volume V and discretized surface covered with boundary elements

To understand the method it is better to assume two different and arbitrary functions which obey the conditions given in the reference [17]**.** These functions are u_f and u_f^*. The function u_f is the variable which is desired to be calculated in reality. The choice of the functions can simplify the complex nature of the equations wanted to be solved. By writing the net flux which is flowing through the boundary in the direction of the normal vector

$$q_f = \frac{\partial u_f}{\partial n} = \vec{\nabla} u_f . \vec{n} \tag{4.48}$$

and the similar expression for the u_f^* is given as :

$$q_f^* = \frac{\partial u_f^*}{\partial n} = \vec{\nabla} u_f^* . \vec{n} . \tag{4.49}$$

By using Green's equation [21] one can write

$$\int_V u_f^* \nabla^2 u_f \, dV - \int_V u_f \nabla^2 u_f^* \, dV = \int_S u_f^* q_f \, dS - \int_S q_f^* u \, dS \tag{4.50}$$

where V is the volume of the solution domain and S is the surface covering the solution domain.

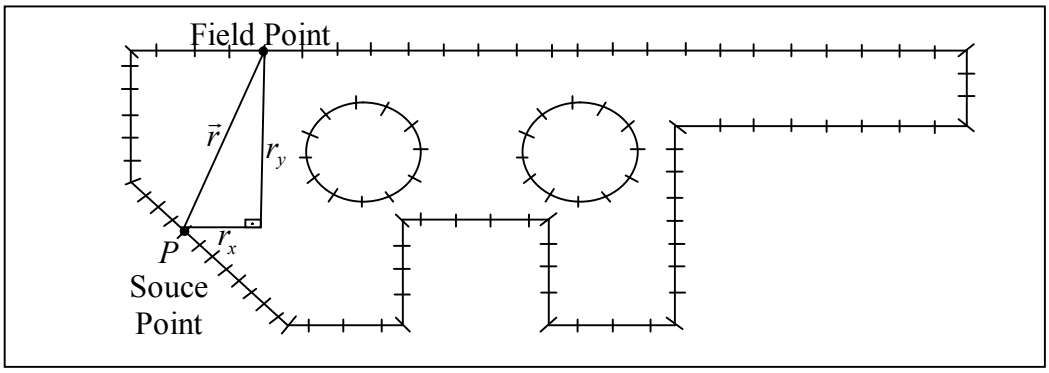

Figure 4.16. Source point and field point on the domain divided into the boundary elements

Point ‘ P ’ which is called the source point can be chosen everywhere in the solution domain. However, in order to form the integral equation it is chosen on the boundary for simplicity. After some definitions given in [17], $u_f(p)$ becomes

$$u_f(p)+\int_S q_f^{\,*} u_f dS = \int_S u_f^{\,*} q_f dS \,. \tag{4.51}$$

$u_f^{\,*}$ and $q_f^{\,*}$ are geometric functions depending only on $\vec{r}$ which is the distance between the source point and the point where the effect of the source is wanted to be calculated. For examle for the isotropic domains $u_f^{\,*}$ can be given as :

$$u_f^{\,*} = \frac{1}{2\pi} ln\left(\frac{1}{\vec{r}}\right) \tag{4.52}$$

and for $q_f^{\,*}$

$$q_f^{\,*} = \frac{\partial u_f^{\,*}}{\partial r}\frac{\partial r}{\partial n} = -\frac{1}{2\pi r^2}(r_x n_x + r_y n_y) \tag{4.53}$$

is obtained.

Since the source point P can be chosen everywhere in the domain $u_f(p)$ is multiplied by the function $c(p)$ which depends on the geometrical position of the source point in the domain. The mathematical definition of $c(p)$ is given as:

$$c(p) = \frac{\theta}{2\pi} \tag{4.54}$$

where θ is the angle related to the part of the source point located in the solution domain.

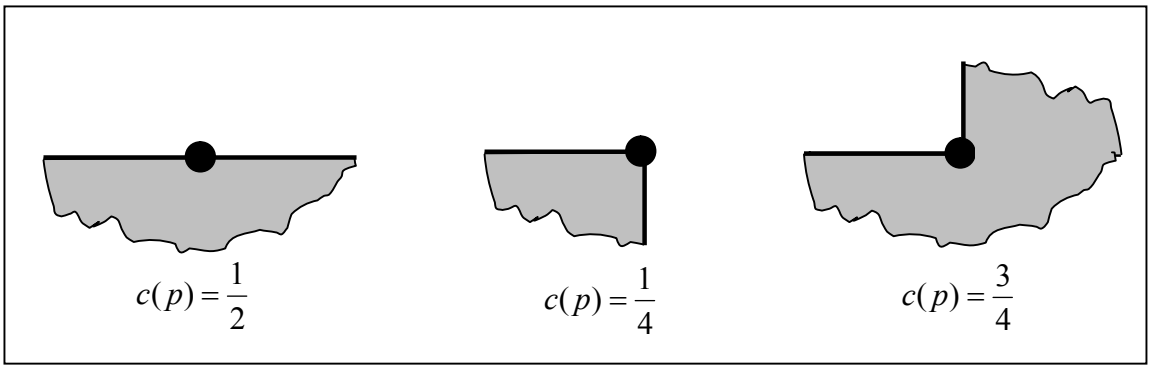

Figure 4.17. The values of $c(p)$ for different geometries

If the source point is chosen to be in the solution domain $c(p)=1$, if it is out of the solution domain $c(p)=0$.

After the multiplication with $c(p)$ is done the integral equation is obtained as:

$$u_f(p)+\int_S \dot{q}_f^{\,*} u dS=\int_S u_f^{\,*} q dS \tag{4.55}$$

This Equation (4.55) can relate all the nodes to each other. After the solution domain is discretized as shown in the Figure 4.16, the boundary integral expression will be

$$c(p)u_f(p)+\sum\int_S q_f^{\,*} u_f dS_i=\sum\int_S u_f^{\,*} q_f dS_i\ . \tag{4.56}$$

The flux of any boundary can be found by doing interpolations. Then the system of equations is transformed to the matrix representations and finally is solved.

Relatively the boundary element method is a new method for discretization compared to the previously mentioned methods. It has some advantages like less time requirement for modelling, the dimensions of the boundaries are reduced by one, for the same accuracy compared with the other methods the element number is less and the computer time used is prominently less, etc. However, there are also some disadvantages in the method such as the need for more complex mathematics, the domains like shells are

difficult domains for solving because of the fact that the elements and nodes are very near each other and this affects the accuracy of solutions, the matrix obtained from the set of equations is not symmetric and there are no zero valued elements.

As a result for the discretization methods mentioned above there are some advantages and disadvantages against each other in different ways.

4.2.5. Matrix Distribution Scheme

This method is a relatively new technique for space discretization. It can be used in MHD equations instead of some conventional discretization techniques such as finite difference, finite element, finite volume. The numerical simulations in this thesis are done in the scope of this matrix distribution scheme. The step by step calculations of MHD equations used in this work are shown below. The main assumption in this scheme is that the value of $\vec{U}$ is changing linearly within the triangles (Equation 4.57). The fluctuations due to these changes are distributed at every node of each triangle by 'distribution matrix' which will be introduced later in this section.

$$U(\vec{r},t) = \sum_{i=1}^{n} N_i(\vec{r})U_i(t) \tag{4.57}$$

In Equation 4.57, $U_i(t)$ is the value of $U(\vec{r},t)$ at node numbered i and $N_i(\vec{r})$ is the linear shape function. If it is assumed that two dimensional space is under consideration then the Equation 4.59 can be written as:

$$U(x,y,t) = \sum_{i=1}^{n} N_i(x,y)U_i(t) \tag{4.58}$$

where $N_i(x_j,y_j) = \delta_{i,j}$ and $\delta_{i,j}$ is Kronecker delta function. Equation 4.1 is in conservative form. The quasi-linear form of it can be written as in Equation 4.59 where A and B are Jacobian matrices.

$$\frac{\partial \vec{U}}{\partial t} + A\frac{\partial \vec{U}}{\partial x} + B\frac{\partial \vec{U}}{\partial y} = \vec{S}_T \tag{4.59}$$

If the pseudo time rate is ignored for now at least and it is multiplied with N_l and integrated the result over the area of triangle given as Ω, will become as:

$$\iint_{\Omega} N_l \frac{\partial \vec{U}}{\partial t} d\Omega = \iint_{\Omega} N_l A\frac{\partial \vec{U}}{\partial x} d\Omega + \iint_{\Omega} N_l B\frac{\partial \vec{U}}{\partial y} d\Omega + \iint_{\Omega} N_l \vec{S}_T d\Omega \ . \tag{4.60}$$

By rearranging the Equation 4.60 a more compact form is obtained

$$\iint_{\Omega}\left(N_l \frac{\partial \vec{U}}{\partial t}\right) d\Omega = \iint_{\Omega} N_l \left(A\frac{\partial \vec{U}}{\partial x} + B\frac{\partial \vec{U}}{\partial y}\right) d\Omega + \iint_{\Omega} N_l \vec{S}_T d\Omega \ . \tag{4.61}$$

By using the definition given in Equation 4.58, the new form for Equation 4.61

$$\iint_{\Omega}\left(N_l \sum_{i=1}^{3} N_i \frac{\partial \vec{U}_i}{\partial t}\right) d\Omega = \iint_{\Omega} N_l \sum_{i=1}^{3} N_i \left(A\frac{\partial \vec{U}_i}{\partial x} + B\frac{\partial \vec{U}_i}{\partial y}\right) d\Omega + \iint_{\Omega} N_l \sum_{i=1}^{3} N_i \vec{S}_T d\Omega \tag{4.62}$$

is obtained. Here the sum inside every triangle runs from 1 to 3, which are the node numbers of the triangle. The global system can be written by a result of summation over the individual triangle T and the final expression can be written in the following way:

$$\sum_{T}\left\{ \iint_{\Omega}\left(N_l \sum_{i=1}^{3} N_i \frac{\partial \vec{U}_i}{\partial t}\right) d\Omega = \iint_{\Omega} N_l \sum_{i=1}^{3} N_i \left(A\frac{\partial \vec{U}_i}{\partial x} + B\frac{\partial \vec{U}_i}{\partial y}\right) d\Omega + \iint_{\Omega} N_l \sum_{i=1}^{3} N_i \vec{S}_T d\Omega \right\} . \tag{4.63}$$

Before proceeding it is better to give some definitions here. If the two dimensional spatial domain Ω, has a triangular shape shown as in Figure 4.18, and 1, 2 and 3 are the local node numbers of the triangle, the inward scaled normals with the length of corresponding faces are given as:

$$\vec{n}_1 = (y_2 - y_3)\hat{x} + (x_3 - x_2)\hat{y} \tag{4.64}$$

$$\vec{n}_2 = (y_3 - y_1)\hat{x} + (x_1 - x_3)\hat{y} \tag{4.65}$$

$$\vec{n}_3 = (y_1 - y_2)\hat{x} + (x_2 - x_1)\hat{y}\,. \tag{4.66}$$

The triangle with the inward normals is shown in the Figure 4.18. [13, 23].

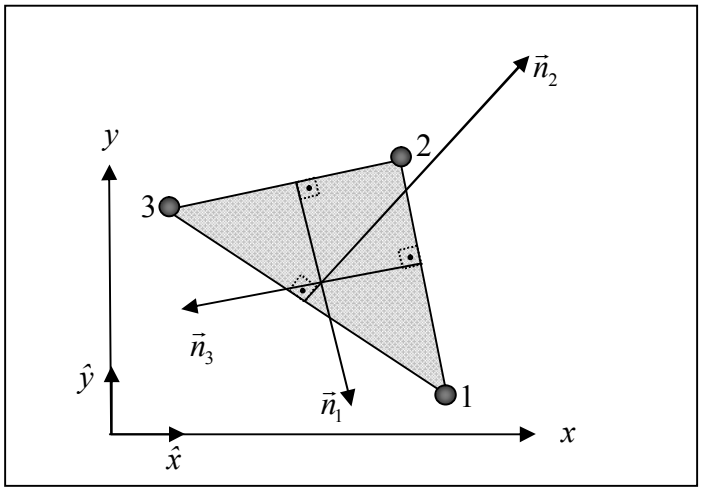

Figure 4.18. Triangle with inward scaled normals

The general formulation for the inward normals is given as:

$$\vec{n}_i = (y_j - y_k)\hat{x} + (x_j - x_k)\hat{y}\,. \tag{4.67}$$

Note that the sum for these three normals vanishes ,

$$\vec{n}_1 + \vec{n}_2 + \vec{n}_3 = (y_2 - y_3)\hat{x} + (x_3 - x_2)\hat{y} + (y_3 - y_1)\hat{x} + (x_1 - x_3)\hat{y} + (y_1 - y_2)\hat{x} + (x_2 - x_1)\hat{y}$$

the result became

$$\vec{n}_1 + \vec{n}_2 + \vec{n}_3 = 0\,. \tag{4.68}$$

This can be written in general representation as:

$$\sum_{i=1}^{3} \vec{n}_i = 0 . \tag{4.69}$$

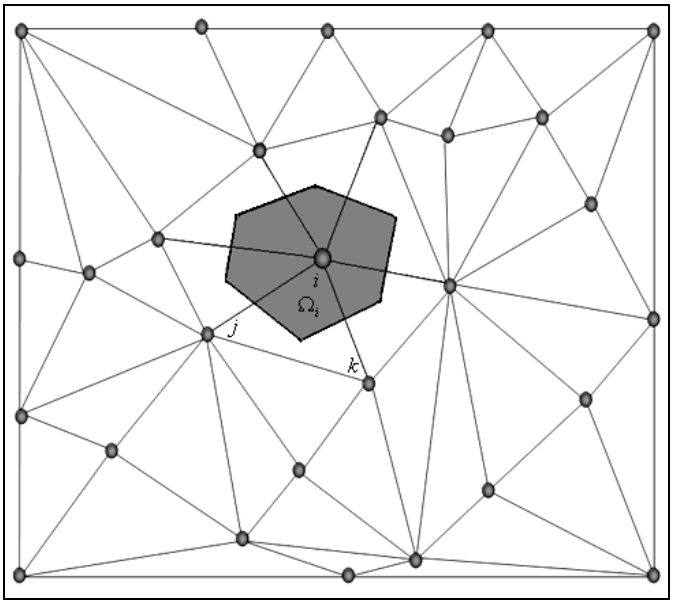

Figure 4.19. Unstructured triangular mesh filling the solution domain

The shaded area in Figure 4.19, is called the median dual cell or Veroni area surrounding the node i. The represenattion of Veroni area is given with the symbol Ω_i.

In order to distinguish the flow direction being inflow and outflow, or the nodes being upstream or downstream it is useful to define the scalar 'inflow parameter' which is mostly given as :

$$k_i = \frac{1}{2} \vec{\lambda} . \vec{n}_i \tag{4.70}$$

where the $\vec{\lambda}$ is constant speed vector in the scalar problem $U_t + \vec{\lambda} . \vec{\nabla} U = 0$ (Figure 4.20).

For inflow face: $k_i \geq 0$ then i is downstream node, and for outflow face: $k_i < 0$ then i is upstream node [23].

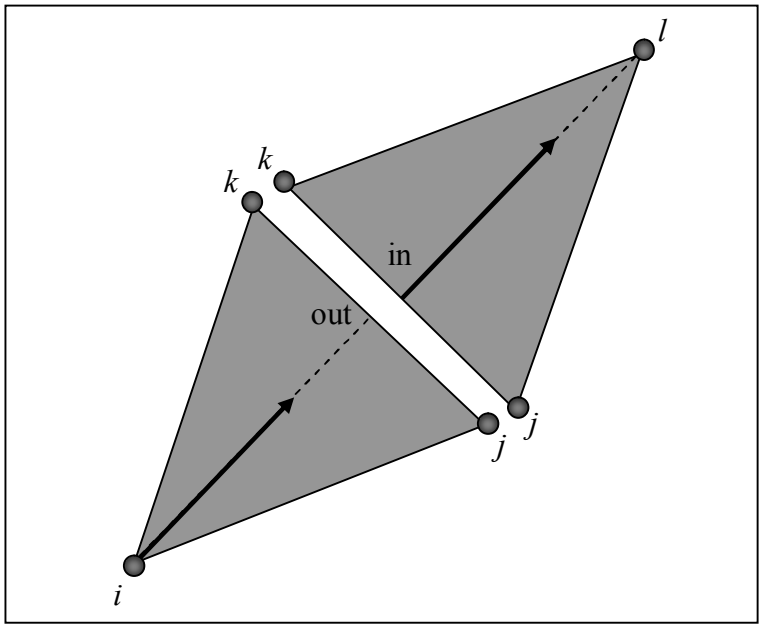

Figure 4.20. One-inflow triangle (upper triangle) with inflow point shown as 'in' and two-inflow triangle with output point shown as 'out'. In both cases the arrow indicaties the direction of the streamline

By using the result obtained in Equation 4.69 one can show that

$$\sum_{i=i}^{3} k_i = 0 . \tag{4.71}$$

For one-inflow triangles only one of the inflow parameters is positive and the other two are negative, for two-inflow triangles two of the inflow parameters are positive and one is negative. By using the definitions given, the gradient of any linearly varying quantity within the triangle can be expressed as:

$$\vec{\nabla}\vec{U} = \frac{1}{2\Omega_T} \sum_{i=1}^{3} \vec{U}_i \vec{n}_i \tag{4.72}$$

where Ω_T is the area of triangle T. Note that the vector sign above U shows that U is a vector of variables, but the vector sign above ∇ (nabla) shows that it is a regular gradient.

The left hand side of Equation 4.63 can be expressed again in the following manner,

$$\sum_T \iint_\Omega \left(N_l \sum_{i=1}^{3} N_i \frac{\partial \vec{U}_i}{\partial t} \right) d\Omega = \sum_T \iint_\Omega \left(\sum_{i=1}^{3} N_l N_i \frac{\partial \vec{U}_i}{\partial t} \right) d\Omega = \sum_{T \in l} \sum_{i=1}^{3} \frac{\Omega_T}{3} \delta_{li} \frac{\partial \vec{U}_i}{\partial t} \qquad (4.73)$$

and as a result

$$\sum_T \iint_\Omega \left(N_l \sum_{i=1}^{3} N_i \frac{\partial \vec{U}_i}{\partial t} \right) d\Omega = \Omega_l \frac{\partial \vec{U}_l}{\partial t} \qquad (4.74)$$

is obtained.

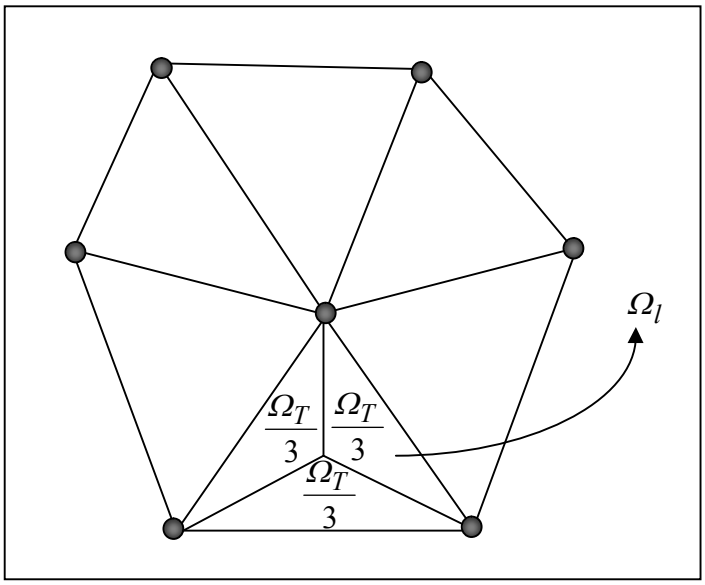

Figure 4.21. The geometrical relation between Ω_T and Ω_l

If some attention is given to the right hand side of the Equation 4.63 and N_l is taken as unity and using the Gauss theorem

$$\iint_{\Omega}\left(A\frac{\partial\vec{U}}{\partial x}+B\frac{\partial\vec{U}}{\partial y}\right)d\Omega=\oint_{\delta\Omega}\left(\vec{F}dn_x+\vec{G}dn_y\right)=\sum_{k=1}^{3}(A_k\vec{U}_k n_{k_x}+B_k\vec{U}_k n_{k_x}) \quad (4.75)$$

is obtained. Another way for obtaining the same result is substituting Equation 4.60 (by using k instead of i as an index) into the flux integral,

$$\sum_T\iint_{\Omega}N_l\left[A\sum_{k=1}^{3}\frac{\partial N_k}{\partial x}\vec{U}_k+B\sum_{k=1}^{3}\frac{\partial N_k}{\partial y}\vec{U}_k\right]d\Omega\ . \quad (4.76)$$

Since it is linear the gradient of the shape function is constant over T, it can be expressed as:

$$\vec{\nabla}N_k=\frac{1}{2\Omega_T}\vec{n}_k \quad (4.77)$$

and by taking $\partial N_k/\partial x=n_{k_x}/2\Omega_T$ and $\partial N_k/\partial y=n_{k_y}/2\Omega_T$ then Equation 4.74 becomes

$$\sum_T\iint_{\Omega}N_l\left[A_k\sum_{k=1}^{3}\frac{n_{k_x}}{2\Omega_T}\vec{U}_k+B_k\frac{n_{k_y}}{2\Omega_T}\sum_{k=1}^{3}\vec{U}_k\right]d\Omega=\left[\frac{1}{\Omega_T}\iint_{\Omega}N_l d\Omega\right]Res_T=B_l\,Res_T \quad (4.78)$$

where

$$Res_T=\sum_{k=1}^{3}\frac{1}{2}\left(An_{k_x}+Bn_{k_y}\right)\vec{U}_k \quad (4.79)$$

is called the 'cell residual' and B_l is the distribution matrix. The cell residual is small in regions of smooth flow and it gives the measure of the accuracy of the discrete solution very precisely. The distribution matrix is used to distribute the total residual to the nodes in appropriate manner. There are some different methods for defining the distribution matrix.

The mostly used numerical schemes which will not be mentioned in detail are listed as follows:

N- Scheme which is the residual distributon formulation of the first-order upwind method. It is only the first order accurate scheme. The distribution matrix expression for this scheme is given as:

$$B_i^N = -\frac{1}{Res_T}\frac{max(0,K_i)}{\sum_j max(0,K_j)}\sum_j min(0,K_j)(U_i^n - U_j^n) \tag{4.80}$$

where $K_i = (An_{k_x} + Bn_{k_y})/2$ is the flux matrix whose eigensystem determines the spatial variation of flow quantities at node i. The superscript n represents the time level.

The PSI (Positive Streamwise Invariant) or limited N- Scheme suggests the distribution matrix expression as :

$$B_i^{PSI} = \frac{max(0,B_i^N)}{\sum_{m=1}^{3} max(0,B_m^N)} \ . \tag{4.81}$$

The requirement for continuity is satisfied by this scheme [24].

The LDA (Low Diffusion A)- Scheme is a linear upwind scheme which satisfies the linearity preservation property. The expression for the distribution matrix is given as:

$$B_i^{LDA} = \frac{max(0,K_i)}{\sum_j max(0,K_j)} \ . \tag{4.82}$$

The Galerkin Scheme is obtained by choosing the the weight functions identical to the nodal basis functions. The distribution coefficients are :

$$B_i^{GAL} = \frac{1}{3} I \tag{4.83}$$

where I is the identity matrix.

This scheme is unstable for convection type of problems. In order to stabilize this scheme some dissipation terms are added and new schemes are obtained [13].

The SUPG (Streamline Upwind Petrov Galerkin) -Scheme is one of the schemes which added some dissipation terms to the Galerkin method and the expression for this method is given as:

$$B_i^{SUPG} = \frac{1}{3} I + \tau_t \frac{K_i}{\Omega_T} \tag{4.84}$$

where τ_t is the positive parameter with the dimension of time [25].

The Lax-Wendroff – Scheme which is the scheme used in this thesis has the expression for the distribution matrix given as:

$$B_i^{LW} = \frac{1}{3} I + \frac{\Delta\tau}{2\Omega_l} K_l \tag{4.85}$$

where $\Delta\tau$ is found from the maximum eigenvalues of K_l and it is called cell based time step. This is different from nodal time step and if they are chosen to be equal this will be the time accurate version for the scheme. Here the term $(\Delta\tau/2\Omega_l)K_l$ represents the Lax-Wendroff dissipation term.

There are different types of distribution matrices B_i and they are used to distribute the total fluctuation to three nodes of the triangle by appropriate fractions. Eventually they all have to satisfy the condition:

$$B_i + B_j + B_k = 1. \tag{4.86}$$

How these distributions are done is shown in Figure 4.22.

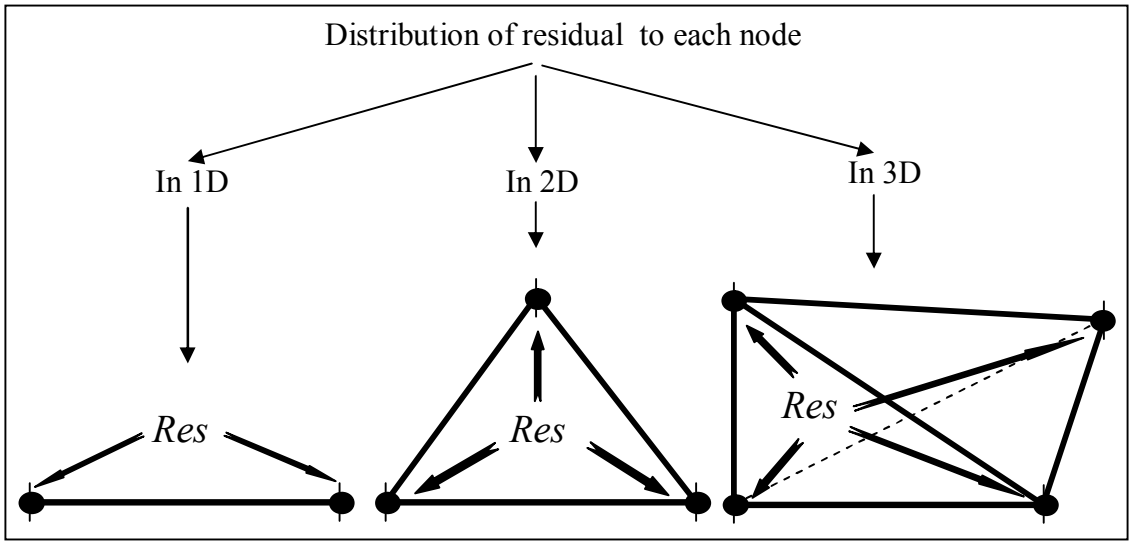

Figure 4.22. Basic distribution scheme for residual distribution processes

The Equation 4.79 can be shown in different form as:

$$Res_T = \sum_{k=1}^{3} K_k \vec{U}_k \,. \tag{4.87}$$

The last term on the right hand side of Equation 4.61 which is the source term and it can be taken as the arithmetic average of the values at the nodes (i, j, k) which belong to the triangle T and can be expressed:

$$\left\langle \vec{S} \right\rangle = \frac{\vec{S}_i + \vec{S}_j + \vec{S}_k}{3} \,. \tag{4.88}$$

After all the terms are expressed the final expression for the residual at the node l of triangle T is defined as:

$$Res_l = \frac{1}{\Omega_l}\left[B_l \sum_{k=1}^{3} K_k \vec{U}_k + \left\langle \vec{S} \right\rangle + \vec{S}_v \right] \tag{4.89}$$

where $\vec{S}_v$ is the viscous term [26].

The solution procedure starts with the calculation of residual given in Equation 4.89 and it is distributed to three nodes of triangles that are visited once at each time step. The analytical boundary conditions are applied by just assigning analytical values at the boundary nodes. The outgoing or zero normal derivative boundary conditions are done by doing no action for these variables at the boundary nodes. The inherent structure of the matrix distribution scheme updates the variables to their correct values automatically.

After the space discretization technique used in this work is introduced in detail it is time to mention about the time discretization technique used here.

4.3. Dual Time Stepping for Time Discretization

By using the preconditioning techniques the careful change for the time evolution of the equations can be obtained. If the time accurate solutions are desired then the procedure must be applied as pseudo time iterations at each real time step. Another way of saying is that when the real time advancement is applied, pseudo iterations only creating the iterations between real time steps in order to reach steady state. In this thesis dual time stepping method was used with pseudo time iterations and real time iterations. This is shown by the dimensionless MHD equations which can be written in the following compact form

$$\frac{\partial \vec{U}}{\partial \tau} + I_m \frac{\partial \vec{U}}{\partial t} + A\frac{\partial \vec{U}}{\partial x} + B\frac{\partial \vec{U}}{\partial y} = \vec{S}_T \quad . \tag{4.90}$$

The better representation of this expression in which the preconditioning matrix is included can be given as:

$$P_m \frac{\partial \vec{U}}{\partial \tau} + I_m \frac{\partial \vec{U}}{\partial t} + A\frac{\partial \vec{U}}{\partial x} + B\frac{\partial \vec{U}}{\partial y} = \vec{S}_T \tag{4.91}$$

where P_m is called preconditioning matrix. Constructing the preconditioning matrix is very important research area in computational fluid dynamics. It is modifying the time derivative in equations. In order to get rid of the P_m in the first term of Equation 4.91 the equation is multiplied by the inverse of the P_m. The best thing here is that this multiplication does not affect the the sources and time evolution of $\vec{U}$. This procedure only modifies the Jacobian matrices changing their eigen-structure. After divergence condition is satisfied by pseudo iterations then the new time level is reached.

4.4. Multistep Methods for Time Integration

Euler method, midpoint method and Runge-Kutta method are the most common methods for solving the initial value problems. Initial value problems are solved basically by using 'one–step methods' and 'multi-step methods' which differ from each other by the fact that the one-step methods depend only on the value of only one old point, whereas in multi-step methods more points are used. In one-step method the value of $y(t_{i+1})$ depends only on the value of $y(t_i)$ and in multi-step method the value of $y(t_{i+1})$ depends on the previous values of $y(t_i)$, $y(t_{i-1})$, $y(t_{i-2})$,… see Figure 4.23.

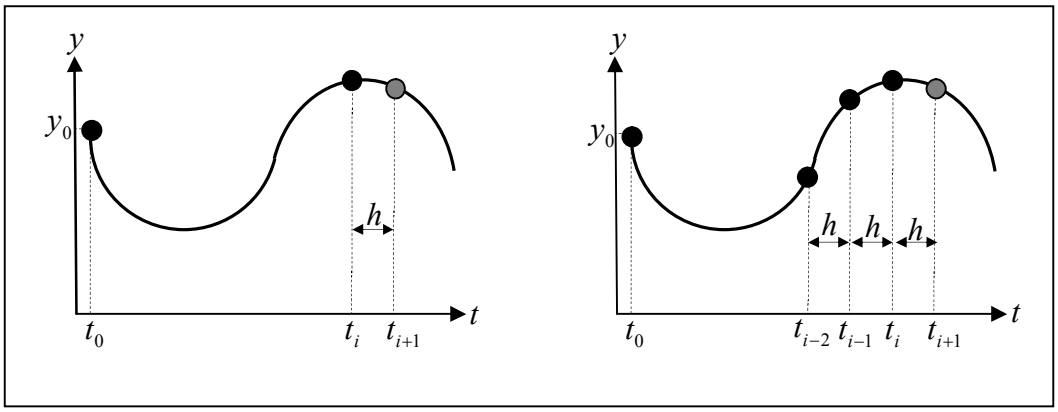

Figure 4.23. One-step method (left) and multi-step method (right) representations

Euler method is the simplest method using the procedure of marching a small step at a time on the right hand side in order to approximate the solution on left hand side of the Equation 4.92. It is a first order accurate method. In order to understand this method a brief description is given as follows:

The problem to be solved is $dy(t)/dt = f(t, y(t))$. The unknown value of $y(t)$ where $t > t_0$ is desired to be obtained. The initial value of $y(t_0)$ is given implicitly. In order to determine the value of it approximately the starting point is the rate of change of y at time t_0, which can be represented as:

$$\frac{dy(t_0)}{dt} = f(t_0, y(t_0)) = f(t_0, y_0). \tag{4.92}$$

If this rate change is constant in time then the value of $y(t)$ will be found exactly on times after t_0:

$$y(t) = y_0 + f(t_0, y_0)(t - t_0). \tag{4.93}$$

A new 'small' number h_t which is called the time step is defined as follows:

$$\begin{aligned} t_1 &= t_0 + h_t \\ t_2 &= t_1 + h_t \\ &\vdots \\ t_i &= t_{i-1} + h_t \end{aligned} \tag{4.94}$$

By using the definition given in Equation 4.94

$$y(t_1) = y_1 = y_0 + f(t_0, y_0)(t_1 - t_0)$$

and consequently

$$y_1 = y_0 + f(t_0, y_0)h_t \tag{4.95}$$

is obtained. This is the approximate value of y at time t_1, $y(t_1) \approx y_1$. The approximate expression for y_1 was obtained and then the rate given by $f(t_1, y_1)$ is used in

$y(t) = y_1 + f(t_1, y_1)(t - t_1)$ for $t > t_1$. By defining next time step as: $t_2 = t_1 + h_t = t_0 + 2h_t$ then

$$y_2 = y_1 + f(t_1, y_1)(t_2 - t_1) = y_1 + f(t_1, y_1)h_t \tag{4.96}$$

is found. Thus, by using Equation 4.94 and Equation 4.95 the general form for Euler method can be written as

$$y(t_{n+1}) \approx y_{n+1} = y_n + f(t_n, y_n)h_t \tag{4.97}$$

where $t_n = t_0 + nh_t$ and $n = 0, 1, 2, 3...$

In midpoint method the time step defined as h_t as done previously for Euler method is divided into two equal parts so that spatial accuracy of the numerical solutions is increased. After this definition the general expression for midpoint method can be written as:

$$y(t_{n+1}) \approx y_{n+1} = y_n + f(t_n + \frac{h_t}{2}, y_n + \frac{h_t}{2} f(t_n, y_n))h_t . \tag{4.98}$$

This method is not so stable and small perturbations in initial values gives rise to growing oscillations. In general, the higher the accuracy, the greater number of function evaluations are necessary. In this thesis, neither Euler nor midpoint methods were used. Runge-Kutta method which is probably the most popular method in engineering was used in this thesis. The name of the method comes from the names of two German mathematicians who developed this method. Runge-Kutta method is essentially an attempt to match a more complex Euler-like formula to a fourth order Taylor method. This method has a high order of accuracy and can be used for time integration. There are several Runge-Kutta methods however the most popular ones are second and fourth order method. In general Runge-Kutta method gives more accurate solutions than the other numerical methods especially compared with Euler's method. However, the implementation of the method is also more complex than the others. In this work the pseudo time iterations were

done by using Runge- Kutta algorithm. The method is self-starting method which can change the step size of integration as often and by the size and by as much as required. One of the main disadvantages of the method is that it requires more function evolutions per step than linear multi-step methods do [27]. As an example the fourth order Runge-Kutta method requires four evaluations on the right hand side of expression per step size h_t. Runge-Kutta method is expressed as:

$$y(t_{n+1}) \approx y_{n+1} = y_n + \frac{1}{6}h_t \left\{ \begin{array}{l} f(t_n, y_n) + 2f(t_n + \frac{1}{2}h_t, y_n + \frac{1}{2}h_t f(t_n, y_n)) + \\ 2f(t_n + \frac{1}{2}h_t, y_n + \frac{1}{2}h_t f(t_n + \frac{1}{2}h_t, y_n + \frac{1}{2}h_t f(t_n, y_n))) + \\ f(t_n + h_t, y_n + h_t f(t_n + \frac{1}{2}h_t, y_n + \frac{1}{2}h_t f(t_n + \frac{1}{2}h_t, y_n + \frac{1}{2}h_t f(t_n, y_n)))) \end{array} \right\} . \quad (4.99)$$

This method will be used to integrate following equation

$$\frac{d\vec{U}}{dt} = f(\vec{U}) \quad (4.100)$$

where $\vec{U}$ is vector of nodal states and $f(\vec{U})$ is the discretized spatial part. In this study the $f(\vec{U})$ is represented by $Res^*(\vec{U})$ which is the residual.

The $m-stage$ Runge-Kutta time integration algorithm is given as follows:

$$\begin{aligned} \vec{U}^{(0)} &= \vec{U}^n \\ \vec{U}^{(k)} &= \vec{U}^{(0)} + \alpha^k \Delta t \, Res^*(\vec{U}^{(k-1)}) \text{ where } k = 1, 2, 3, \ldots m \\ \vec{U}^{n+1} &= \vec{U}^{(m)} \end{aligned} \quad (4.101)$$

where n is the counter used for counting the consecutive time levels, α^k are constant numbers changing between 0 and 1 depending on the characteristic of the method used.

Δt is the time step. If Runge-Kutta method is used for iterations, this is the local time step used to speed up the convergence to the steady-state.

Table 4.1. Coefficients for multi stage Runge-Kutta integration [13]

$m=1$	$\alpha^1=1.00$					
$m=2$	$\alpha^1=0.70$	$\alpha^2=1.00$				
$m=3$	$\alpha^1=0.28$	$\alpha^2=0.61$	$\alpha^3=1.00$			
$m=4$	$\alpha^1=0.16$	$\alpha^2=0.32$	$\alpha^3=0.57$	$\alpha^4=1.00$		
$m=5$	$\alpha^1=0.10$	$\alpha^2=0.21$	$\alpha^3=0.34$	$\alpha^4=0.55$	$\alpha^5=1.00$	
$m=6$	$\alpha^1=0.07$	$\alpha^2=0.14$	$\alpha^3=0.23$	$\alpha^4=0.34$	$\alpha^5=0.53$	$\alpha^6=1.00$

The real time derivative in Equation 4.90 can be approximated such as done in reference [28] as follows

$$\frac{\partial \vec{U}}{\partial t}=\frac{3}{2\Delta t}(\vec{U}^{n+1}-\vec{U}^{n})-\frac{1}{2\Delta t}(\vec{U}^{n}-\vec{U}^{n-1}) \tag{4.102}$$

and pseudo time iterations were approximated by a third order Runge-Kutta algorithm. After the pseudo iterations converges such as $\partial\vec{U}/\partial\tau\to 0$, the time accurate solution $I_m\left(\partial\vec{U}/\partial t\right)=Res(\vec{U},\beta^2,\delta^2)$ is recovered from the Equation (4.90). $Res(\vec{U},\beta^2,\delta^2)$ is expressed as:

$$Res(\vec{U},\beta^2,\delta^2)=\vec{S}^T-A\frac{\partial\vec{U}}{\partial x}-B\frac{\partial\vec{U}}{\partial y}. \tag{4.103}$$

This is called the ‘ residual vector’ which in this thesis is discretized by using matrix distribution scheme which is described in detail previously. After combining the real time and pseudo time levels

$$\frac{\vec{U}^{n+1,m+1}-\vec{U}^{n+1,m}}{\Delta\tau}+I_m\left[\frac{3}{2\Delta t}(\vec{U}^{n+1}-\vec{U}^{n})-\frac{1}{2\Delta t}(\vec{U}^{n}-\vec{U}^{n-1})\right]=Res^{n+1,m+1} \tag{4.104}$$

is obtained. In Equation (4.104) $\vec{U}^{n}$ and $\vec{U}^{n-1}$ do not change in pseudo iterations. In order to make the real-time derivative term explicit in pseudo iterations Equation 4.104 can be written as:

$$\frac{\vec{U}^{n+1,m+1}-\vec{U}^{n+1,m}}{\Delta\tau}=-I_m^*\left[\frac{3}{2\Delta t}(\vec{U}^{n+1}-\vec{U}^{n})-\frac{1}{2\Delta t}(\vec{U}^{n}-\vec{U}^{n-1})\right]+Res^{n+1,m+1} \quad (4.105)$$

where I_m^* is called the modified diagonal matrix and is given as:

$$I_m^*=\left[I+\frac{3}{2}\left(\frac{\Delta\tau}{\Delta t}\right)I_m\right]^{-1}.I_m \quad (4.106)$$

where I is the unit matrix. Since the residual requires implicit treatment, the accuracy of pseudo time derivative is improved by the following third- order Runge-Kutta method. After this treatment the residual calculation for the next pseudo time iteration is more accurate. By using the parameters given in the Table 4.1.

$$\begin{aligned}
\vec{U}^{(0)}&=\vec{U}^{n+1,m}\\
\vec{U}^{(1)}&=\vec{U}^{(0)}+0.28\Delta\tau\, Res^*(\vec{U}^{(0)},\vec{U}^{n},\vec{U}^{n-1})\\
\vec{U}^{(2)}&=\vec{U}^{(0)}+0.61\Delta\tau\, Res^*(\vec{U}^{(1)},\vec{U}^{n},\vec{U}^{n-1})\\
\vec{U}^{(3)}&=\vec{U}^{(0)}+\Delta\tau\, Res^*(\vec{U}^{(2)},\vec{U}^{n},\vec{U}^{n-1})\vec{U}^{n+1,m+1}
\end{aligned} \quad (4.107)$$

where

$$Res^*(\vec{U})=-I_m^*\left[\frac{3}{2\Delta t}(\vec{U}^{n+1}-\vec{U}^{n})-\frac{1}{2\Delta t}(\vec{U}^{n}-\vec{U}^{n-1})\right]+Res^{n+1,m+1}. \quad (4.108)$$

The new pseudo values $\vec{U}^{n+1,m+1}$ are obtained from $\vec{U}^{n+1,m}$ in three steps as shown in the algorithm given as Equation 4.107. After pseudo iterations converge $\vec{U}^{n+1,m+1}\to\vec{U}^{n,m}$ so that $Res^*(\vec{U})\to 0$ the desired second-order accurate solution is obtained at new time level from

$$I_m \frac{\partial \vec{U}}{\partial \tau} = Res(\vec{U}) \tag{4.109}$$

or

$$\vec{U}^{n+1} = \vec{U}^n - \frac{1}{3}(\vec{U}^n - \vec{U}^{n-1}) + \frac{2}{3}\Delta t I_m^{*-1} Res(\vec{U}, \beta^2, \delta^2). \tag{4.110}$$

In this part of the thesis the space and time discretization techniques used in order to solve the equations are described. The spatial discretization method which is the matrix distribution was used in the numerical simulations. The time integration method was Runge-Kutta method. The numerical results obtained for different problems and given in 'Numerical Problems and Results' part of the thesis were found in very good agrement with the references.

5. THE CODE AND ITS FEATURES

In order to solve the incompressible MHD (Navier-Stokes and Maxwell's) equations on structured and unstructured meshes with triangular mesh elements a new generation and original code was used**.** The two dimensional code which was running in Cartesian coordinate system was used for simulations. Since the code was running on two dimensions, the first step which is the mesh generation procedure for three dimensions was finished. As a postdoctoral study the mesh generation part is planned to be adapted to the original code.

5.1. Code Properties

5.1.1. General Properties

The code is a two-dimensional incompressible (constant mass density) magneto-hydrodynamic code which can be used to solve the steady state (time independent) and transient magnetized or neutral convection problems with or without the effect of heat transfer. By using the numerical method which is called 'Matrix Distribution Scheme', and was described in previous chapter, Navier-Stokes and Maxwell's equations in two dimensions in Cartesian coordinate system can be solved numerically. The code can be run under the Linux operating system. In order to start running the console should be used under Linux operating system.

In computational fluid dynamics, the commercial solvers or codes operate as 'black box' which obtain the raw output data correspoding to a set of numbers that give the values of each field variable at each point of mesh. Some of the popular commercial codes are Ansys, Fluent, and Flowscience. Informally, CFD which is the acronym for the Computational Fluid Dynamics that is the science which can make numerical expriments on computers is sometimes used as 'colourful fluid dynamics'. This name comes from the fact that the codes provide very colourful graph plots as a result of the solved problem. These colourful plots are very helpful for easy analysis of the results.

In this non-commercial and original code which initial version was implemented as in reference [26], the solutions are done and the results were collected in the data files which contain only the numbers, or the results are shown on the screen with some graphs changing simultaneously. The refresh time of the graphs can be given by the user by specifying the step numbers for iteration. The code provides the plots such as: shaded contour plots in which the areas with the same colour represents the same mathematical value for a calculated field variable such as velocity, temperature, pressure, etc. (Figure 5.1). Vector plots which show the vector quantities such as velocity, electric and magnetic fields lines are also drawn by the code (Figure 5.2). The magnitude of the vectors are directly related to the calculated magnitude of the variable. The vectors are giving an idea about the direction of the variable. The mesh plots which are showing the computational mesh are also a part of the code used. The computational elements are visualized by mesh plots (Figure 5.3).

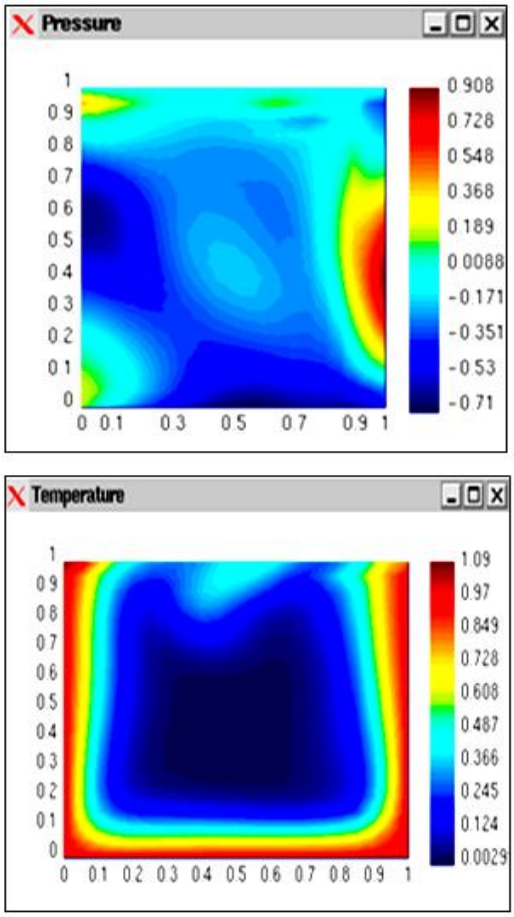

Figure 5.1. Shaded contour plots for the pressure and temperature

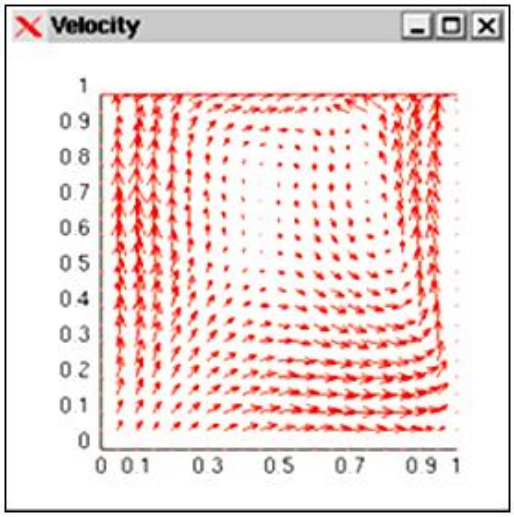

Figure 5.2. Vector plot for the velocity

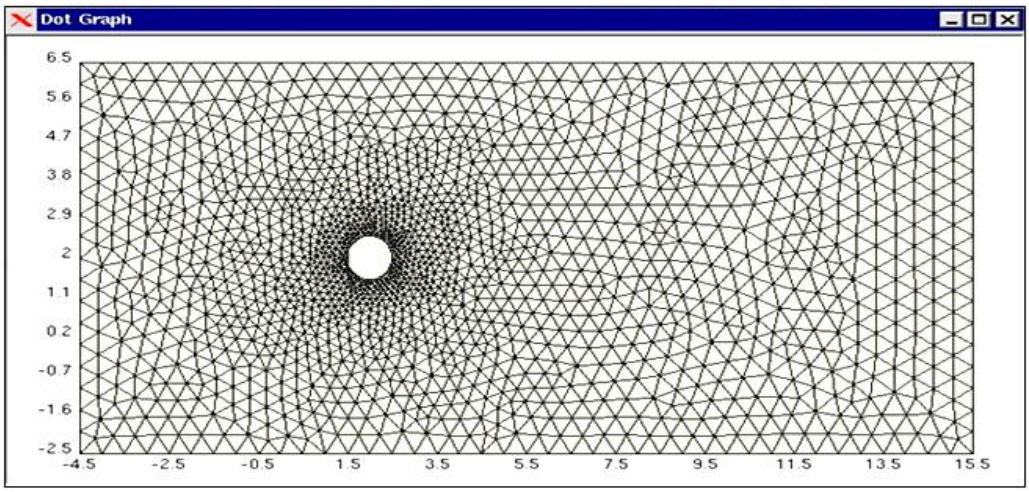

Figure 5.3. Unstructured mesh plot done by the code

The code has very friendly graphical user interface. It is used to create complex meshes, the boundary and initial conditions can be specified by the user directly, colour vector graphs can be created etc. This code utilizes the matrix distribution scheme which is running on the structured and unstructured triangular meshes. For time discretization the dual time stepping with multidimensional Runge-Kutta algorithm was used. The code can easily be used for simulating the nonlinear time dependent evolution for heated and magnetized liquids, natural convection with internal heat generation and absorption, conductive fluids under the electric and magnetic fields, etc.

There is a first step display on the screen in order to start the code in Figure 5.4. After the the code was started to execute another menu appears on the screen (Figure 5.5). There are some control buttons such as quit (quitting from execution), generate mesh (generates the mesh for solution domain), run (starts simulation done by the code), pause (pauses the execution), graph (it gives the permission for choosing the graphs which can be displayed on the screen) on the menu.

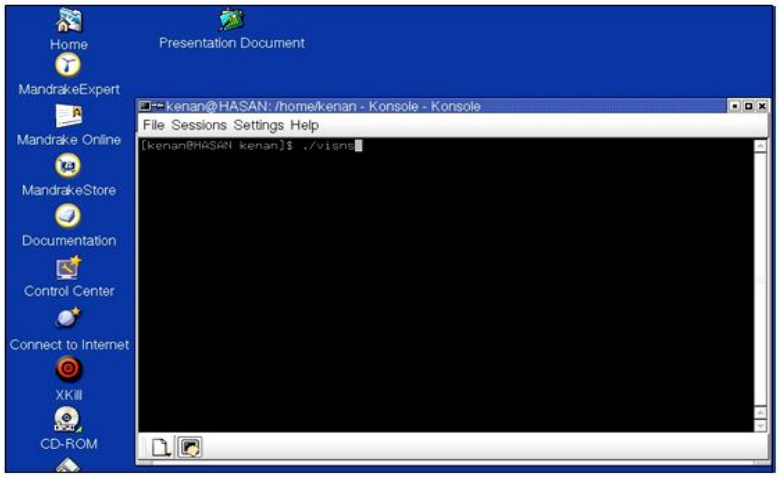

Figure 5.4. A snapshot showing starting step of the code

5.1.2. Using The Code and Mesh Generation

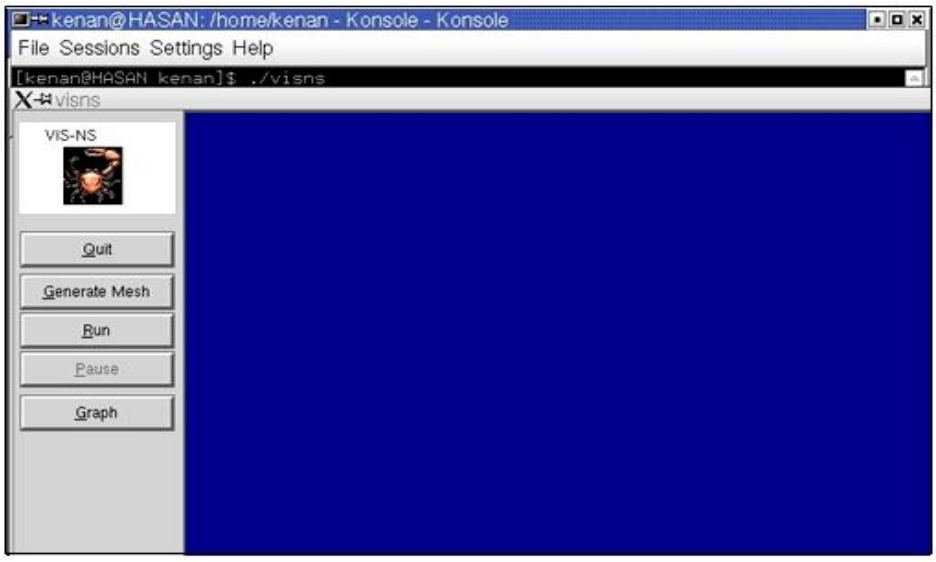

Figure 5.5. Control buttons for the code

5.1.2.1. Structured Mesh Generation

In order to solve the problem numerically firstly the mesh must be generated. Structured and unstructured triangular meshes can be generated by the code but also three dimensional (tetrahedron) mesh is also wanted to be embedded in the code as a postdoctoral study. After the generation of the mesh the screen is seen as in Figure 5.6.

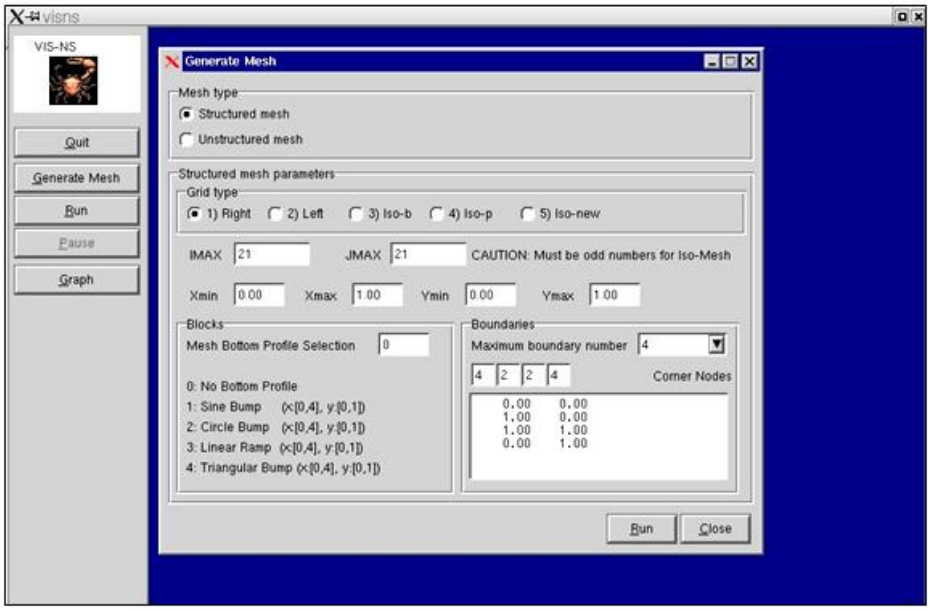

Figure 5.6. Menu for mesh generation process

There are five different stuctured grid types in the code. They have different forms which are shown in the Figure 5.7.

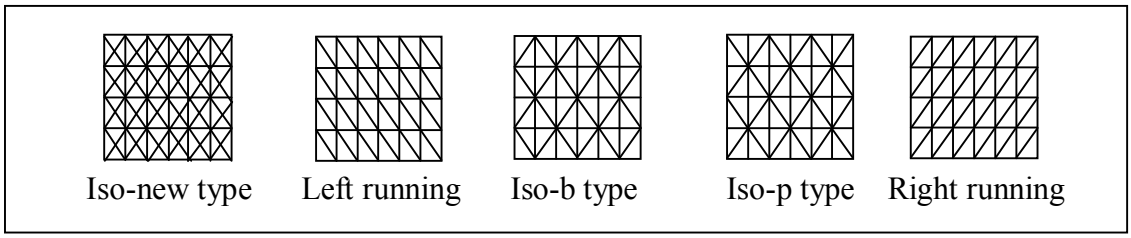

Figure 5.7. Grid types for structured mesh

After the mesh type was chosen, the dimensions for the solution domain (Xmin, Xmax, Ymin, Ymax) and maximum node (the specific points on which the discrete solutions are done) numbers for different dimensions (Imax for x coordinate and Jmax for

y coordinate) are also put externally. The next step is deciding about maximum boundary number for the solution domain and the boundary numbers for the corner nodes.

5.1.2.2. Unstructured Mesh Generation

Not only structured meshes but also unstructured meshes can be used for the computer simulation of the problem in the code. The unstructured mesh can be generated after it is chosen from the menu shown in the Figure 5.6. After unstructured mesh is chosen another different menu will appear on the screen. It is given below in Figure 5.8.

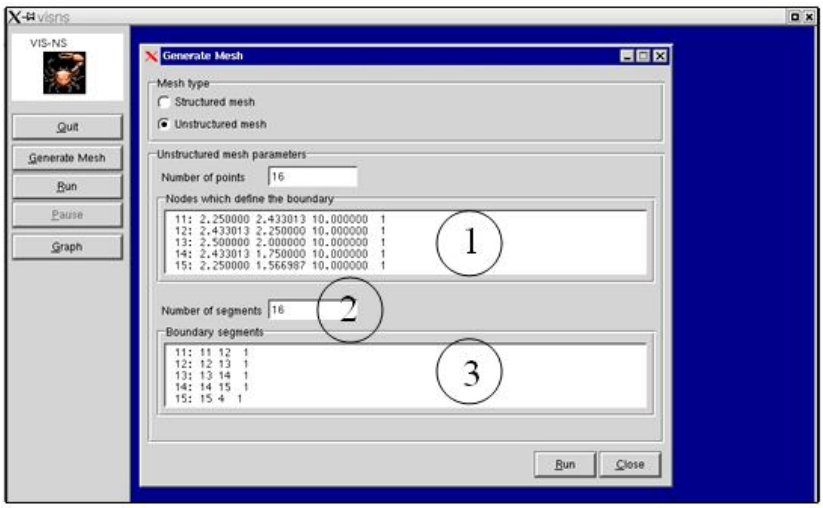

Figure 5.8. Parameters used for creating the unstructured mesh

For creating the unstructured mesh there are three different parts which must be filled. In the first part the number of the node, x cordinate value, y coordinate value, displacement dx and the number of the boundary which own the nodes mentioned must be given. In the second part the number of segments must be given. In the last part for creating the unstructured mesh the boundary segments must be put in proper way.

5.1.3. Example Problem

To understand the descriptions given above the example below will be very useful. Let us give the initial values and boundary conditions for the one of the very well known benchmark problem. The formal name for this problem can be called as ‘Lid driven cavity

test'. In this problem the sliding upper lid which has the constant velocity u on the upper boundary drives the circulation in the cavity Figure 5.9.

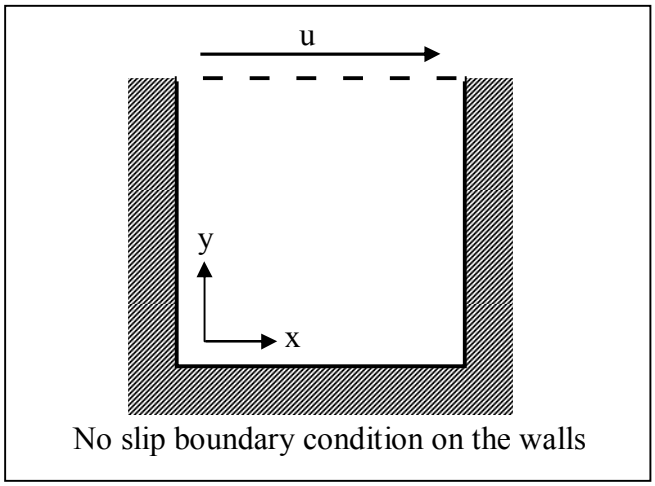

Figure 5.9. Scheme for the lid driven cavity test

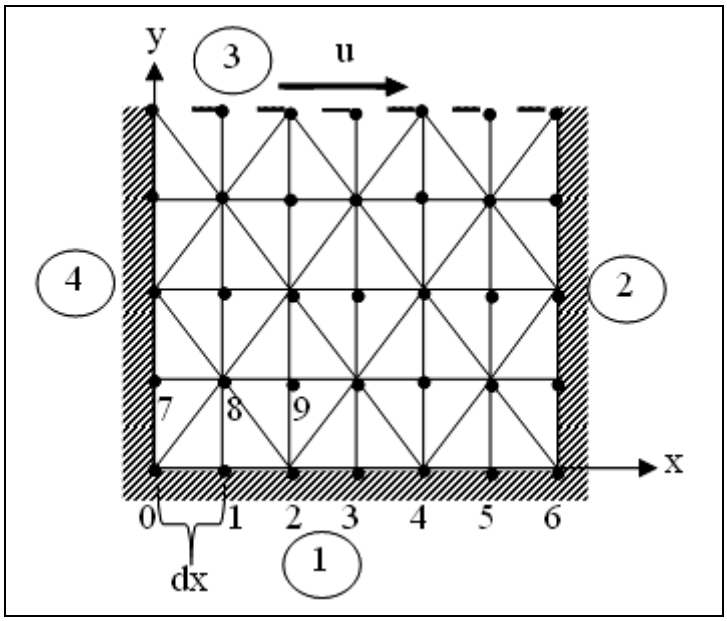

Figure 5.10. Scheme for the lid driven cavity test after the maximum node numbers are given and structured mesh type was chosen

In Figure 5.10, there are the nodes, the node numbers (only for the first row and the half of the second row), assigned boundary numbers (numbers in the circles) and the structured mesh for the solution domain. Before start the code the important boundary and

initial conditions must be considered and it is better to see all these things together on the solution domain.

5.2. Running the Code

After the steps in the example are completed another important step is the next. Here the simulation almost will start. However some blank spaces must be filled. Before code starts solving the problem the scheme in the Figure 5.11 is displayed on the screen.

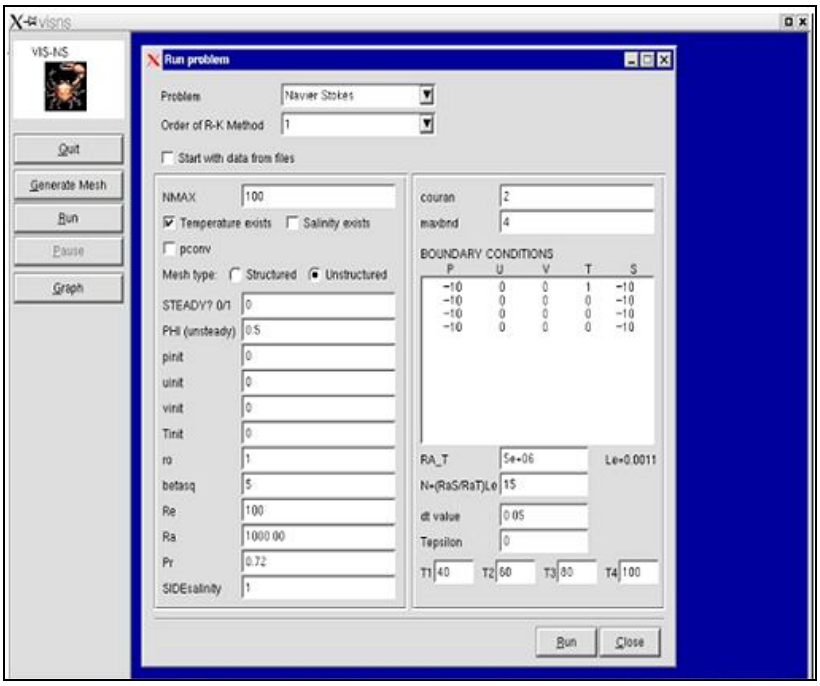

Figure 5.11. Scheme for running part of the code

At that point first of all the problem type (Navier- Stokes, MHD, Electromagnetic Braking etc.) must be chosen. Then the order of Runge-Kutta algorithm, temperature, salinity existences, the initial conditions such as pinit (initial pressure), uinit (the initial value for x component of the velocity), vinit (the initial value for y component of the velocity), Ra (Rayleigh number), Pr (Prandtl number), Tinit (initial temperature) etc. must be chosen and filled in the blanks. After all the requirements which are the initial conditions, boundary conditions, problem type, order for Runge-Kutta method etc. are finished the code is ready to start running. As a last step pushing the 'Run' button will start

the code to simulate the problem. During the simulation the graphs on the screen can also be controlled. In order to change the graphs on the screen firstly the button with the name 'Pause' is pushed and then the button with the name 'Graph'. Then another one menu appears on the screen (Figure 5.12). Here the graph selection for different graphs (vector graph of velocity, colour graph of pressure, color graph of temperature, vector graph of magnetic field, colour graph of density, vorticity, energies etc.) can be done and also the graph refresh intervals can be chosen in proper and desired way. By putting the thick sign in the blank squares the graphs which are wanted to be seen during the execution of the code will be chosen and step by step changes can be observed on the screen easily.

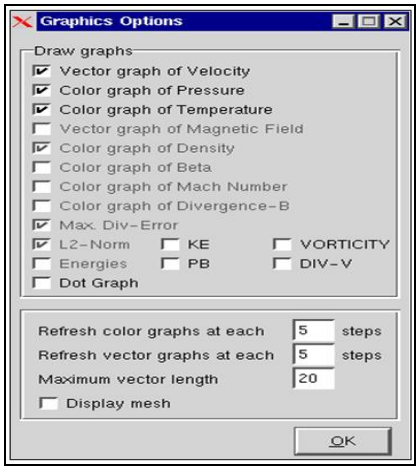

Figure 5.12. The graph selection menu

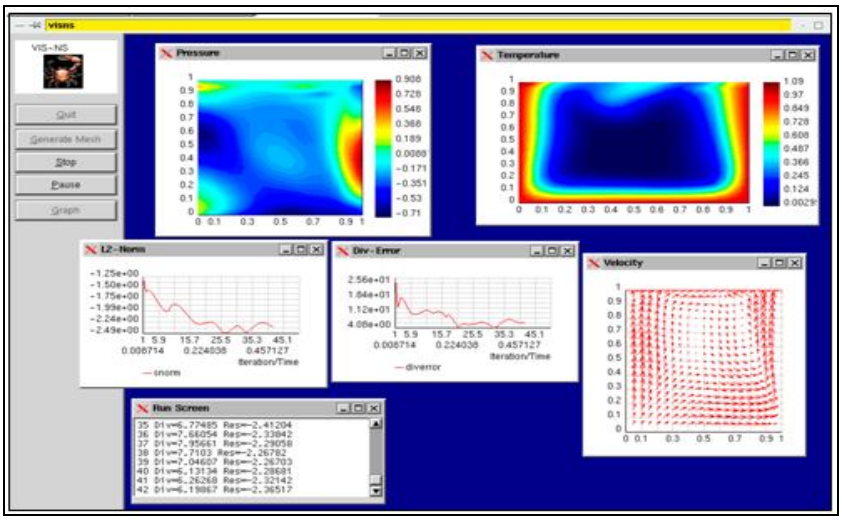

Figure 5.13. The schemes on the computer screen when the code is running

During the execution of the code the screen is seen like in the Figure 5.13.

5.3. Three Dimensional Mesh Generation Procedure

Since all the things are observed in three dimensions in the real life, another challenge is wanted to be realized. This challenge is to expand the code in three dimensions. Instead of the triangles now the tetrahedra will be used. In order to reach this purpose firstly the mesh generation menu of the code is changed and the '3D mesh' part is added (Figure 5.14).

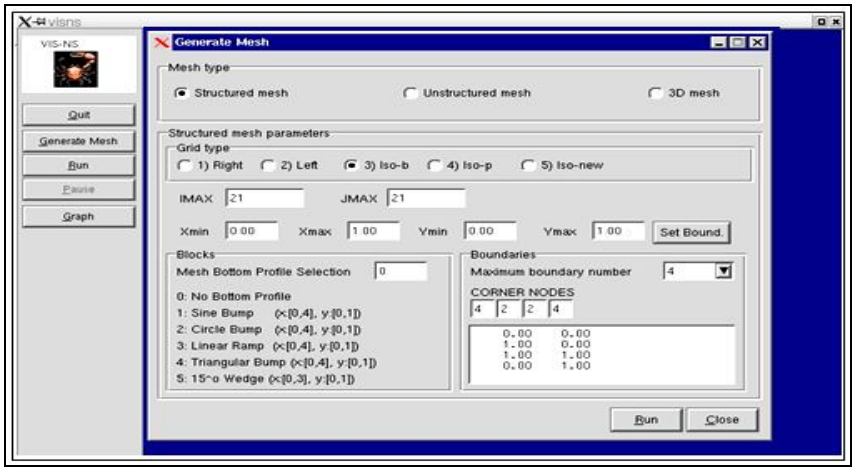

Figure 5.14. The new mesh generation part including the 3D mesh choice

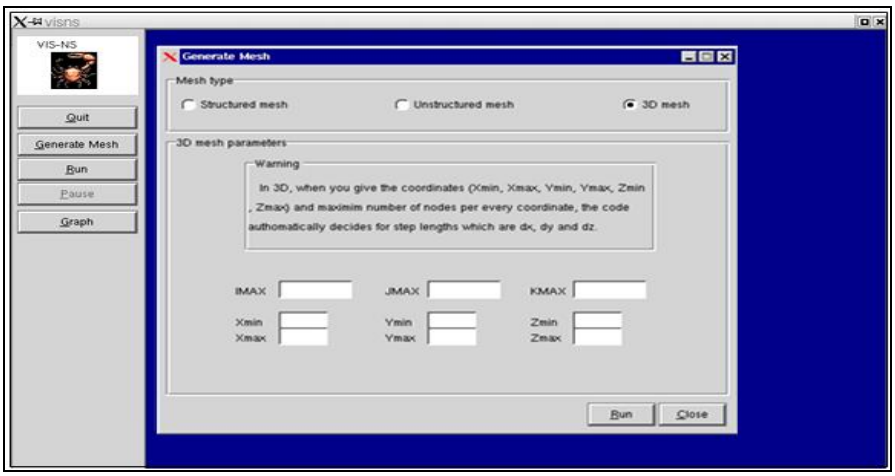

Figure 5.15. Menu for deciding about the size of the solution domain and number of nodes for the 3D mesh

In order to get this three dimensional objective firstly the tetrahedra geometry was studied and understood. Then the cube which has six tetrahedra in it is chosen as primitive cell which will form the whole mesh that will fill the whole solution domain. This cube can be named as a 'molecule'. By adding the molecules in a suitable manner the whole mesh is planned to be attained. The number of every node is wanted to be generated automatically by the code and an expression for doing this numbering in three dimensions was found. This expression is a function of the maximum numbers of the nodes in x, y and z directions. Maximum node number for x direction is given as I, maximum node number for y direction is given as J and maximum node number for z direction is given as K.

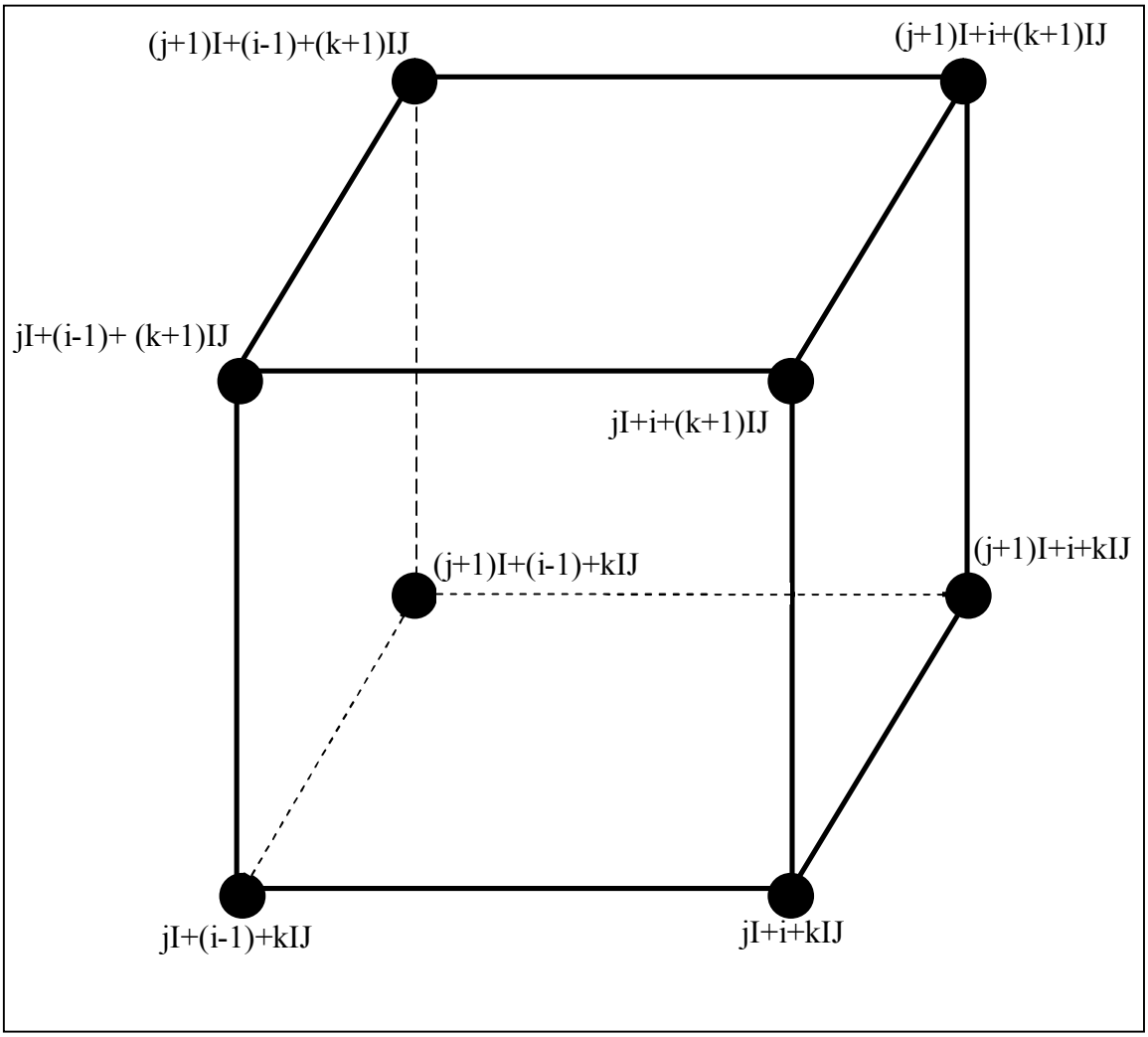

Figure 5.16. The shape and node number expression for every node in one molecule

The molecule shown above will be broken into six pieces which are all tetrahedra. The shape for every singular tetrahedral forming the molecule is given below together with the node number expressions formulated by us.

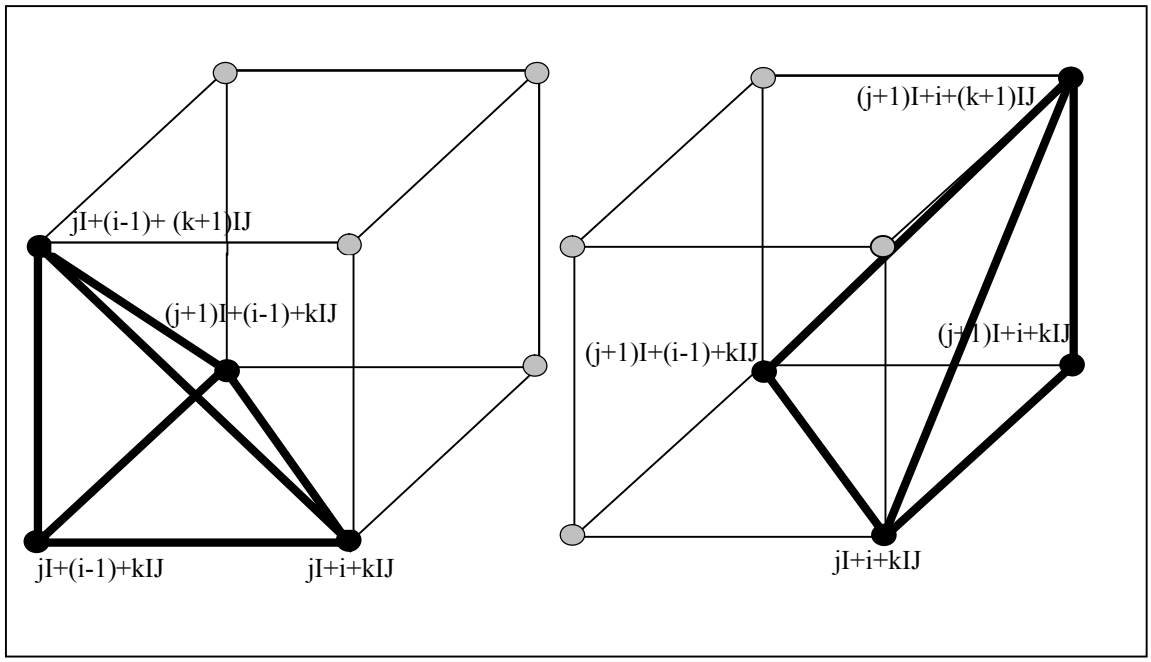

Figure 5.17. The first and second tetrahedra for the molecule

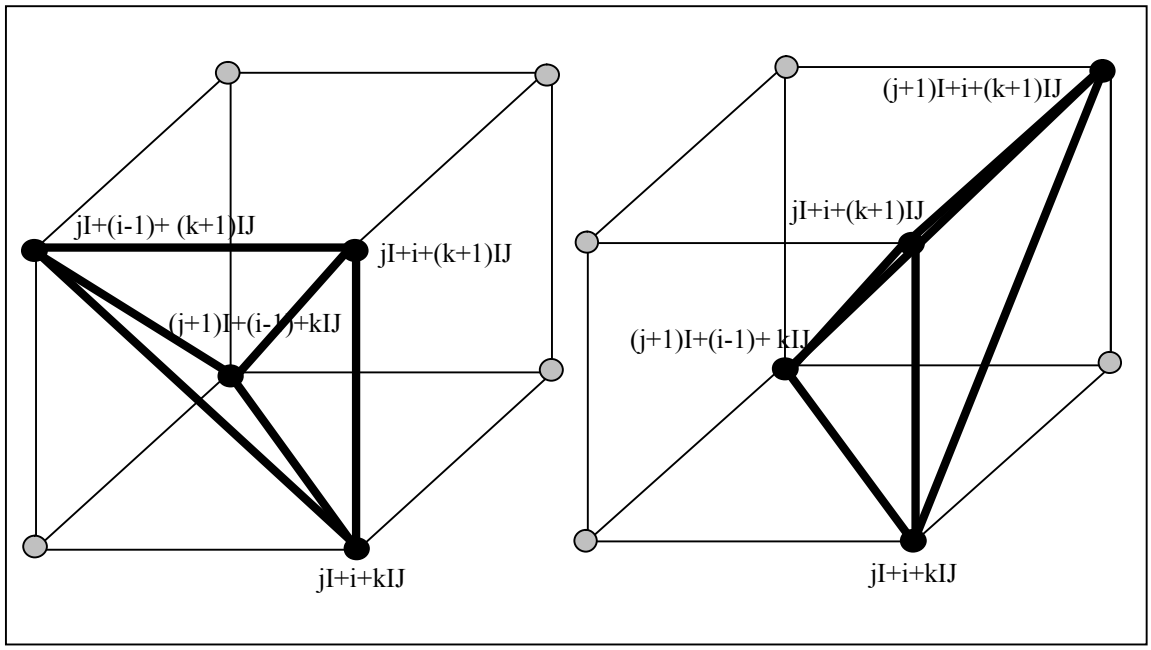

Figure 5.18. The third and fourth tetrahedra for the molecule

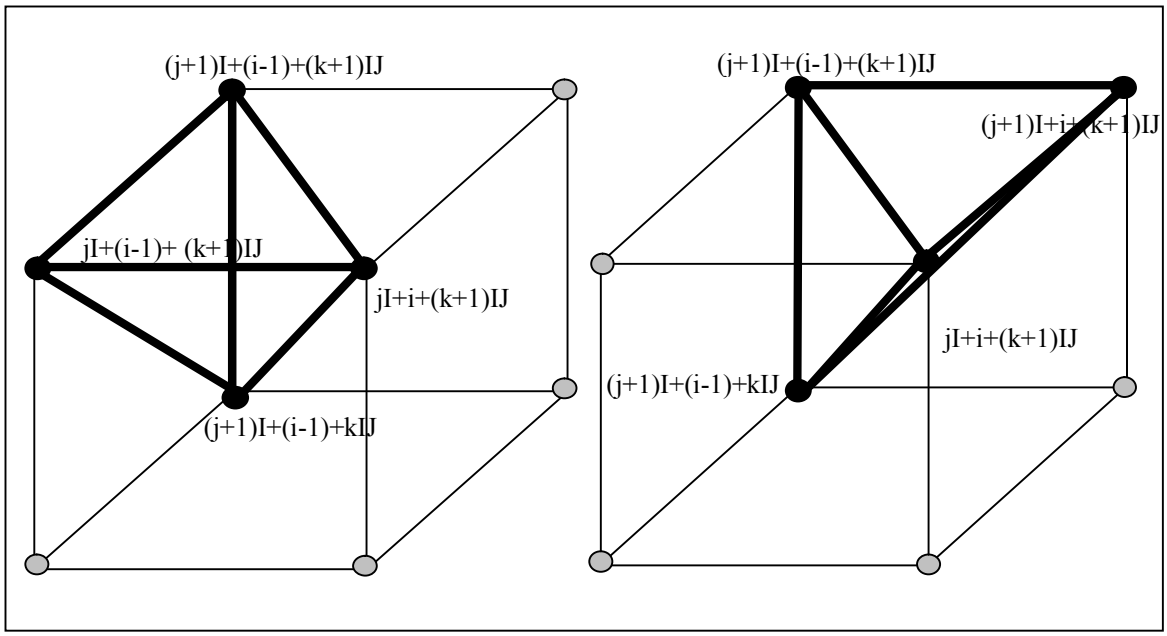

Figure 5.19. The fifth and sixth tetrahedra for the molecule.

Since it is very difficult to imagine the mesh shape by using only the drawn graphs above as an additional work real molecules were built by using the cardboard (Figure 5.21). They are built in order to use them as a model when the computer code is written for the three dimensional mesh. By using the model it is relatively easy to see the needed properties of the tetrahedra. It is easy to see which triangular faces of tetrahedra coincide with the other mutual faces. Since they are neighbours the information will be transmitted between them directly. It is also easy to calculate the areas for the four faces of the tetrahedra and also the volumes of every tetrahedron separately. Also the normal vectors are needed to be calculated for every face of the tetrahedron. Most of these things are done and ready in the code. Also in order to check the calculations of the volumes the total volume form the whole three dimensional mesh is calculated and is compared with the summation of every tetrahedron's volume separately and results are very encouraging. To generate the mesh in three dimensions all the node numbers must be known and must be put in the suitable order. The expression for automatical node number generation is checked also in the way shown in the Figure 5.20. The arbitrary nodes are chosen and by using the expression which was $jI+i+kIJ$ the node numbers can be found. They are compared with the real node numbers. The results are exactly right.

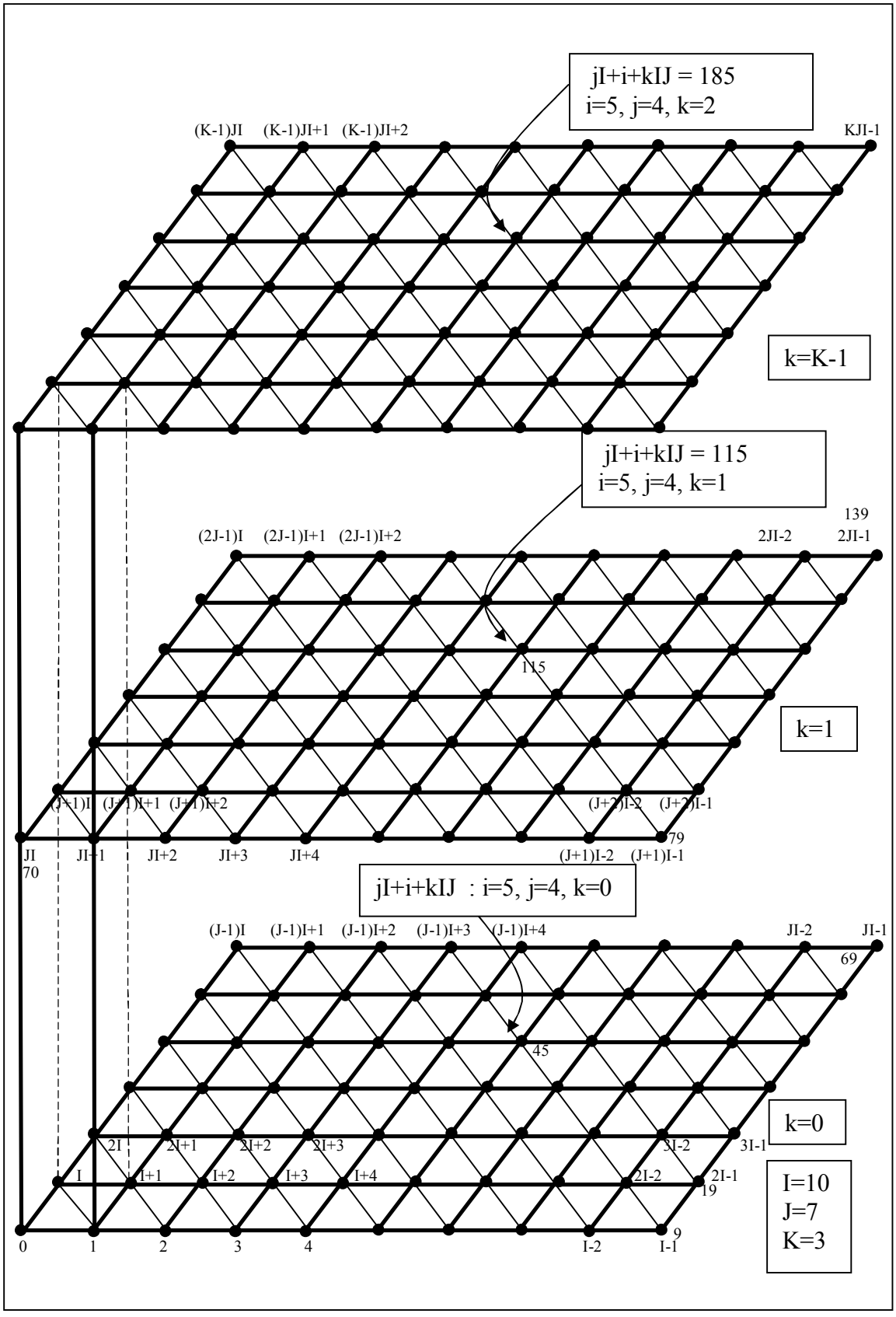

Figure 5.20. The expression for node number control (I=10, J= 7 and K=3)

The step by step advance of the proccess in which the real three dimensional model was built is given in the Figure 5.21.

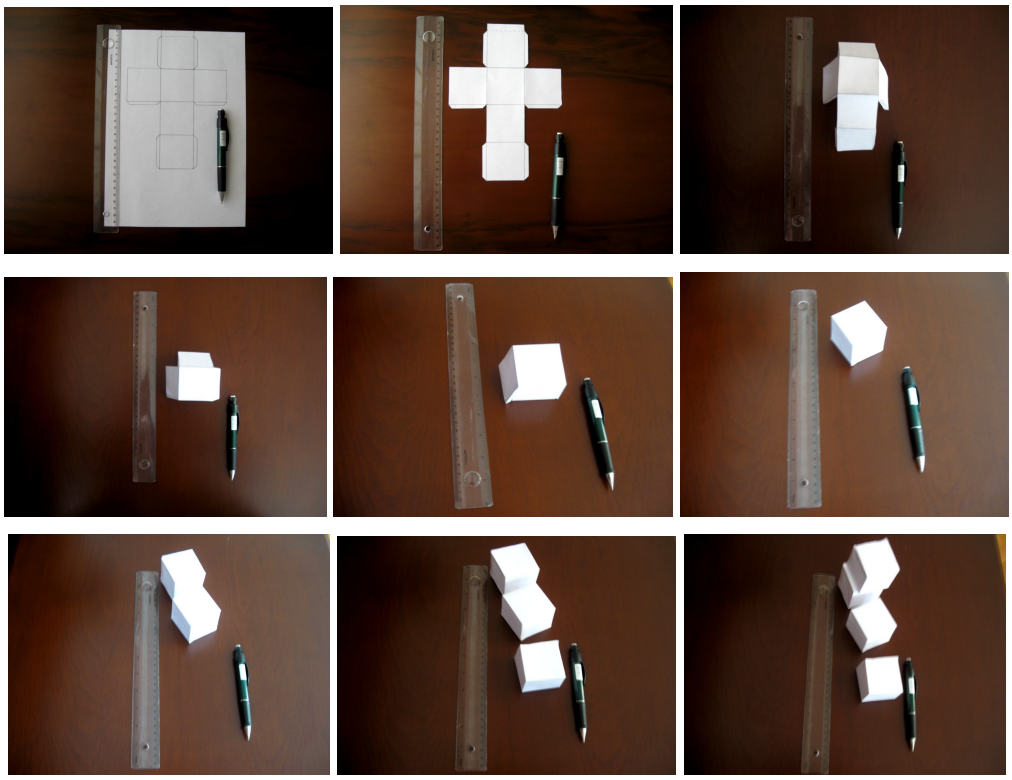

Figure 5.21. The process for making the model for three dimensional molecule

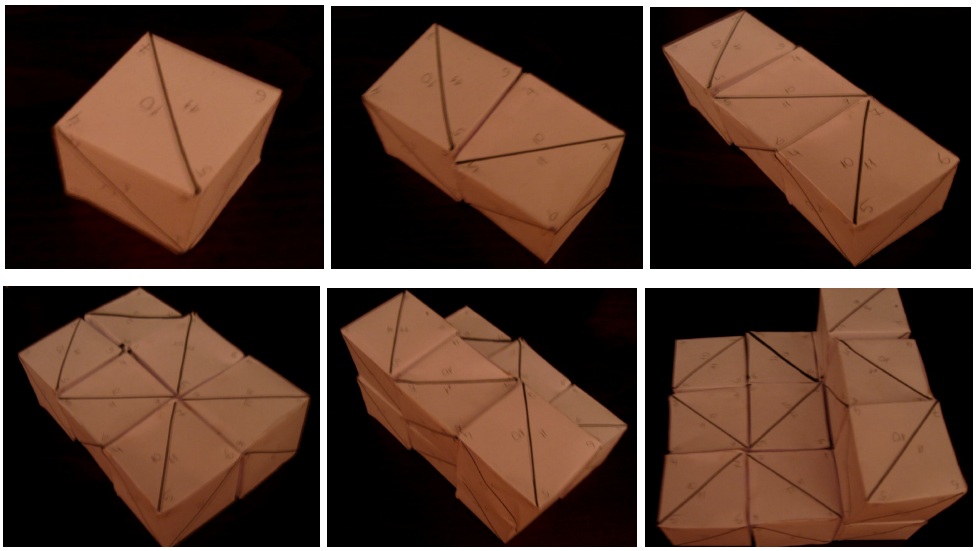

Figure 5.22. Three dimensional mesh structure preparation in order to see the orientation of the molecules

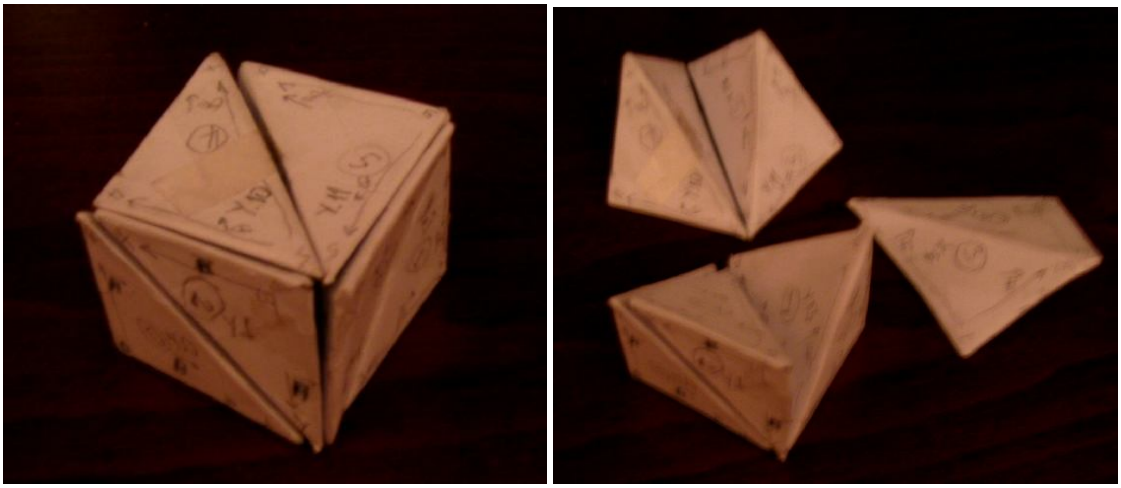

Figure 5.23. Three dimensional view of one molecule and its tetrahedron shaped elements

After the shapes of all the molecules and tetrahedra were seen the computer code is written for these new elements.

As it is seen above the three dimensional geometry was seen obviously and three dimensional mesh generating procedure was finished. The code which is producing the node coordinates, calculates the volume of each tetrahedron, the four surfaces of each tetrahedron, the inward normal vectors magnitude and vectoral coordinates, etc. is originally developed. It is given in Appendix A. The adaptation of this code to the main solver is left as a postdoctoral study.

As it was said before, the main feature of the code can be summarized as: it has a very user friendly graphical user interface (GUI), it can run for steady and transient problems, it can create color and vector graphs, structured and unstructured meshes can be created, the initial and boundary conditions can be specified easily.

The solver used here most importantly provides flexibility of creating the meshes (both structured and unstructured), specifying the initial and boundary conditions, starting stopping and pausing the calculations, displaying desired colourful and vector images on the screen.

In the numerical part of the thesis benchmark problems such as the steady-state lid-driven cavity, the unsteady lid-driven cavity, unsteady oscillatory lid-driven cavity test, vertical obstructed flow through square channels, natural flow in thermally driven cavity by different side wall temperatures, liquid metal flow past a circular cylinder in open channels exposed to external magnetic field, electromagnetic braking of liquid metals in vertical channels and levitation were solved by using this code.

6. NUMERICAL PROBLEMS AND RESULTS

6.1. The System of Equations Used in Numerical Solutions

The equations which are to be solved in this thesis are Navier-Stokes plus Maxwell equations which are the magnotohydrodynamic (MHD) equations. During the simulation of physical problems some assumptions will be done. The flow will be considered as incompressible and the fluid to be electrically conductive in some problems. The equations for continuity, momentum and energy can be given respectively as:

$$\vec{\nabla}.\vec{v} = 0 \tag{6.1}$$

$$\rho\left[\frac{\partial\vec{v}}{\partial t} + \vec{v}\vec{\nabla}.\vec{v}\right] + \vec{\nabla}P = \mu\nabla^2\vec{v} + \rho\vec{g} + \vec{F}_L \tag{6.2}$$

$$\vec{F}_L = \rho_e\vec{E}^T + \vec{J}^T \times \vec{B}^T \tag{6.3}$$

$$\rho C_v\left(\frac{\partial T}{\partial t} + \vec{v}\vec{\nabla}T\right) = k_T\nabla^2 T + \eta\vec{J}^T \cdot \vec{J}^T \tag{6.4}$$

where $\vec{v}$ is the velocity, P is the pressure, ρ is the density, μ is the viscousity, $\vec{g} = -g\hat{j}$ is the gravitational acceleration, $\vec{F}_L$ is Lorentz force , ρ_e is the charge density, $\vec{E}^T$ is the total (external+internal) electric field, $\vec{B}^T$ is total magnetic field, $\vec{J}^T$ is total current density, C_v is the specific heat, k_T is thermal conductivity, T is temperature, and η is electrical resistivity [29]. The last term in Equation 6.4 is called Joule heating term. It occurs in the equations due to the heating effect of the currents passing through the conductive fluid. The Maxwell equations which are the set of four equations that are used to describe all the known electromagnetic phenomena on the macroscopic scale must be related to the Navier-Stokes equations. Since the flow is assumed to be conductive $\vec{J}^T$, the total current density term makes a link to (Equation 6.7) the Maxwell's equations which can be given as:

$$\vec{\nabla} \cdot \vec{B} = 0 \tag{6.5}$$

$$\vec{\nabla}.\vec{J} = 0 \tag{6.6}$$

$$\vec{\nabla} \times \vec{B} = \mu_0 \vec{J} \tag{6.7}$$

$$\frac{\partial \vec{B}}{\partial t} - \vec{\nabla} \times (\vec{\nabla} \times \vec{B}) - \frac{\eta}{\mu_0} \nabla^2 \vec{B} = \vec{S}_{MAG} \tag{6.8}$$

where $\vec{S}_{MAG}$ is the source term driving the magnetic field, μ_0 is the magnetic permeability, $\vec{B}$ is the magnetic field. It is known that the total current density also satisfies Ohm's law given in the form :

$$\eta \vec{J}^T = \vec{E}^T + \vec{v} \times \vec{B}^T \tag{6.9}$$

where $\vec{J}^T$, $\vec{E}^T$, and $\vec{B}^T$ are total current density, total electric field and total magnetic field respectively which can be given as:

$$\vec{J}^T = \vec{J} + \vec{J}^{ext} \tag{6.10}$$

$$\vec{E}^T = \vec{E} + \vec{E}^{ext} \tag{6.11}$$

$$\vec{B}^T = \vec{B} + \vec{B}^{ext} . \tag{6.12}$$

Since the externally applied electric and magnetic fields can affect the current density their effects must also be taken into account during the calculations. If there are external effects existing there, the Maxwell equations written below must also be satisfied.

$$\vec{\nabla} \times \vec{E}^{ext} = 0 \tag{6.13}$$

$$\vec{\nabla}.\vec{B}^{ext} = 0 \tag{6.14}$$

$$\vec{\nabla}.\vec{E}^{ext} = \frac{\rho^{ext}}{\varepsilon_0} \tag{6.15}$$

$$\vec{\nabla} \times \vec{B}^{ext} = \mu_0 \vec{J}^{ext} \tag{6.16}$$

As previously said, Navier-Stokes and Maxwell equations are linked with the total current density $\vec{J}^T$ and this leads to the charge conservation equation which can be given as :

$$\frac{\partial q}{\partial t} + \vec{\nabla}.\vec{J}^T = 0 \tag{6.17}$$

$$\frac{\partial q_{ext}}{\partial t} + \vec{\nabla}.\vec{J}^{ext} = 0\,. \tag{6.18}$$

The Equation 6.17 says that the both $\vec{\nabla}.\vec{J}^T = 0$ and $\vec{\nabla}.\vec{J}^{ext} = 0$ under the condition that internal and external charges are constant in number and are not changing in time [6]. The definition of current density given in Equation 6.9 includes the effects of both external electric and magnetic fields existing around the flow itself. In order to represent $\vec{S}_{MAG}$ in more correct form it must include the external magnetic field as in the form given below in Equation 6.19.

$$\vec{S}_{MAG} = -\vec{\nabla} \times (\vec{v} \times \vec{B}^{ext}) \tag{6.19}$$

Here an assumption can be easily done since the localized charge neutrality the internal electric field can be neglected comparing with the externally applied electric field so that the Equation 6.11 can be rewritten as :

$$\vec{E}^T = \vec{E} + \vec{E}^{ext} \approx \vec{E}^{ext}\,. \tag{6.20}$$

Since in this thesis we are interested in low speed flows, the temperature effect on the density can have a significant effect. Because of the fact that the gravitational forces can be in comparable ranges with the inertia and viscous forces the temperature which will affect

the density and implicitly the gravitational force will play an important role in calculations. To take the temperature effect into account the Boussinesq approximation named for Joseph Valentin Boussinesq is used. The concentration and pressure also can have some effect on the density. In this approximation the variation of the density is neglected everywhere except in the buoyancy term since the little temperature change results with a little change in density which affects the buoyancy which is driving the motion. The mathematical representation for Boussinesq approximation is given as:

$$\rho = \rho_0\left[1 - \beta_T\left(T - T_0\right)\right] \tag{6.21}$$

where $\beta_T = -\left(1/\rho_0\right)\left(\partial\rho/\partial T\right)\big|_{C,P}$ is the expansion coefficient due to temperature. As an example the coefficient of volume expansion of water at $20^\circ C$ is $\beta_T = 210\times10^{-6}(^\circ C)^{-1}$ [30]. Note that ρ_0 and T_0 are reference density and reference temperature respectively. In some sources they are called the ambient density and temperature. The Equation 6.2 with a little rearrangement will have the form as:

$$\rho\left[\frac{\partial\vec{v}}{\partial t} + \vec{v}\vec{\nabla}.\vec{v}\right] + \vec{\nabla}P - \rho\vec{g} = \mu\nabla^2\vec{v} + \vec{F}_L. \tag{6.22}$$

After the Boussinesq approximation is taken into accout one can write

$$\vec{\nabla}P - \rho_0\vec{g} = \vec{\nabla}(P - P_0) = \vec{g}\left[\beta_T\left(T - T_0\right)\right]. \tag{6.23}$$

For Equation 6.24 one can take $\partial P/\partial y = \rho_0 g$ and $\partial P/\partial x = 0$ because of the fact that $P_0 = \rho_0 g y$. Before all the open form of MHD equations are written, the dimensionless form must be defined. The equations can produce useful solutions only when they are written in dimensionless forms in terms of some parameters. The number of these flow parameters depends on the number of equations used. The dimensionless form of the quantities can be written as:

$$P' = \frac{P}{P_0}, \quad \theta_t = \frac{T - T_c}{T_h - T_c}$$

where P' and θ_t are dimensionless pressure and temperature respectively, T_h is 'hot wall' T_c is 'cold wall' temperatures. The other dimensionless parameters are

$$t' = \frac{t}{t_0}, \ \rho' = \frac{\rho}{\rho_0}, \ \vec{r}' = \frac{\vec{r}}{\vec{r}_0}, \ \vec{v}' = \frac{\vec{v}}{\vec{v}_0}, \ \vec{E}' = \frac{\vec{E}}{\vec{E}_0}, \ \vec{B}' = \frac{\vec{B}}{\vec{B}_0}.$$

In MHD equations there are some important parameters. One of the most important numbers is Reynold's number, which is a unitless number, mathematically defined as:

$$Re = \frac{L_0 v_0}{\upsilon} \tag{6.24}$$

where L_0 is characteristic length (m), v_0 is velocity (m/s) and υ is kinematic viscosity (m^2/s). Reynold's number basically gives the ratio between the inertial and viscous forces in flow. It is mostly used in prediction of the flow nature if it is laminar or turbulent. Since turbulent regime is different in some properties from the laminar flow it is important to distinguish the flow type in engineering in order to avoid from the increased viscous losses. In turbulent flows the viscous loses are generally much higher then those in laminar flow.

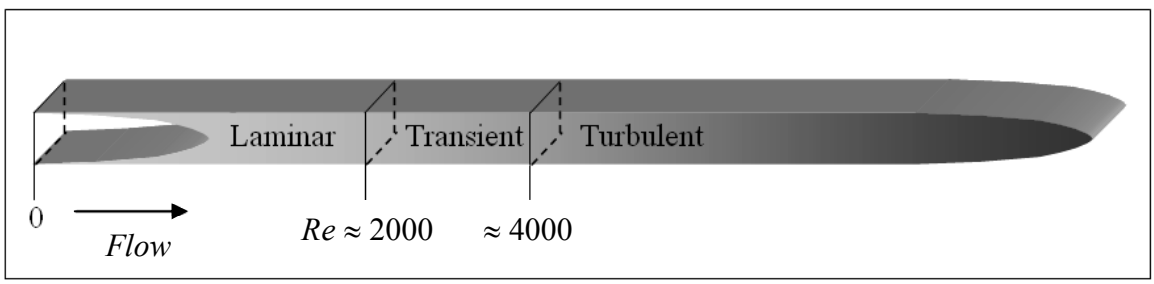

Figure 6.1. Diagram of flow regimes in pipe flow

Another parameter is called ‘magnetic Reynold’s number’. Basically it is the ratio of the induced magnetic field to the applied magnetic field [31].

$$R_{em} = \mu_0 \sigma V_0 L_0 = \frac{\mu_0 V_0 L_0}{\eta} \tag{6.25}$$

Prandtl number, Pr is the ratio of momentum diffusivity to the thermal diffusivity. If the value of Prandtl number is small it means that the heat diffusses more quickly than the diffusion of momentum. It also gives the information about the velocity and heat boundary layers ratio. If $Pr = 1$ the boundary layers coincide. The mathematical representation is given as:

$$Pr = \frac{\upsilon}{\alpha_t} \tag{6.26}$$

where υ is kinematic viscosity and α_t is thermal diffusivity.

Eckert number is another dimensionless parameter which gives the ratio between the kinetic energy of the flow to the boundary layer enthalpy.

$$E = \frac{v_0^2}{C_p \Delta T} \tag{6.27}$$

where C_p is the heat capacity under constant pressure and ΔT is the temperature difference.

Rayleigh number, Ra , which has a mathematical expression as :

$$Ra = \frac{g \beta_T \Delta T L_0^3}{\upsilon \alpha_t} \tag{6.28}$$

where g is gravitational acceleration, β_T is thermal expansion coefficient, υ is kinematic viscosity and α_t is thermal diffusivity constant. Rayleigh number physically gives an idea if the heat transfer is due to the conduction or convection in fluid. It is mostly used in heat transfer and free convection calculations.

Hartmann number, Ha is a dimensionless number defining the relative importance of the forces due to the magnetic induction to the viscous forces. It is the ratio of the magnetic forces to the viscous forces.

$$Ha = \sqrt{NR_e} = B_0 L_0 / \sqrt{\sigma / \mu} \tag{6.29}$$

where B_0 is magnetic field, L_0 is characteristic length, σ is electrical conductivity and μ is dynamical viscosity coefficient. The relation between Hartmann number and Reynold's number is given with the 'interaction parameter', N ,

$$N = \frac{Ha^2}{Re} \ . \tag{6.30}$$

Actually $'N'$ can be defined as the ratio between the electromagnetic forces and inertial forces. By using the defined dimensionless parameters and approximations the final MHD equations for incompressible flow are written in two dimensional Cartesian geometry as [29]:

$$\frac{\partial u}{\partial \tau} + \frac{\partial u}{\partial t} + u\frac{\partial u}{\partial x} + v\frac{\partial u}{\partial y} + \frac{\partial P'}{\partial x} + \frac{N}{R_{em}} B_y{}^T \left(\frac{\partial B_y}{\partial x} - \frac{\partial B_x}{\partial y} \right) = \frac{1}{R_e} \nabla^2 u \tag{6.31}$$

$$\frac{\partial v}{\partial \tau} + \frac{\partial v}{\partial t} + u\frac{\partial v}{\partial x} + v\frac{\partial v}{\partial y} + \frac{\partial P'}{\partial y} - \frac{N}{R_{em}} B_x{}^T \left(\frac{\partial B_y}{\partial x} - \frac{\partial B_x}{\partial y} \right) = \frac{1}{R_e} \nabla^2 u + \frac{R_a \theta}{P_r R_e{}^2} \tag{6.32}$$

$$\frac{\partial \theta}{\partial \tau} + \frac{\partial \theta}{\partial t} + u\frac{\partial \theta}{\partial x} + v\frac{\partial \theta}{\partial y} = \frac{1}{R_e P_r} \nabla^2 \theta + NE \left[E^{ext2} + (uB_y{}^T - vB_x{}^T)^2 \right] + \frac{R_a{}^i}{R_a R_e P_r} \tag{6.33}$$

$$\frac{\partial B_x}{\partial \tau} + \frac{\partial B_x{}^T}{\partial t} - B_x{}^T \frac{\partial u}{\partial x} + u\frac{\partial B_x{}^T}{\partial x} - B_y{}^T \frac{\partial u}{\partial y} + v\frac{\partial B_x{}^T}{\partial y} + \frac{\partial \psi_m}{\partial x} = \frac{1}{R_{em}} \nabla^2 B_x{}^T \tag{6.34}$$

$$\frac{\partial B_y}{\partial \tau} + \frac{\partial B_y{}^T}{\partial t} - B_x{}^T \frac{\partial v}{\partial x} + u\frac{\partial B_y{}^T}{\partial x} - B_y{}^T \frac{\partial v}{\partial y} + v\frac{\partial B_y{}^T}{\partial y} + \frac{\partial \psi_m}{\partial y} = \frac{1}{R_{em}} \nabla^2 B_y{}^T \tag{6.35}$$

$$\frac{\partial \psi_m}{\partial \tau} + \delta^2 \left(\frac{\partial B_x}{\partial x} + \frac{\partial B_y}{\partial y} \right) = 0 \tag{6.36}$$

$$\frac{\partial P'}{\partial \tau} + \beta^2 \left(\frac{\partial u}{\partial x} + \frac{\partial v}{\partial y} \right) = 0 \tag{6.37}$$

In Equations from 6.31 to 6.37 there are some new terms, such as τ which is pseudo-time, δ^2 which is magnetic relaxation constant, β^2 is an artificial compressibility parameter, and ψ_m is an artificial magnetic relaxation function. Since we are interested in the incompressible fluids the artificial compressibility parameter defined here has a significant meaning. This parameter is firstly defined by Chorin [32] in order to be used in the modification of the continuity equation. In incompressible flows the pressure is affected instantaneously by the disturbance in flow. However, with the effect of artificial compressibility there is a time lag between the flow disturbance and its effect on the pressure. The artificial compressibility relaxes the strict condition for mass conservation in each step. In order to have time- dependent solutions for this method, an iterative method can be applied to each physical step by satisfying the continuity equation. Mathematically the effect of artificial compressibility parameter can be shown as :

$$\frac{\partial P'}{\partial \tau} = \beta^2 \vec{\nabla}.\vec{v} \tag{6.38}$$

where $\vec{v} = u\hat{i} + v\hat{j} + w\hat{k}$.

Eventually the need for artificial compressibility parameter is coming from the desire to use the incompressible fluids in algorithms obtained for the compressible fluids.

In Equation 6.36, there is ψ_m artificial magnetic relaxation function. This function is also used to correct the magnetic fields in the same way that the artificial pressure corrects the velocity fields. These newly introduced parameters are used to satisfy the divergence constraints $(\vec{\nabla}.\vec{v} = 0, \vec{\nabla}.\vec{B} = 0)$ by solving the equations in subiterations in each time step. After the sub iterations converge $(i.e., \partial/\partial\tau \to 0)$, pressure and artificial magnetic relaxiation function are having the values which are used in correcting the magnetic fields and velocities in order to satisfy the divergence conditions.

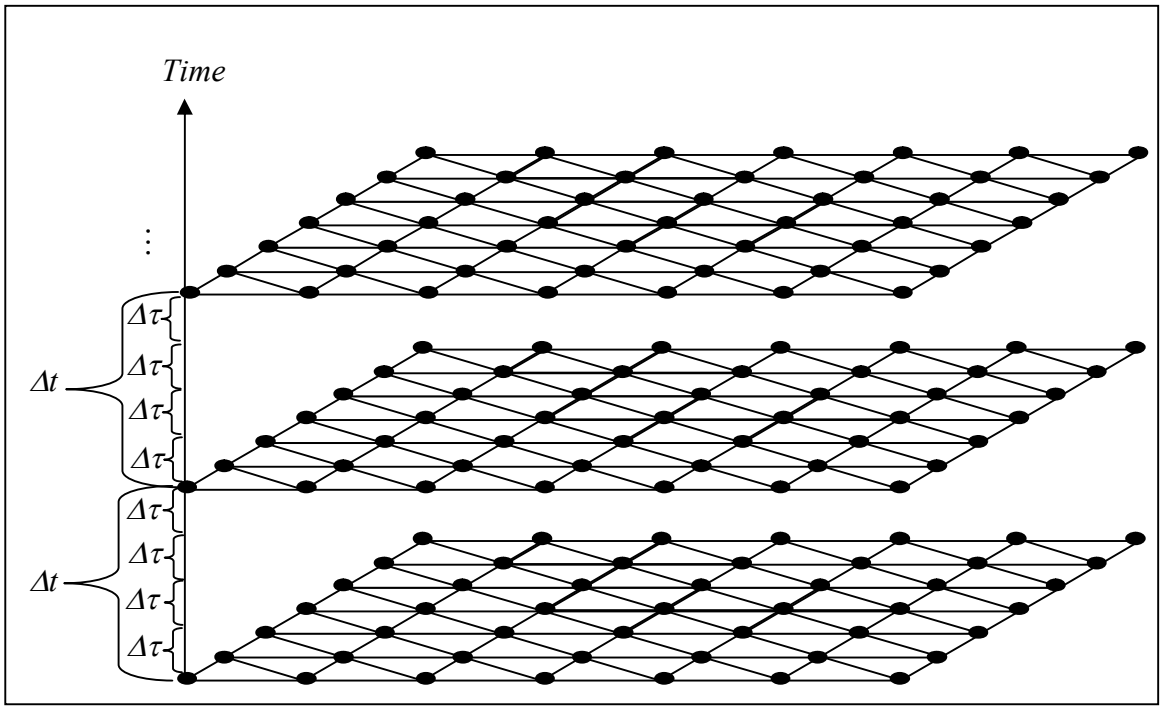

Figure 6.2. Dual time stepping sheme for a 2 dimensional mesh where $\Delta\tau$ is the pseudo time step and Δt is real time step

In numerical time derivatives it is better to utilize the implicit time stepping by Newton type of algorithm. Since in this thesis not only structured but also unstructured mesh types are used and this algorithm is very complicated for unstructured triangular meshes. This is the main reason for using the explicit multistage Runge-Kutta algorithm in pseudo time stepping. The time discretization process will be mentioned later in a more intensive manner. By using the dimensionless parameters the dimensionless MHD equations can be written in the following compact form:

$$\frac{\partial \vec{U}}{\partial \tau} + I_m \frac{\partial \vec{U}}{\partial t} + A\frac{\partial \vec{U}}{\partial x} + B\frac{\partial \vec{U}}{\partial y} = \vec{S}_T \tag{6.39}$$

where

$$\vec{U} = \left[P', u, v, \theta, B_x, B_y, \psi_m\right]^T \tag{6.40}$$

is the conservative state vector of fluid variables in which P' is dimensionless pressure, u is the x component and v is the y component of velocity, θ is dimensionless temperature

B_x and B_y are the x and y components of the magnetic field and the last term ψ_m, is the artificial magnetix relaxation function. In Equation 6.39 there is a diagonal matrix which is used to eliminate the pressure and artificial magnetic relaxation functions from the real time advancements. So the diagonal matrix I_m is given in the form as:

$$I_m = diag\ [0,1,1,1,1,1,0]^T . \tag{6.41}$$

A and B are Jacobian matrices which include the coefficients of $\left(\partial\vec{U}/\partial x\right)$ and $\left(\partial\vec{U}/\partial y\right)$directions respectively. $\vec{S}_T$ is the total source vector which has viscous and external parts and can be given as:

$$\vec{S}_T = \vec{S}_v + \vec{S}^{ext} . \tag{6.42}$$

By using the definition given above Jacobian matrices in Equation 6.39 can be written as:

$$A = \begin{bmatrix} 0 & \beta^2 & 0 & 0 & 0 & 0 & 0 \\ 1 & u & 0 & 0 & 0 & \frac{NB_y}{R_{em}} & 0 \\ 0 & 0 & u & 0 & 0 & \frac{NB_x}{R_{em}} & 0 \\ 0 & 0 & 0 & u & 0 & 0 & EB_x \\ 0 & -B_x^T & 0 & 0 & u & 0 & 1 \\ 0 & 0 & -B_x^T & 0 & 0 & u & 0 \\ 0 & 0 & 0 & 0 & \delta^2 & 0 & 0 \end{bmatrix},$$

$$B = \begin{bmatrix} 0 & 0 & \beta^2 & 0 & 0 & 0 & 0 \\ 0 & v & 0 & 0 & \frac{NB_y}{R_{em}} & 0 & 0 \\ 0 & 0 & v & 0 & \frac{NB_x}{R_{em}} & 0 & 0 \\ 0 & 0 & 0 & v & 0 & 0 & EB_y \\ 0 & -B_y^T & 0 & 0 & v & 0 & 0 \\ 0 & 0 & -B_y^T & 0 & 0 & v & 1 \\ 0 & 0 & 0 & 0 & \delta^2 & 0 & 0 \end{bmatrix}$$

and source vectors are given as

$$\vec{S}_v = \begin{bmatrix} 0 \\ \left(Re\nabla^2 u\right)^{-1} \\ \left(Re\nabla^2 v\right)^{-1} \\ \left(RePr\nabla^2\theta\right)^{-1} \\ \left(R_{em}\nabla^2 B_x\right)^{-1} \\ \left(R_{em}\nabla^2 B_Y\right)^{-1} \\ 0 \end{bmatrix}, \quad \vec{S}^{ext} = \begin{bmatrix} 0 \\ \left(-NB_y^{ext}/R_{em}\right)\left(\partial B_y^{ext}/\partial x - \partial B_x^{ext}/\partial y\right) \\ \left(NB_x^{ext}/R_{em}\right)\left(\partial B_y^{ext}/\partial x - \partial B_x^{ext}/\partial y\right) + Ra\theta/PrRe^2 \\ NE\left[E_{ext}^2 + \left(uB_y - vB_x\right)^2 + \left(uB_y^{ext} - vB_x^{ext}\right)\right] \\ 0 \\ 0 \\ 0 \end{bmatrix}.$$

So that the explicit form of Equation 6.39 is

$$\frac{\partial}{\partial\tau}\begin{bmatrix} P' \\ u \\ v \\ \theta \\ B_x \\ By \\ \psi_m \end{bmatrix} + I_m\frac{\partial}{\partial t}\begin{bmatrix} P' \\ u \\ v \\ \theta \\ B_x \\ By \\ \psi_m \end{bmatrix} + \begin{bmatrix} 0 & \beta^2 & 0 & 0 & 0 & 0 & 0 \\ 1 & u & 0 & 0 & 0 & \frac{NB_y}{R_{em}} & 0 \\ 0 & 0 & u & 0 & 0 & \frac{NB_x}{R_{em}} & 0 \\ 0 & 0 & 0 & u & 0 & 0 & EB_x \\ 0 & -B_x^T & 0 & 0 & u & 0 & 1 \\ 0 & 0 & -B_x^T & 0 & 0 & u & 0 \\ 0 & 0 & 0 & 0 & \delta^2 & 0 & 0 \end{bmatrix}\frac{\partial}{\partial x}\begin{bmatrix} P' \\ u \\ v \\ \theta \\ B_x \\ By \\ \psi \end{bmatrix} + \begin{bmatrix} 0 & 0 & \beta^2 & 0 & 0 & 0 & 0 \\ 0 & v & 0 & 0 & \frac{NB_y}{R_{em}} & 0 & 0 \\ 0 & 0 & v & 0 & \frac{NB_x}{R_{em}} & 0 & 0 \\ 0 & 0 & 0 & v & 0 & 0 & EB_y \\ 0 & -B_y^T & 0 & 0 & v & 0 & 0 \\ 0 & 0 & -B_y^T & 0 & 0 & v & 1 \\ 0 & 0 & 0 & 0 & \delta^2 & 0 & 0 \end{bmatrix}\frac{\partial}{\partial y}\begin{bmatrix} P' \\ u \\ v \\ \theta \\ B_x \\ By \\ \psi_m \end{bmatrix} =$$

$$\begin{bmatrix} 0 \\ \left(Re\nabla^2 u\right)^{-1} \\ \left(Re\nabla^2 v\right)^{-1} \\ \left(RePr\nabla^2\theta\right)^{-1} \\ \left(R_{em}\nabla^2 B_x\right)^{-1} \\ \left(R_{em}\nabla^2 B_Y\right)^{-1} \\ 0 \end{bmatrix} + \begin{bmatrix} 0 \\ \left(-NB_y^{ext}/R_{em}\right)\left(\partial B_y^{ext}/\partial x - \partial B_x^{ext}/\partial y\right) \\ \left(NB_x^{ext}/R_{em}\right)\left(\partial B_y^{ext}/\partial x - \partial B_x^{ext}/\partial y\right) + Ra\theta/PrRe^2 \\ NE\left[E_{ext}^2 + \left(uB_y - vB_x\right)^2 + \left(uB_y^{ext} - vB_x^{ext}\right)\right] \\ 0 \\ 0 \\ 0 \end{bmatrix}. \qquad (6.43)$$

Equation 6.43 is the final equations which are to be solved. Note that there are two newly defined artificial parameters, β^2, the artificial compressibility parameter and ψ_m, the artificial magnetic relaxation function which are used in correction of velocity fields and magnetic fields respectively. The pressure P' which was related to the artificial

compressibility parameter such as given in Equation 6.38 and artificial magnetic relaxation function are put only in pseudo time derivation part in equation and they are eliminated from the real time derivation parts by using the diagonal unit matrix. By using the defined equations above the numerical problems below were solved by using matrix distribution scheme which is explained in the previous chapter.

6.2. Numerical Tests

6.2.1. The Steady State Lid Driven Cavity Test

This is the classical two dimensional lid-driven cavity test. It is assumed there is no heat transfer and externally applied electromagnetic fields. There is a sliding lid on the upper boundary which has a constant horizontal velocity (i.e. $u = 1$) in $+x$ direction. This sliding lid generates a circulation in the cavity. The solution domain for this test was chosen as a square-shaped cavity which is filled with isotropic triangles with 41×41 nodes (Figure 6.3). Starting with no flow initial condition within the cavity, this test problem was run for *Re*=100, *Re*=400, *Re*=1000, and *Re*=5000 together with no-slip wall conditions (i.e. $u = v = 1$) on the walls of the cavity and *u*=1,*v*=0 condition along its upper boundary. The resulting velocity vectors within the cavity, after steady state is achieved at *t* =2, are shown in Figure 6.4. There are velocity profiles for four different *Re* (Reynolds) numbers. As can be seen, the constant flow along the upper lid drives the flow circulation whose centers shift as the *Re* number is increased.

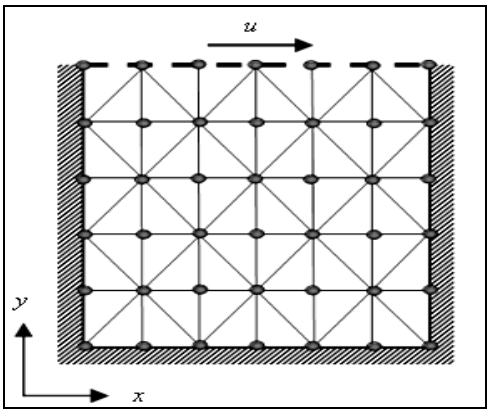

Figure 6.3. Solution domain shape for the lid driven cavity test problem

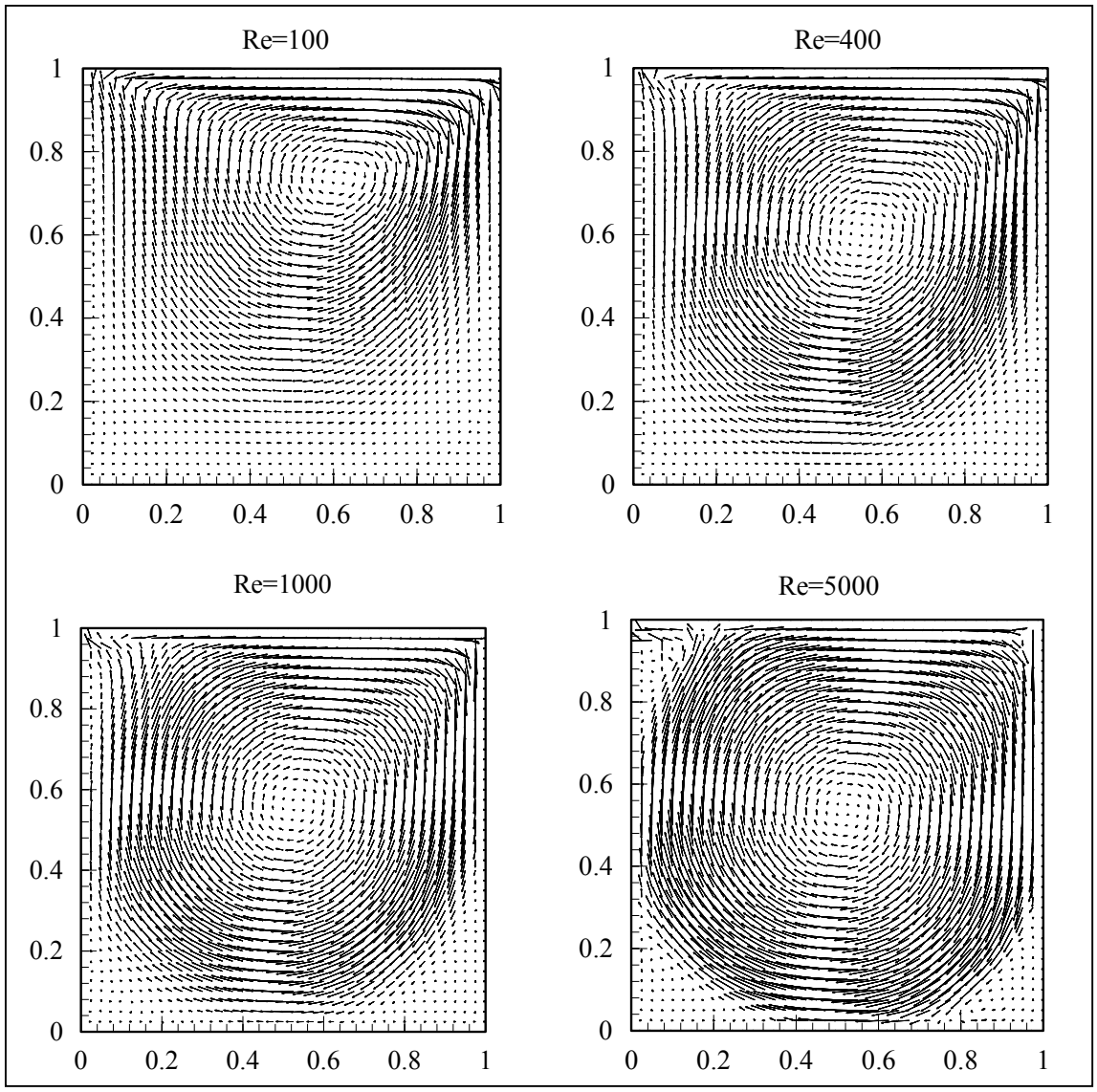

Figure 6.4. The velocity vectors formed in the square shaped cavity

As it is seen in Figure 6.4 for different Reynolds numbers the velocity vectors have different shapes. The centres of circulations for different Reynolds numbers took shape in different places in the cavity. It seems that for high Reynolds numbers the circulation center can coincide with the centre of square shaped cavity and the corner circulating regions on the bottom get similar.

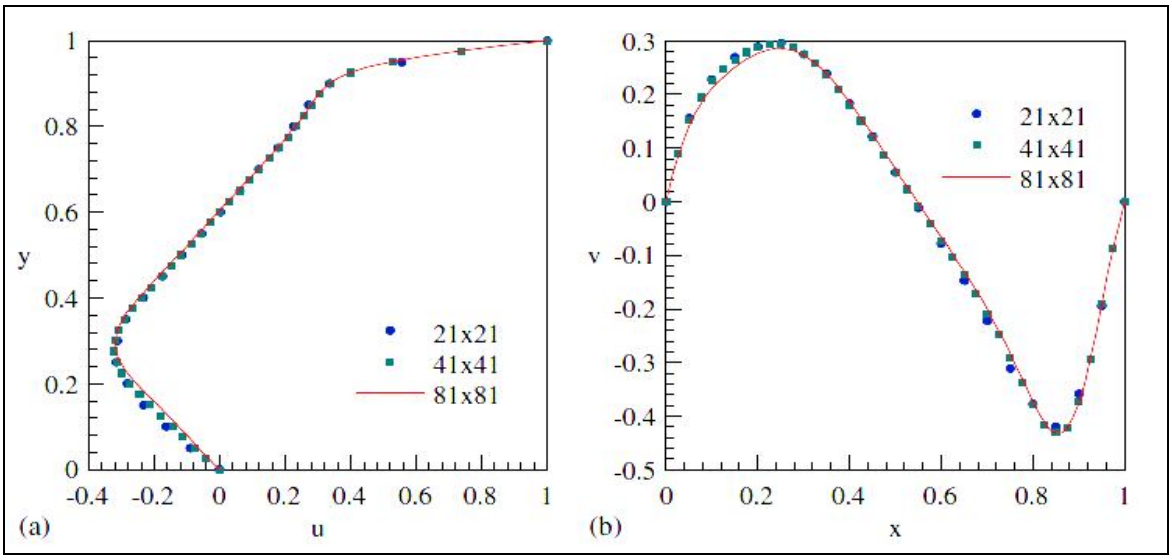

Figure 6.5. $y-u$ and $v-x$ profiles passing through the midpoint of the cavity

In order to see the convergence of the numerical solutions, the same problem for different mesh types is solved. The generated meshes were $21\times21, 41\times41, 81\times81$. There are y profile of velocity u and x profile of velocity v passing at the midpoint of the cavity presented in Figure 6.5 (a) and (b) respectively. As seen, the mesh gets finer the solutions converged to the correct solution. There were some deviations in Figure 6.5 (a) especially for y profile of u velocity between the limits 0.3 -0 for y , and -0.4-0 for u values. However, the differences got smaller as the mesh was refined.

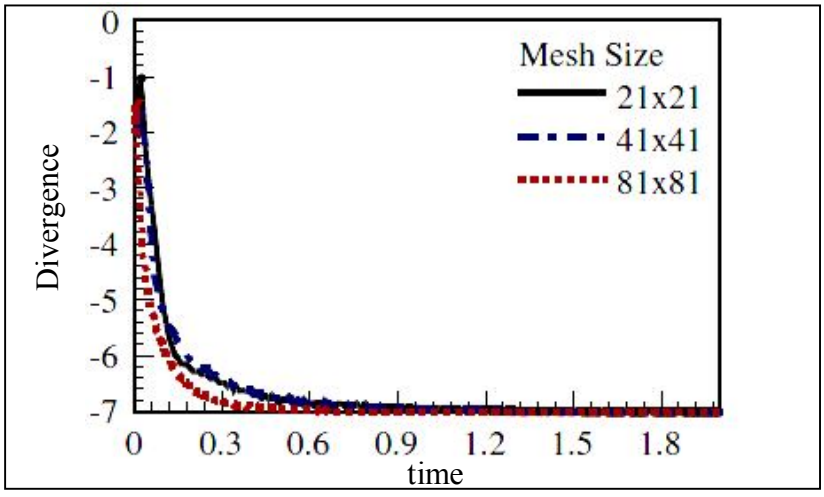

Figure 6.6. Divergence – time graph for three different mesh types

In order to see how the divergence decreases depending on time and depending on the mesh types the graph in Figure 6.6 was drawn. It is easily seen that for finer meshes the divergence decreases quickly. The results were found in very good agreement with references [6] and [33] .

6.2.2. The Unsteady Lid Driven Cavity Test

In this test problem the boundary and initial conditions were chosen as the same as in the steady state lid driven cavity test. The problem was solved for two different Reynolds numbers, the cavity had again the square shape. However, the investigated property of the fluid was the velocity behaviour of the mid point of the cavity. The problem was solved by using relatively fine mesh which was 81×81. The velocity in this problem had a step shape which was given as $u = 0$ *for* $t < 0$ and $u = 1$ *for* $t \geq 0$. The results shown that the velocity was nearly constant after t=5 for the flow with Reynolds number 100 , but it was not possible to say the same thing for the flow with Reynolds number 400. The velocity in the centre decreased up to t=5 and it increased later. There was a something like a turning point for velocity values at centre at that time .

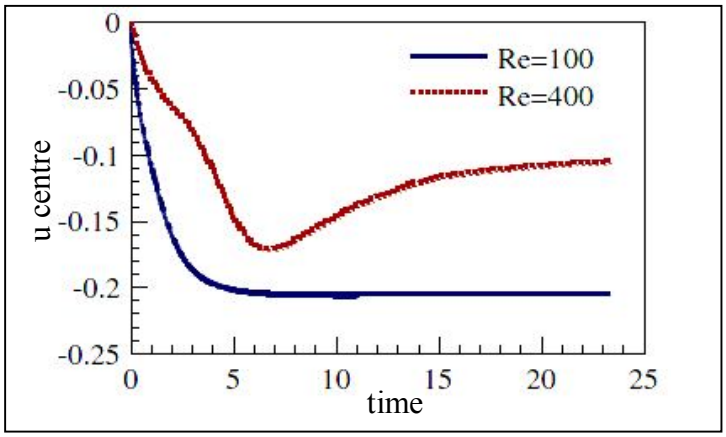

Figure 6.7. u centre – time graph for flows with two different Reynolds numbers

The results were found in very good agreement with reference[33].

6.2.3. The Unsteady Oscillatory Lid Driven Cavity Test

Differently from the previous tests there were periodic velocity in the upper boundary. The flow inside the cavity was controlled by the velocity which had a sinusodial profile. The velocity function on the upper boundary was assumed to be $u(t) = u_0 Cost$. Since the profile of the velocity driving the fluid is periodic, the oscillatory solutions will be formed in the cavity. In this problem the drag on the upper boundary was calculated by using the following formula which is $D = \int_0^1 (\partial u/\partial y) dx$. In order to see how the drag is changed depending on time for different meshes ($33\times33, 65\times65, 133\times133$). The results were given in Figure 6.8.

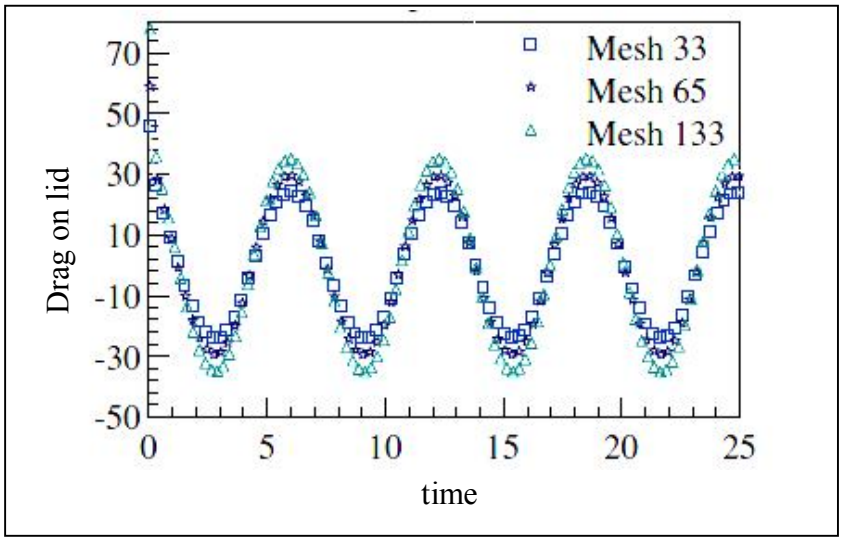

Figure 6.8. Drag on lid – time graph for different meshes

In this problem Reynolds number was taken to be 400. Not only for different meshes but also for different time steps the same problem was solved. In this part the mesh was constant and was taken to be 65×65 additionally time steps were chosen to be $\Delta t = 0.01$, $\Delta t = 0.05$ and $\Delta t = 0.1$. The results were presented in Figure 6.9.

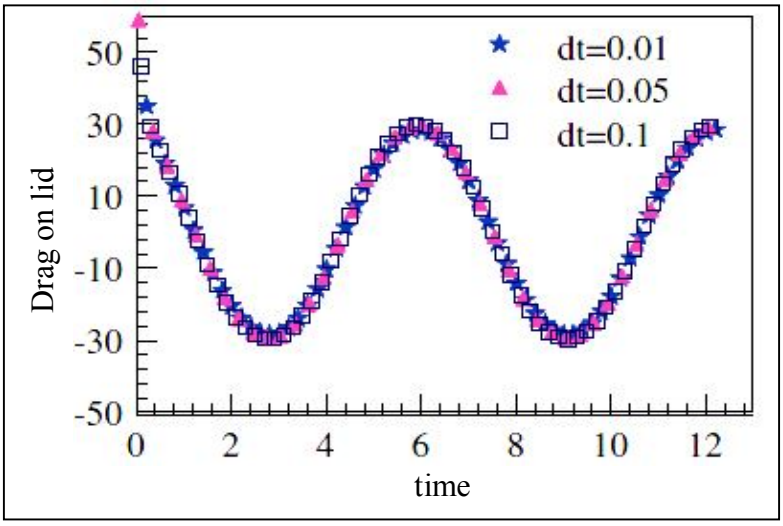

Figure 6.9. Drag on lid – time graph for different time steps

In conclusion these results were found in very good agreement with the results given in the reference [34].

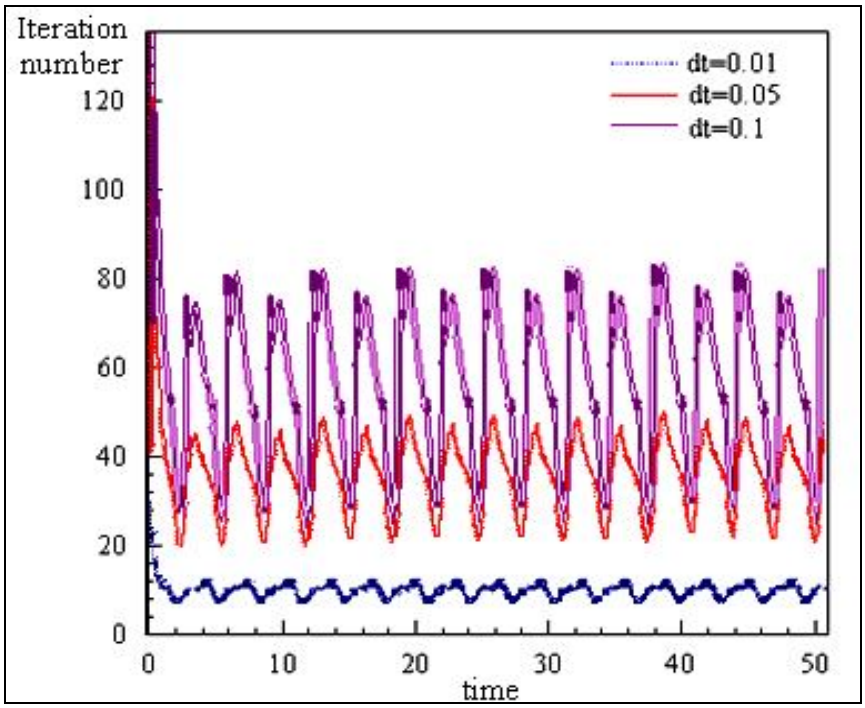

Figure 6.10. Iteration number graph for different time steps

The iteration number decreased for smaller time steps as seen in Figure 6.10.

6.2.4. Vertical Obstructed Flow Through the Square Channels

In this test problem the flow in channel was investigated. The flow here was driven by the pressure difference. This kind of problems are very important in pipe flows, internal flow cavities etc. The solution domain had an aspect ratio 4. The x component of the mesh was between 0-1 and, y component was between 0-4. One important point here is that the mesh was made finer at the top and at the bottom of the channel (Figure 6.11 (a)). The mesh node numbers were chosen to be 21×41, $Re=100$, $\beta^2=10$ and $Pr=0.72$. The boundary conditions were given in the following manner: no slip condition for the walls $(u=0, v=0)$, there was open outlet in the right wall and its velocity there was $u=1$, the pressure at the upper boundary was 0 and the pressure in the bottom boundary was set to -1. This pressure gradient will drive the flow through the negative y $(-y)$ direction. When there is no obstruction in the channel the vertical parabolic velocity profile bends towards the opening on the side wall and a small circulation region was created on the lower left corner as clearly seen from Figure 6.12(b).

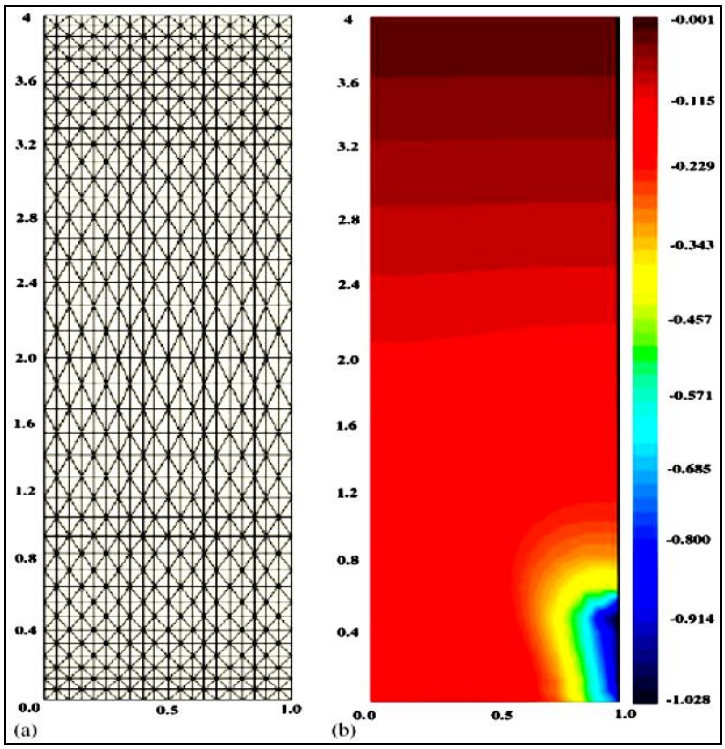

Figure 6.11. (a) The structured mesh grid finer at the bottom and at the top (b) The pressure contours in the vertical channel

Another interesting challenge occurs for the same test when some obstructions are put in the channel. In this test the obstructions were rectangular in shape. The velocity profiles in the channel without obstruction, with obstuction on the left and with the obstuction on the right walls separately were shown in Figure 6.12. The velocity profiles were found different for these three different cases. These results can be helpful for designing the pipes because the nature of the flow is seen easily in this simulation.

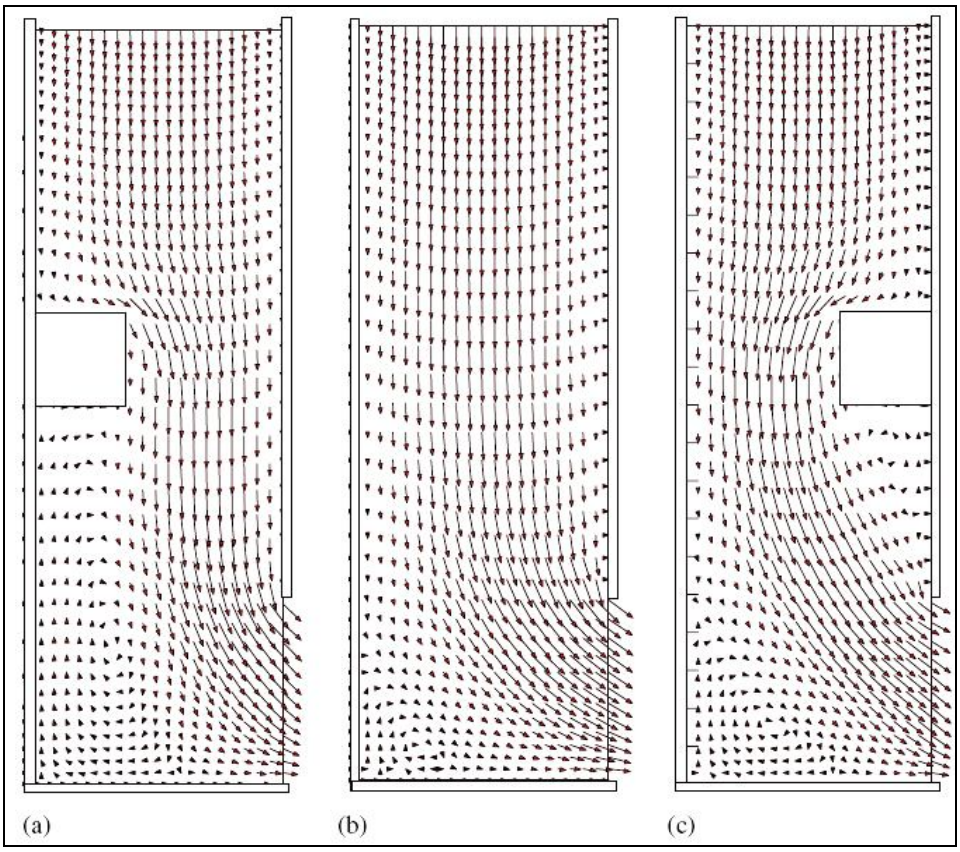

Figure 6.12. (a) The vertical natural flow with the presence of the obstacle on the left wall (b) The vertical natural flow without the presence of the obstacle (c) The vertical natural flow with the presence of the obstacle on the right wall

6.2.5. Natural Flow in Thermally Driven Cavity by Different Side Wall Temperatures

This is the classical benchmark problem of Davis [35]. The test is about the natural convection heat transfer inside the cavities. It is very important in a wide range of applications such as room insulation, ventilation etc. In this test problem $Pr = 0.71$ was

taken and the left wall was kept hot, the right was kept cold, $Ra = 10^4$ and $Ra = 10^5$ were taken, artificial compressibility parameter was chosen to be $\beta^2 = 100$. The test was solved on 61×61 isotropic mesh. In this problem naturally circulating flow was developed because of the temperature gradient existing between the walls. The temperature contours for two different Ra numbers were shown in Figure 6.13.

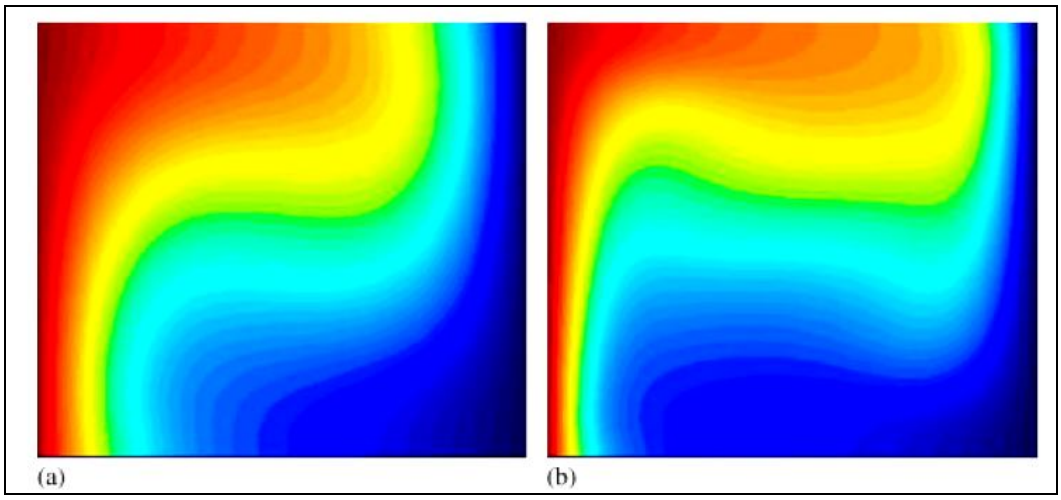

Figure 6.13. Temperature profile for (a) $Ra = 10^4$ and (b) $Ra = 10^5$ for thermally driven cavity

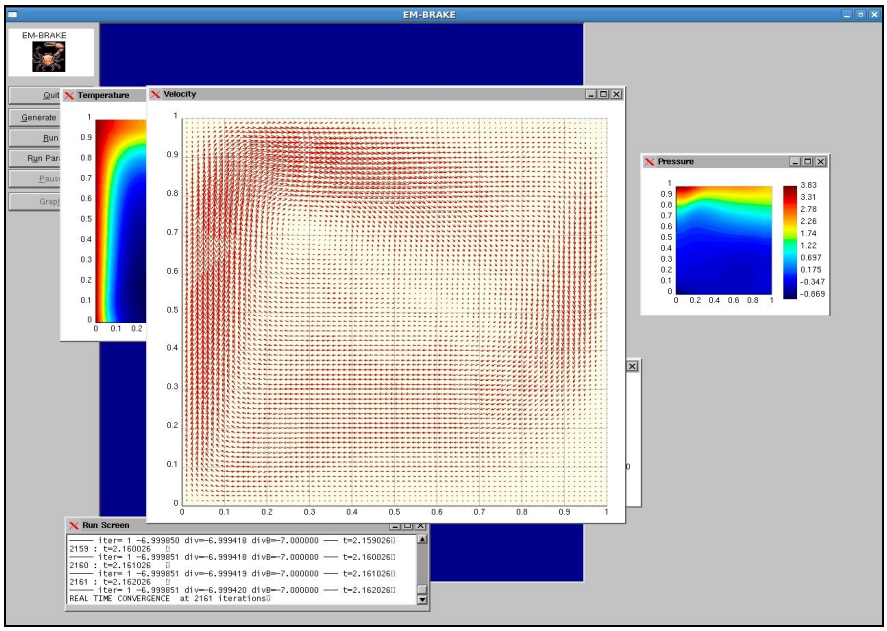

Figure 6.14. The view of the programme when the problem was solving

Numerical solutions for this test agreed very well with the results in reference [35].

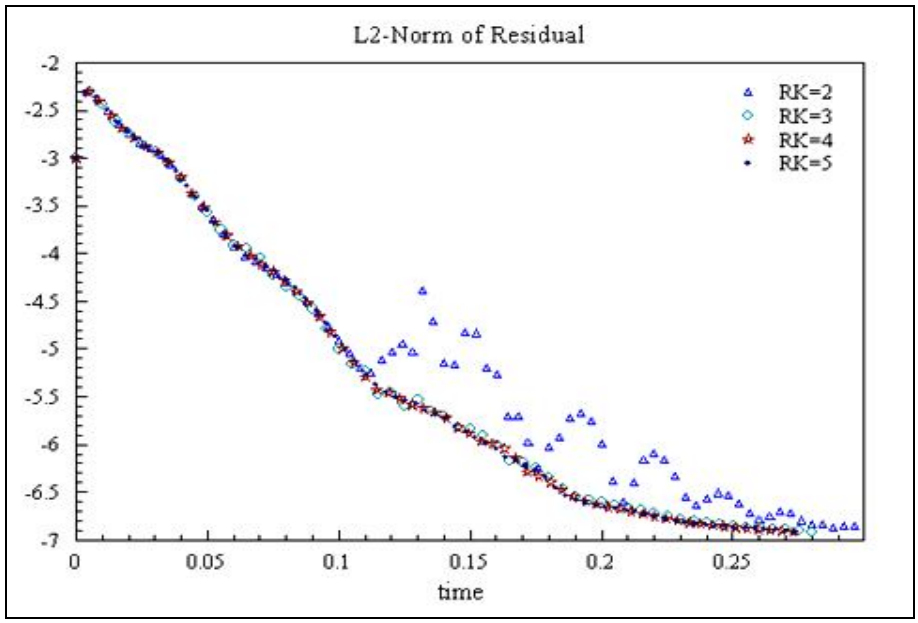

Figure 6.15. L2 norm of residual – time graph for different orders of Runge-Kutta method

In order to see the residual drop for different Runge-Kutta orders, the problem was solved from 2^{nd} to 5^{th} order. The solutions reach the steady state when the L2 norm of residuals droped to -7 as seen in Figure 6.15. It was seen that there were some fluctuations for second order of Runge-Kutta level but the other levels had nearly the same profiles. These results were used in order to compare the different orders of Runge-Kutta discretization method.

6.2.6. Liquid Metal Flow Past a Circular Cylinder in Open Channels Exposed to External Magnetic Field

This is one of the relatively new test problems which can be thought as an original one. In this test the conducting incompressible liquid metal flow past a circular cylinder when the medium includes both vertical and parallel magnetic fields. The flow around the cylinder becomes unstable and vortices start to shed from the cylinder surface behind which a periodic flow is obtained for both $Re = 100$ and $Re = 400$. It was shown in this test that such flows can be stabilized by using an externally applied magnetic field. The

cylinder with a radius of unity was placed at $x = 0$ and $y = 0$ in a computational domain of $-4.5 \le x \le 15.5$ and $-4.5 \le y \le 4.5$. The inflow boundary condition was used on the left surface with $u = 1, v = 0, B_{x,y} = 1$ and reflecting boundary conditions were used on the upper and lower boundaries with $v = 0, B_{x,y} = 1$. The right boundary was chosen to be the outgoing boundary on which no condition was imposed on velocity but $B_{x,y} = 1$ was taken when magnetic fields exist. The cylinder surface was taken as no-slip boundary with $u = v = 0$ and $B_{x,y} = 1$. This problem was run for three different cases which were with no magnetic field, with a parallel field (in x direction) and with that in y direction for $Re = 100$ and $Re = 400$. The interaction parameters, N, were chosen to be $0, 0.001, 0.0625, 0.25$ corresponding to Hartmann numbers of $0, 1, 2.5, 5$ respectively and magnetic Reynolds number was 10^{-5}. These parameters were chosen to compare the results with those presented by [36] who solved the problem with only a horizontal magnetic field (i.e. $B_x \neq 0$ and with only $Re = 100$); however, the effects of vertical field were also examined additionally in this work. Figure 6.16 shows the time behavior of x-velocity contours at times $t = 0, 30, 60, 90, 120, 150$ for $Re = 100$ and $Re = 400$ with no magnetic field .

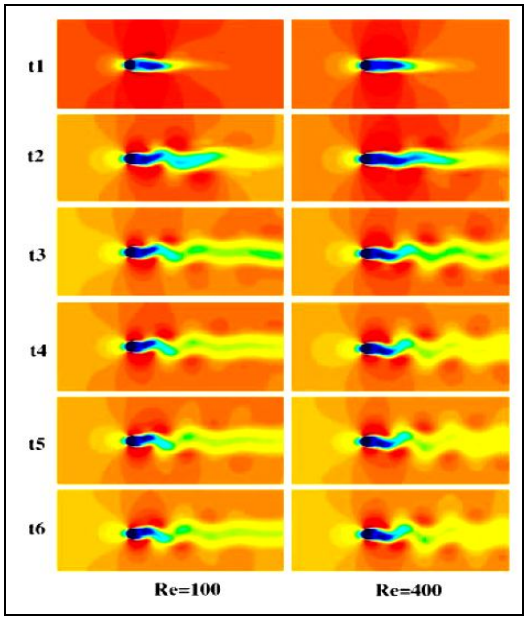

Figure 6.16. The contour graphs and time behaviour of u - velocity for two different Reynolds numbers when no magnetic field exists, $N = 0$, $Ha = 0$

From the results, temporal behavior of the solutions at $Re = 100$ and $Re = 400$ for $N = 0.25\ (Ha = 5)$ showed that the vertical magnetic field eliminates oscillations for $Re = 100$ but does not eliminate for $Re = 400$ as seen in Figure 6.17.

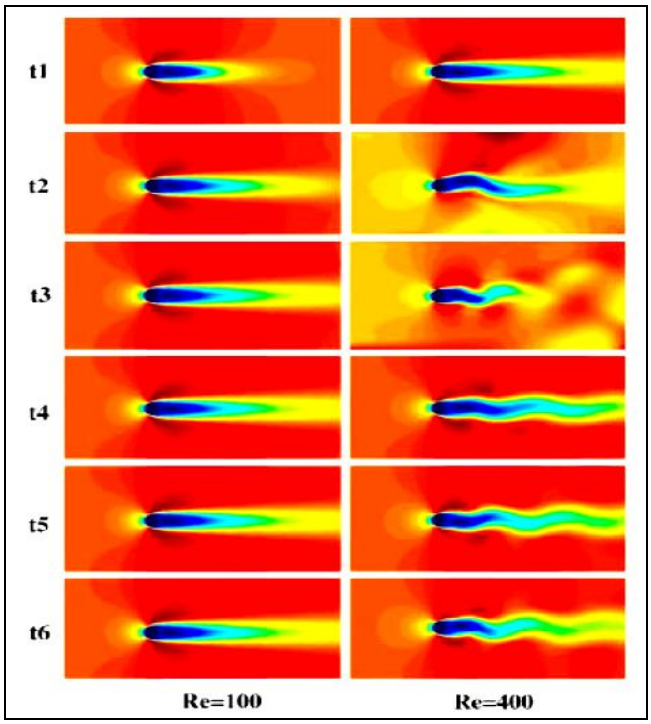

Figure 6.17. The contour graphs and time behaviour of u - velocity for two different Reynolds numbers when a perpendicular field , B_y , exist for $N = 0.25$ which corresponds to $Ha = 5$

Horizontal magnetic field $(B_y = 0, B_x \neq 0)$ with different Hartmann numbers (different strengths) was applied to the same problem for $Re = 100$. Even at lower Hartmann numbers eliminated the oscillations as it is seen in Figure 6.18. The important effect of magnetic field on the conducting fluid is its ability to create an extra drag on the immersed body by adding extra viscosity in the fluid. These effects are of great importance especially for metal casting in atmospheric pressures and thin film deposition in vacuum chambers.

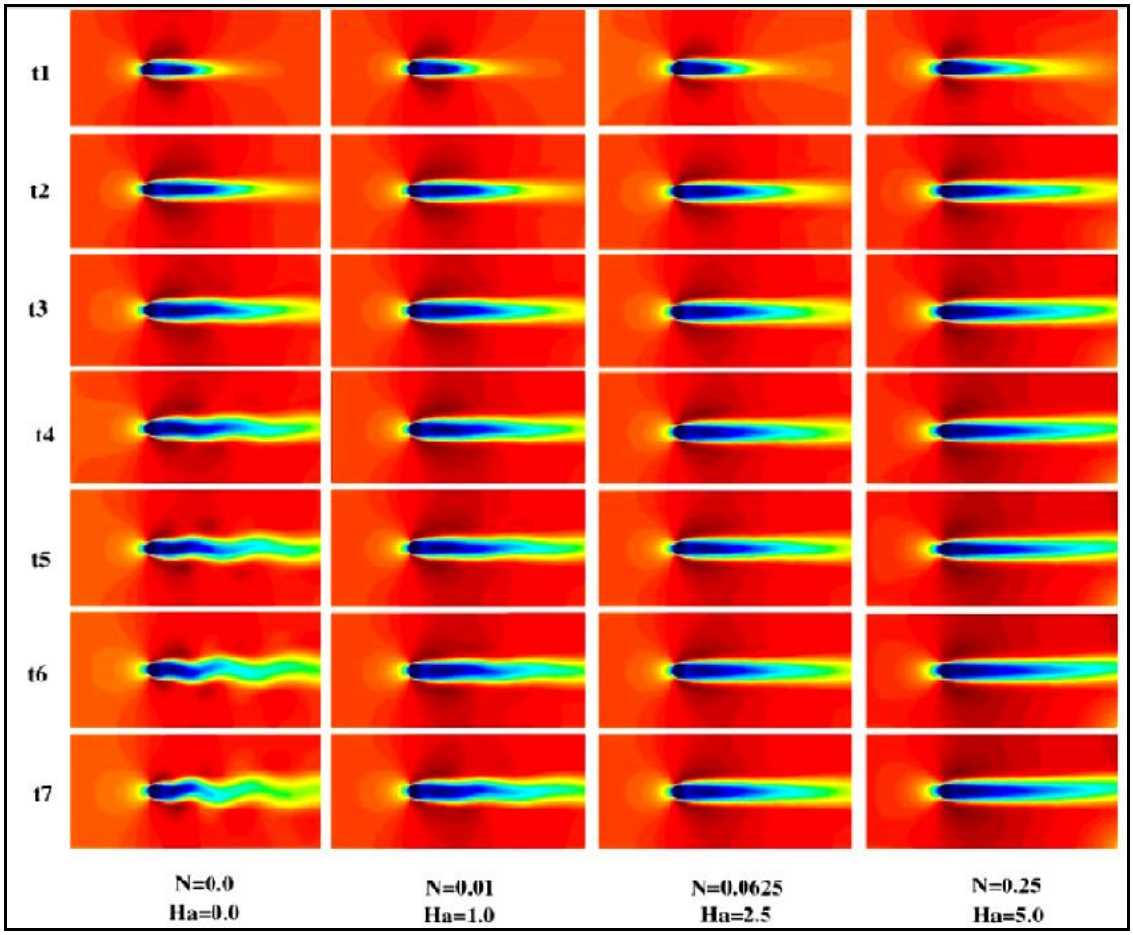

Figure 6.18. The time behaviour of the flow around the cylinder at different interaction parameters for $Re = 100$ and $By = 0, Bx \neq 0$

Vertically applied magnetic field results are relatively new in comparing with the results for horizontally applied magnetic field that were found in very good agreement with reference [36].

6.2.7. Electromagnetic Braking of Liquid Metals in a Vertical Channel and Levitation

The flow control of liquid metals is important especially for both heat transfer problems and MHD generator problems flow control has very high importance. In the reference [37] it is proposed that in order to slow down or levitate liquid metals both externally applied DC electric and perpedicularly applied magnetic fields can be used. If the strenghts for externally applied fields are appropriate, the liquid metal flowing down

($-y$ direction) through a rectangular channel can be slowed down. In the work done in reference [37], the averaged vertical velocity, which reached its steady value of -1.5m/s dropped to zero exhibiting a series of damped oscillations when perpendicular electric and magnetic fields were switched on. The same numerical experiment was done here with two-dimensional simulation. In order to understand the shape of the problem better, three dimensional structure of the liquid metal flow control region was shown in Figure 6.19. The rectangular solution domain was shown in Figure 6.20.

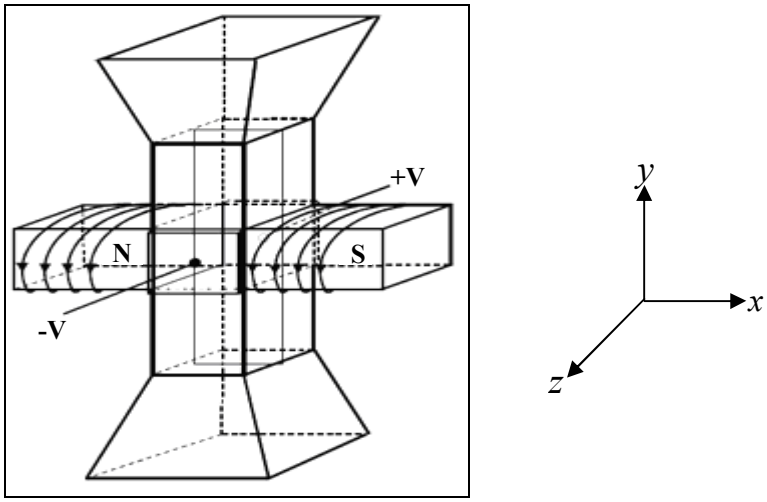

Figure 6.19. The proposed shape of a system for electromagnetic braking test problem

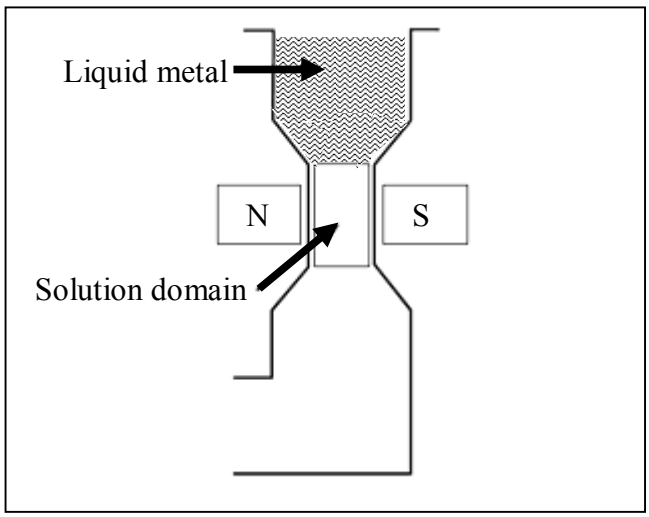

Figure 6.20. Two dimensional view of solution domain

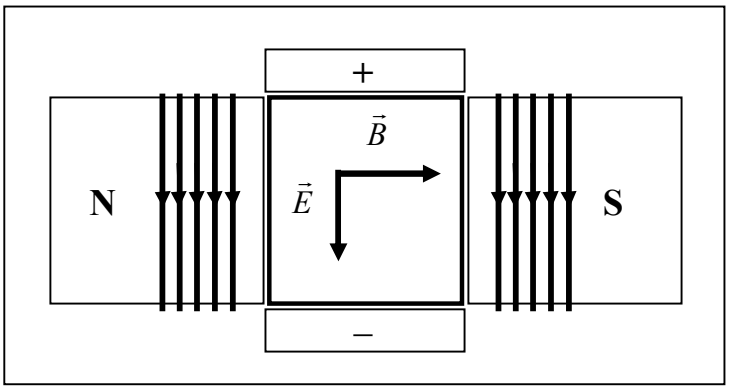

Figure 6.21. The top view of the solution domain in which the directions of externally applied fields were depicted

External magnetic field was applied perpendicular (x direction) to the flow direction ($-y$ direction) through coils and the external electric field was applied in z direction (perpendicular to solution domain). In that case, the direction of $\vec{E}\times\vec{B}$ force opposes the gravitational force, which is in $-y$ direction. The externally applied electric and magnetic field vectors and the coil-winding directions were shown in Figure 6.21 as top view. Analytically the external magnetic field is given as the following by solving $\nabla^2\vec{A}_z = 0$ where $\vec{A}_z$ is the vector potential satisfying $\vec{B}^{ext} = \vec{\nabla}\times\vec{A}$ where $\vec{B}^{ext}$ satisfies $\vec{\nabla}\times\vec{B}^{ext} = 0$ and $\vec{\nabla}.\vec{B}^{ext} = 0$. The solution to the vector potential is $A_z = Cosh(\lambda_f x)Sin(\lambda_f y)$ where λ_f is a free parameter. The value of this parameter can be adjusted according to *s*uitable boundary conditions.

In that case, the external field becomes

$$B_x^{ext} = B_0 Cosh(\lambda_f x)Cos(\lambda_f y) \tag{6. 44}$$

and

$$B_y^{ext} = -B_0 Sinh(\lambda_f x)Sin(\lambda_f y) \tag{6. 45}$$

where $B_0 = 1$ was taken.

Figure 6.22 gives the temperature contours, standard vertical parabolic velocity vectors and the vector graph of total magnetic field within the solution domain (with $\lambda_f = 1$) just after the switch was turned on at t =2. Since at that instant the internal magnetic field is negligible in comparison with the external one; hence, Figure 6.22 (c) can be considered to be the graph of only $\vec{B}^{ext}$.

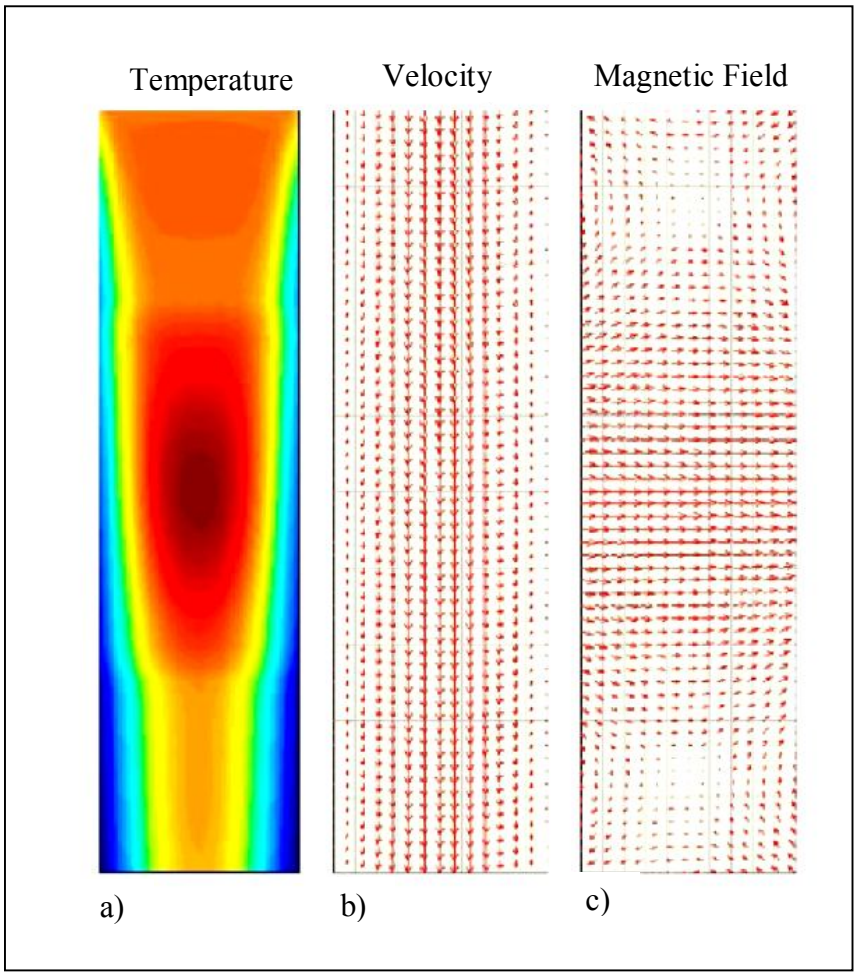

Figure 6.22. Temperature profile, velocity and magnetic field vectors in the channel just after external fields were turned on

The initial conditions were taken as $Re = 1000$, $Ra = 100$, $Rem = 5$, $Pr = 0.72$, $\Delta t = 0.005$ when the externally applied fields were turned on by a switch

when the vertical flow was $v = -1.5$. As the initial condition steady vertical flow under gravity can be provided or it can be obtained by running the code without fields. After a prescribed time by switching on the fields the vertical flow was modified. It began to display small oscillations whose intensity and period depend on the interaction parameter, N and the strength of external electric field, i.e. E_0, and that of the external magnetic field, B_0. As the boundary conditions, no-slip $(u = 0, v = 0)$ and constant temperature $(T = 0.5)$ were applied along the walls at $x = \pm 0.5$. These walls were assumed to be non-ferromagnetic and non-conducting (i.e. $\partial \vec{B} / \partial x = 0$). The top boundary which is the inlet was considered to be at constant temperature $(T = 1)$ and pressure $(P = 0)$, the bottom boundary was taken as outgoing boundary at which pressure was defined to be $P = -1$. The other fields were kept untouched. In this case, the pressure difference and gravity cause the increase in vertical downward flow and external fields slow it down in a short span of time after the switch is turned on.

A DC electric field perpendicular to solution domain was applied by connecting the electrodes (Figures 6.19 and 6.21). The magnetic field was also applied simultaneously by turning on coil currents. Since the electric field was perpendicular to the solution domain, one needs no boundary condition for electric field. Note that the hydrodynamic flow state can be obtained in two different ways before the application of external fields. In the first, a homogeneous vertical velocity $(u = 0, v = -1.5)$ can be given everywhere in the mesh as the initial condition. In that case, the code converges quickly to the homogeneous parabolic velocity profile as shown in Figure 6.22 (b). In the second, zero velocity and constant pressures on the top and bottom boundaries $(Ptop = 0, Pbottom = -1)$ can be given as the boundary condition. In that case, hydrodynamic convergence takes time (as shown in Figure 6.23).

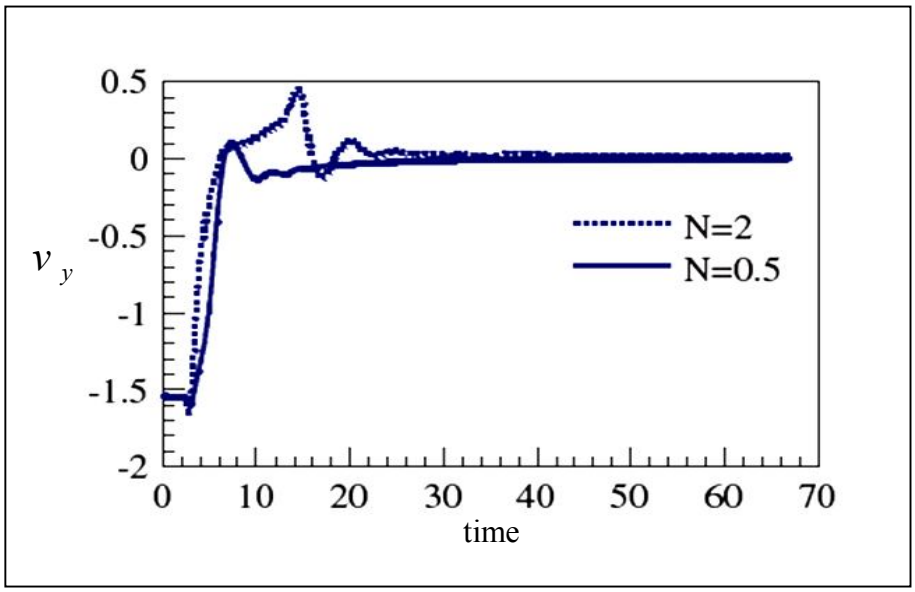

Figure 6.23. The effect of the interaction parameter, N, on the vertical velocity when external electric and magnetic fields are turned on at $t = 2$ simultaneously

The time dependence of the vertical velocity at the centre of exit after its steady value which was $v_y = -1.5$ changed when the switch was turned on, as shown in Figure 6.23. When the external fields were applied, the vertical flow slowed down and stopped after a short time period after passing through minor oscillations. This behaviour is obvious from Figure 6.23 with two different values of interaction parameters, $N = 2$ and $N = 0.5$. For small value of interaction parameter, $N = 0.5$, a better control with less oscillations was obtained. After running this problem with different N values it was found that the optimum value is $N = 0.4$. The time rate of central vertical velocity at the outlet with $N = 0.4$ and its long time behaviour were presented in Figure 6.24.

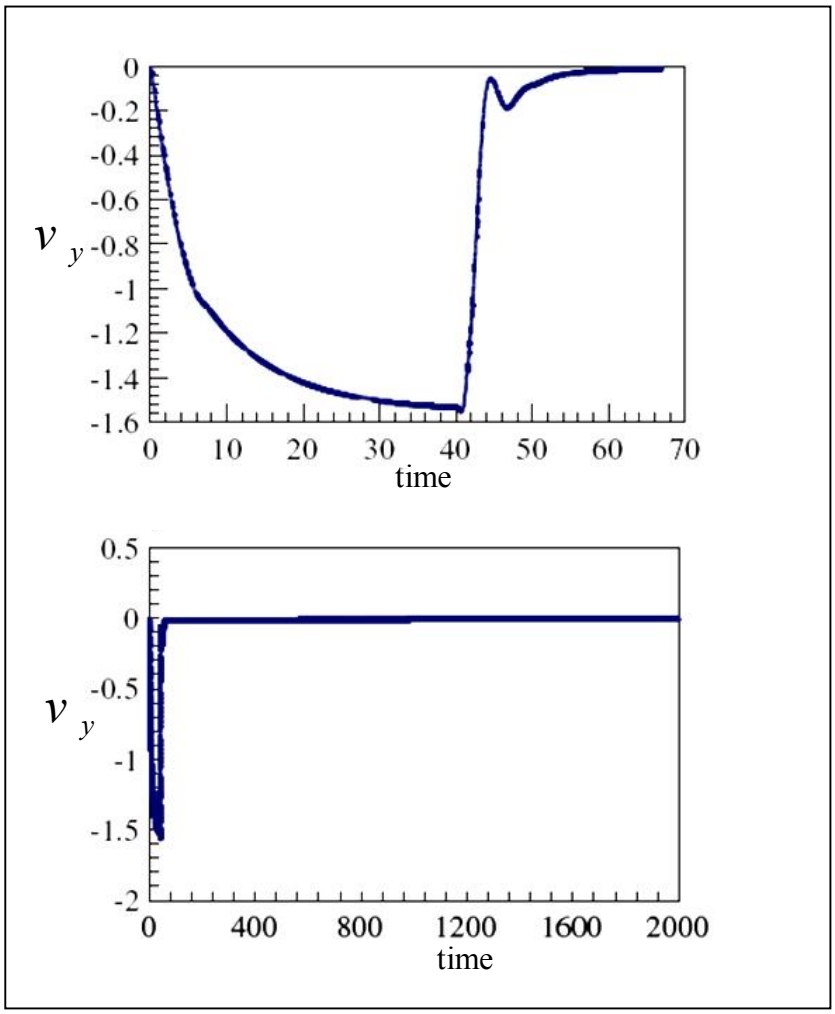

Figure 6.24. Vertical velocity profile and its long-time behaviour with $N = 0.4$ when the external fields are applied at $t = 40$ after steady state is reached

As can be seen, as far as the external fields are kept on, the flow remains stopped at the outlet of the channel for a very long time. In this part of the thesis some benchmark and newly designed test problems were implemented and meaningful results were taken.

7. TECHNOLOGICAL AND EXPERIMENTAL STUDIES

7.1. Liquid Metals: General Information

Great progress has been made in the area of industrial technology of metallurgy in the second part of the 20^{th} century. Particularly in the area of high quality metallic materials there was a great need for knowledge about the physical properties of liquid metals and alloys. Many elements are metallic in liquid states. Especially over the last three decades, researchers have made a lot of studies in order to understand the processing mechanism of the liquid metals. Since these materials have a very important place in industry and technology liquid metals deserved these studies and investigations. The properties such as thermal and electrical conductivities, surface tension, atomic structure, density, viscosity etc. are very important for technological developments. Unfortunately the behaviours of liquids can be explained with a greater difficulty in comparison with the behaviours of solids. Sometimes it can be said that the liquids have intermediate properties between the solids and gases. The diffusivities of liquids are higher but the viscosities are lower than those of the solids. However, the densities of two states of metals near to their melting point differ by only $2-5$ per cent [38]. The best known liquid metal is Mercury (Hg). It has a long-time stability against the effects arising from the environment. However it has a poisonous nature. Therefore Hg is not prefered by the scientists who are doing the experiments in order to understand the nature of liquid metals. It can be said that the structure of liquids resemble the structure of the amorphous solids. The structures of liquids are described by using the pair distribution functions mathematically but they will not be mentioned in this thesis. The pair distribution function gives an idea about the probability of finding another atom at the same time interval from the reference atom at any chosen distance. There is another one function which is called the pair potential which is the potential energy between an atom and its surroundings. The pair potential can be measured experimentally and by the help of it the pair distribution function can be calculated. The very well known Lennard-Jones potential is one of the examples for pair potentials. The difficulties for explaining the structure of alloys increase very considerably since the need for the functions mentioned above increase in number. As an example for binary alloys the number of distribution functions is three because the first distribution

function is for the first metal, the second is for the second metal and the third one is for interaction of atoms for two different metals.

One of the most important properties of metals and alloys is their density. Unfortunately the experimental data for every liquid metal or alloy are not easily obtained because they have some disadvantages such as chemical reactivity at their liquid states. There are some experimental methods which can be used to measure the density of liquid metals such as Archimedean Method, Pycnometric Method, Dilatometric Method, Manometric Method etc. [38]. Experimentally it is found that the density of the liquid metals and alloys have linear temperature dependence. The temperature gradient in liquids causes the transport process. The very well known transport processes are mass transport which is related to diffusion, momentum transfer which is related to the viscosity and the energy transport related to the thermal conduction. Another one of the important properties of liquids is their viscosity which can be thought as a friction between the atoms. Viscous forces arise as a result of the rate of momentum interchange between the atoms. There are some different methods used for viscosity measurements. They are the rotational method in which the viscosity can be calculated from the torque source used in the experiment, oscillating-plate method in which there is a plate immersed in the liquid metal and the motion of this plate is resisted by the force exerted by the liquid metal. Another one method is called 'oscillating vessel method' in which the liquid is put in the vessel which is suspended to the torsional suspension and damping of oscilation due to the energy dissipation and absorption within the liquid is observed. The last method which is mentioned here is called capillary method in which the viscosity is determined by measuring and using the flow times of the liquid flowing through the capillary. Together with experimental measurements there are some theoretical expressions for viscosity calculations. Some of these equations such as Born and Green equation are based on the pair distribution function, some of them are based on a moment method and the hard-sphere theory. For liquid alloys the viscosity calculations are very difficult since the atomic masses and atomic sizes are different and the interaction between them is not very well mathematically describable. The viscosity of metals such as Iron, Bismuth, Nickel, and Zinc is inversely proportional to the temperature.

The diffusion, which is described as transfer of mass from one to another place in atomic scales. For example the diffusion of reactant species is a very important for the liquid metals which can make heterogeneous reactions. The diffusion of solvents can change the rate of the chemical reactions. Actually diffusion occurs as a result of density gradient and concentration gradient. The SI unit for diffusion is $length^2/time$, (m^2/s). Some of the methods used for calculating the diffusion are shear-cell method which is used for mesurements at low temperatures, the plane source method, diffusion couple method which is mostly used for two metal samples which melt at the similar temperatures, etc. There is a direct proportion between the temperature and diffusion.

Table 7.1. The temperature and corresponding diffusion values of Iron , Fe [38]

Temperature (°C)	Diffusion ($10^{-9} m^2 s^{-1}$)
1600	4.91
1700	5.85
1800	6.90
1900	8.08
2000	9.46

Not only the properties mentioned above but also the electrical and thermal conductivities of metals are very important for technology. In solid states of metals both the electrical and thermal conductivities are high. Freely moving electrons and conduction electrons are mostly responsible for both conductivities. Electrical conductivities of liquid metals are very important in electromagnetic stirring, electrical furnace steelmaking, etc. The thermal conductivities of liquid metals are very important in some different areas. One of the important application areas is where heat is removed from nuclear reactors with mostly known name ‘cooling’. The electrical resistivities of most metals differ between their solid and liquid phases just above melting point by $1.5-2.3$ times. The disordered arrangement of ions in liquid state cause to increase in the electrical resistivity. The ratio of resistivity of liquid state to resistivity at solid state is 2.18 for In and 2.10 for Sn. Similar to electrical conductivity the thermal conductivities of liquid metals are less because of

their disordered arrangement in comparing with the crystalline solid metals regular arrangement.

Temperature gradient in the liquid metal causes a thermoelectric current and by applying magnetic fields externally, Lorentz force is induced. The thermoelectric effect might change the flow pattern and the heat transfer in the presence of a magnetic field. Instead of thermoelectric current, direct application of DC electric current and magnetic field is one of the alternatives to produce the electromagnetic force for the material processing [39]. DC electric current can be used under a magnetic field for the surface wave suppression of molten metal. The conclusion was done that the combination of magnetic field and electric current can affect and can cause the suppression of the surface wave [40]. The Lorentz force can be put as an external force term in the momentum equation. It is a very nice tool to play with in order to control the flow. It can be arranged as needed and it generates a contactless action which is perfectly controllable. Different magnetic fields can be used for different purposes. Such as : DC fields are used for flow damping, AC fields with low frequencies are used for stirring and pumping of liquid metals, AC fields with high frequencies can be used for heating, melting and levitations. Combined fields, AC and DC are used in crystal growth processes.

If electrically conductive fluids which are exposed to magnetic fields are moving, additional currents are induced. These induced currents give rise to additionally induced magnetic fields. Magnetic Reynolds number, is the ratio of the induced magnetic field to applied magnetic field. A motor driven propeller can reach rotation rates up to 2000 rpm which corresponds to a magnetic Reynolds number of approximately 0.4 [31].

The electric current density can be determined by Ohm's law.

$$\vec{J} = \sigma(-\vec{\nabla}\phi_P + \vec{v} \times \vec{B}) \tag{7.1}$$

where $\vec{J}$, $\vec{v}$, $\vec{B}$ are current density, velocity and magnetic field respectively. ϕ_P is electric potential which is determined by solving the Poisson equation.

$$\nabla^2 \phi_P = \nabla(\vec{v} \times \vec{B}) \tag{7.2}$$

During the interaction of flow and magnetic field, the currents are induced in the fluid and they cause Joule dissipation or Joule heating.

7.2. Technological Applications

Parallel to improvements in computer performance the heat generation in the chips also increases. This is a big problem for operating performance of computer chips. Cooling with liquid metals is one of the newest methods. The dimensions of central processing units (CPU) are decreasing but on the contrary, the heat generation increases. In order to extract this heat some cooling materials such as oil, water, organic fluids can be used. Because of the fact that, the thermal conductivity of liquid metals are higher they are preferable than the other cooling materials. Additionally to high thermal conductivity liquid metals can be pumped effectively by using electrohydrodynamic micro pumps, electrowetting pumps and peristaltic pumps. The liquid metals have low viscosity, heat capacity, low melting point etc. Temperature change can easily affect the properties mentioned above. Gallium is the metal which expands during cooling process. During the solid-liquid phase transition most of the metals exhibit a volume increase about 3.8 per cent as an average [38]. Gallium has also antimicrobial effects. In order to increase the conductivity of liquid metals or alloys in some sources it is proposed a new method in which depends on some nano particles addition. As an example the thermal conductivity for Gallium is $28 W/mK$ [41] and the thermal conductivity of water is $0.6 W/mK$ [42]. One of the main problems for cooling is the pumping procedure. There are some conventional pumps such as mechanical and peristaltic pumps. However, the high density of liquid metals is the main drawback in pumping. One of the most popular pumps used to drive the liquid metals is magnetohydrodynamic pumps which do not have any moving parts which will not give rise to the noise production. However, there is one important drawback in liquid metal cooling. If the ambient temperature is low such as almost $0^\circ C$ the liquid metal can freeze. However it is obvious that computers won't be put in very cold places with an ambient temperature near the freezing point of liquid metal used.

There are some technological applications in which different liquid metals are used. Some of the inventions mentioned below are patented.

1. Liquid Metal Solar Power System: The aim of this system is to get the electricity from solar energy. There is a transparent reflector envelope through which a reflective liquid metal can be circulated in the improved solar collector (U. S. Patent 4 454 865).

2. Liquid Metal Heat Exchanger: Effective heat exchange is a very important process especially in fast breading reactors. The liquid metal heat exchanger is used to transfer the heat from primary liquid metal reactor coolant to suitable secondary liquid metal. The heat exchanger here is contructed with improved maintenance and repair features and reduced thermal stresses (U. S. Patent 3 656 543).

3. Liquid Metal Capacitively Monitored Sensors: The measurable changes in capacitance of the devices occur when the liquid metal move in response of stimulus. The capacitive sensors using liquid metals can be fabricated by using high technology devices (US 2007/0125178 A1).

4. Liquid Metal Electrical Contact Compositions: These compositions are mostly useful for high current applications in order to get effective current transfer (U. S. Patent 5 281 364).

5. Tokamak with Liquid Metal Toroidal Field Coil: This device can be used to produce a toroidal plasma with the help of the electric current which is passed through the liquid metal over a conductive path. The liquid metal is used to form coils for developing the toroidal magnetic fields (U. S. Patent 4 305 783).

6. Liquid Metal Electric Current Limiter: This device utilizes the electromagnetic pinch effect. The pinch effect can be described as the reduction of the cross section of the fluid. This causes a very big increase in the resistance. The cross section reduction of the liquid metal is the result of the Lorentz force produced by the current flowing through the liquid metal and magnetic field. After short circuit effect finished differently from mechanically restored limiters the liquid metal current limiters healing themselves. As a

result these kinds of devices can be used in protecting the people, animal and equipment against the problems may occur due to the high electrical currents [43].

7. Liquid Metal Microstrips: Microstrips are some kind of transmission lines for delivering the microwave frequency signals. The advantage of these microstrips is their tunability due to the fluidic nature of the liquid metals [44].

There are some other application areas such as liquid metal radio frequency reflective and absorptive switches, Mercury free liquid metal thermometers etc.

In order to use the liquid metals some other inventions are also needed, there are some of them given below.

1. Liquid Metal Level Indicator: This device is made of a number of separate, substantially identical coils supported in a vertical array and adapted to be extended to a liquid metal bath. In order to indicate the liquid level the change at the impedance of the coils due to the presence of liquid metal surrounding them is used. The liquid metal which surrounds the coils changes the inductance of the coil. The level of the liquid is detected by sensing the change in inductance or the corresponding change in impedance (U. S. Patent 4 007 636).

2. Liquid Metal Droplet Generator: These droplet generators are used when the small quantities of metal are desired. As a methodology the magnetic pressure of the current which is flowing through the liquid metal is used. This current is separating the small amounts of the liquid metal. Later these small drops are directed through the orifice (US 2006/0102663 A1).

3. Liquid Metal Mechanical Pump: This pump is used for pumping the liquid metals. This kind of inventions are reduced the drawbacks of the other types of mechanical pumps by preventing the damage of the upper mechanical bearing and seal (U. S. Patent 4 511 315).

4. Electromagnetic pumps for liquid metals: This device can be used especially in the nuclear power engineering in order to pump the liquid metal which is the responsible agent for heat carrying in nuclear reactors. It can be used also for transporting the molten metals in the area of metallurgy (U. S. Patent 3 708 246).

5. Electromagnetic stirring pump for liquid metals: This pump is used for stirring or circulating the liquid metals in a vessel. The pump is put in the immersion box which is metal resistant. It can be immersed in the bath by suspension device. These pumps have an increased importance in the technology. They are suitable for long-term use. An electromagnetic pump has an approximately horizontal pump channel with the openings on two opposite sides. The advantage of this stirring pump is that no moving parts come into contact with metal melt and this prevents the system from many problems (U. S. Patent 4 668 170).

7.3. General Study of GaInSn Alloy

The experiments in this thesis were done by using the eutectic alloy GaInSn. This alloy is formed from Gallium, Indium and Tin. For alloys the composition of the layers which form the surface can have some differences from the layers inside the bulk. The density of GaInSn is higher than these of Na, Li or NaK etc. but eventually Hartmann and Steward numbers are lower. If the GaInSn is exposed to the air it is easily oxidized to form Ga_2O_3. Oxidized thin layer can easily be removed by cleaning. GaInSn can wet easily to the glass surfaces. Contrarily to Ga, GaInSn is not chemically reactive and it is compatible with plastics and metals. However, GaInSn is reactive especially to Al [45]. If GaInSn is spoiled at room temperature it would not evolve any constituent metal vapour. It has been adopted as a replacement for Mercury in oral thermometers and has been successfully used as a dental filling alloy. The spilled GaInSn can be cleaned by mechanical means such as spatula, plastic scoop and then soap and water or other commercial cleaners to clean the floor. GaInSn is a good choice to study liquid metal flow without the safety concerns of high temperature operation [46]. During the experimental work with liquid metals chemical reactions between liquid metals and air, reactions between liquid metals and water, liquid metals and CO_2 etc. must be taken into account. Direct energy releases can occur from chemical reactions which can lead to the increse in temperature and pressure.

As a result of chemical reactions the possibility of H_2 gas release can be dangerous during the experiments.

GaInSn is corrosive, non-flammable or explosive alloy. If it comes to contact with the skin it can easily be cleaned by using water and soap. If it comes to contact with the eyes it is better to wash them with warmish water. During the washing the eyelid must be opened. If it is not used it is better to keep GaInSn in closed container which must be placed in dry and cool place. It is suggested to use the rubber protective gloves during the experiments. GaInSn is an odourless alloy, the colour is silvery, it does not have fire promoting properties. It is insoluble in water or in organic solvents. If GaInSn comes into contact with Al and water is added subsequently, exothermic reactions can be seen. Actually it is not miscible with water. As a cleansing material, 2% hydroclorid acid heated up to $60^{\circ}C$ can be used. Since it has a very low vapour pressure its risk of toxicology is negligible. If it is handled in unpacked conditions the purity and degree of quality will decrease, it is easily oxidized. There are some melting point values for different alloys and the alloys from GaInSn alloy family.

Table 7.2. Some melting point values for different alloys [47]

Alloy	Melting Point (°C)
$GaIn_{15}Sn_{13}Zn_{1}$	3
$Ga_{62.5}In_{21.5}Sn_{16}$	10.7
$GaIn_{10}Sn_{60}$	12
$Ga_{75}In_{25}$	16
$GaZn_{16}In_{12}$	17
$GaSn_{8}$	20
$GaIn_{25}Sn_{13}$	5
$Ga_{69.8}In_{17.6}Sn_{12.6}$	10.8
$GaIn_{29}Zn_{4}$	13
$GaSn_{12}$	17
$GaZn_{5}$	25
$K_{78}Na_{22}$	-11.1

Table 7.3. The physical properties for different metals and GaInSn alloy

Composition	$Ga_{67}In_{20.5}Sn_{12.5}$	Ga	Li	Hg	Na
Melting Point (°C)	10.5	29.8	180.5	-38.8	97.8
Boiling Point (°C)	〉1300	2204	1342	357	883
Density (kg/m^3)	6360	6080	534	1353	927
Conductivity ($\Omega^{-1}m^{-1}$)	3.1×10^{6}	3.7×10^{6}	2.8×10^{6}	1.0×10^{6}	3.7×10^{7}
Viscosity (m^2/s)	2.98×10^{-7}	3.24×10^{-7}	6.4×10^{-7}	13.5×10^{-7}	7.4×10^{-7}
Surface Tension (N/m)	0.533	0.7	0.35	0.5	0.2
Sound Speed (m/s)	2730	2860	4500	1450	2550
Water compatibility	Insoluble	Insoluble	Reactive	Soluble	Reactive

The viscosity value for $Ga_{67}In_{20.5}Sn_{12.5}$ is given by UCLA (University of California, Los Angeles) and surface tension is given by PPPL (Princeton Plasma Physics Laboratory) [48].

7.4. Experiments With GaInSn

7.4.1. Thermal Expansion of GaInSn

The GaInSn alloy used in these experiments was purchased from MCP HEK GmbH Kaninchenborn 24-28D-23560 Lübeck, Germany. Some of the physical properties for the alloy which was used in the experiments were given below in Table 7.4. These values were provided by the manufacturer mentioned above.

In this preliminary experiment the constant volume glass chamber with volume of $V_g = 100ml$ was filled with GaInSn alloy. Additionally the connecting rubber tubing which was used to make connection between the spherical glass chamber and the scale shown in Figure 7.2 is also filled with GaInSn. The volume of this tubing was $V_t = 30ml$. The experiment was done under the constant ambient temperature of $T_a = 25^{\circ}C$.

Table 7.4. The physical properties for GaInSn used in the experiments in this thesis

Eutectic Temperature (°C)	10.7
Melting Point (°C)	11
Boiling Point (°C)	$\rangle$ 1300
Density (kg/m^3) at 20 °C	6440
Electrical Conductivity (S.m^{-1}) at 20 °C	3.46×10^6
Viscosity (Pa·s) at 20 °C	0.0024
Surface Tension (N/m) at 20 °C	0.718
Vapour pressure (Torr) at 5000 °C	$\langle 10^{-8}$
Water compatibility	Insoluble
Organic Solvents compatibility	Insoluble
Thermal Conductivity (W.m^{-1}.K^{-1})	16.5
Specific Electrical Resistance (Ω.mm^2 m^{-1})	0.435
Specific Heat liquid (J/g.°C)	0.34
Specific Heat solid (J/g.°C)	0.32
Latent Heat (J/g)	67.8

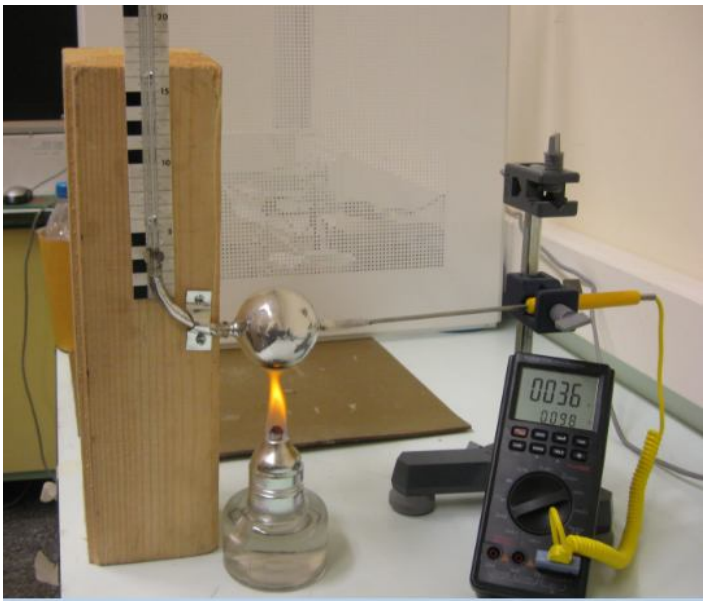

Figure 7.1. The photograph of the experimental setup

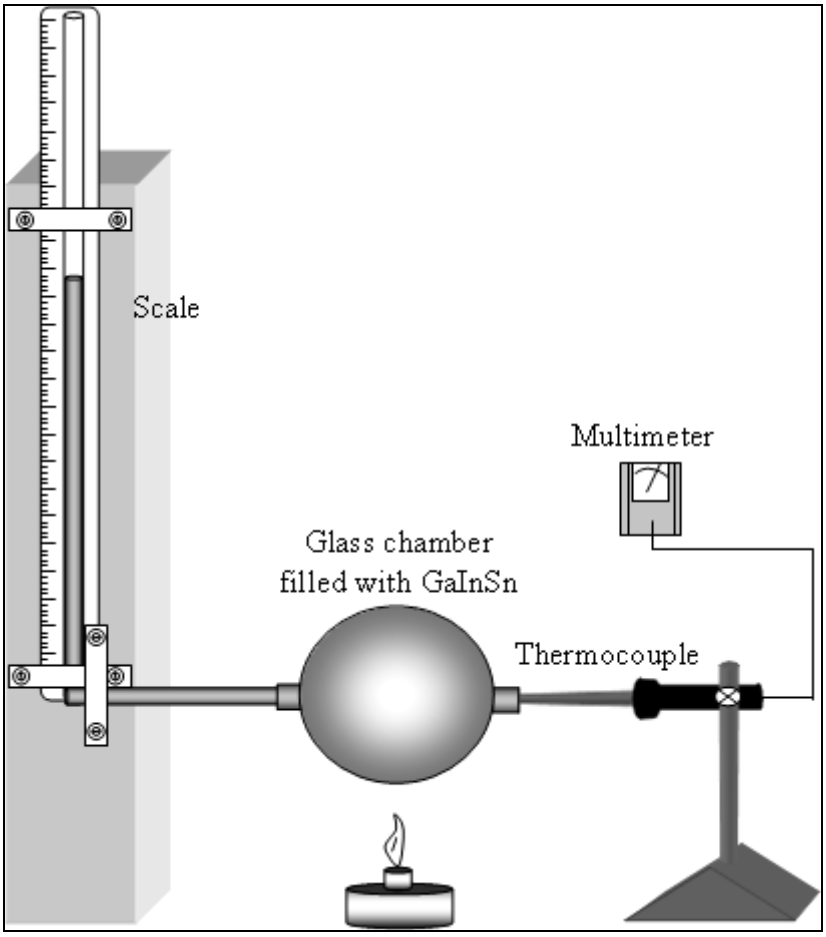

Figure 7.2. The representation of the experimental setup

The temperature measurements were done by using Protek multimeter which had the thermocouple with the range from -17 to $1200^{\circ}C$ *(0 to* $2000^{\circ}F$*)* with resolution $1^{\circ}C$ and $1^{\circ}F$, and accuracy $\pm 3\%$. The multimeter can be connected to PC by using RS-232 serial port and the data were collected by its own software.

The total initial volume of GaInSn which was filled in both glass chamber and tubing was

$$V_0 = V_g + V_t$$
$$V_0 = 100ml + 30ml = 130ml \qquad (7.3)$$
$$V_0 = 0.130l.$$

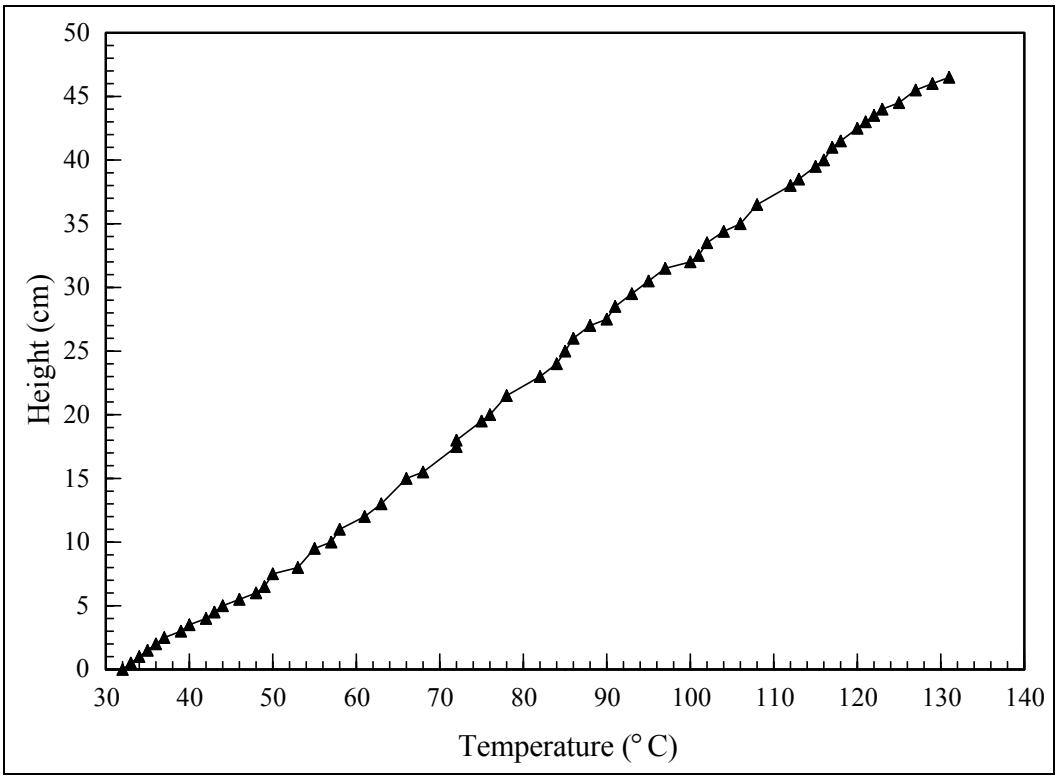

Figure 7.3. The linear nature of GaInSn alloy under heating process

During the heating process the level (height) of GaInSn in the scale was measured as a function of the temperature change. The results were presented in Figure 7.3. As seen, the height increases linearly as temperature gets higher. The expression for volume expansion or thermal expansion is given as :

$$\Delta V = \beta_T V_0 \Delta T \tag{7.4}$$

where ΔV is the volume increase, β_T is thermal expansion coefficient, V_0 is initial volume of alloy which filled the spherical chamber and tubing, and ΔT is the temperature difference. The inner radius of the scale r was $1\,mm$. Since the shape of the glass scale is cylindrical the volume change can be given as

$$\Delta V = \Delta h_e . \pi r^2 . \tag{7.5}$$

So that $V_0 \beta_T \Delta T = \Delta h_e . \pi r^2$ or $h_e = h_{e0} + V_0 \beta_T (T - T_0) / \pi r^2$ by solving these equations one can calculate the thermal expansion coefficient.

By using the data given in Figure 7.3 and the equations between Equation 7.3 and 7.5 β_T was found as $10.9 \times 10^{-5}\ K$ with $\%5$ difference from the reference value given in [49]. This shows that the experiment done to find the thermal expansion coefficient was accurate.

The coefficient of expansion of Hg and the GaInSn were found suitable to be used in thermometers. Geratherm Medical AG (Geratherm Medical AG, Fahrenheitstrasse 198716 Geschwenda, Germany) is one of the manufacturers of Mercury free thermometers in which GaInSn is used. From the Figure 7.3 it is seen that the temperature dependence of GaInSn is linear (direct proportion between the expansion and temperature) at least for the temperature limits used in this thesis. This expansion coefficient will be used later in the experiments in which the dependence of reflection to temperature change in GaInSn will be studied.

In this part of the experiment the characterization graphs for the light source used in these experiments are given. Three different detectors were used for measuring the light properties of the lamp. They were a UV-Vis spectrometer, a luxmeter and a thermopile.

Figure 7.4. The lamp and electronic transformer used in the experiments related to GaInSn alloy (Halogen lamp 12V, 20W, Osaka Light)

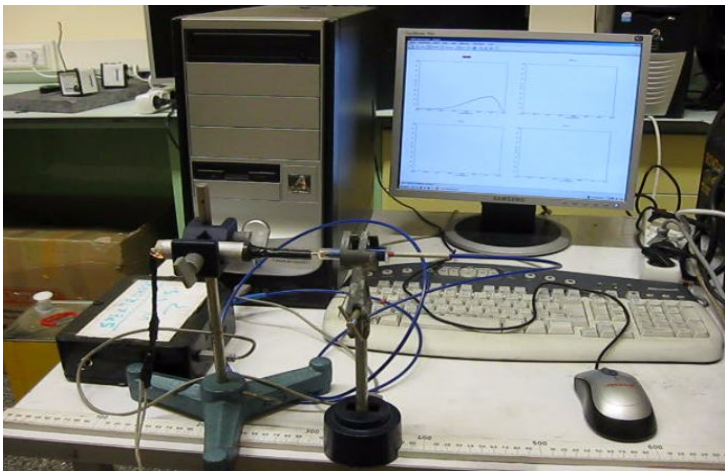

Figure 7.5. The experimental setup for investigating the light source's (halogen lamp) light intensity versus displacement from UV-Vis spectrometer's detector

7.4.2. UV-Vis Measurements

In this experiment the light intensity from the halogen lamp (see Figure 7.4) was measured as a function of distance by the spectrometer as shown in Figure 7.5. The UV-Vis results are given in Figure 7. 6.

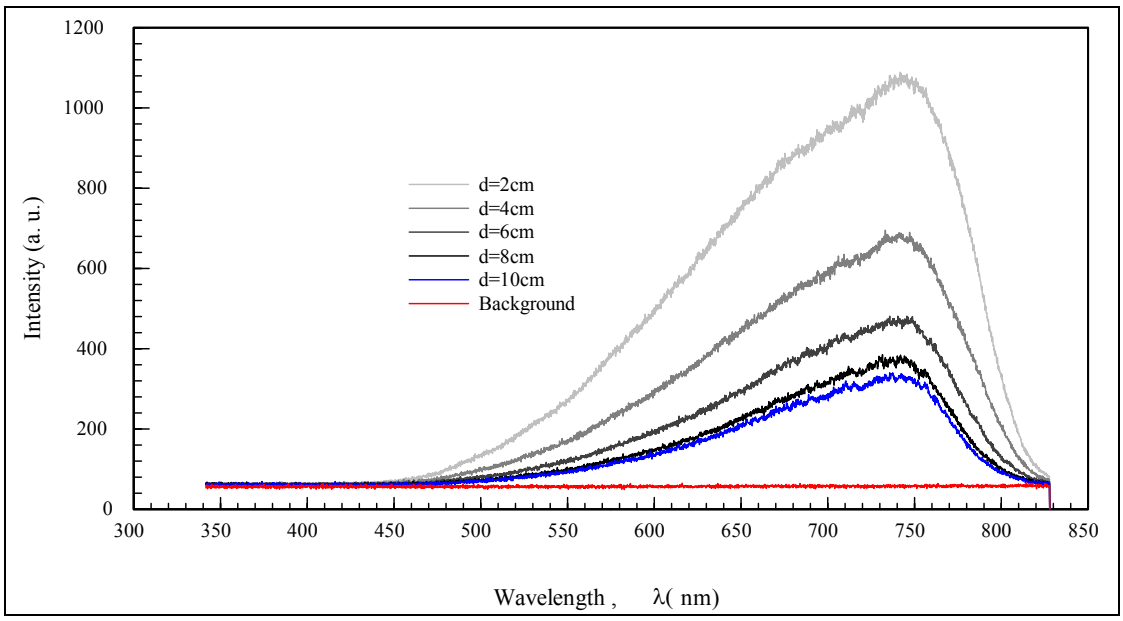

Figure 7.6. The intensity of light versus wavelength depending on the distance between the ligth source and UV-Vis detector

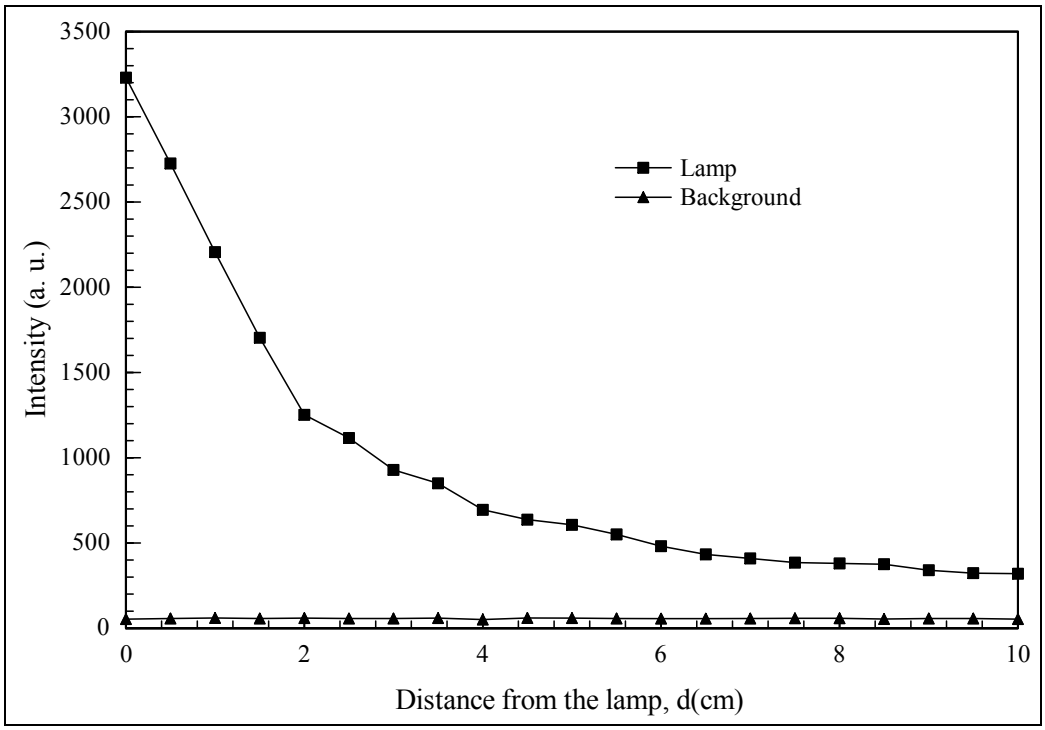

Figure 7.7. The maximum intensity values of every spectrum versus different distances between light source and UV-Vis detector

As seen the whole spectrum reduces when the distance from light source increases. It can be seen that the maximum intensity reduces exponentially with the distance from the light source as shown in Figure 7.7. Note that the background light intensity is nearly constant and very small for all wavelengths. The UV-Vis spectrometer produced by BAKI at Kocaeli University, Turkey used in these experiments had the resolution of 600 *lines / mm* diffraction grating density, 100 μm slit aperture, 100 *mm* focal length, and aperture ratio *fl*3.93 .

7.4.3. Luxmeter Measurements

The same experiment was done by using a luxmeter as light detector (Figure 7. 8). The luxmeter with product number 07137-00 is provided by the manufacturer PHYWE, Germany. It is a hand-held instrument which is used to measure the light intensity both in laboratory or outdoors. Some of the important properties of the instrument are large liquid crystal display (40 x 50 mm), analog bar display with a very good resolution (2 per cent),

data interface (RS-232) for transmitting the measured values to a computer, microprocessor control of all measuring, operating and evaluating functions etc. The probe for luxmeter which is Selenium-PN planar-photoelement with colourfilter was also manufactured by PHYWE with the product number 12107-01.

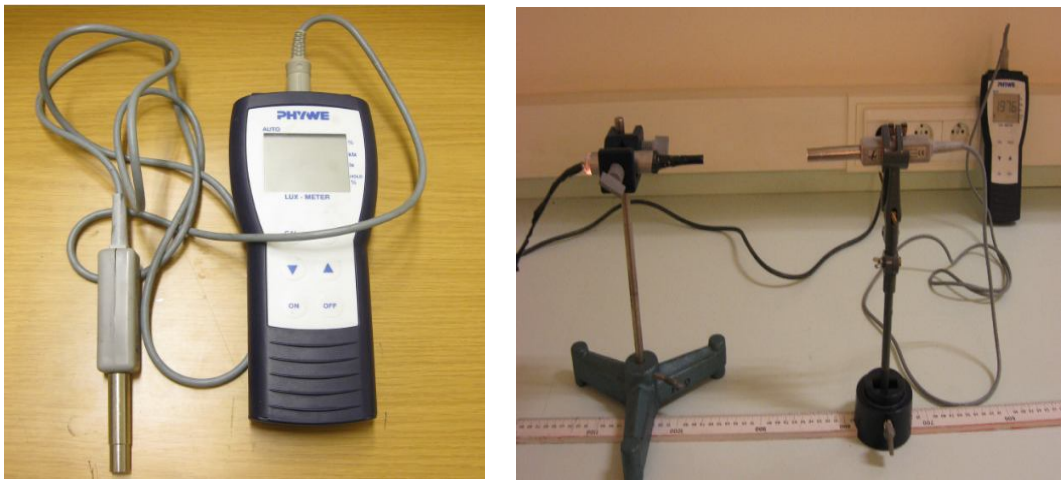

a-) b-)

Figure 7.8. The view of a-) the luxmeter and probe which were used in the experiments b-) the experimental setup

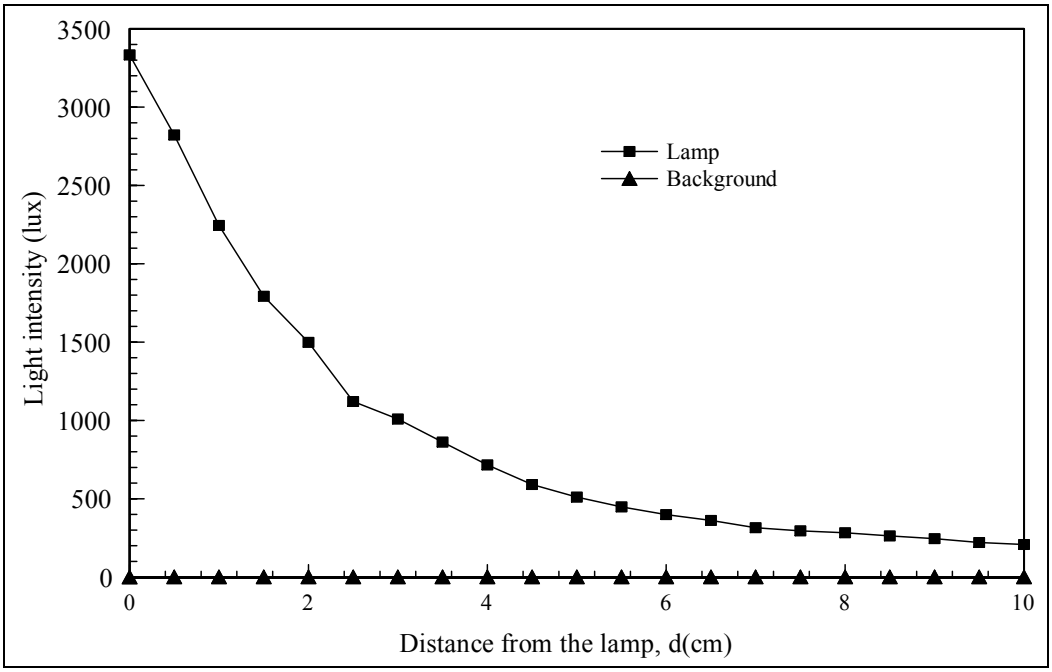

Figure 7.9. The light intensity detected by luxmeter versus distance between light source and luxmeter

Similar to the measurements with UV-Vis the intensity decreases exponentially with the distance from the light source.

7.4.4. Thermopile Measurements

Thermopile was also used to detect or at least to have an idea about the irradiated light change depending on the distance from the light source. The experimental setup is given in Figure 7.10. The thermopile is the device which is used as a radiation sensor. The thermopile used in this experiment is produced by PHYWE company with production number 08479-00. It works in a very broad spectral area from UV to far IR longwave. The thermopile was connected to the universal measuring amplifier with production number 13626-93 and can be used for DC and AC voltage amplification. The amplification factor was 10^3 during the experiment. The results obtained from this experiment were given below in Figure 7.11.

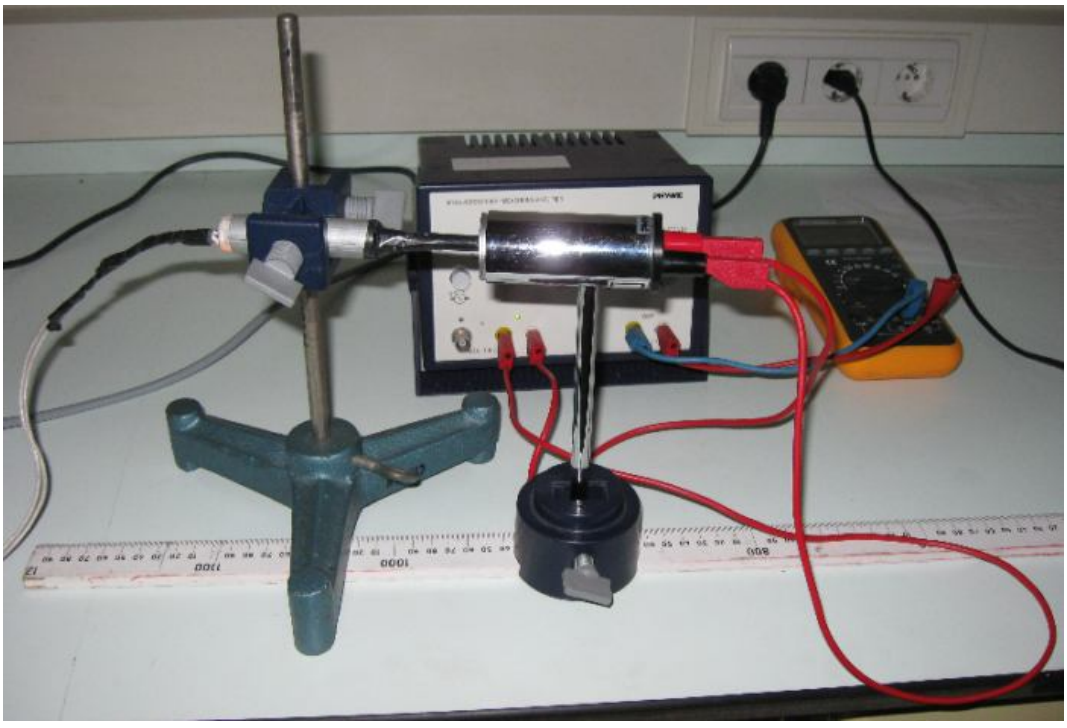

Figure 7.10. Experimental setup in which the thermopile was used

Results of these lamp characterization processes also showed that the light intensity emitted by the light source (lamp) decreases exponentially as the distance from the lamp increases. However, the results taken by the thermopile were more interesting. The results taken by thermopile did not change significantly in the first $4\,cm$ distance. This is due to the circular detector area of thermopile having a relatively big diameter ($d = 10\,mm$). The radiation emitted from the light source has shined on this area without any significant loss. All the experiment about the characterization of the light source were done in total darkness. The light source was put into the holder which was formed from two concentric cylinders. The light was emmitted from the tip of the black coloured cylinder with diameter $d_l = 8\,mm$ (Figure 7.8(b), 7.10) and whole light was directly sent through the detectors. During the experiments the light source and the detectors were aligned along a straight line carefully.

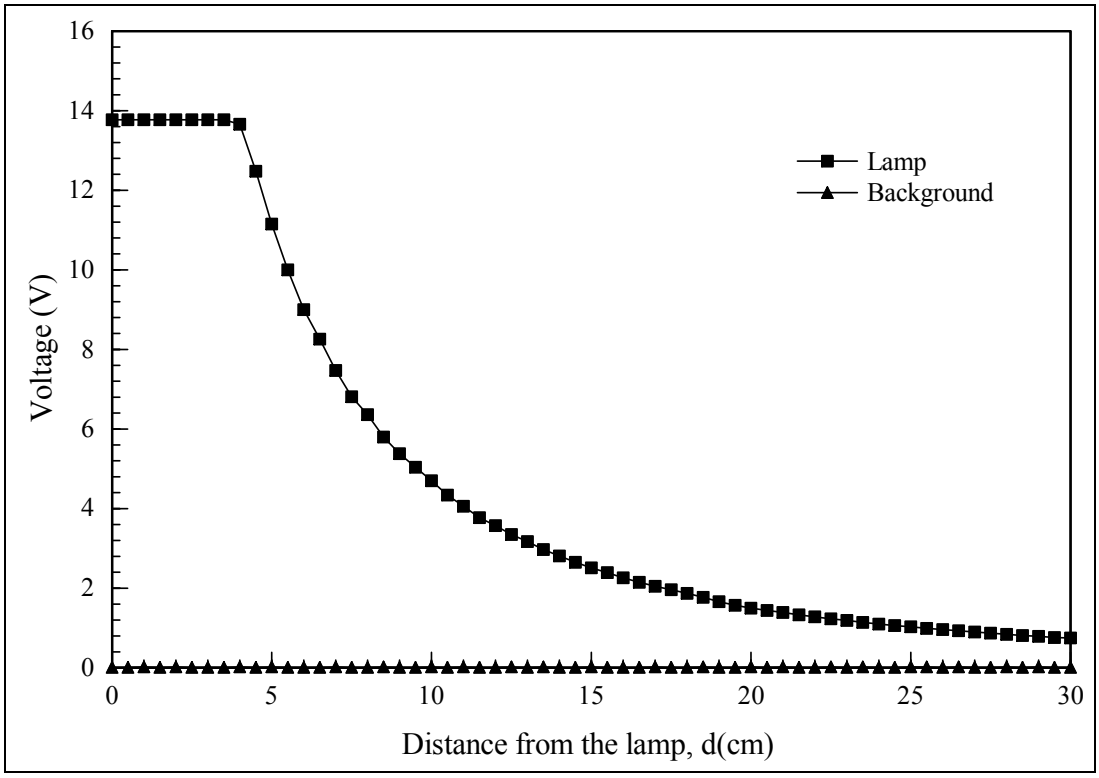

Figure 7.11. The voltage data taken from the thermopile versus distance between light source and thermopile

After the results obtained here it is decided to put the light source as near as possible to the surface of GaInSn where the light will be reflected. The arrangement of the experimental setup affected the distance between the lamp and studied surface appreciably.

It was interesting that the results for both experiments done by UV-Vis spectrometer and luxmeter were found similarly. This shows that the UV-Vis spectrometer gives light intensity as the dimensions of lux. The results were put in the same graph as can be seen in Figure 7. 12.

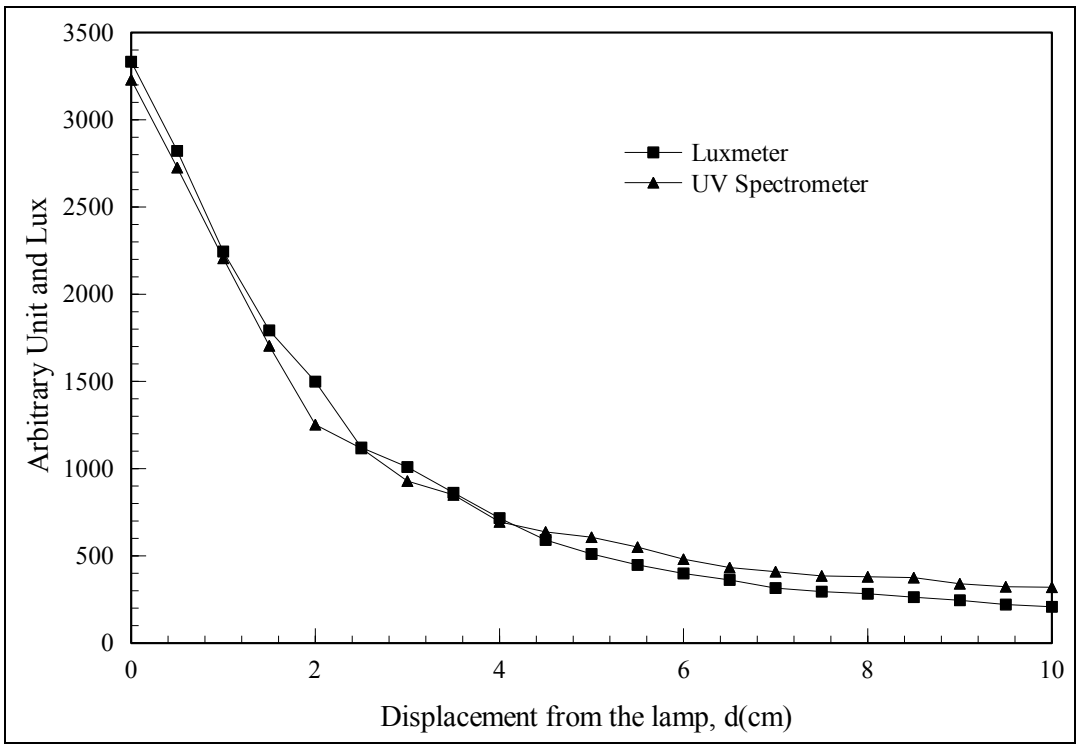

Figure 7.12. The comparison of UV-Vis spectrometer and luxmeter results

The results taken from UV-Vis spectrometer and luxmeter were very similar to each other. As a conclusion it can easily be said that the quantities which were measured from the luxmeter and UV-Vis spectrometer used in these experiments are the same.

After the investigations about the light source and spectrometer was completed the other experiments were conducted.

7.4.5. Oxidation of GaInSn Surface

One of the main experiments which is done in this thesis is checking the temperature dependence of reflectivity of GaInSn. The surface of the reflecting media is a most important agent in these kinds of experiments. The experiment was done to see if GaInSn is oxidized easily under normal room conditions by studying the reflectivity of its surface. Oxidation process depends on the humidity conditions of the experimental environment. In this experiment the oxidation process of GaInSn was studied in laboratory with the ambient temperature of $T_a = 25 \pm 2^{\circ} C$ and humidity of $52 \pm 5\%$. In order to understand if the surface is oxidized the halogen lamp was used as a light source (see Figure 7.4) and UV-Vis spectrometer was used as a detector. The light was sent on to the surface of GaInSn and its spectrum was monitored by an emmision spectrometer developed at Kocaeli University, Turkey by BAKI and the data were recorded. The surface of the alloy previously was very smooth and the reflection from this surface can be considered as 'specular reflection' (Figure 7.13). After oxidation started there were some contaminations on the surface which caused to diffuse reflection (Figure 7.14). Since during the experiment the locations of the lamp and detector are kept constant, the surface changes will affect the intensity of reflected light detected by the UV-Vis spectrometer and recorded by PC. In this experiment the reflected light's spectrum was recorded depending on different time intervals (Figure 7.15). It is seen from Figure 7.15 that the spectrum of reflected light intensity decreases with time. However, the intensity of the reflected light did not change significantly after approximately 400 hours when the initial value was taken at unoxidized state. It can be concluded that the surface shape of the GaInSn was not changing very significantly after a certain time. Figure 7.16 shows an exponential decay of spectrum maximum at $740nm$ as a function of time. This shows an exponential increase in surface oxidation. This time can be thought as a time instance until which the whole surface is totally oxidized. The oxidation changes not only the surface shape of GaInSn but also its viscosity. The dominantly responsible agent for oxidation in GaInSn is Ga. The possible states for Ga with increasing valence can be given as

$$Ga^0 < (Ga^{1+}{}_2O)_n \sim Ga^{1+}OH < Ga^{2+}O < Ga^{3+}{}_2O_3 \sim Ga^{3+}OOH < GaO_{x\geq 2}.$$

The most stable oxide phase for Ga is Ga_2O_3 and less stable one is Ga_2O. In and Sn are nearly stable in their metallic states which means that they are not so much responsible for oxidation. The increase in humidity causes an increase in oxidation and eventually an increase in viscosity. The oxide thickness changes rapidly in wet conditions. High humidity results in a further growth of the oxide films. Actually the humidity effect is more significant than time for oxidation of GaInSn alloy. The change in structure of an alloy may be also seen. Since the humidity was almost constant at laboratory where the experiment was done the only change of oxidation can be assumed to be dependent on time [50].

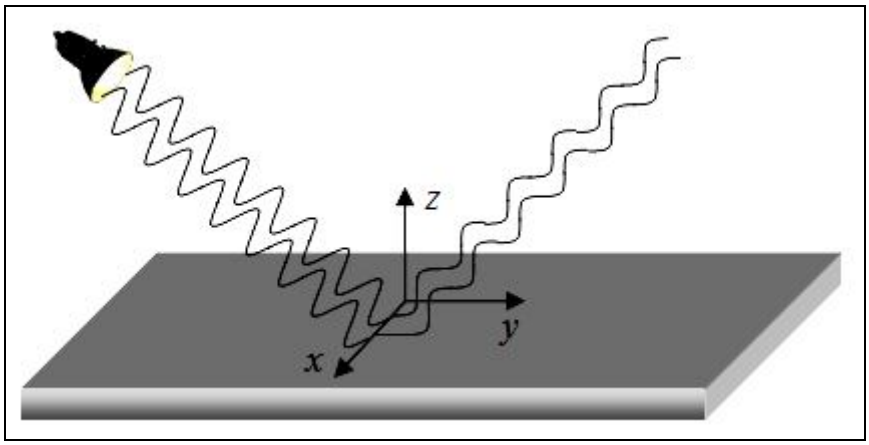

Figure 7.13. Specular reflection

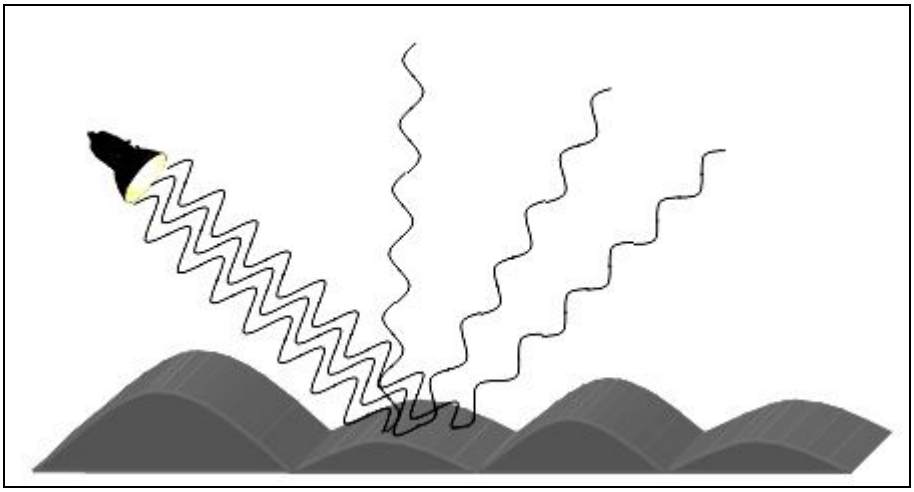

Figure 7.14. Diffused reflection

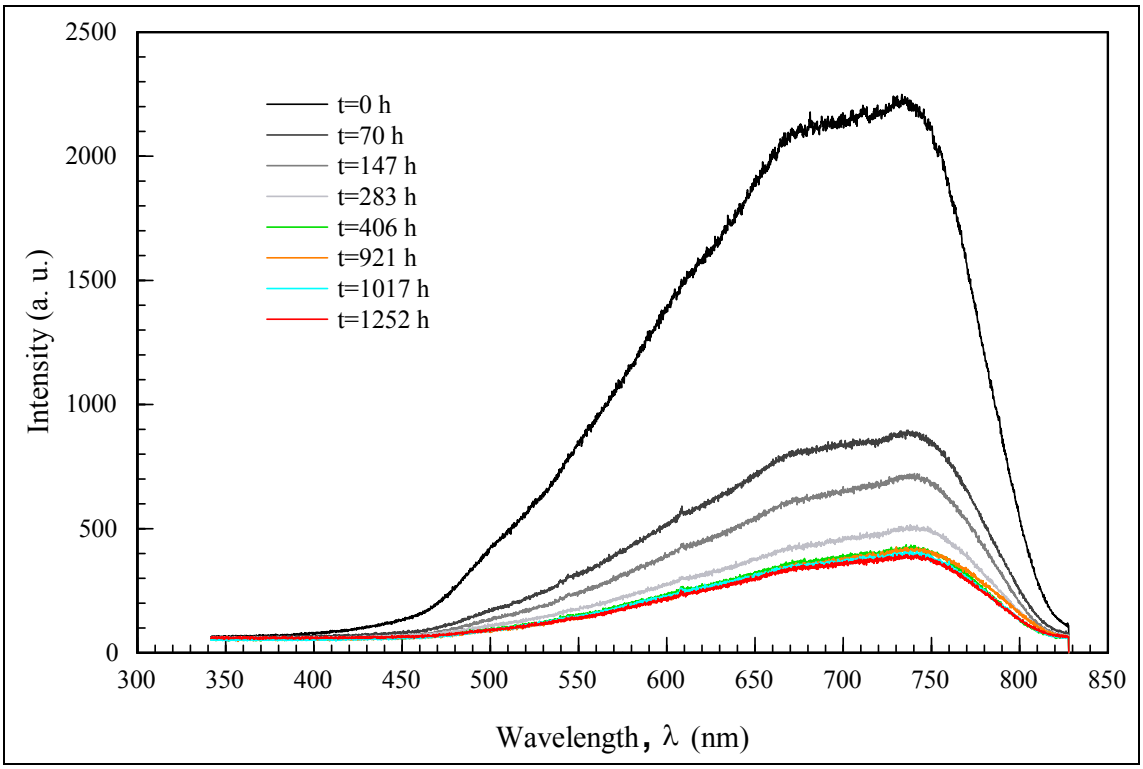

Figure 7.15. The intensity of the reflected light depending on the time elapsed

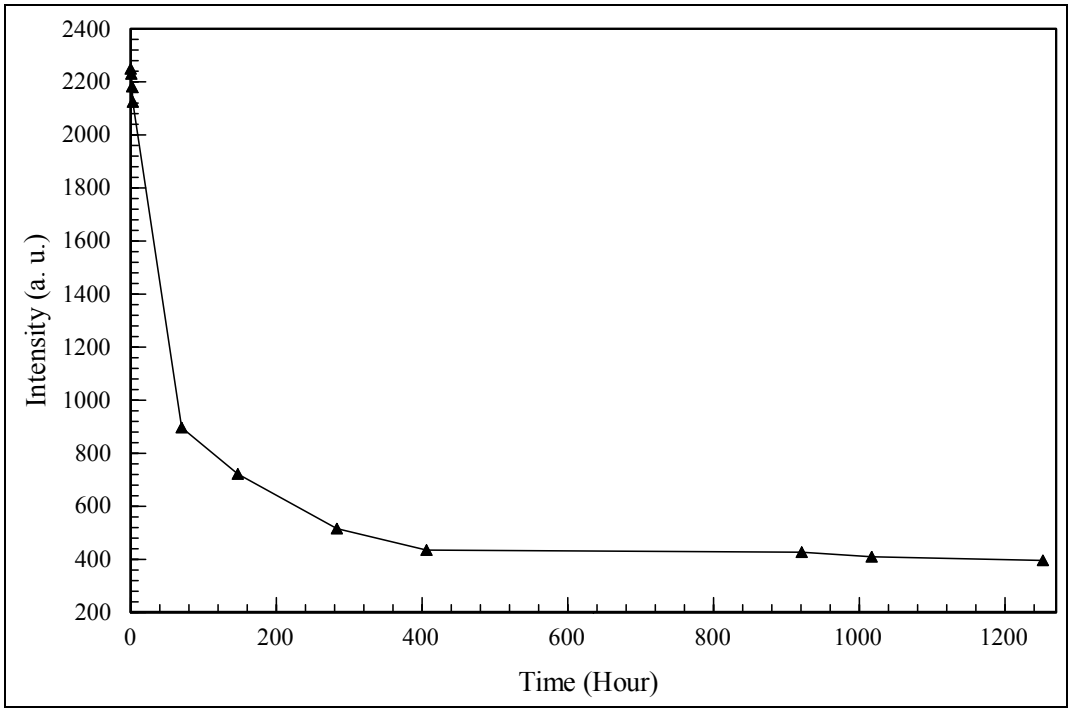

Figure 7.16. The maximum intensity values for the spectra of reflected light depending on time elapsed

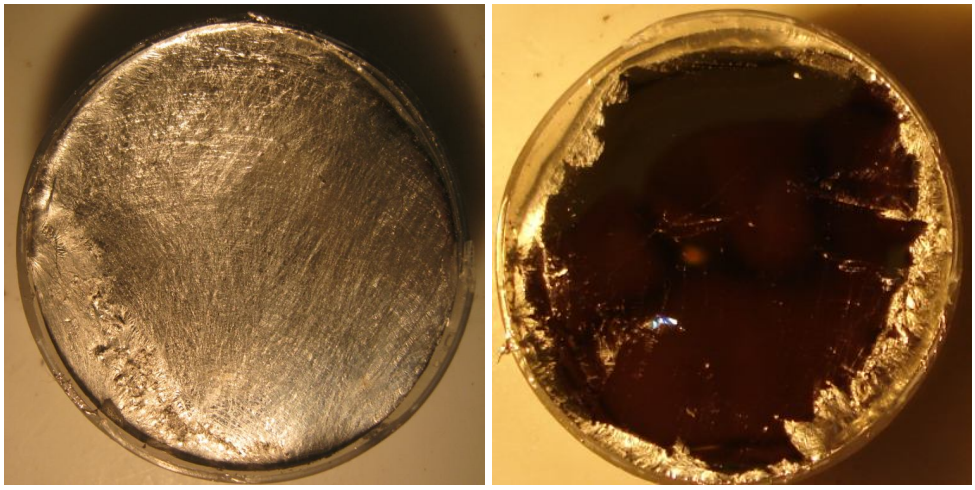

a-) b-)

Figure 7.17. The surface difference on an a-) oxidized and b-) cleaned surface of GaInSn alloy

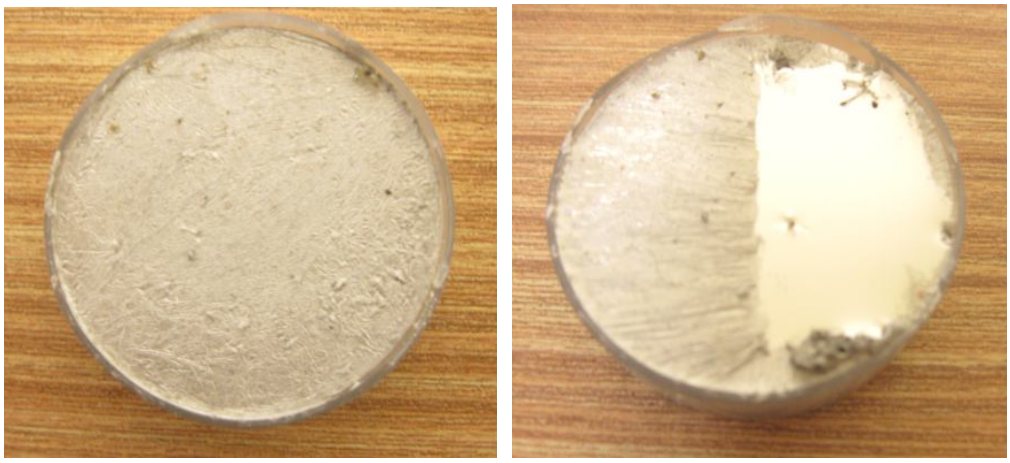

a-) b-)

Figure 7.18. GaInSn alloy a-) totally oxidized b-) half oxidized and half cleaned surface

Since the surface of GaInSn was oxidized relatively fast as seen in the experiment done and described above, the reflection experiments in air are suggested to be done as quickly as possible to prevent this additional effect. Otherwise, vacuum is needed to eliminate oxidation. There are oxidized shapes of GaInSn in Figures 7.17 and 7.18.

7.4.6. Reflection from GaInSn Surface

Light scattering experiments are very important especially in physics because of the fact that they can be used in determining the structure of matter under interest. At the beginning of the twentieth century Ernest Rutherford designed an experimental setup in order to understand the structure of the atom. Scattering is often accompanied by absorption. Both of them remove energy from a beam of light which is traversing the medium. Extinction occurs after scattering and absorptions were occurred and the beam is attenuated. This can be formulated for these processes easily as

$$Extinction = Scattering + Absorption\ . \tag{7.6}$$

In the experiments related to the scattering the most important property of scattered wave is thought to be its intensity. Intenstiy can be described as the energy flux per unit area. Some amount of the total energy of the incident wave will be absorbed by the plane on which the wave is falling. The other part of the energy of the incident wave will be carried by the scattered wave or let us say by the reflected wave.

All the problems in theoretical optics are problems in Maxwell's theory. One of the most important outcomes of Maxwell's equations is that the light does not carry only the energy but also the momentum. The direction of momentum is the same with the direction of propagation of a wave. The amount of momentum is given as

$$Momentum = Energy/c \tag{7.7}$$

where c is the speed of the light. Some amount of the momentum of the incident wave is given to the scatterd particles. A certain force is exerted on the scattering particles in the same direction of propagation of the incident light. This phenomenon is also known as 'radiation pressure'. For a highly conducting medium, like metallic conductors the fields applied by outside sources can penetrate into a skin depth of the conducor. The fields below the skin are virtually zero [51](Figure 7.19).

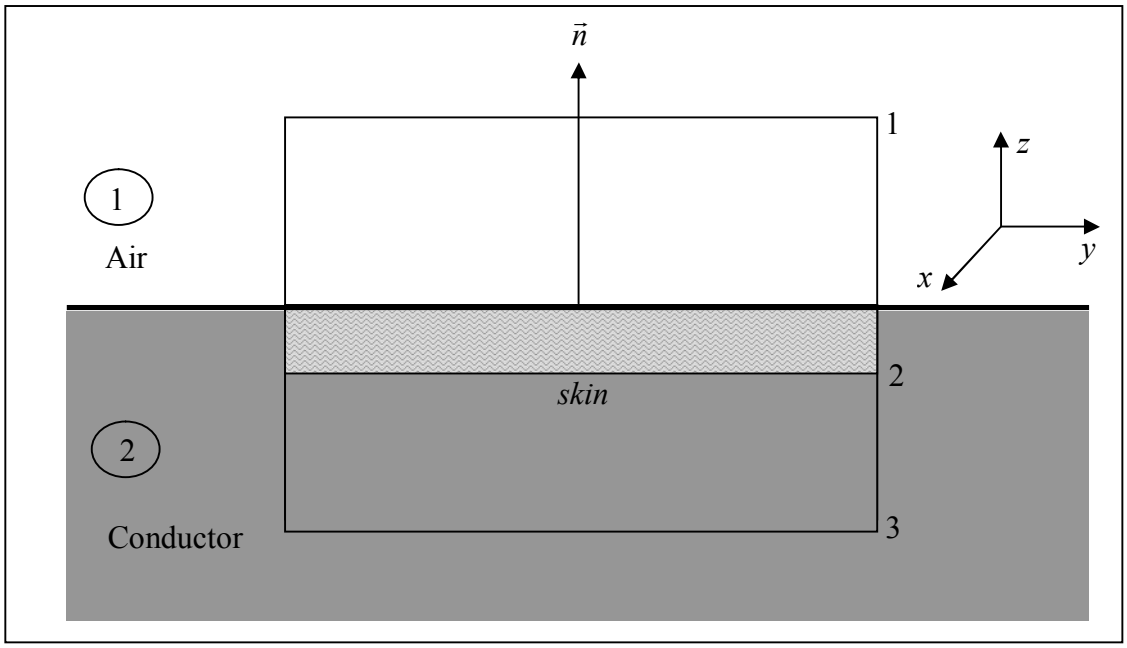

Figure 7.19. The skin condition at the boundary of conductor and air [51]

The boundary condition on the liquid metal surface is given by

$$\vec{n} \times \vec{H}_1 = \frac{4\pi}{c} \vec{J}_{qs} \tag{7.8}$$

where $\vec{H}_1$ is the magnetic field strength in medium 1 and $\vec{J}_{qs}$ is quasi-surface current. The magnetic field strength in y direction can be written as

$$-H_{1y} = \frac{4\pi}{c} \int I_x dz \tag{7.9}$$

and

$$\vec{J}_{qs} = \int \vec{I}_{tang} dz \,. \tag{7.10}$$

where $\vec{I}_{tang}$ is the tangential component of the volume current. The quasi-surface current can be formed by integrating the tangential components of the volume current over the

depth of the skin. During the same time the normal components of the volume current exists which cause to the actual surface charges. If the metal is assumed to be a perfect conductor then the $\vec{J}_{qs}$ is an actual surface current. The boundary condition for an electric field is given by [51] as

$$\vec{n} \times \vec{E}_1 = 0 \tag{7.11}$$

where $\vec{n}$ is the normal vector as shown in Figure 7.19. The tangential components of the volume currents when integrated over the depth of the skin is forming the quasi-surface current.

As an experimental study about reflection from GaInSn surface there were four different cases done. In the first case no external magnetic field and current was applied through the alloy but only the temperature was changed by heating it up. In the second case the current was applied through the alloy but the temperature was kept constant and external magnetic field was not applied. In this experiment different current values were applied under the same conditions and the reflectance was studied. One additional experiment was also done to check if the alloy was affected only by an externally applied magnetic field alone. The change in reflectance for different valued magnetic fields were studied. In the other case both magnetic field and current were applied externaly through the alloy and the reflection from surface was observed. In the last case again externally applied magnetic field and current were used but here the direction of the current was inverted.

7.4.6.1 Temperature Dependence

In this experiment the setup shown in Figure 7. 20 was used. GaInSn was heated up by using the heater seen from Figures 7. 20 and 21. The alloy was put into the glass container and during the heating process the reflection data against temperature were taken. The light source was the same as in the previous experiment which was 12 V_{DC}, 20 W Halogen lamp.

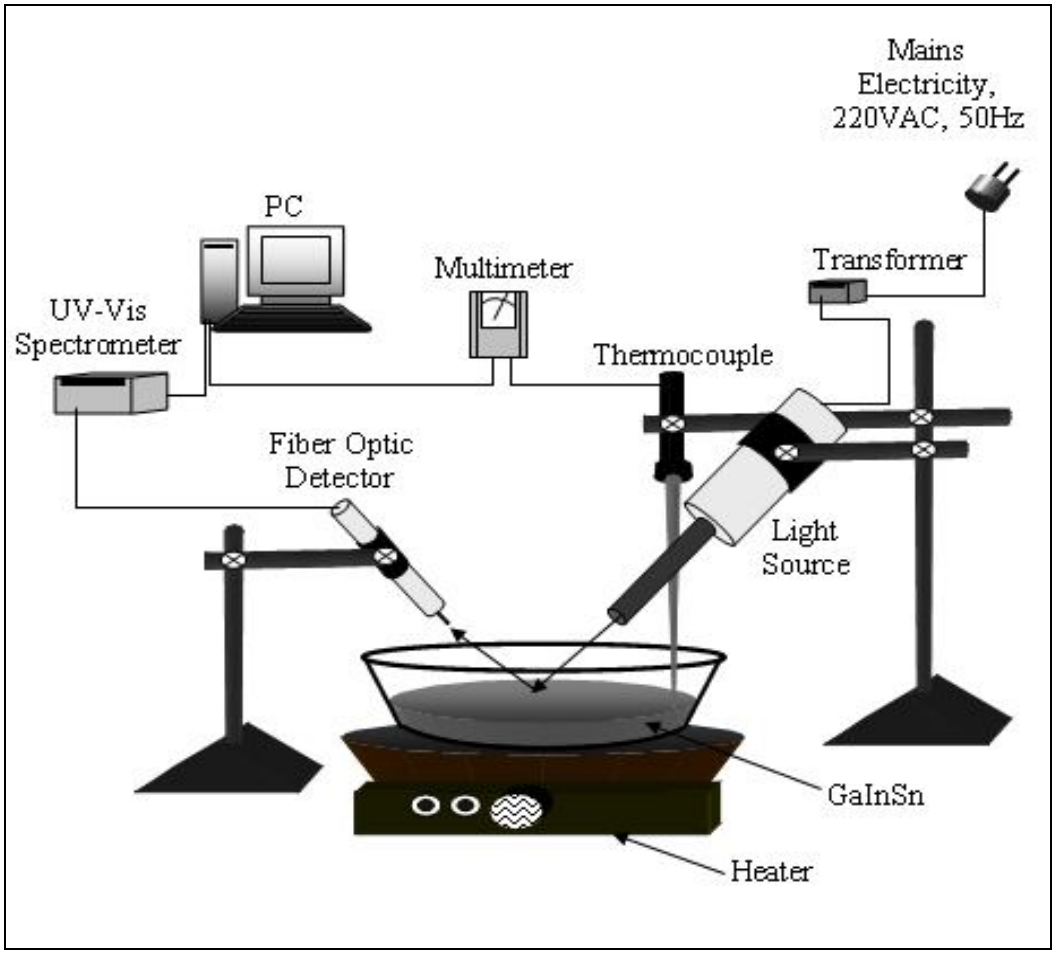

Figure 7.20. The setup of temperature dependence of reflectivity experiment

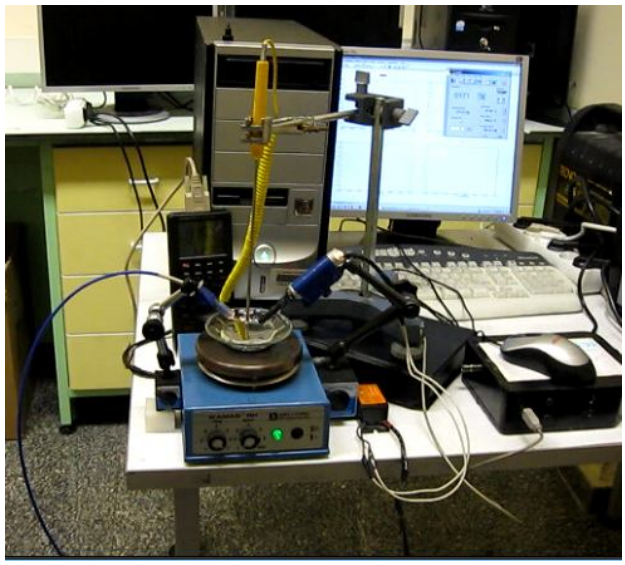

Figure 7.21. The photograph of the experimental setup for temperature dependence

UV-Vis spectrometer was used to collect the spectrum data for the reflected light. The multimeter connected to the thermocouple was used to take the temperature data. It was connected to the computer by using the serial RS 232 port in order to record the data.

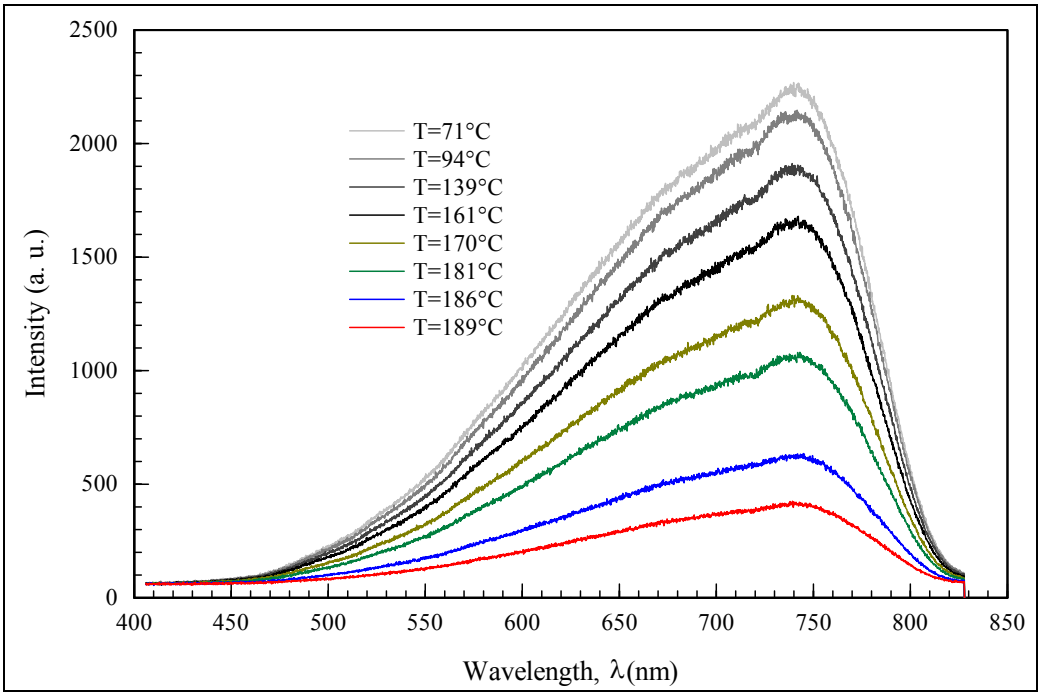

Figure 7.22. The reflectance spectrum taken for different temperatures of GaInSn alloy

Before the heating process started GaInSn volume inside the glass plate was $V_0 = 10^{-2} lt$ and after the heat addition finished the change in volume due to the expansion was $\Delta V = 0.013 \times 10^{-2} lt$ which corresponded to $0.1mm$ rise in surface level of GaInSn (Figure 7. 23). This level change will change the data taken by the fixed UV-Vis detector and stable light source. Due to the finite size of UV-Vis detector this level change may be effective in observations.

In reflection there are a lot of additional effects. In some cases such as described in the previous experiment the surface can have temporal changes such as oxidation. If roughness of surface increases the energy scatters in different directions. The real surfaces can not be known in a very detailed way so it is difficult to give any deterministic equation.

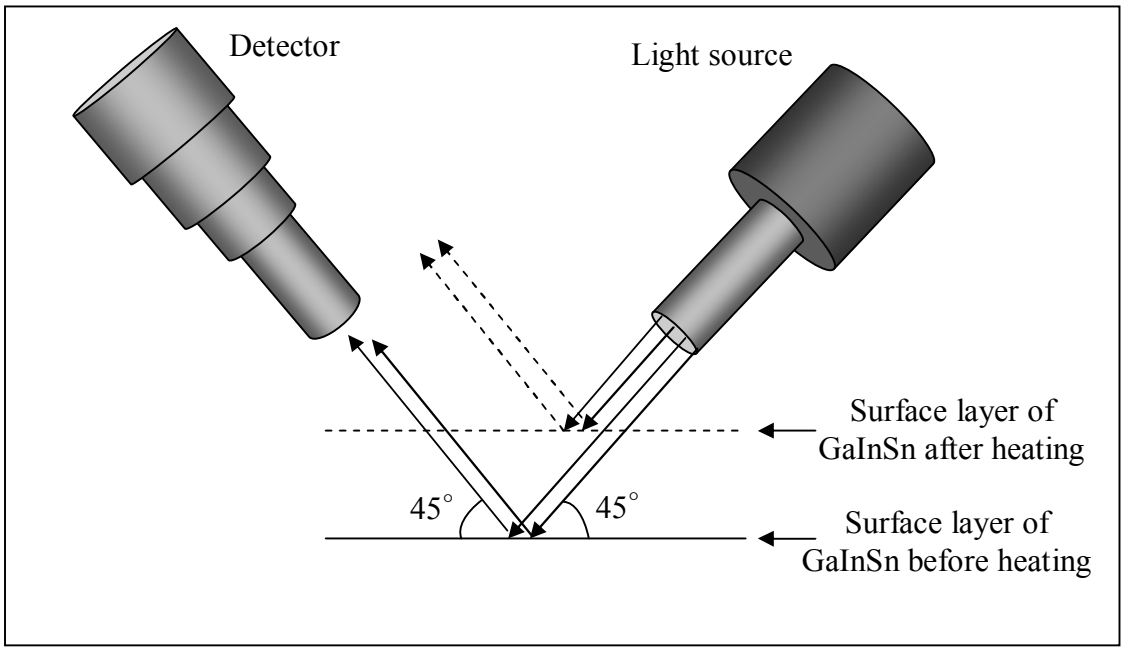

Figure 7.23. The effect of surface layer level change on the intensity detected

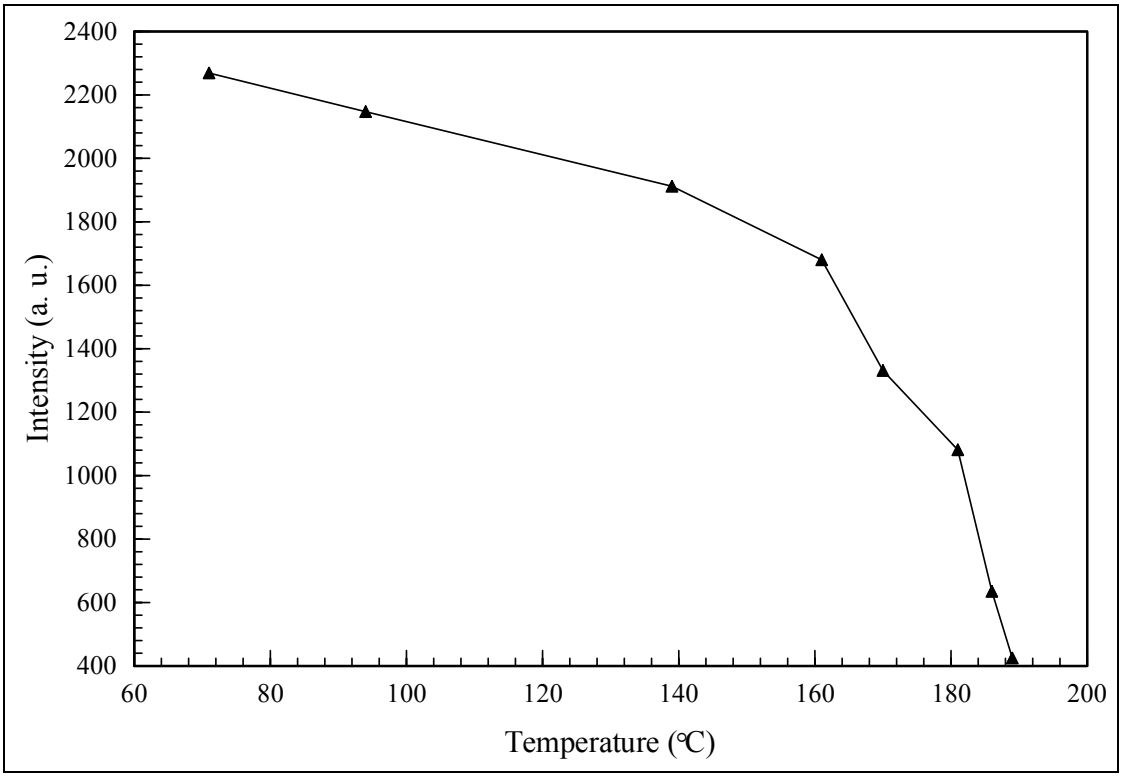

Figure 7.24. The maximum values for different spectra with different temperatures

Maximum values for reflection spectra for different temperatures were given in the table below (Table 7.5). The results did not show any wavelength shift for maximum reflected values from surface depending on temperature increment. Therefore it can be said that the temperature increase of GaInSn alloy did not affect remarkably the maximum reflection wavelength.

Table 7.5. Maximum reflection values for different temperatures and corresponding wavelengths

Temperature (°C)	Maximum Reflection Value (a. u.)	Corresponding Wavelength (nm)
71	2269	739.811
94	2147	741.645
139	1912	739.105
161	1680	742.21
170	1331	739.105
181	1081	743.057
186	635	744.895
189	425	739.246

The graph drawn in order to see the temperature and maximum reflection value's wavelength is given as in Figure 7.25.

During the experiment the incident angle for light was chosen to be 45° and the UV-Vis spectrometer's detector was also placed in order to have the same angle of 45°. During the heating process occuring under air pressure the physical properties of GaInSn may change and especially surface tension will be changed. By adding more heat to the alloy it will cause its surface tension to decrease.

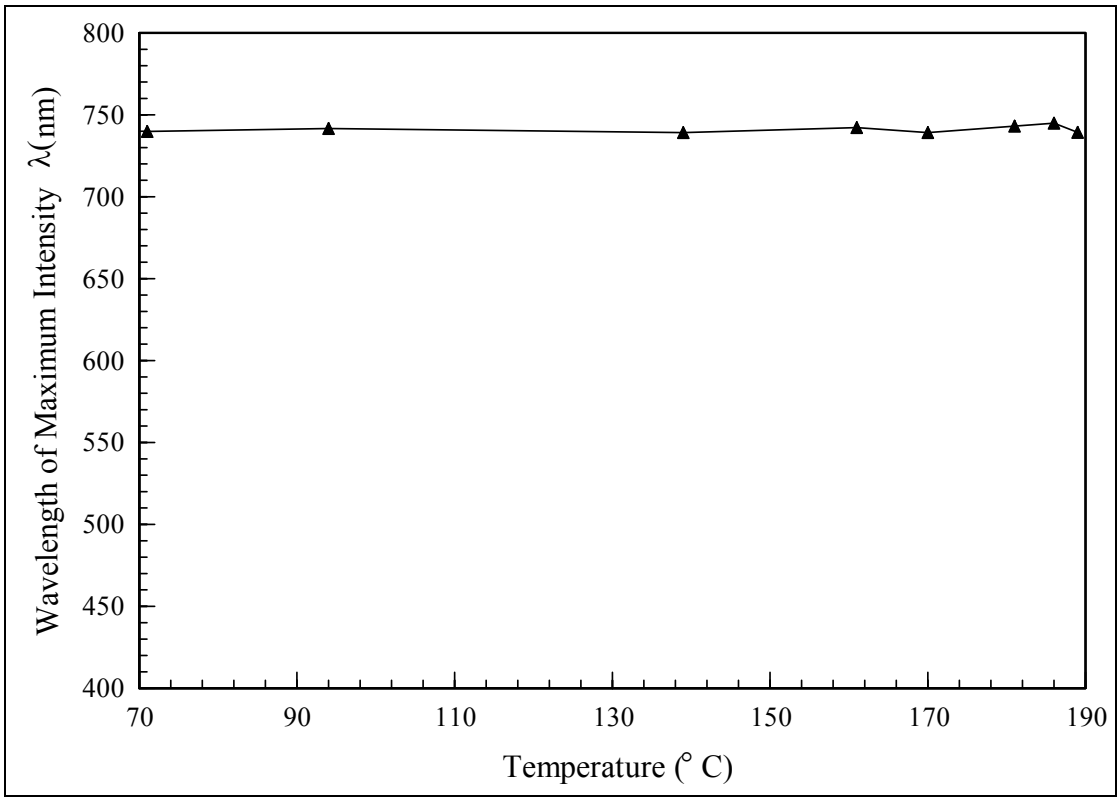

Figure 7.25. Temperature dependence of wavelength of maximum intensity of reflected light

The bulk structures of liquid metals and simple dielectric liquids are similar. However, at the surface of liquid metals there is an oscillatory electron density profile normal to the surface. This phenomenon comes from the fact that the interactions at the surface are changing from metallic interactions in liquid phase to Van der Wals interactions in gas phase. Actually the surface of elemental liquid metal can easily be modified by adding a second or third liquid metal such as in GaInSn alloy. The interactions between these different atoms may lead to directional bonding. The surface of alloy is very much affected by the properties of different atoms. The presence of oxygen in gas phase can affect the the compounds of ternary alloy GaInSn differently. For example the oxidation of Ga forms a homogeneous layer but oxidation of In forms nonhomogeneous island-like shapes [52]. Actually below activation pressure which is given as $\sim 5.0\times10^{-6}\,Torr$ the pure liquid Sn does not react with oxygen. If once the oxidation started it proceeds even if the pressure is less than critical or not. The oxidation of liquid Sn appears in the shape of islands which have very rough surfaces. The surface oxide on

liquid Ga is amorphous [53]. Since there are different structures, In has many free electrons in its liquid state contrarily Ga has partially localized electrons due to their covalent bonds. After the alloying process the reflectivity differs from the reflectivity of any individual metal surface forming an alloy. There are many parameters which can affect the reflectivity such as the density of surface adlayer, electron density and sizes of atoms. The electron density of In is 5 per cent larger than that of Ga.

The results obtained in these experiments showed that the reflected light intensity decreased with increasing temperatures. According to reference [54] liquid eutectic systems are not completely mixed but they consist of some regions rich with one component and the other with the others. There were large concentration fluctuations. By increasing the temperature of the alloy the atoms are redistributed and heterogeneity decreases. The interatomic distances also decrease. The last distribution of the elements in the alloy will change the electron density profile wich can affect the reflection of the light considerably. The number of electrons can change the energy of incident light during the reflection process. The absorbed energy from the incoming light will increase with the increase of the number of electrons accumulated at the top of the surface of reflectance which will lead to the decrease of the intensity after reflection. The results shown in Figure 7.22 and 7.24 are in good agreement with this explanation. Second effect can be the expansion of the alloy itself by heating. The level of surface of the alloy will change and the reflected light will be directed to a different direction in which the detector does not stay (Figure 7.23). The level change of the surface of GaInSn alloy was calculated to be $0.1mm$ in this experiment by using the expansion coefficient calculated previously. This effect also must be taken into account. Actually the structure of the alloy can also change with increasing temperature and this can affect the reflection. However, the temperature change during the heating process in this experiment was kept in a very narrow range which was between $71-189^{\circ}C$ this effect will be less significant with the other mentioned above.

The surface tension of GaInSn alloy also decreases with increasing temperature even though Gallium makes an increase in In-Sn alloy surface tension [55].

The agitation of the surface of an alloy by temperature decreased the intensity of reflected light. There is a graph given below as Figure 7.26 taken from [56] in which the electron density profile change is given for liquid-vapour interface of Gallium.

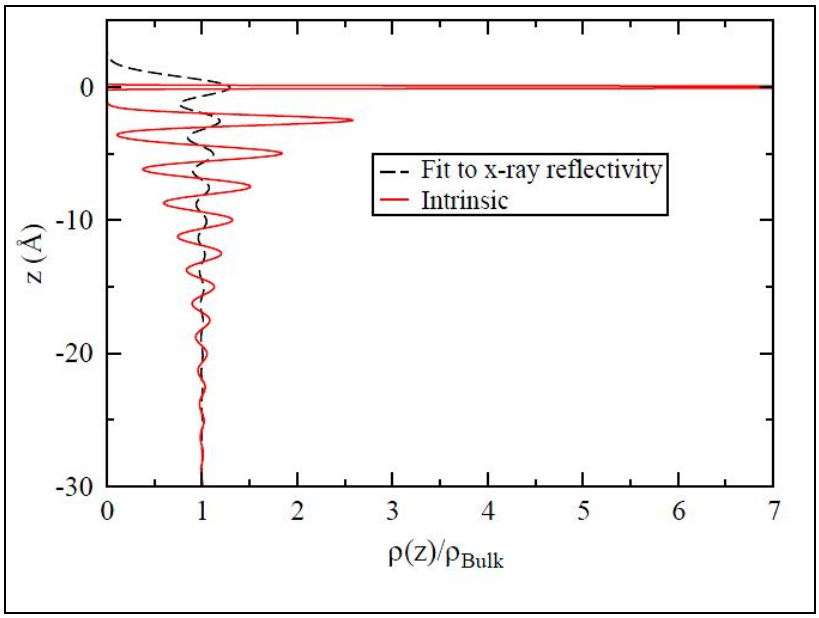

Figure 7.26. The electron density profile for density liquid-vapour interface of Gallium [56]

In Figure 7.26 it is seen that the electron density $\rho(z)$ for lquid metal which is Gallium has an oscillatory nature. However, a more important thing which is very remarkable is the value of $\rho(z)$ which is bigger on the surface than the bulk electron density ρ_{Bulk}. This means that the number of electrons accumulated on the surface is more that that are in the bulk of liquid metal.

It is obvious that the heating process can modify this density. This can easily be seen from the reflected light's intensity change as a function of temperature in Figure 7.22 and 7.24. These results agree also with [57] in which it is said that by increasing the temperature of illuminated surface generally is accompanied with the decrease in reflectivity.

Since the effect of the gravity makes the surface of a liquid smooth and macroscopically flat there are thermally induced capillary fluctuations in the height of the surface. The dominant effect which decreased the reflection from GaInSn surface must be this capillary wave effect. According to [58] the surface of liquid can be roughened by thermally induced capillary waves. The contribution of capillary is determined by using the balance between the thermal energy kT with the surface tension γ and gravity. The formula showing the relation between the temperature and capillary width is given as

$$\sigma_{cw}^2 = \sigma_0^2 + \frac{kT}{2\pi\gamma} ln\left(\frac{k_{max}}{k_{min}}\right) \tag{7.12}$$

in [58] and [59] where σ_0 is the intrinsic contribution $(= 0.37 \pm 0.027\ A^\circ$ for Ga $)$, γ is surface tension, k_{max} and k_{min} are short and long wavelengths respectively

$$k_{max} = \frac{\pi}{d} = 1.26\ A^{\circ -1} \tag{7.13}$$

where d is the molecular size.

$$k_{min} \propto \sqrt{\Delta\rho g/\gamma} \tag{7.14}$$

where $\Delta\rho$ is mass density difference.

For an alloy such as GaIn the electron density profile can be modified in the way in which the contribution of each element can be added to each of the layers in the expression given as

$$\langle \rho(z) \rangle = \frac{d}{2\pi} \sum_{j=0}^{\infty} \frac{1}{\sigma_j} \left[n_{Ga}(j) f_{Ga}(z) + n_{In}(j) f_{In}(z) \right] \otimes exp\left[\frac{-(z - jd)^2}{2\sigma_j^2} \right] \tag{7.15}$$

where d and σ_j defined similarly as for pure Ga, $f_{In}(z)$ and $f_{Ga}(z)$ are the electron density distributions for atomic In and Ga respectievely. The number densities in each layer are given by $n_{In}(j) = x_j n_{In}$ and $n_{Ga}(j) = (1 - x_j) n_{Ga}$ with x_j the concentration of In in the j^{th} layer [59].

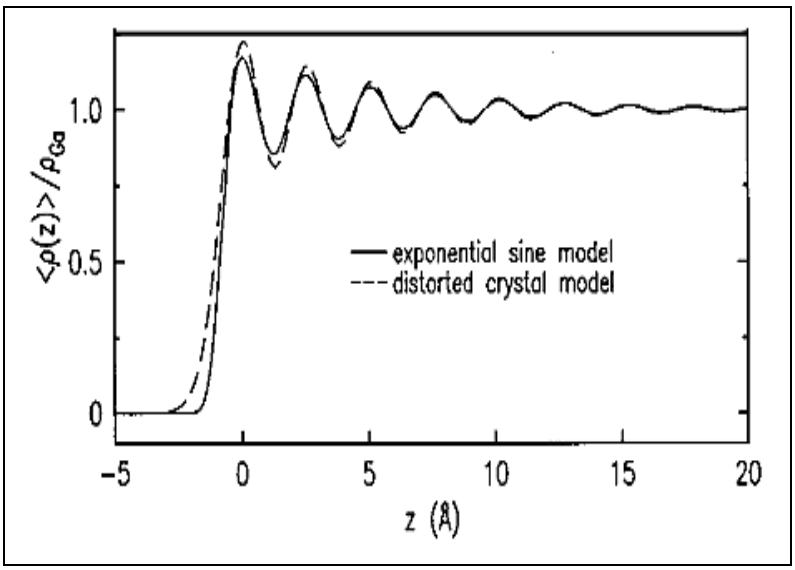

Figure 7.27. Electron density profiles for liquid Ga at room temperature [59]

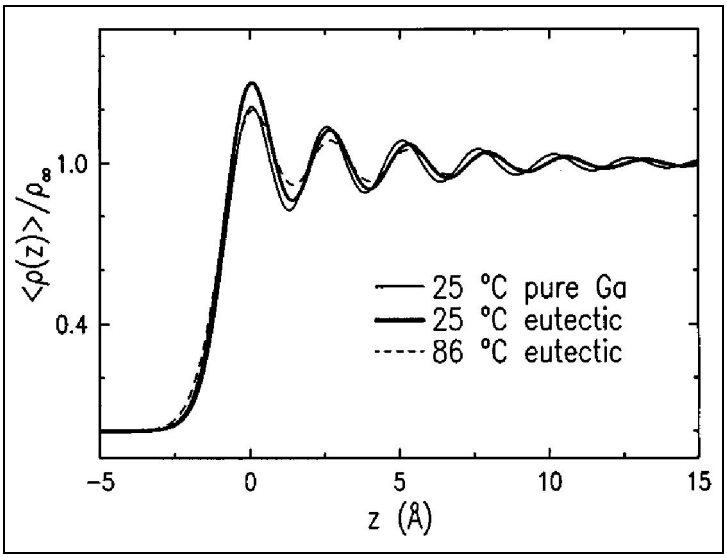

Figure 7.28. Models of the electron density profiles for GaIn alloy compared to pure Ga [59]

The electron density ratios for Ga and GaIn alloys which are given in Figure 7.27 and Figure 7.28 are taken from the reference [59]. These results are similar to the results of reference [56] which are given in Figure 7.26. It can be easily said that the electron density at the surface of both liquid metal (Ga) and liquid alloy (GaIn) has higher values from the bulk electron density. Since the alloy used in the experiments in this thesis is GaInSn its electron density profile can be assumed to be similar to that which was given in Figure 7.28.

The reflection expression given in [59] is

$$R(q_z) = Rf(q_z)\left|\frac{1}{\rho_0}\int \frac{d\langle\rho(z)\rangle}{dz} e^{iq_z z} dz\right|^2 \tag{7.16}$$

where $Rf(q_z)$ is Fresnel reflectivity, q_z is the wave vector. From this equation it is seen that reflection is directly proportional to the density gradient of electrons. If the density gradient increases the reflectivity will increase meaning that the reflected intensity will increase. By heating the alloy this gradient can be less since heating the alloy will cause a more homogeneous distribution of electrons on the surface and bulk. Therefore the maximum peak at $z = 0$ which is given in Figure 7.28 will decrease. This will result with decreasing reflection and reflection intensity detected by UV-Vis will decrease as it was seen from the experimental results in Figure 7.22 and Figure 7.24.

However, it is also seen from Equation 7.12 that increasing temperature results with the increase at surface roughening which leads to decrease in reflectance. By comparing two effects mentioned above the dominant one must be the capillary wave effect since it is changing directly the shape of the reflection surface. The change in electron density profile will also affect the reflectance but probably less than the one previously mentioned.

Not only the effects mentioned above can change the reflectivity but also the light falling on the surface can corrugate the surface of liquid metal [60] which will also have similar effects on the reflecivity. The spatially periodic heating due to applied irradiation occurs which causes the evaporation of the surface which results with stimulated growth of

the corrugation. However, the light source in our experiment was a $20W$ halogen lamp operating in the range of visible spectrum, the effect can be neglected during this experiment.

Actually it is very difficult to say that the specular reflection can exist for heated liquid surfaces [61].

The maximum intensity values for different temperatures were also studied. It was found that in the etween the temperature limits used in this thesis there were no significant changes in the wavelengths for the intensity maxima (Figure 7.22).

Similar tests were also carried out by different groups but they used X-ray sources in order to study the reflectance from liquid metal surfaces [59]. However, in that study the light source was a halogen lamp which had the wavelengths in visible region of electromagnetic spetrum. The results as mentioned above were found in good agreement with these obtained by the groups which mostly using X-ray scattering.

It must be noticed that before reflection experiment starts the surface of GaInSn was cleaned by using thin clean glass spatula like material in order to remove any macroscopic oxide particles formed there.

7.4.6.2 Current Dependence

In this experiment the reflection from the surface of GaInSn is monitored continuously during the application of external current. Actually only current was applied through the GaInSn, the ambient temperature was not changed $T_a = 25 \pm 2^{\circ}C$ and humidity was measured as $52 \pm 5\%$. The applied current values were chosen to be 50, 80 and 100 A. During the experiment two different geometries were used as given in Figure 7.29 and Figure 7.30.

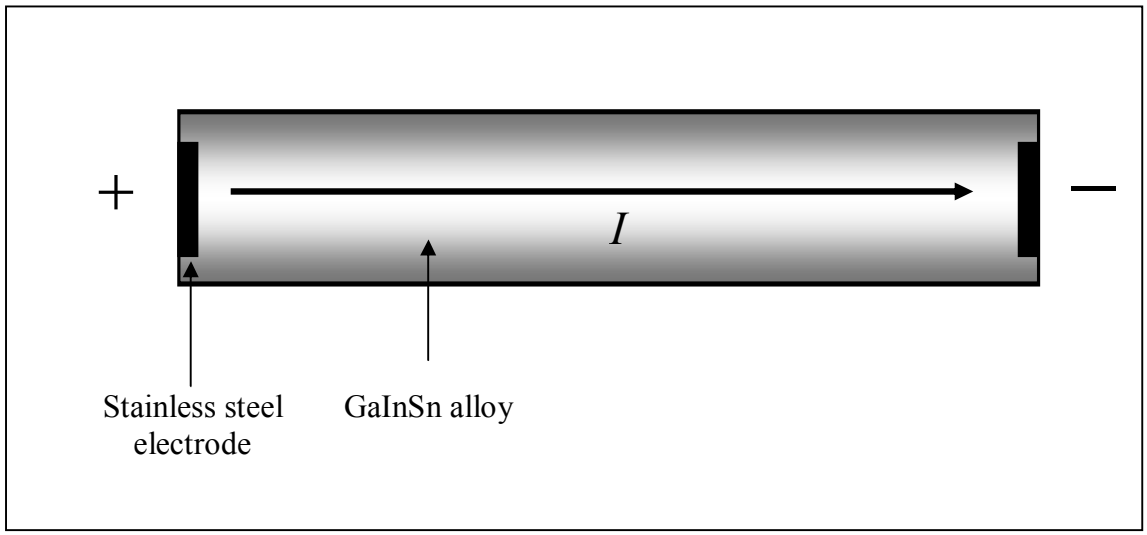

Figure 7.29. The top view of the electrodes' locations for the first part of the experiment (case A)

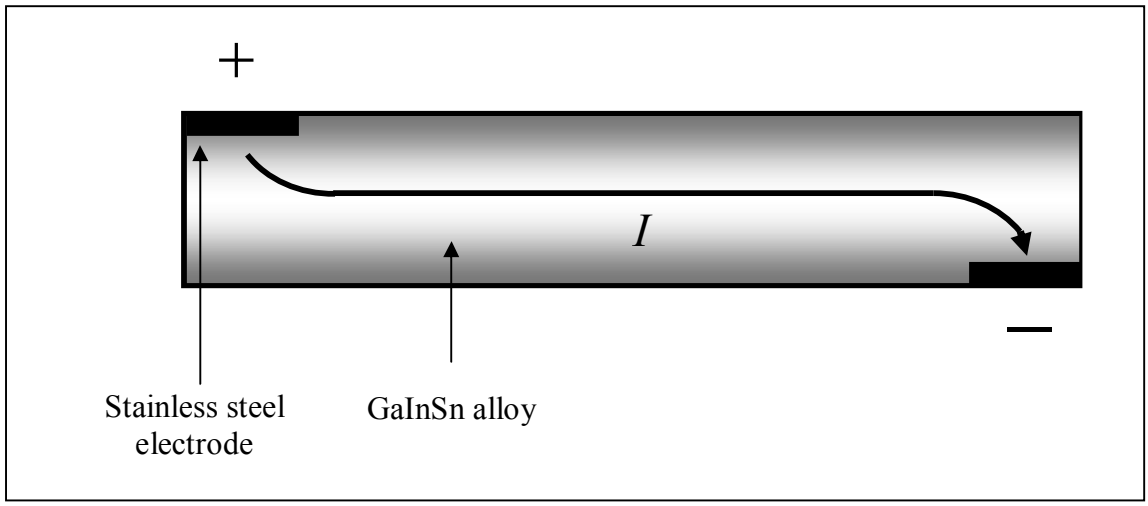

Figure 7.30. The top view of the electrodes' locations for the second part of the experiment (case B)

The intensity changes for both cases (A and B) are given below in Figure 7.31 and Figure 7.32.

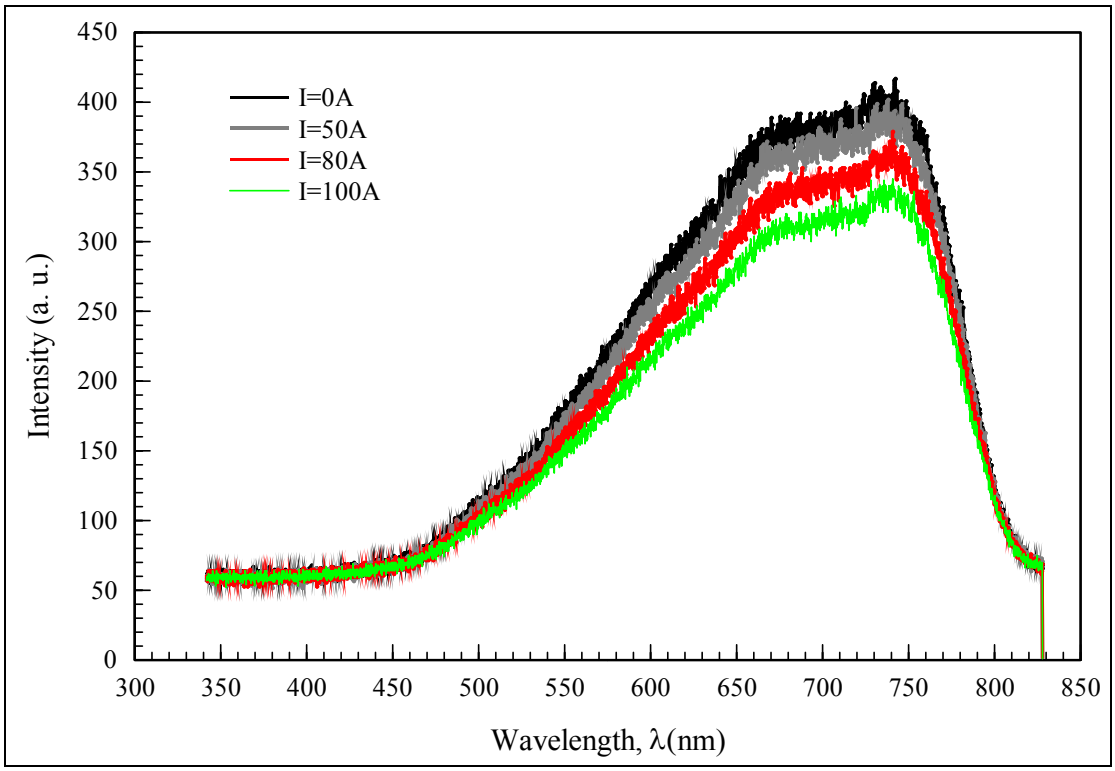

Figure 7.31. Intensity of reflected light versus wavelength graph for case A

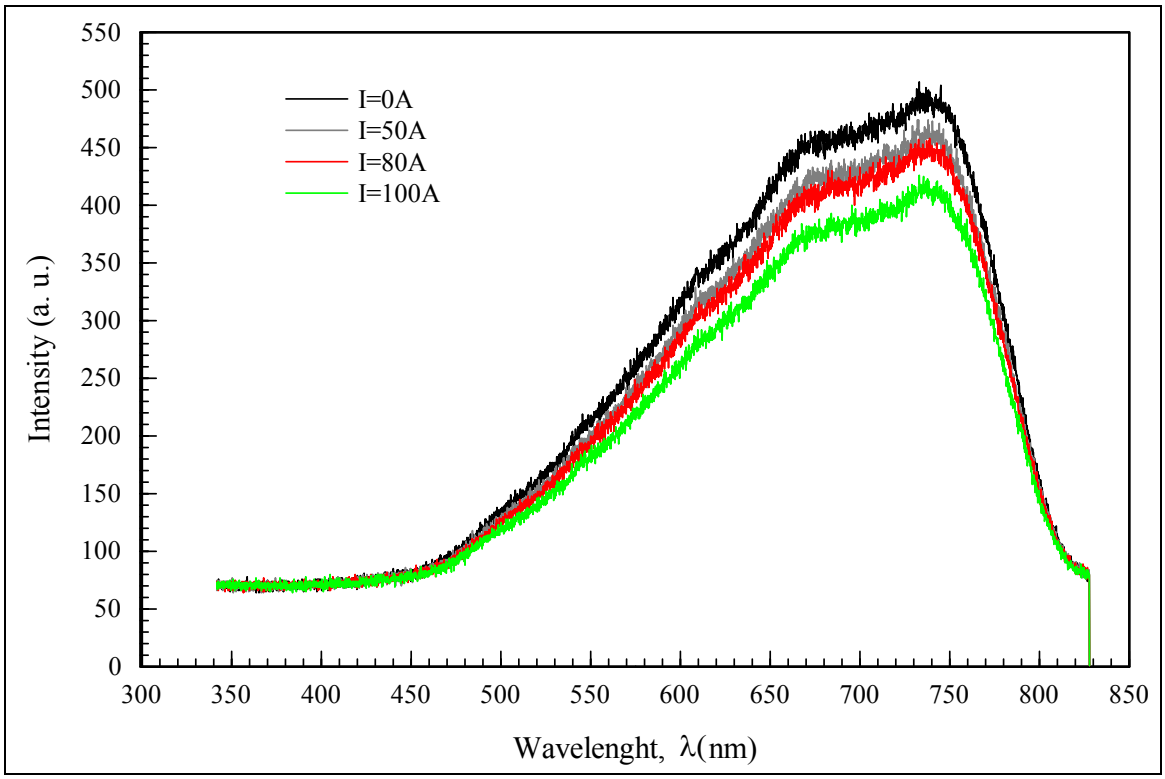

Figure 7.32. Intensity of reflected light versus wavelength graph for case B

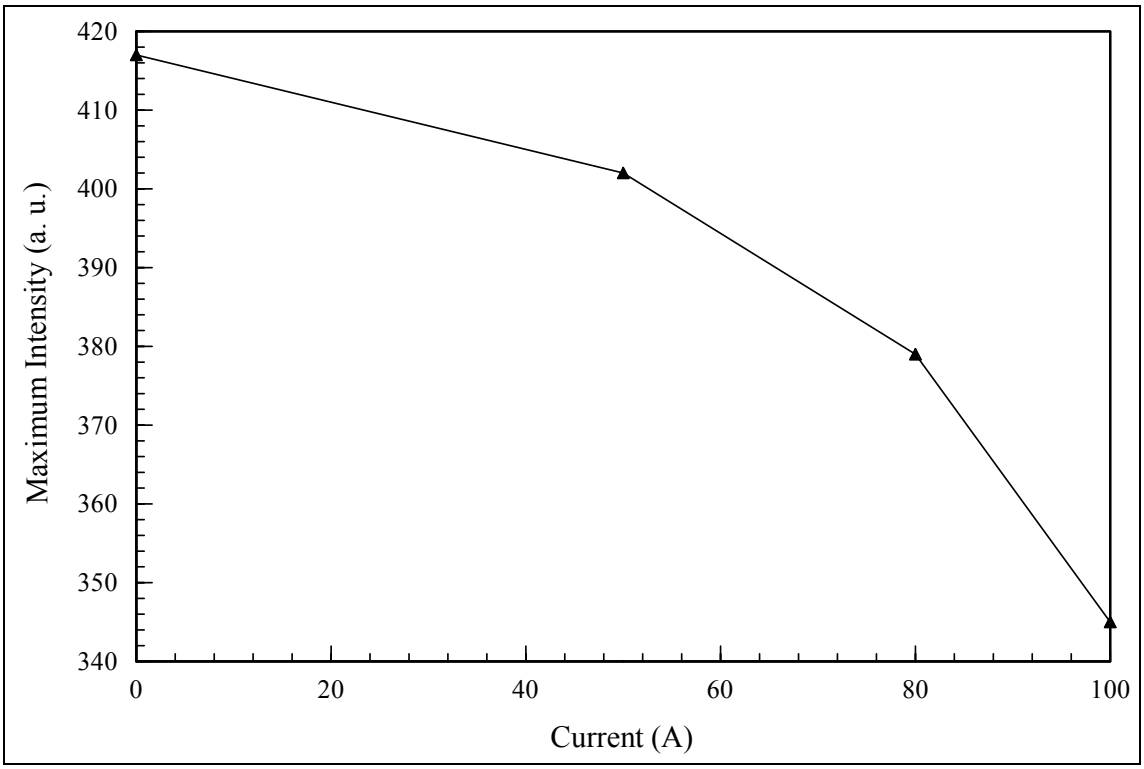

Figure 7.33. Maximum intensity of reflected light versus current graph for case A

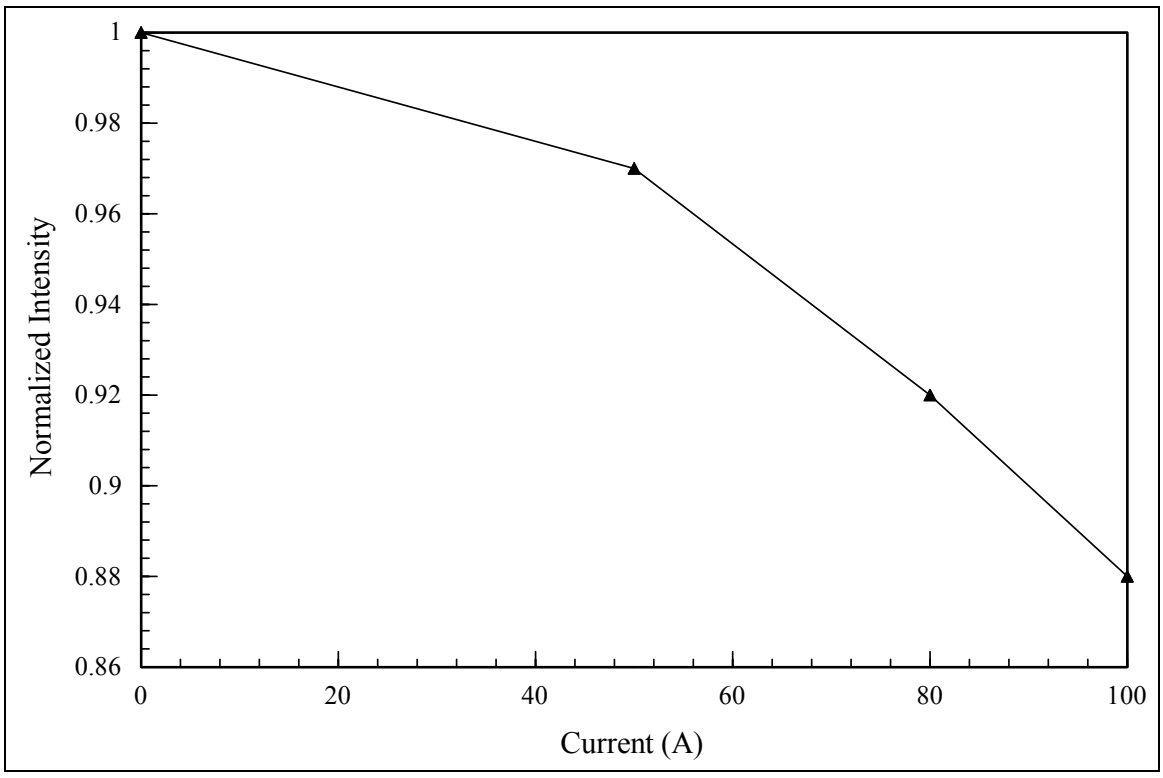

Figure 7.34. Normalized intensity of reflected light versus current graph for case A

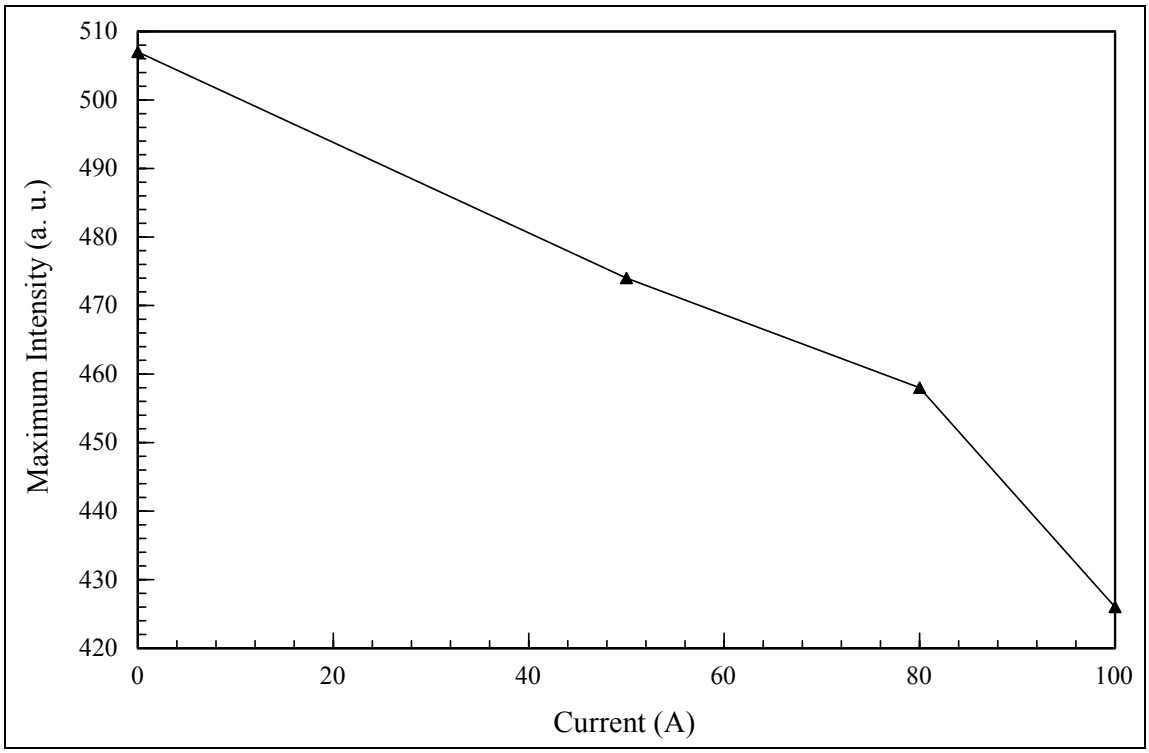

Figure 7.35. Maximum intensity of reflected light versus current graph for case B

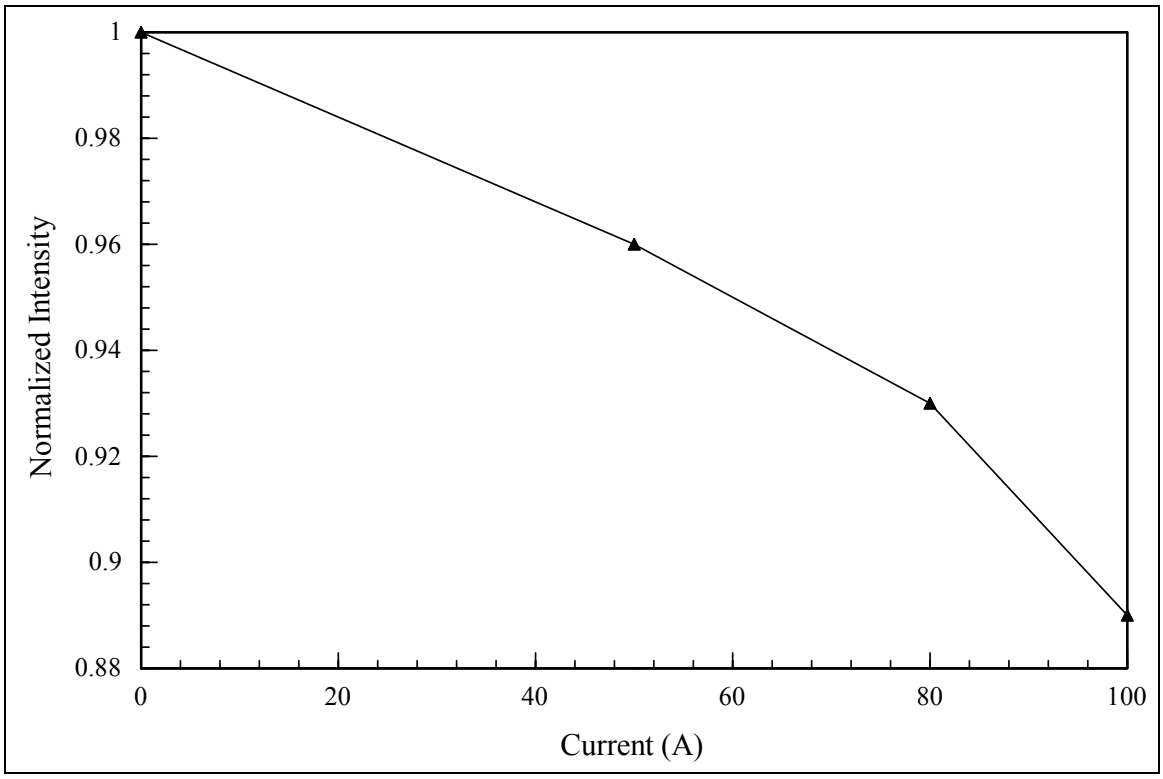

Figure 7.36. Normalized intensity of reflected light versus current graph for case B

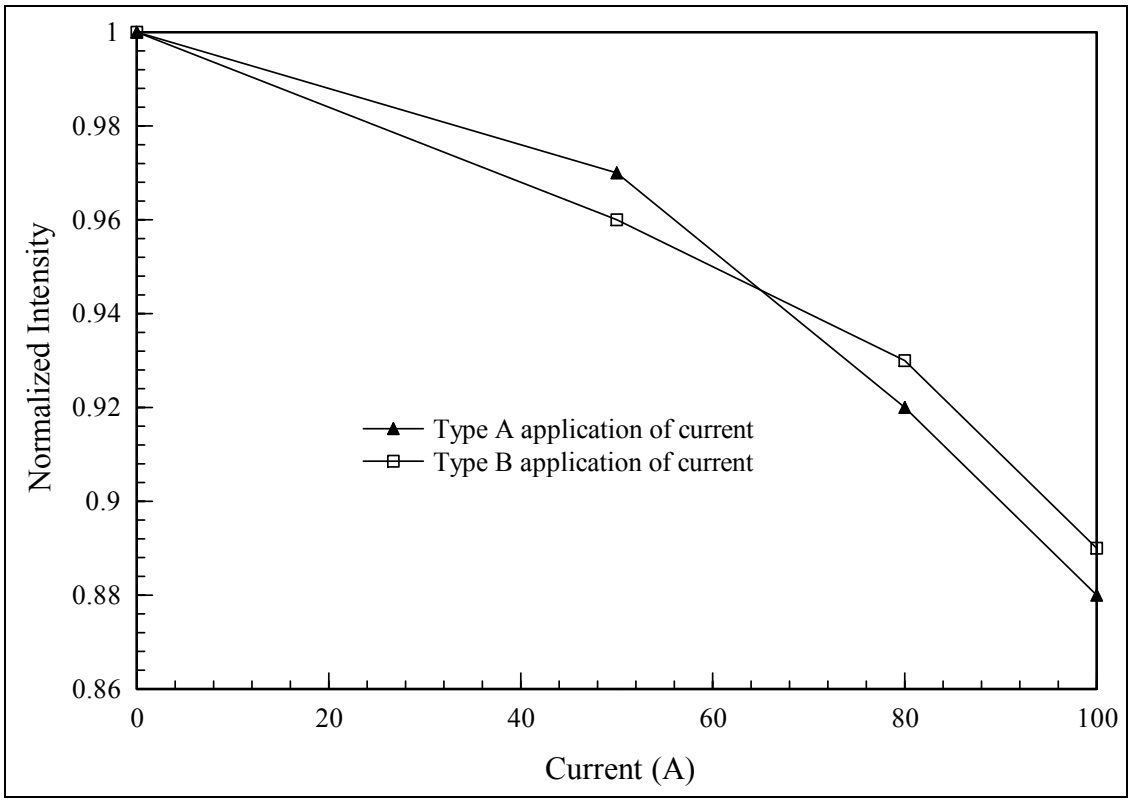

Figure 7.37. Normalized intensity versus current graph for case A and case B

Results obtained from the application of current showed that the reflection decreased with increasing current similar to the reflection dependence of temperature. It will not be an overstatement to say that with increasing current the temperature of the alloy will increase due to Joule heating. This temperature increase can again generate capillary wave effect which will decrease the intensity of reflected light. However, fast moving electrons due to the applied current can produce diffuse scattering on the surface and they can form some instabilities which can also decrease the reflection.

The Figures between 7.33 and 7.36 are showing similar results for both current application geometries (case A and case B). The normalized intesities were calculated by dividing each spectrum to the maximum intensity of the spectrum taken without current application for case A and case B separately. Figure 7.37 shows similar profiles for different application geometries.

In order to check the reflection polarization from the GaInSn surface two different polarizers were put in the opposite ends of the container filled with GaInSn. The light was sent through the first polorizer. In order to send the light through the polarizer easily the angle of light falling on the surface of GaInSn alloy was arranged to be 30°, first polarizer angle was set to 0°. Second polarizer which is put in front of the UV-Vis spectrometer's detector which was also arranged to be 30° with the horizontal. Polarization angle second polarizer was firstly arranged to be 0°. It was desired to change the second polarizer's angle between $0-90^\circ$ in order to see if there is maximum intensity value for reflected light different from 0° polarization. The experimental setup is given in Figure 7.38 and a photograph of the experiment is given in Figure 7.39.

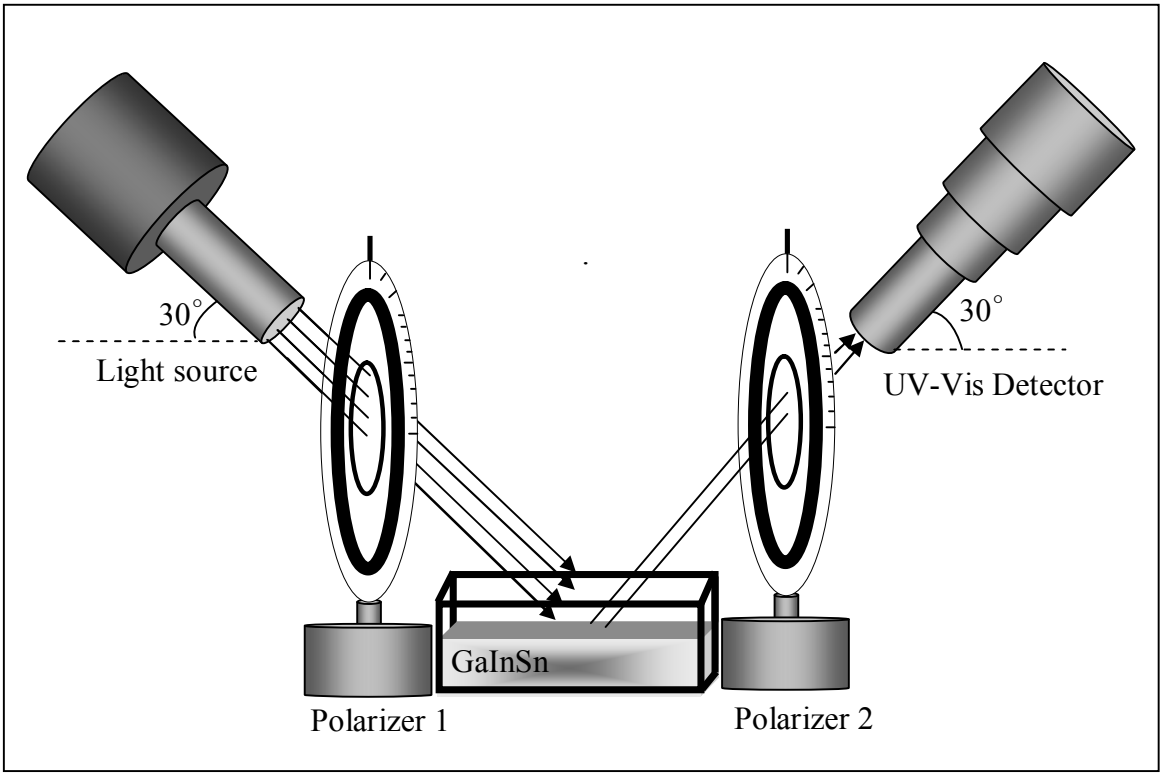

Figure 7.38. The schematic view for light source, detector, polarizers and GaInSn chamber

This part of the experiment was done with three different cases. In first case no current was applied through the GaInSn, in second case $60A$ current, and in the third case $100A$ current was applied through the alloy. The polarizer in front of the light source

(polarizer 1) is set to be at 0° and it wasn't changed during the experiment. The second polarizer (polarizer 2) in front of the UV-Vis detector was previously set to 0° then its polarization angle is changed to 30°, 45°, 60°, 75° and 90° angles. The results are given below.

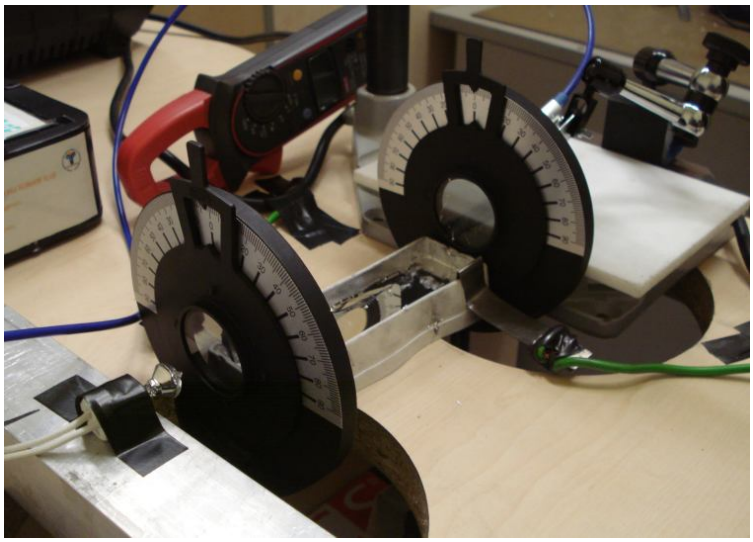

Figure 7.39. The photograph of the experiment for polarization study

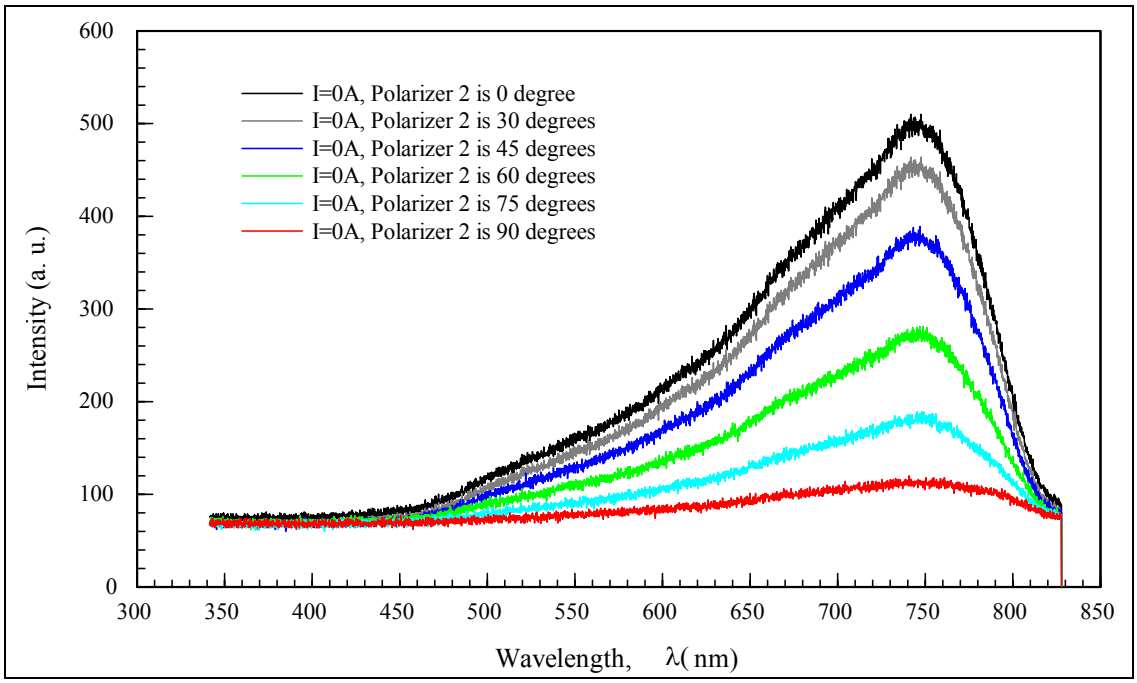

Figure 7.40. Intensity versus wavelength graph for no current application

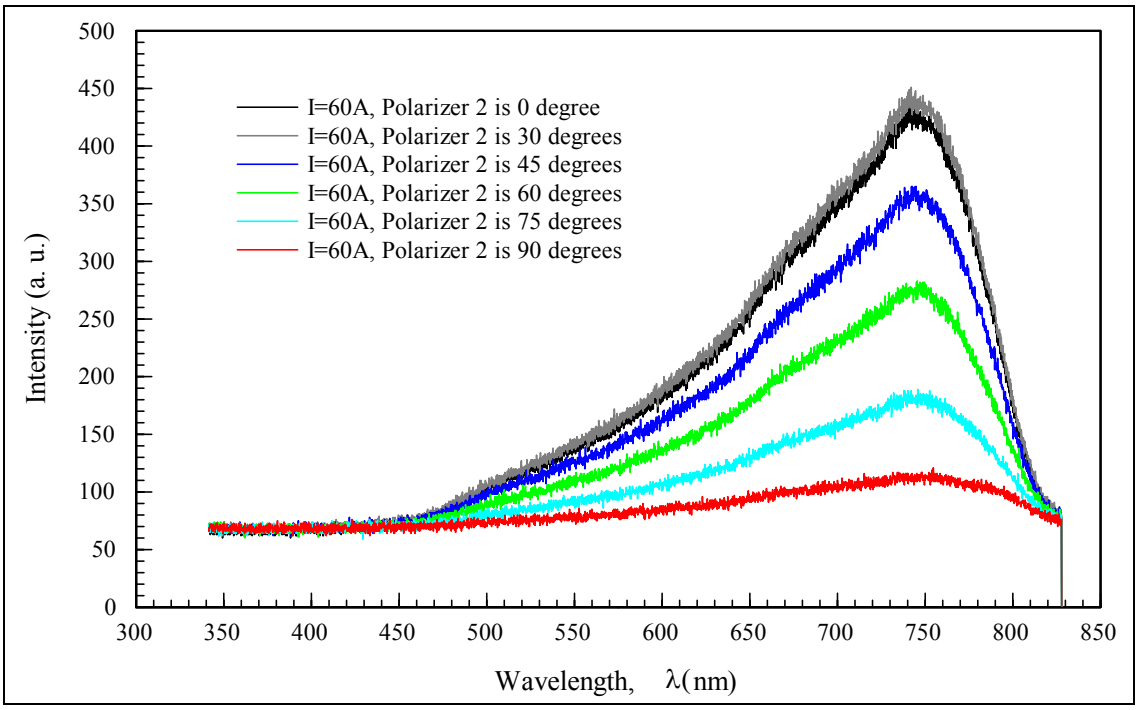

Figure 7.41. Intensity versus wavelength graph for 60 A current applied throug GaInSn

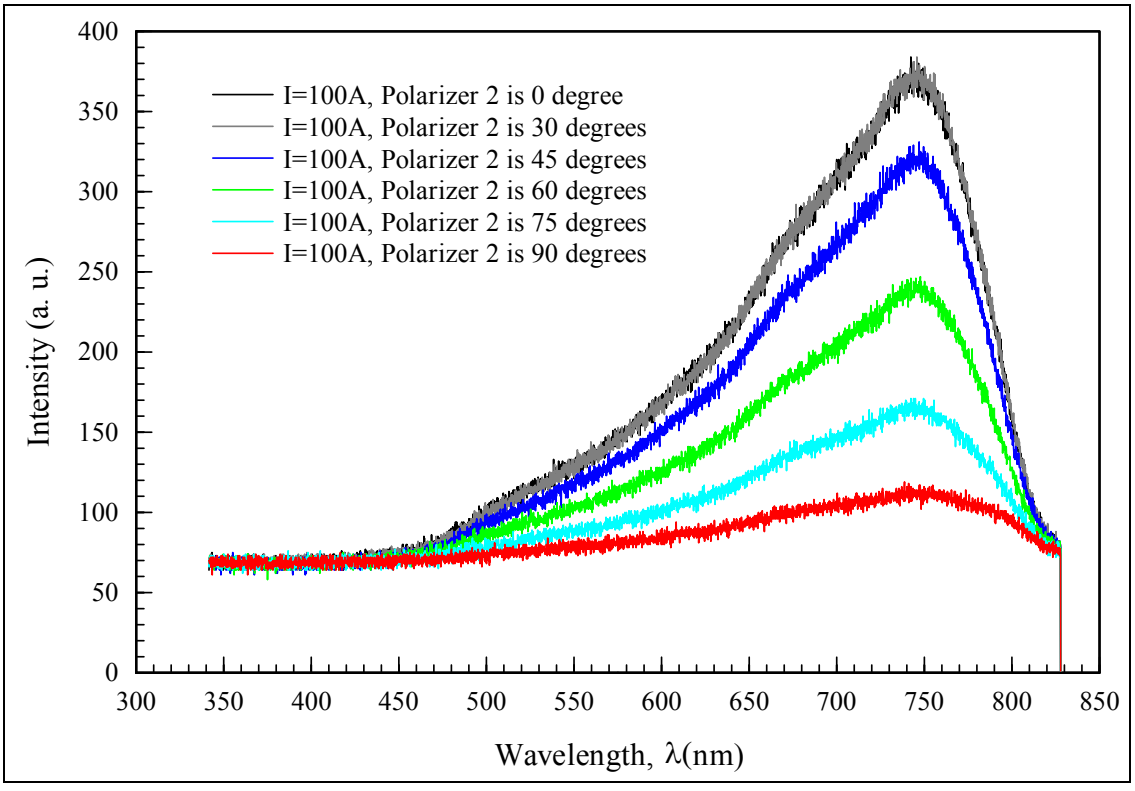

Figure 7.42. Intensity versus wavelength graph for 100 A current applied through GaInSn alloy

The polarising filter used in this experiment is used to produce and determine the linearly polarized light. It has $+/-90$ degrees range with diameter $32mm$ and product number was 08610-00. Manufacturer is PHYWE. From the graphs given as in Figure 7.33, 7.34 and 7.35 it is obviously seen that when the current flowing through GaInSn alloy increases the intensity of reflected light decreases. In the first part of polarization experiment when no current was applied, the intensities decreased when the angle of polarizer 2 increased. According to Malus' law the intensity of the light can be calculated

$$I(\theta) = I_0 Cos^2\theta \tag{7.17}$$

where I_0 is the initial intensity and θ is the difference of angle between the first polarization direction and the direction of the axis of the polarizer.

It is seen that when the angle of polarizer 2 is changed and if there is no polarization after scattering from the surface of GaInSn the intensity of light must decrease. The results when the current is passing through GaInSn showed different character from the results obtained for currentless experiment. It can be said that after reflection from the surface there is polarization of the light when curent is flowing through the alloy. This part of experiment can be studied by using more sensitive devices since the change of the nature of scattering is seen. However, since the detector used here is measuring the intensity of the total light falling on the aperture the effect of polarization will not be taken into account. The total amount of the reflected light will be measured during the experiments.

If the attention is focused on the current application part it was seen that by increasing current the reflection intensity decreased. For two different arrangements of electrodes the same decreasing nature was seen. However, in case B there are some perturbations at current flow due to the electrodes positions. This perturbation can affect the reflectance. In case B the intensities of reflectances were observed higher than these in case A. Since the electrodes' positions were changed this caused an obligatory rearrangement of the chamber filled with GaInSn. Therefore it was meaningful to compare their maximum intensity ratios. The results were given in Table 7.6. It was seen that the intensity change in case B is more significant from case A for currents with magnitudes

$50A$ and $80A$. This can be because of perturbated and nonhomogeneous motion of electrons for case B. For high enough currents this effect is seen to be decreased as given in the results for $100A$ current application for both cases.

Table 7.6. Comparison of the intensity ratios for cases A and B

Current Geometry	$I_{50A.max}/I_{0A.max}$	$I_{80A.max}/I_{0A.max}$	$I_{100A.max}/I_{0A.max}$
Case A	0.96	0.91	0.83
Case B	0.94	0.90	0.84

The current magnitude increase caused the decrease in reflected light intensity. The current increase will heat up GaInSn resulting with capillary wave effect which will decrease the reflection. This kind of heating is called Joule heating. This heating term was mentioned in the previous chapters and in Equation 2.131 and Equation 6.4.

7.4.6.3 Magnetic Field Dependence

AC magnetic fields with high frequencies can be used to control and shape the surfaces of liquid metals [62]. For high values of magnetic fields the observed waves occured on the surface are structured. High frequency magnetic field can create electromagnetic pressure which can be used in shape forming of liquid metals. The instabilities formed on the surface of liquid metals can be controlled by the externally applied magnetic fields. This kind of control can be used in the metallurgical Technologies especially in levitation, cold crucible etc.

In this part of the experiment only externally applied magnetic field was changed, temperature was kept constant and no current was applied through GaInSn alloy. The externally applied magnetic fields were constant in time (DC). The magnitudes of magnetic fields were measured by using PHYWE produced teslameter with product number 13610-93. The operating temperature range is $5-40^{\circ}C$, relative humidity $\langle 80\%$, accuracy for used DC magnetic fields were $\mp 2\%$. Together with the teslameter a tangential Hall probe was also used and it was also produced from the same company with production number 13610-02. The experiment was done with both detectors UV-Vis and luxmeter. The light source was arranged in the way that the incoming light is making 45°

with the surface of the GaInSn. The data for reflected light were collected for different arrangements of luxmeter which was moved from 20° to 90° with 5° degree increases of the reflection surface. For different magnetic field values applied externally the same procedure was repeated and the results were presented in the figures given below.

The magnetic fields were generated by using the home made electromagnet which is shown in Figure 7.43 and 7.44. The effect of DC magnetic field on stationary and currentless GaInSn must be negligible. Since there are randomly moving free electrons in GaInSn alloy Lorentz force which can act on these electrons will be isotropical and the effect of it can be reduced by its differently directed components. In order to undertstand the properties of the electromagnet which was used in these experiments some preliminary experiments were done and the results are given below in Figure 7.45-7.47.

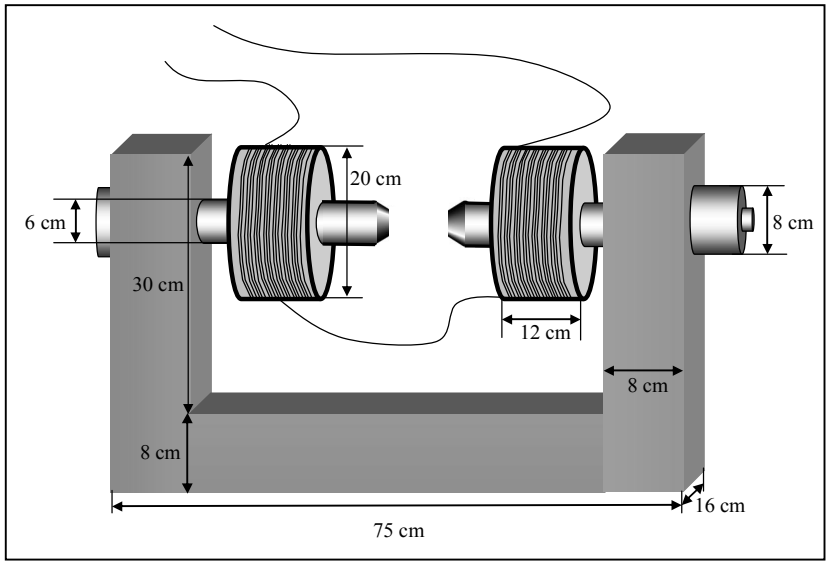

Figure 7.43. The dimensions for the electromagnet used in the experiments

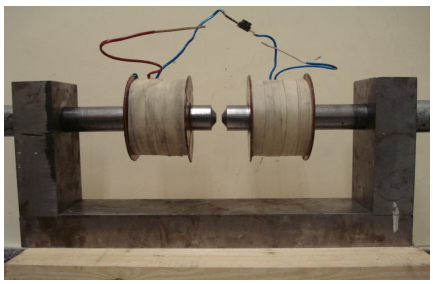

Figure 7.44. The photograph of the electromagnet

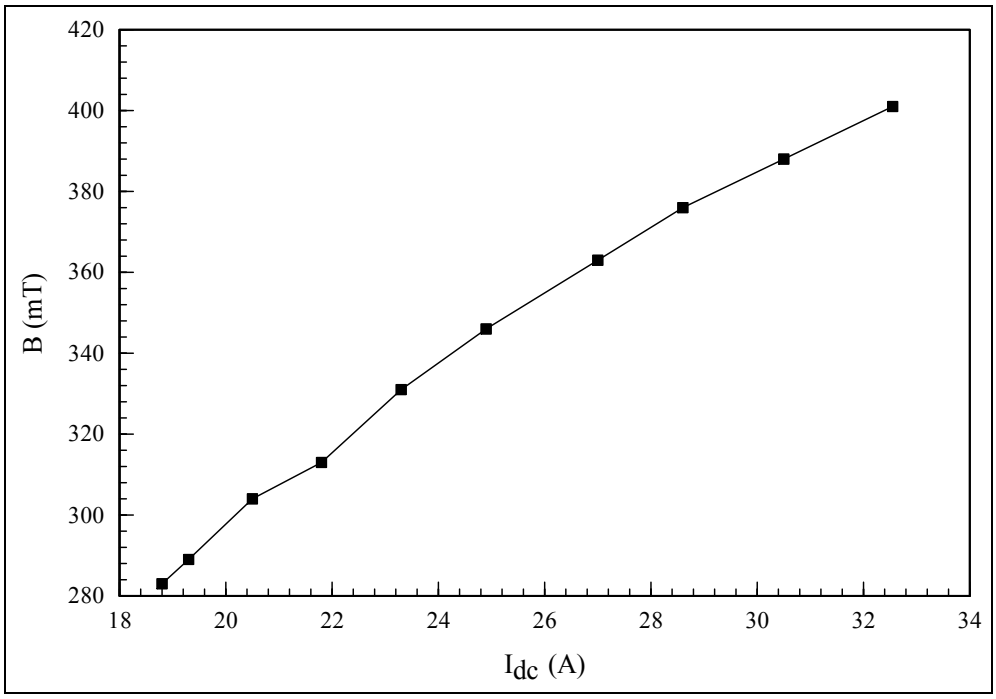

Figure 7.45. Magnetic field change with respect to the applied current when the displacement between the coils is set to be constant at 4 cm

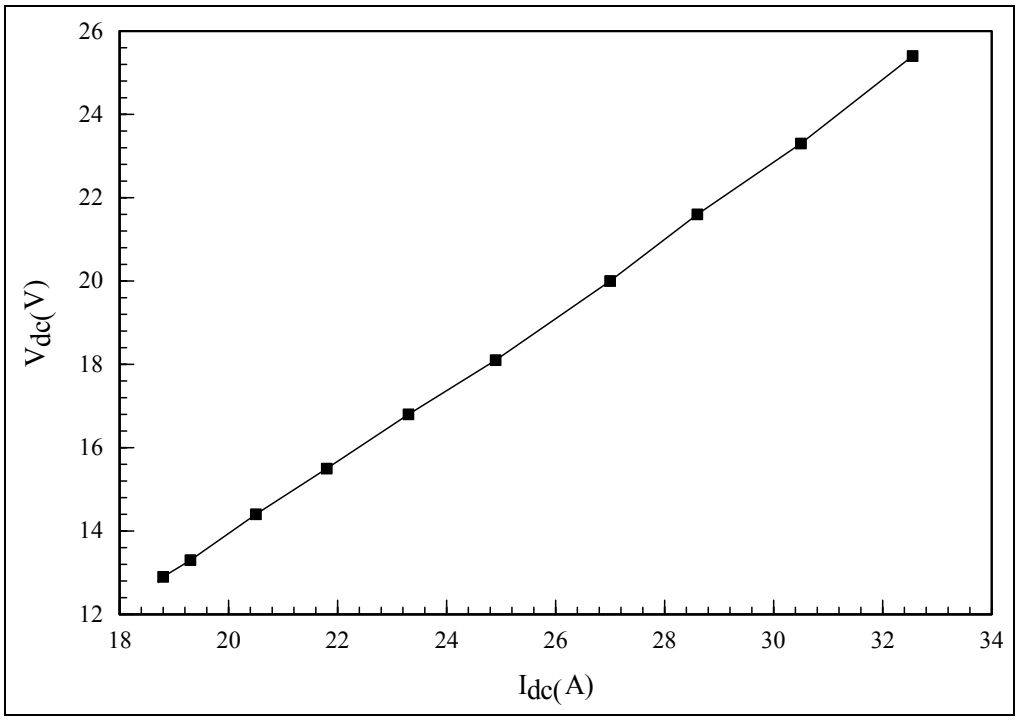

Figure 7.46. Voltage drop between two ends of the coils versus current (two coils were connected in series)

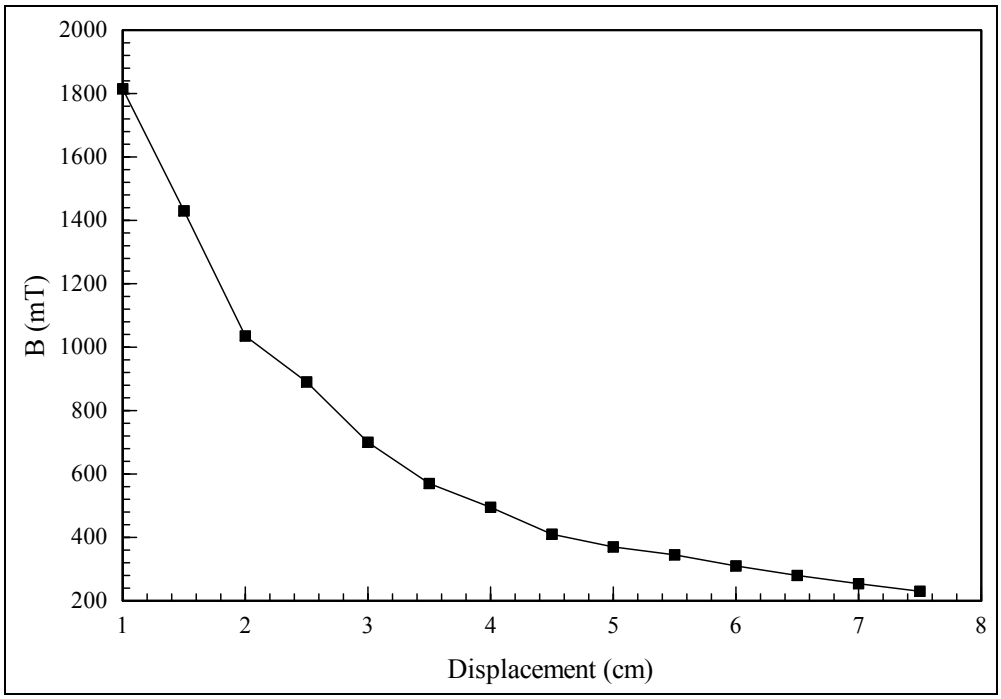

Figure 7.47. Magnetic field strength change versus the displacement of coils when the current was set to be constant at 35 A_{DC}

In this experiment only the magnetic field effect on reflection was studied by using the experimental setup given in Figure 7.48. Different magnetic fields were applied to GaInSn alloy. At the same time the light from halogen lamp was sent on the surface of it. The reflected light was detected by using two different detectors which were luxmeter and UV-Vis spectrometer.

During the experiments the light source was directed to GaInSn surface with 45° above the horizontal. In the first part of the experiment luxmeter's direction was changed from 20° to 90° above the horizontal. The luxmeter direction was changed by 5°. After the angle of luxmeter was arranged the reflectance was measured in two different cases. In the first case the magnetic field is applied and the reflectance was measured. In second case the magnetic field is turned off and again the reflectance was measured. Externally applied magnetic field strenghts were $202\,mT$, $304\,mT$, $406\,mT$, $500\,mT$, and $600\,mT$. The results for this procedure were given between Figure 7.49-7.53.

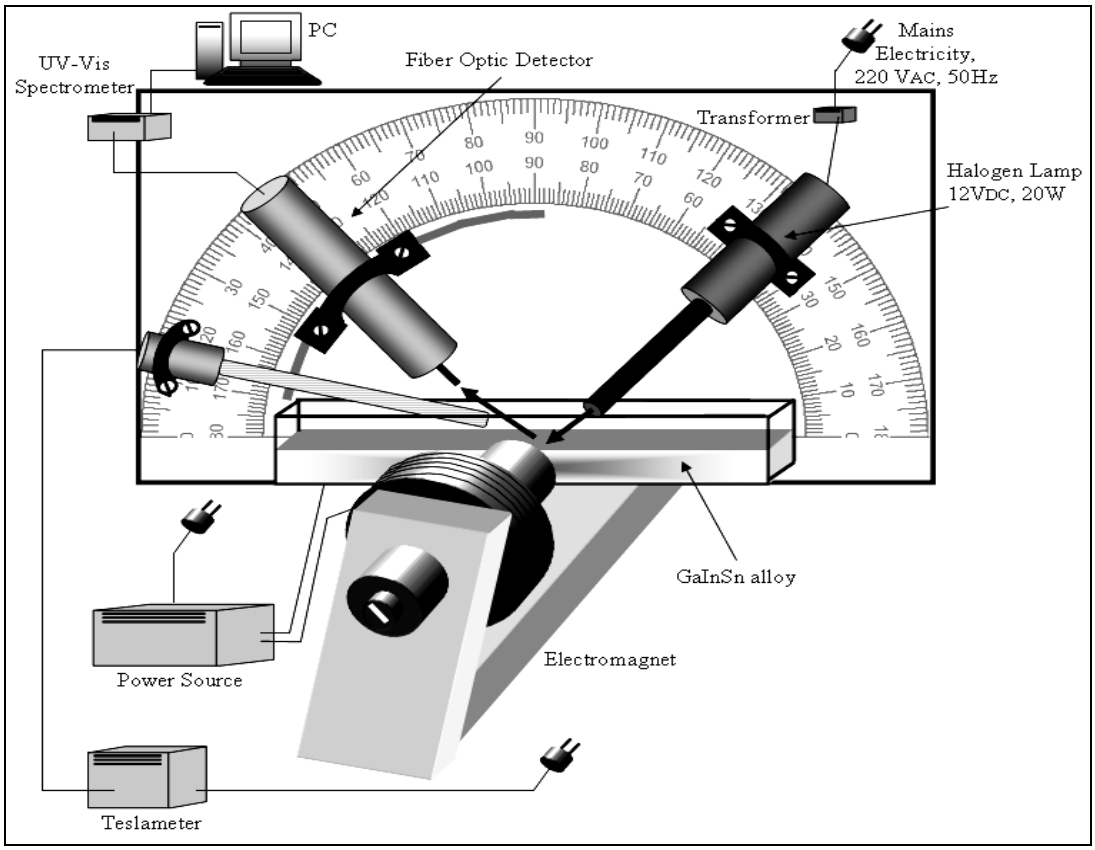

Figure 7.48. Experimental set up for studying magnetic field effect

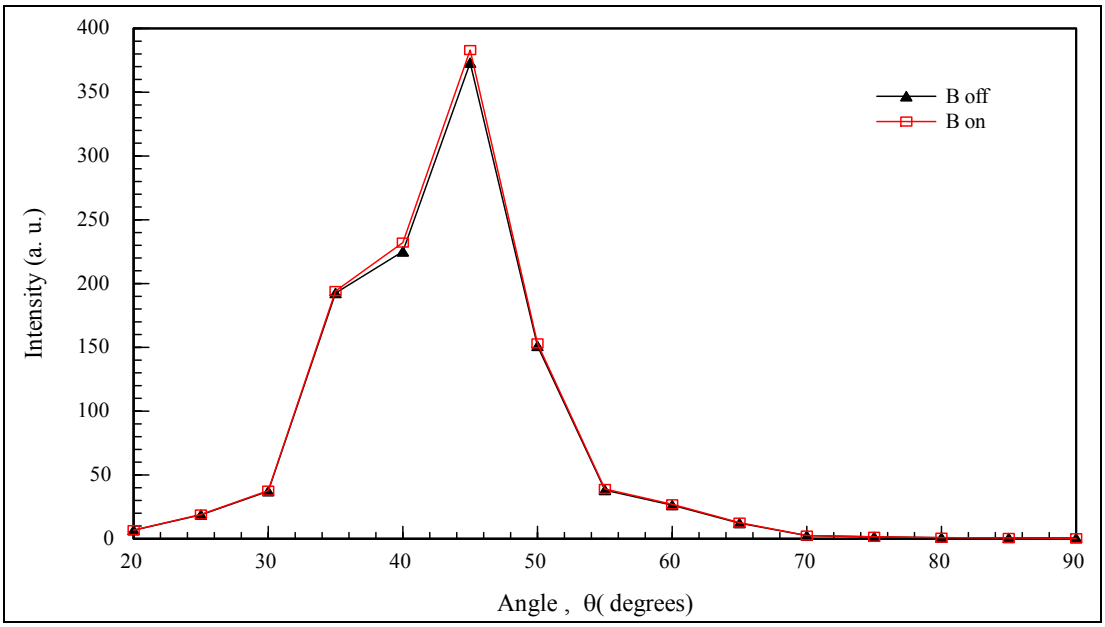

Figure 7.49. The intensity versus angle of detector graph for magnetic field with the value of $B^{ext} = 202\ mT$

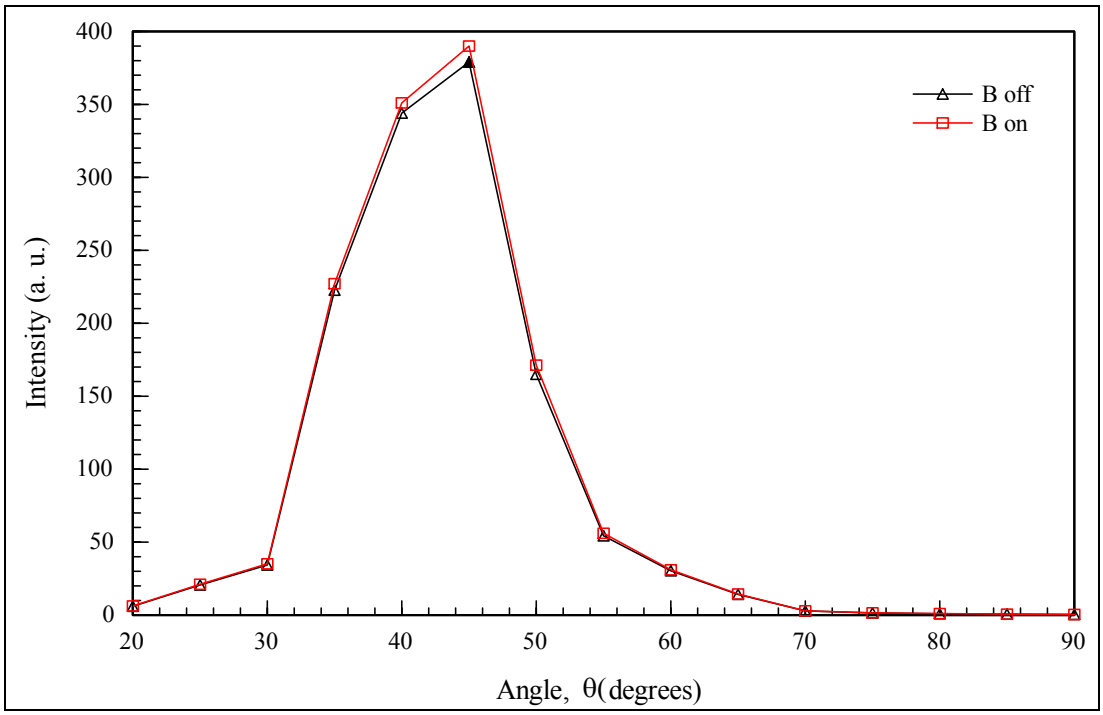

Figure 7.50. The intensity versus angle of detector graph for magnetic field with the value of $B^{ext} = 304\ mT$

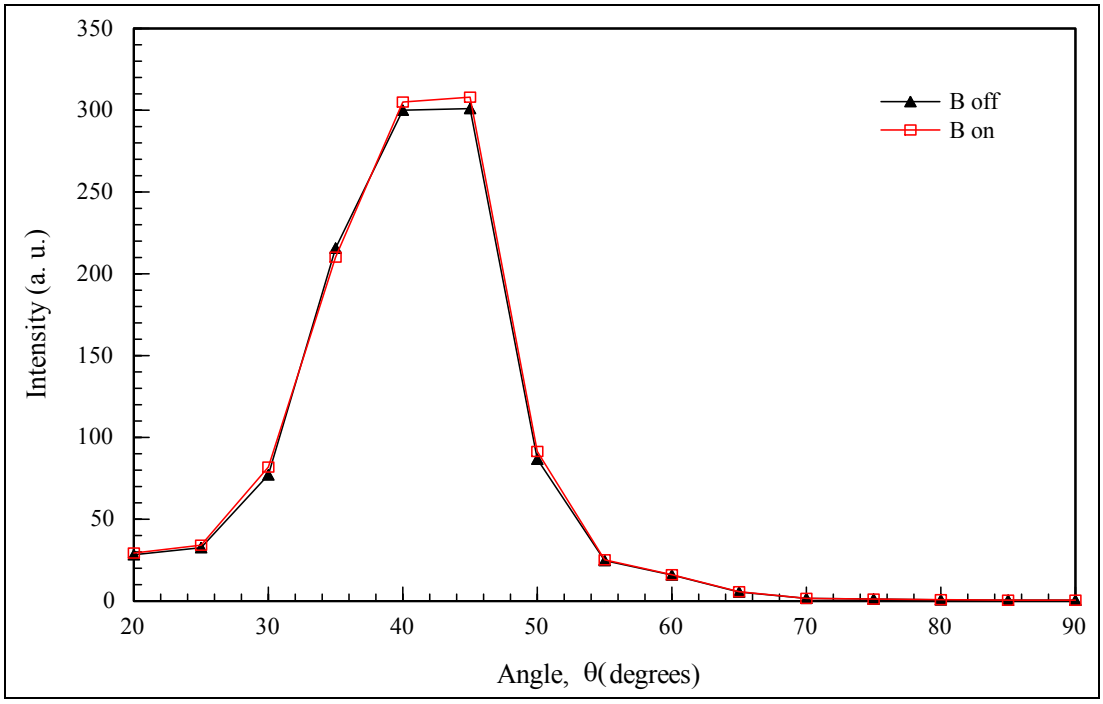

Figure 7.51. The intensity versus angle of detector graph for magnetic field with the value of $B^{ext} = 406\ mT$

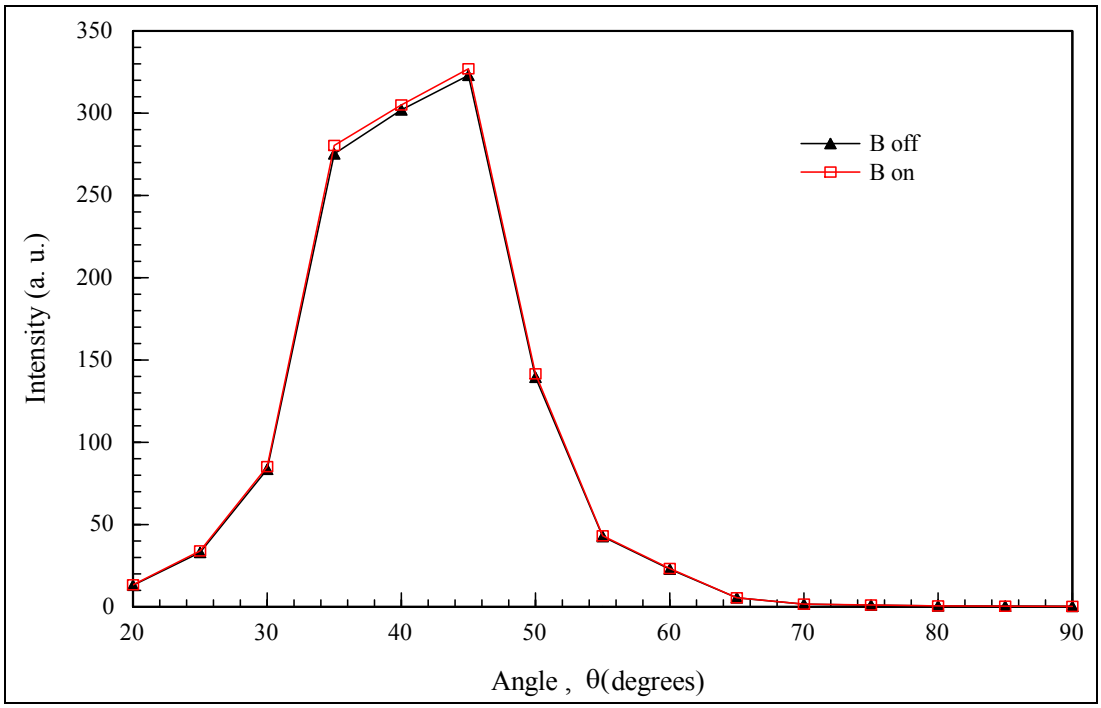

Figure 7.52. The intensity versus angle of detector graph for magnetic field with the value of $B^{ext} = 500\ mT$

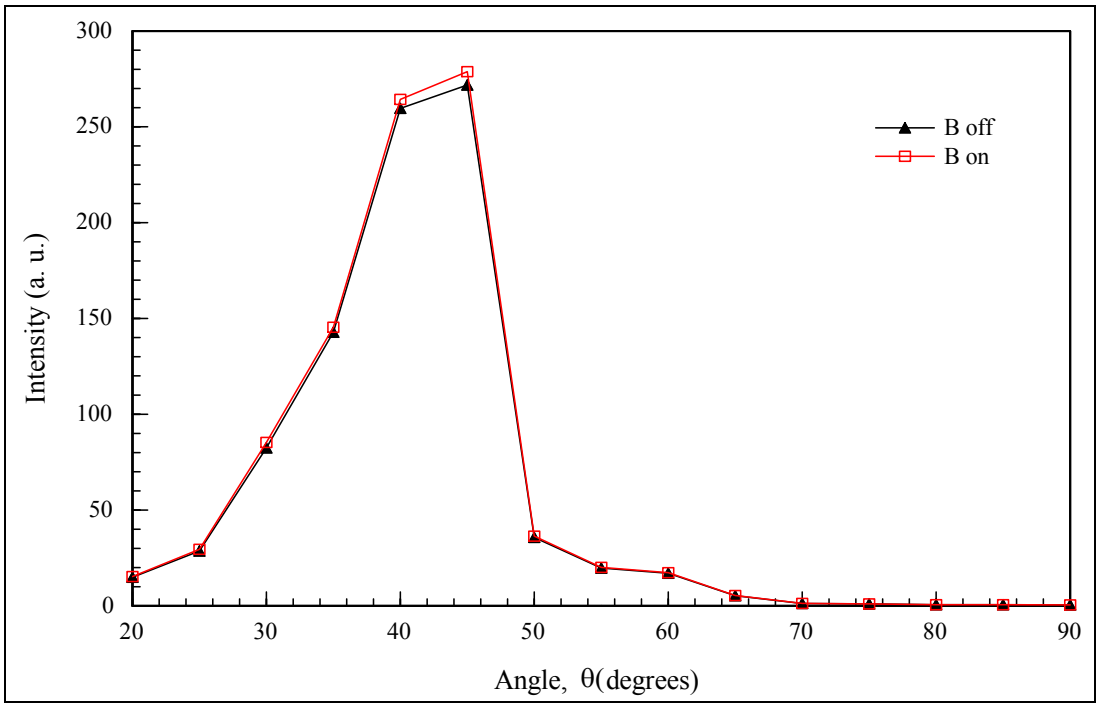

Figure 7.53. The intensity versus angle of detector graph for magnetic field with the value of $B^{ext} = 600\ mT$

The reflection results before and after an external magnetic field is applied were found similar to each other. In order to see how they differ from each other $Bon/Boff$ ratio versus angle graphs were drawn as a function of angle for each externally applied magnetic field used in previous experiment.

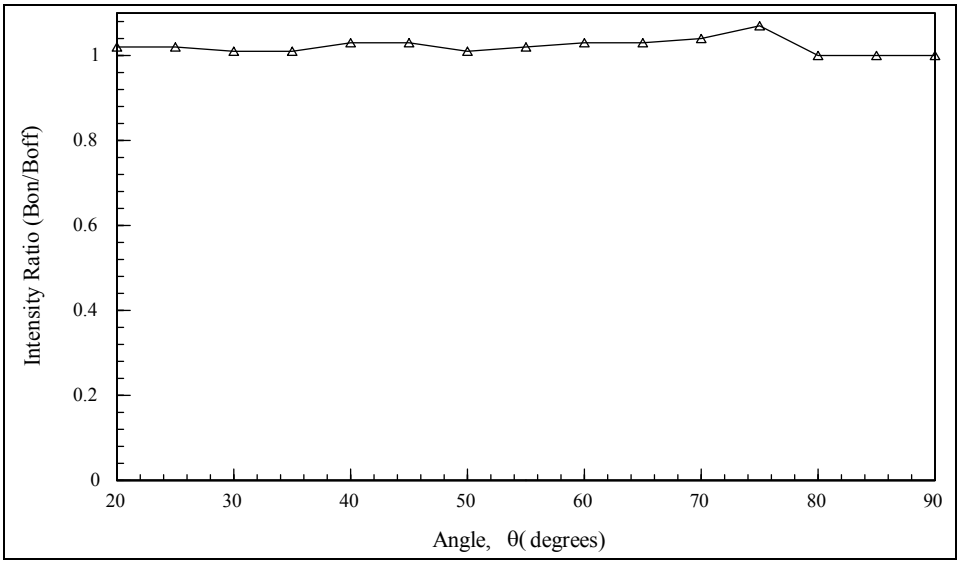

Figure 7.54. The intensity ratio $B^{ext}{}_{on}/B^{ext}{}_{off}$ for $B^{ext} = 202\ mT$ versus angle of detector graph

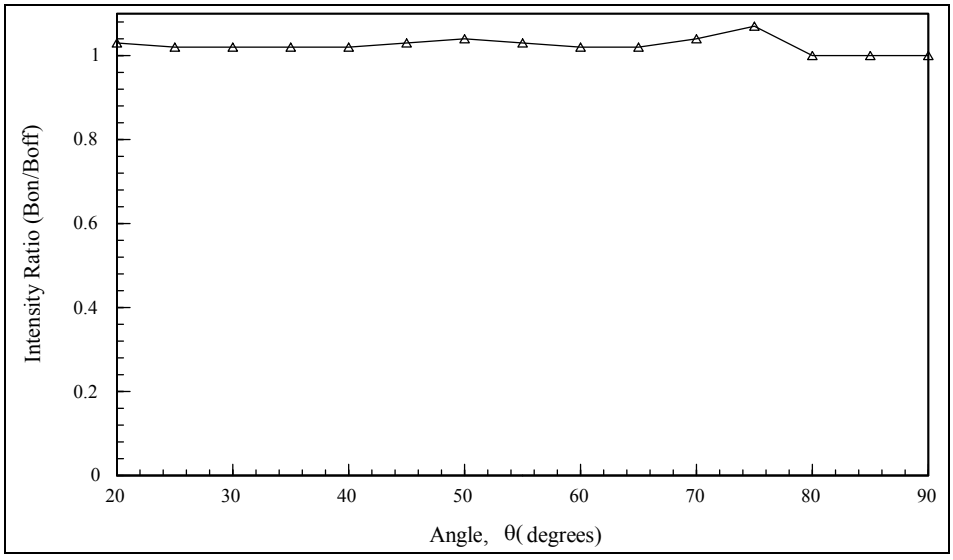

Figure 7.55. The intensity ratio $B^{ext}{}_{on}/B^{ext}{}_{off}$ for $B^{ext} = 304\ mT$ versus angle of detector graph

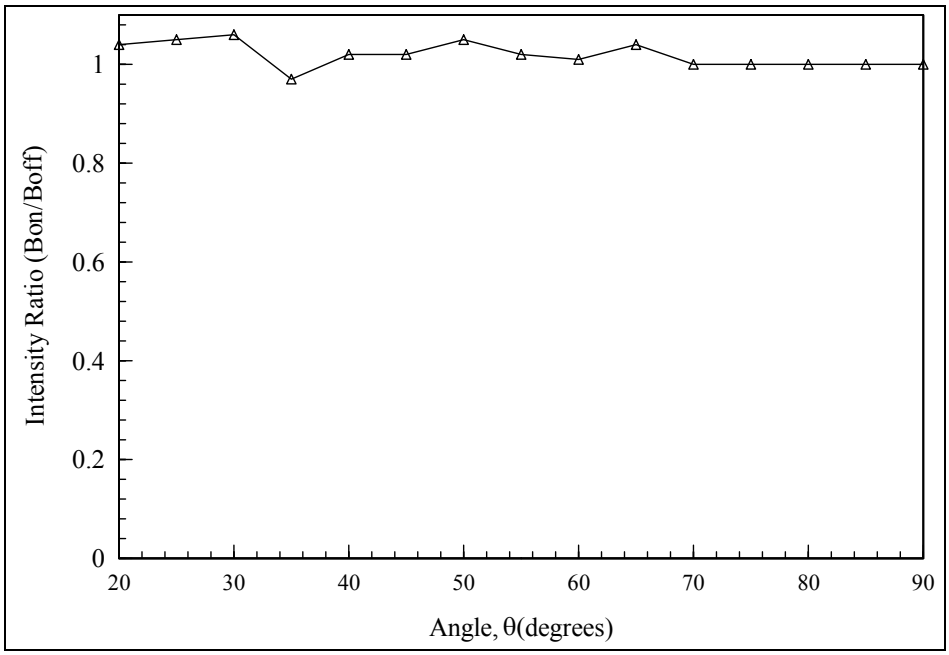

Figure 7.56. The intensity ratio $B^{ext}{}_{on} / B^{ext}{}_{off}$ for $B^{ext} = 406\, mT$ versus angle of detector graph

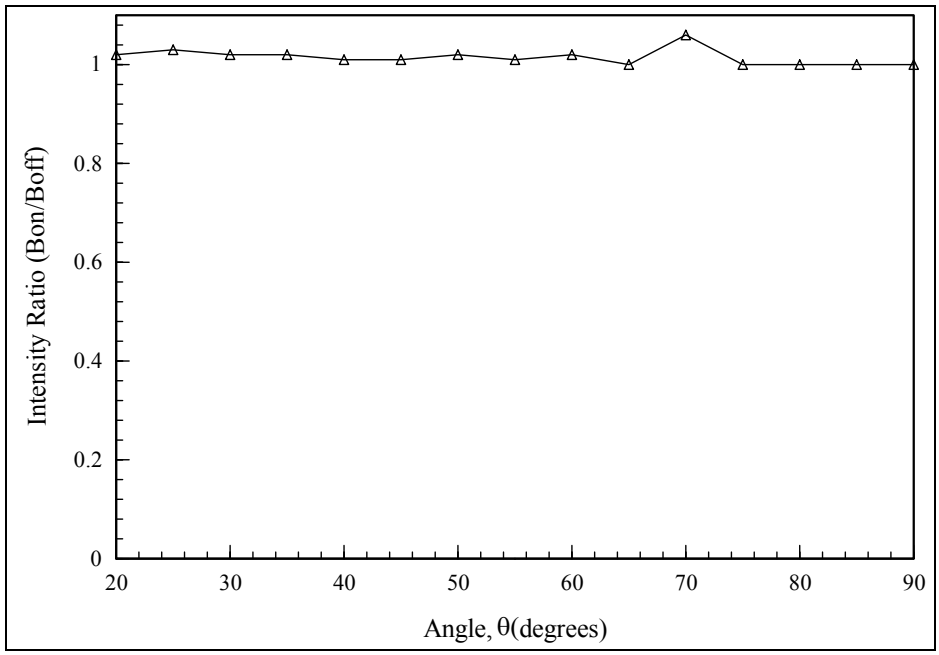

Figure 7.57. The intensity ratio $B^{ext}{}_{on} / B^{ext}{}_{off}$ for $B^{ext} = 500\, mT$ versus angle of detector graph

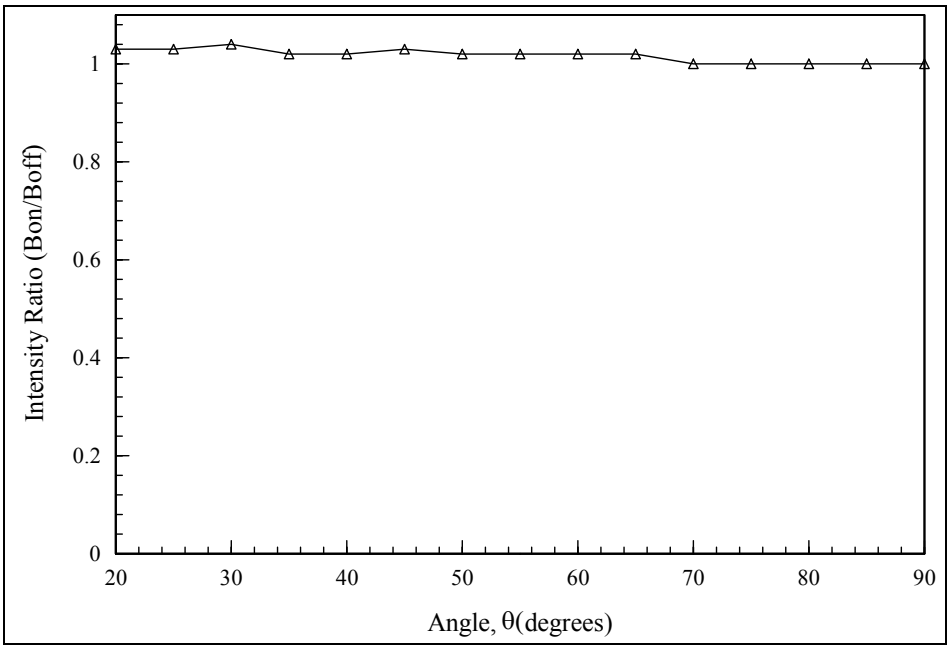

Figure 7.58. The intensity ratio $B^{ext}{}_{on} / B^{ext}{}_{off}$ for $B^{ext} = 600\ mT$ versus angle of detector graph

After the last five graphs are drawn it is seen that the effect of magnetic field is very less and maximum difference for these data is about 6 per cent in favour of *Bon* which means that magnetic field is turned on.

The same experiment was repeated by using UV-Vis detector. The difference in this experiment from the previous one is that the UV-Vis angle was also kept constant at 45° with the horizontal. The intensities of reflected light were taken versus wavelength.

Since in the previous experiment it was seen that the reflectance from GaInSn alloy surface was not so much affected by the externally applied DC magnetic field in this experiment the same was tested and the data were collected by using UV-Vis spectrometer.

After the intensities of reflected light were taken as a function of wavelength the intensity ratio fluctuation were also checked. The intensity ratio versus wavelength graph were also drawn below.

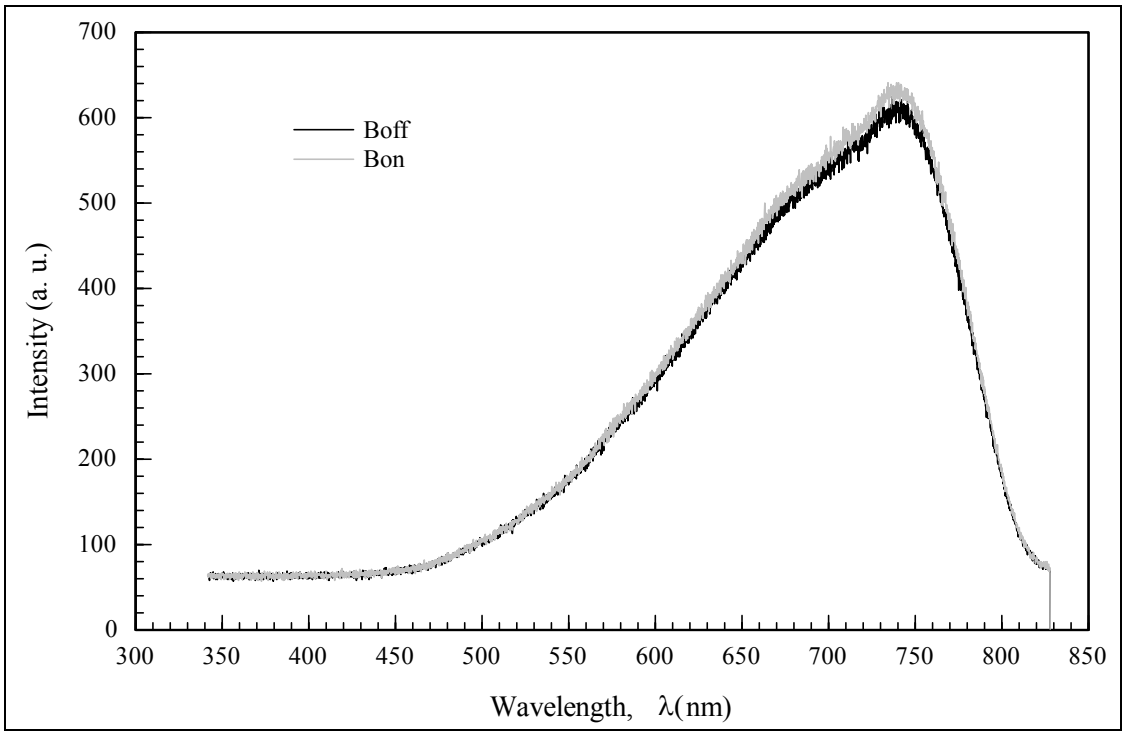

Figure 7.59. The intensity versus wavelength graph for magnetic field with the value of $B^{ext} = 200\ mT$

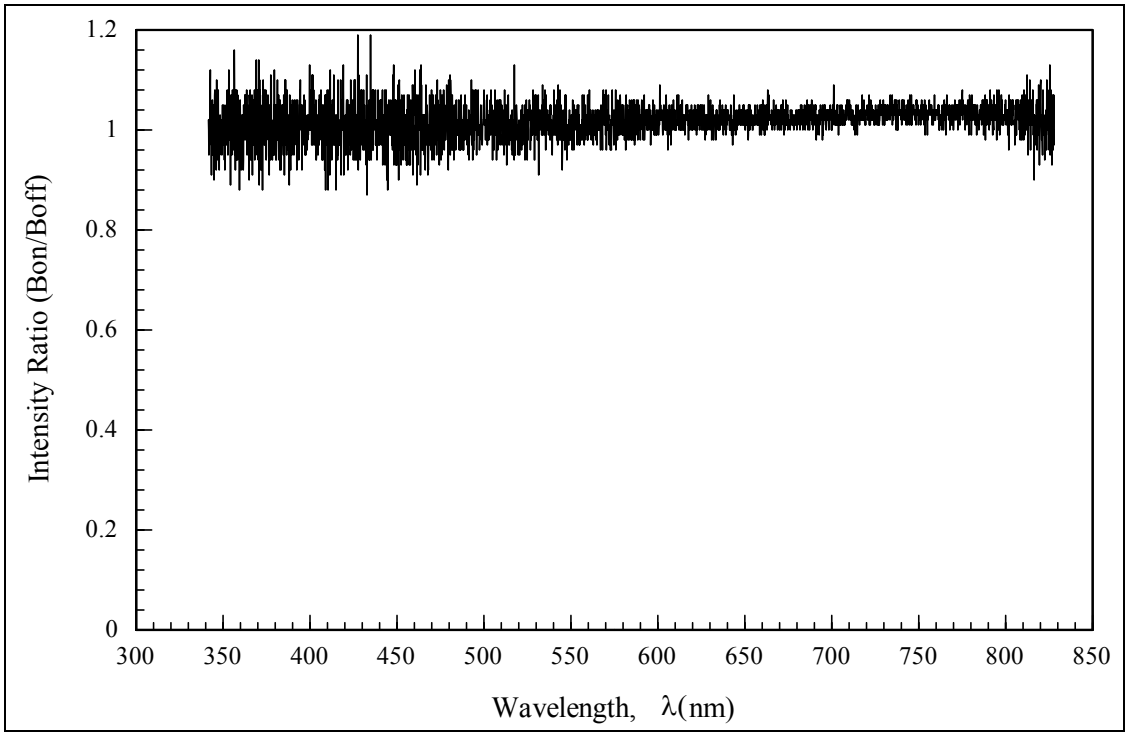

Figure 7.60. The intensity ratio $B^{ext}{}_{on} / B^{ext}{}_{off}$ for $B^{ext} = 200\ mT$ versus wavelength graph

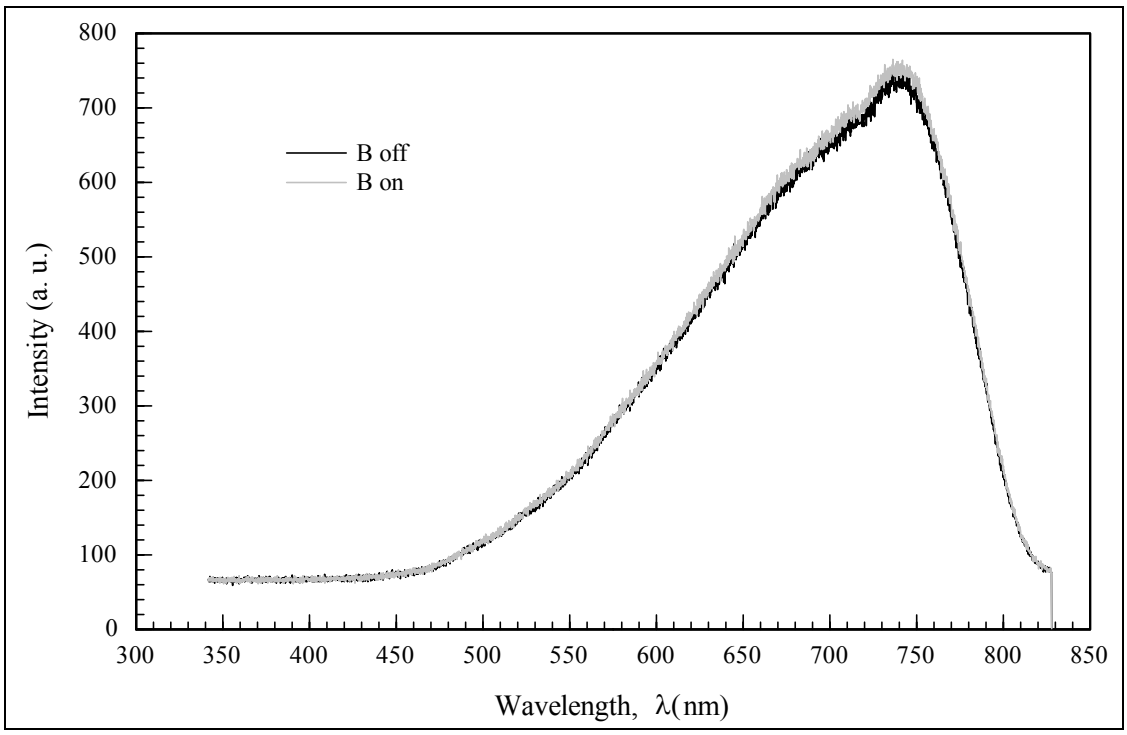

Figure 7.61. The intensity versus wavelength graph for magnetic field with the value of $B^{ext} = 300\ mT$

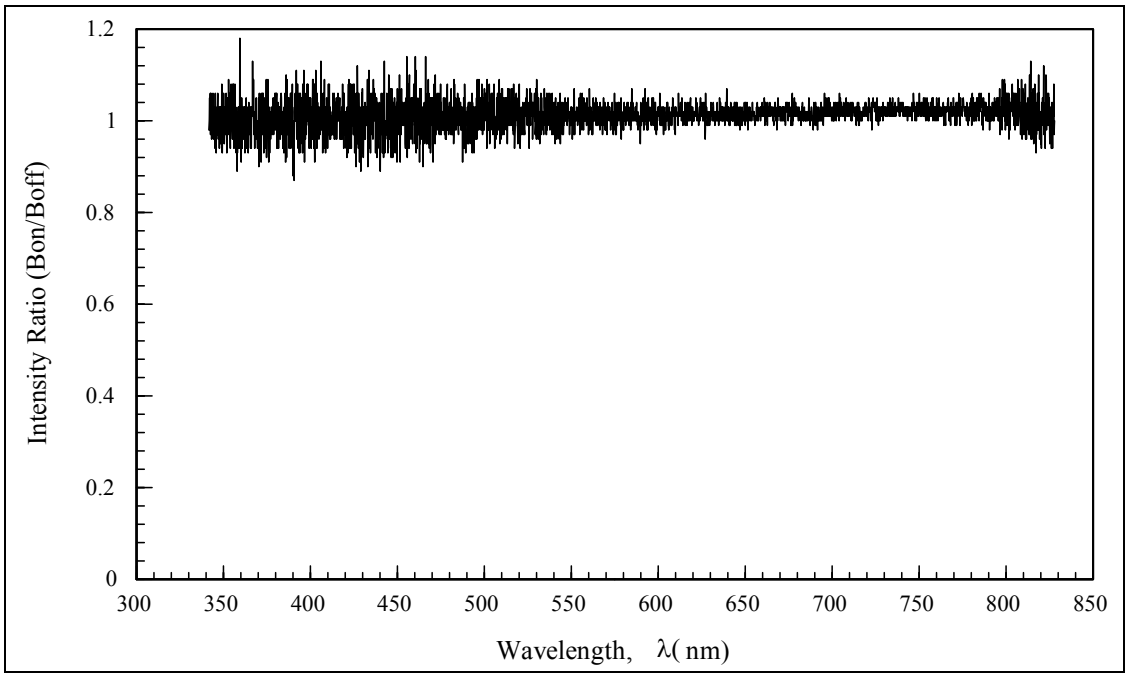

Figure 7.62. The intensity ratio $B^{ext}{}_{on} / B^{ext}{}_{off}$ for $B^{ext} = 300\ mT$ versus wavelength graph

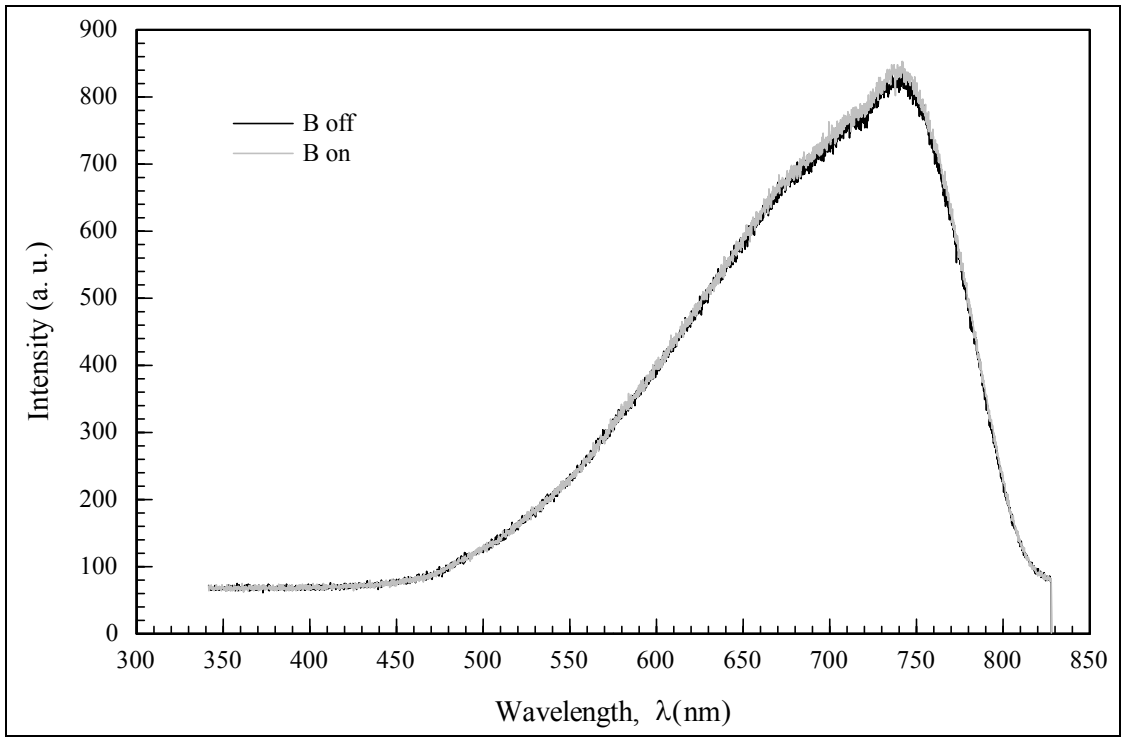

Figure 7.63. The intensity versus wavelength graph for magnetic field with the value of $B^{ext} = 400\ mT$

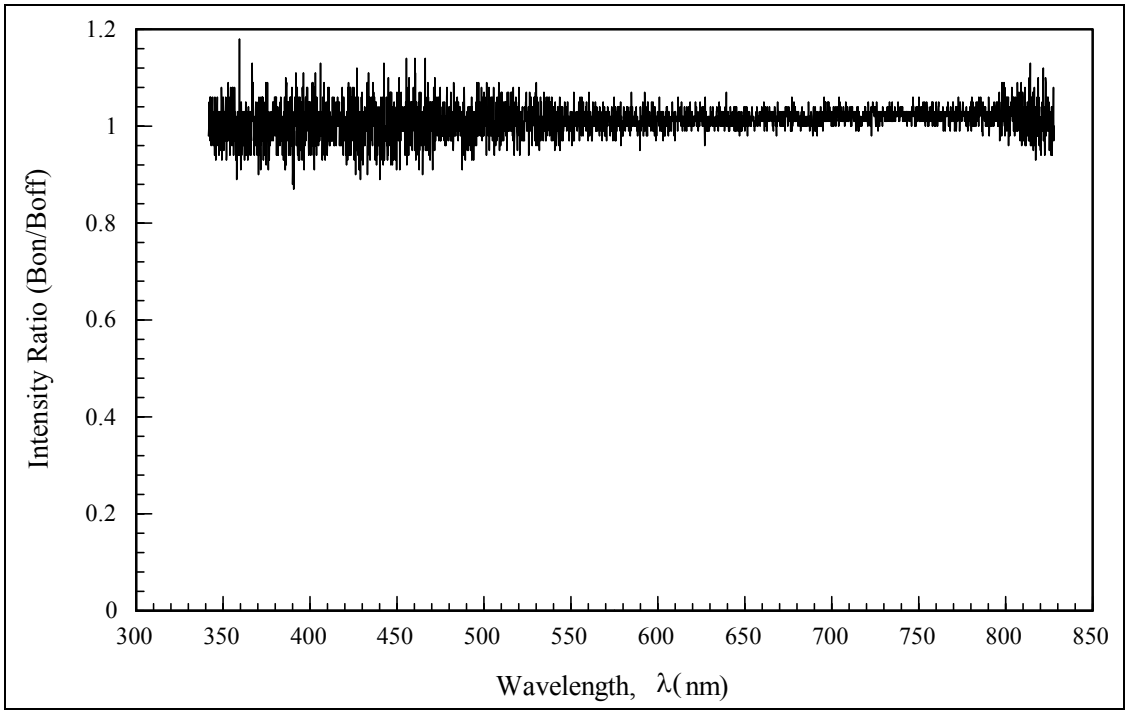

Figure 7.64. The intensity ratio $B^{ext}{}_{on} / B^{ext}{}_{off}$ for $B^{ext} = 400\ mT$ versus wavelength graph

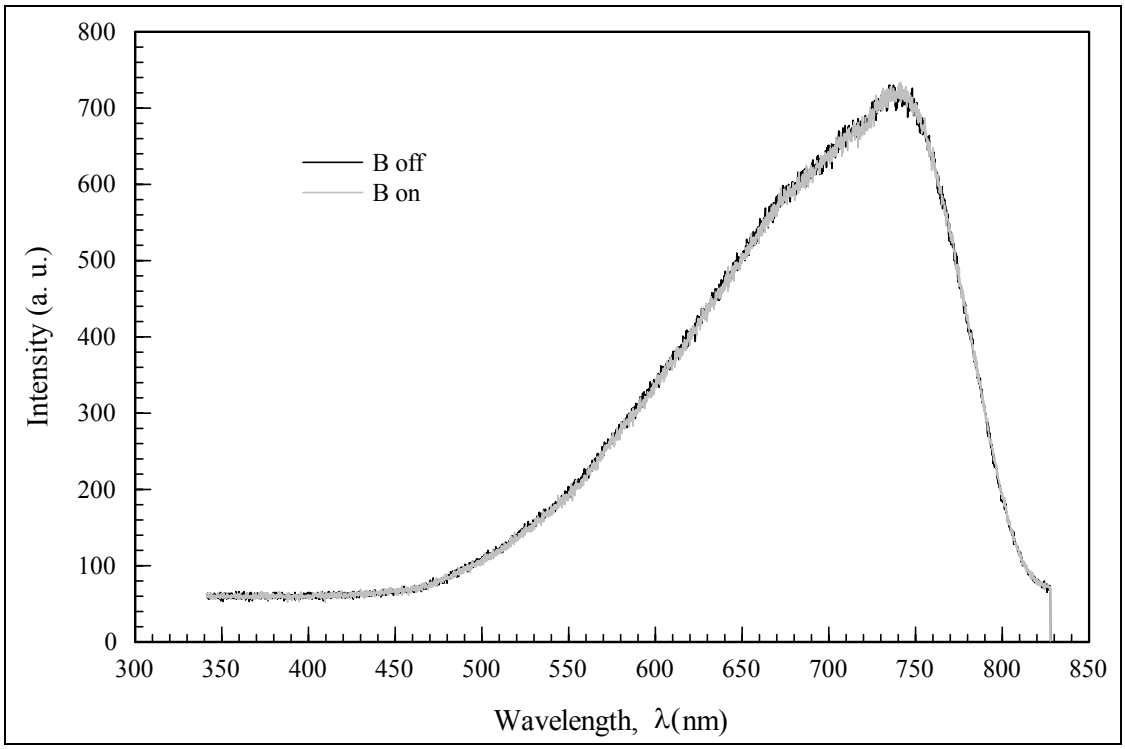

Figure 7.65. The intensity versus wavelength graph for magnetic field with the value of $B^{ext} = 500\ mT$

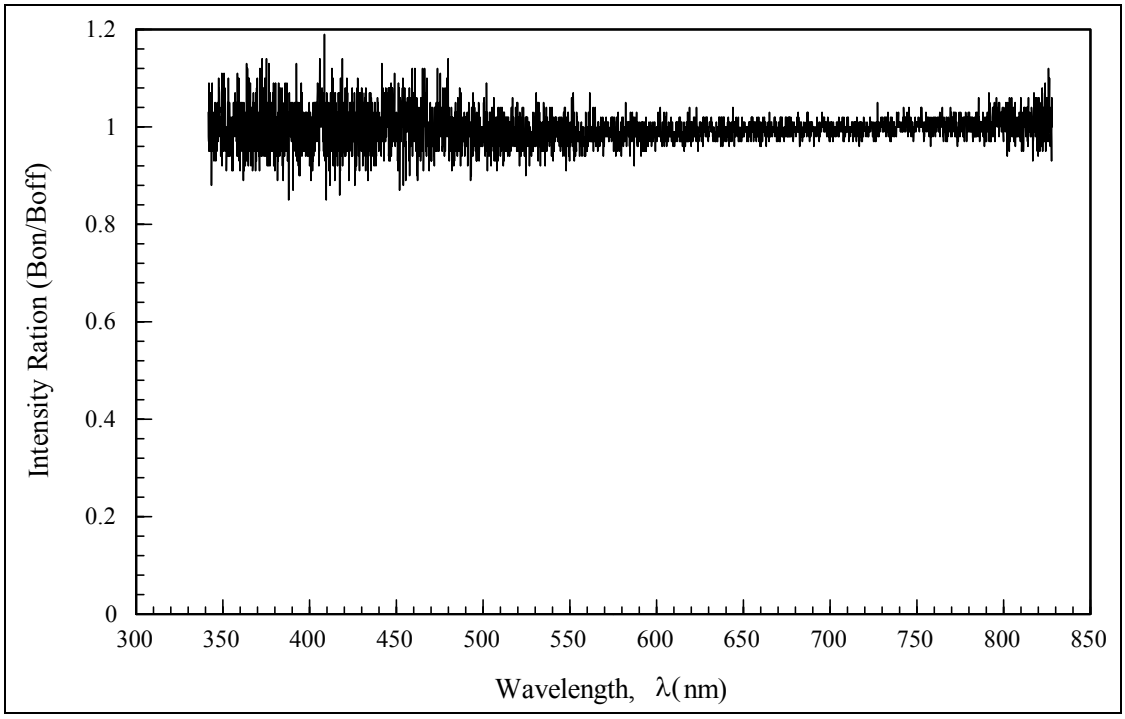

Figure 7.66. The intensity ratio $B^{ext}{}_{on} / B^{ext}{}_{off}$ for $B^{ext} = 500\ mT$ versus wavelength graph

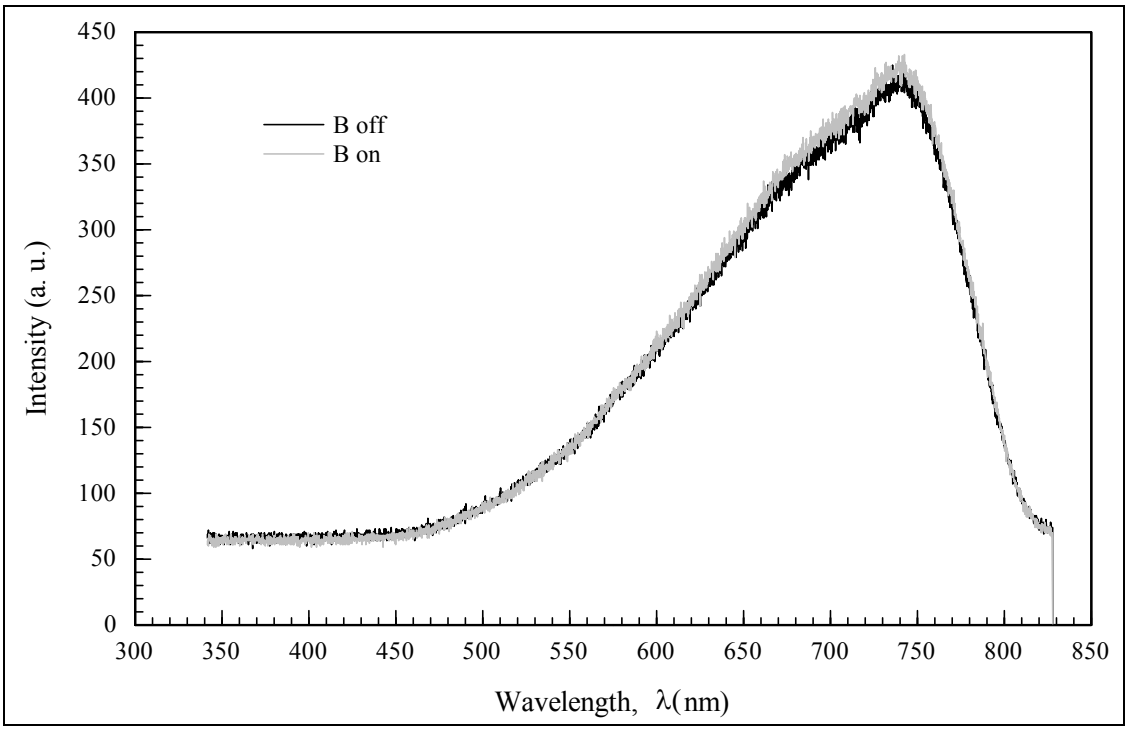

Figure 7.67. The intensity versus wavelength graph for magnetic field with the value of $B^{ext} = 600\ mT$

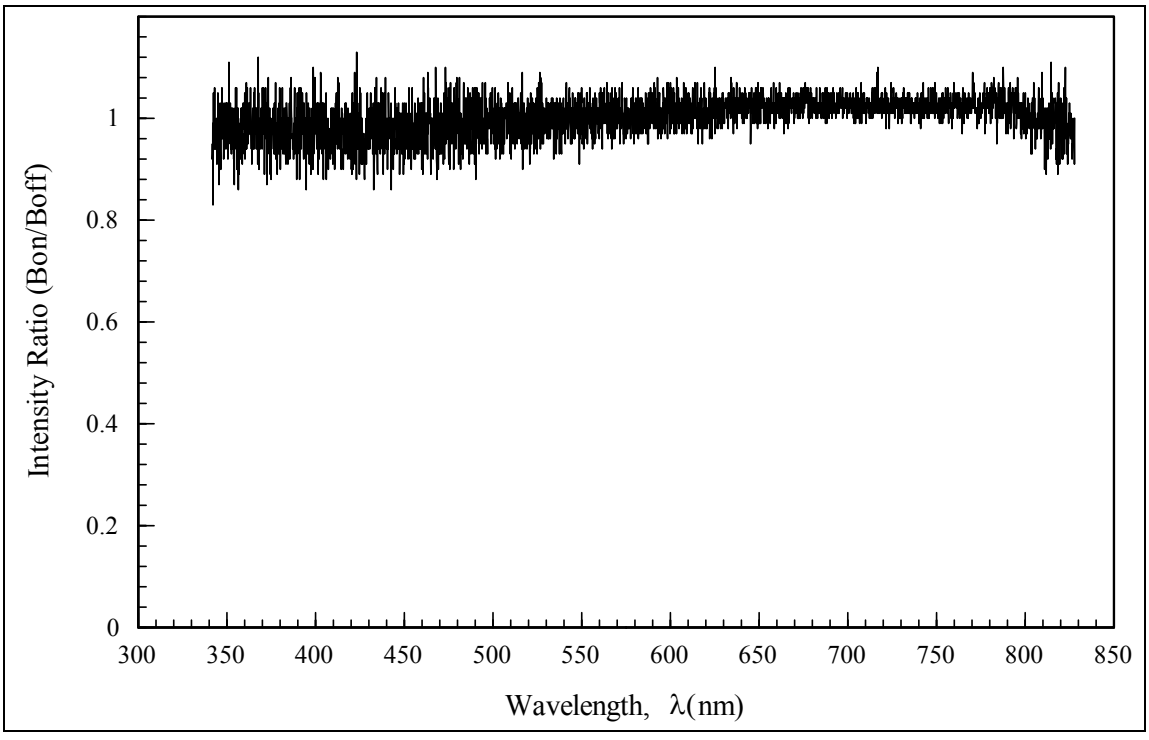

Figure 7.68. The intensity ratio $B^{ext}{}_{on} / B^{ext}{}_{off}$ for $B^{ext} = 600\ mT$ versus wavelength graph

When the light interacts with matter either reflection or absorption or both can happen. The effect of stationary magnetic field on the reflectance from GaInSn alloy surface was studied and there wasn't seen a very significant change but some fluctuations were found especially for small wavelengths.

In contrary to the stationary magnetic fields the alternating magnetic fields affect the surface of liqiuid metals. In [63] three different kinds of instabilities were observed. They were long-wavelength instability which is producing the deformation on the surface of alloy, surface waves instability and electromagnetic pinch which is developing a pinch channel inside the alloy.

Actually high frequency electromagnetic fields can be used to reduce the convective heat losses within melts [64]. However, in this thesis both the electric current and magnetic field used were stationary (DC) but their strengths were changed externally. If there was a propagation direction for fluid and the magnetic field was applied parallel to it there could be the damping effect for waves on surface. The perpedicularly applied magnetic field does not have this effect [65].

7.4.6.4 Dependence on Both Magnetic Field and Current Applied Together

As was seen in the experiments done previously the current was strongly affecting the measured reflectance intensity from the surface of GaInSn. However, the stationary magnetic field effect was not so much significant. In this part of the experiment both current (DC) and magnetic field (DC) were applied through the GaInSn alloy. The externally applied current and magnetic field were applied perpendicularly to each other. The experimental setup is also given in Figure 7.69. Figure 7.70 gives the photograph for the same experimental setup. There were two different cases as shown in Figure 7.71 and Figure 7.72. In this experiment the current value was kept constant at $20A$. The externally applied magnetic fields were $200mT, 300mT, 400mT, 500mT,$ and $600mT$. The light source was again halogen lamp, the detector was UV-Vis spectrometer, magnetic field was measured with the same teslameter used in previous experiments.

In this experiment due to the effects of current and magnetic field Lorentz force will be induced. Actually the induced Lorentz force can excite the waves on the surface. These

waves are dependent on current frequencies for low current values. For high currents the frequency dependence is negligible and nearly stationary waves can be formed on the surface of an alloy [62]. However, in this experiment the current was constant in value ($20A$) and it was DC. Induced Lorentz force will affect the charged particles inside the GaInSn alloy. The movement of electrons will be dominated by this force. The moving electrons will be accumulated in different places inside the chamber carrying GaInSn alloy. This accumulation and movement of electrons will affect also the reflectance from the surface of an alloy. The reflectance spectra for case I and case II are given below from Figure 7. 73 to Figurer 7.77.

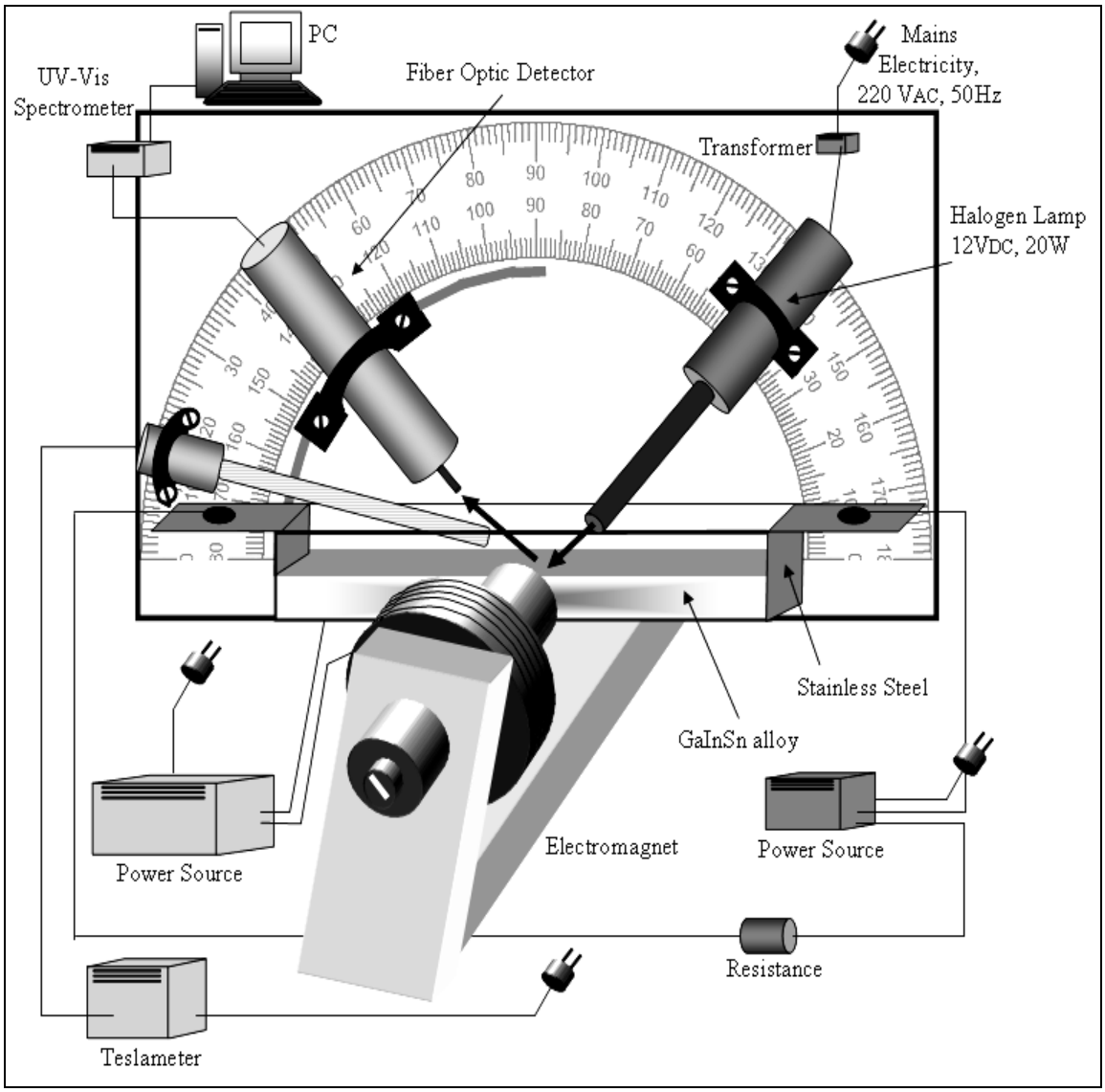

Figure 7.69. Experimental set up for studying Lorentz force effect

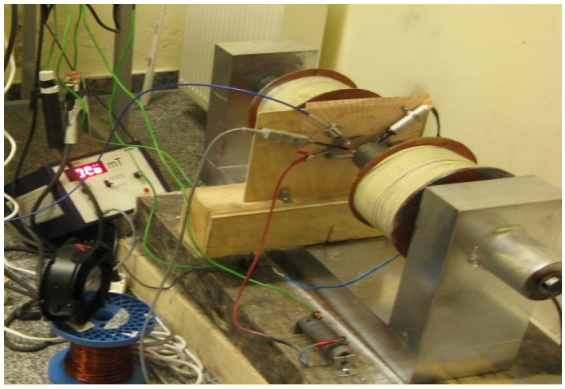

Figure 7.70. Photograph of experimental set up for studying Lorentz force effect

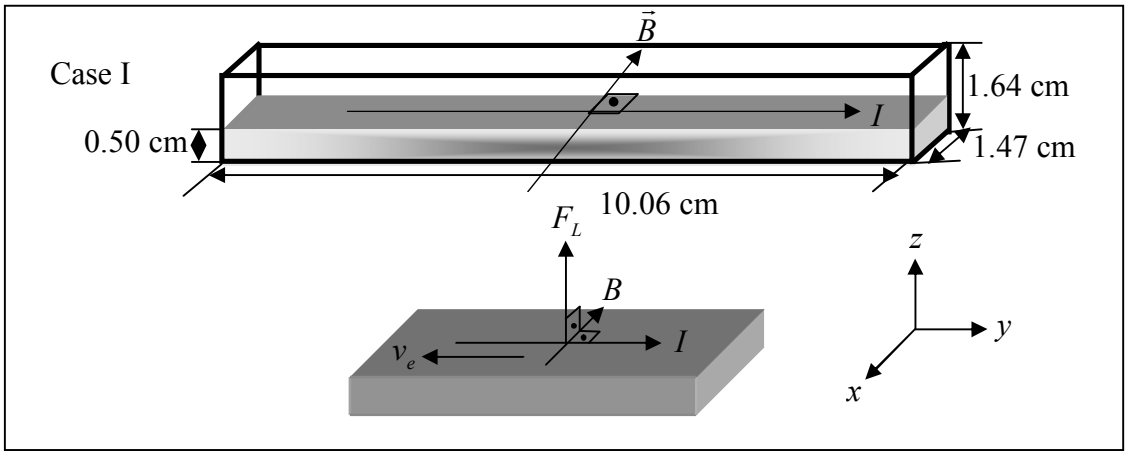

Figure 7.71. The scheme for externally applied magnetic field and current together with the direction of induced Lorentz force and electrons' velocity (case I)

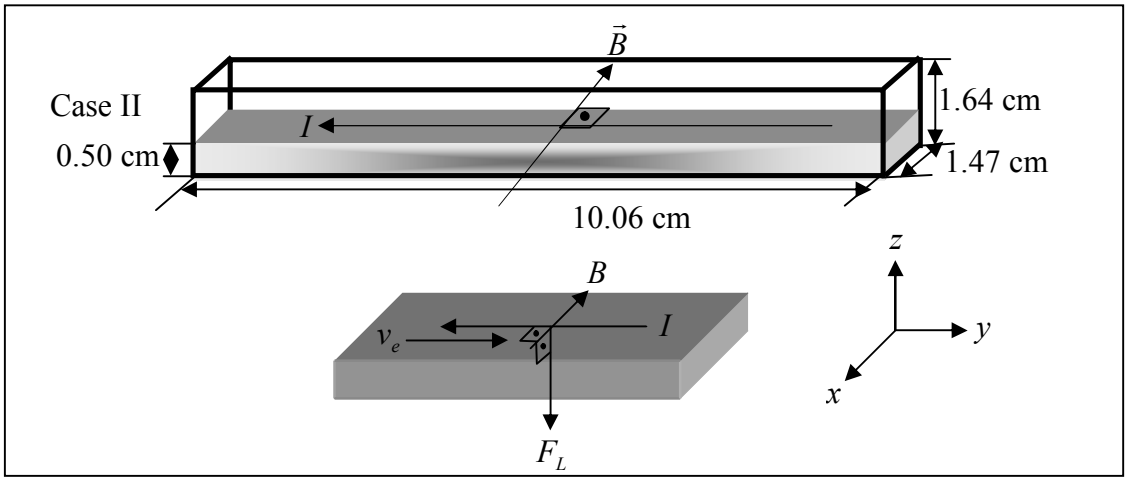

Figure 7.72. The scheme for externally applied magnetic field and current together with the direction of induced Lorentz force and electrons' velocity (case II)

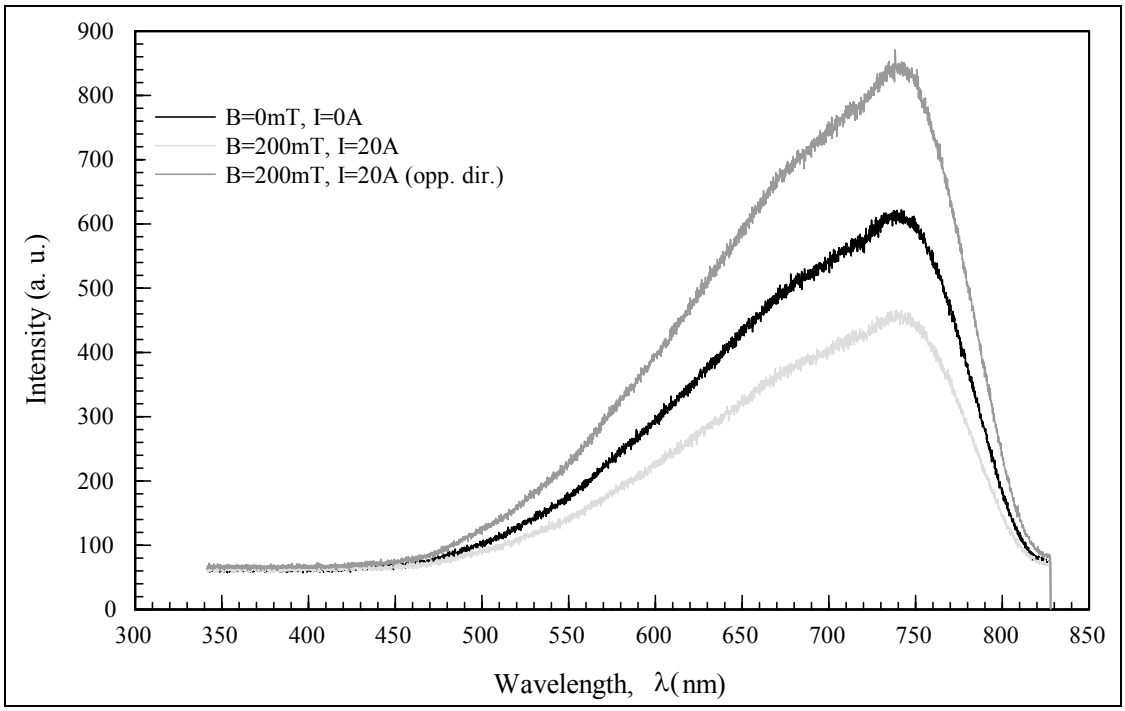

Figure 7.73. The reflectance versus wavelength graph for $B^{ext} = 200\,mT$ magnetic field and $20A$ current

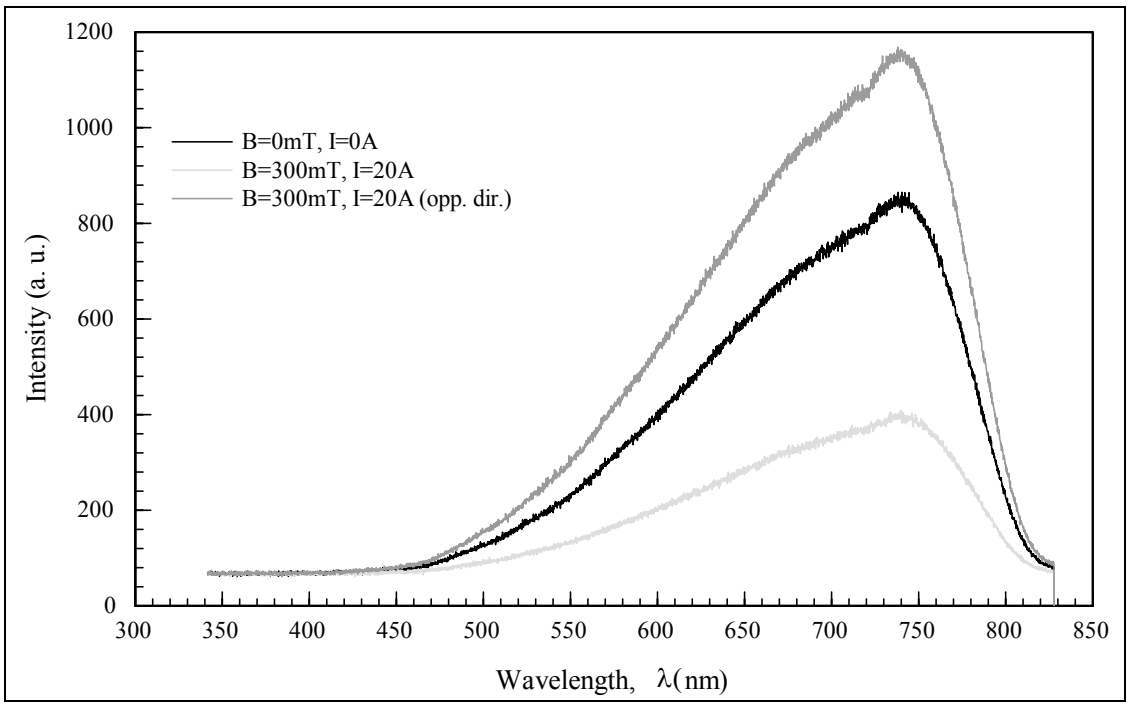

Figure 7.74. The reflectance versus wavelength graph for $B^{ext} = 300\,mT$ magnetic field and $20A$ current

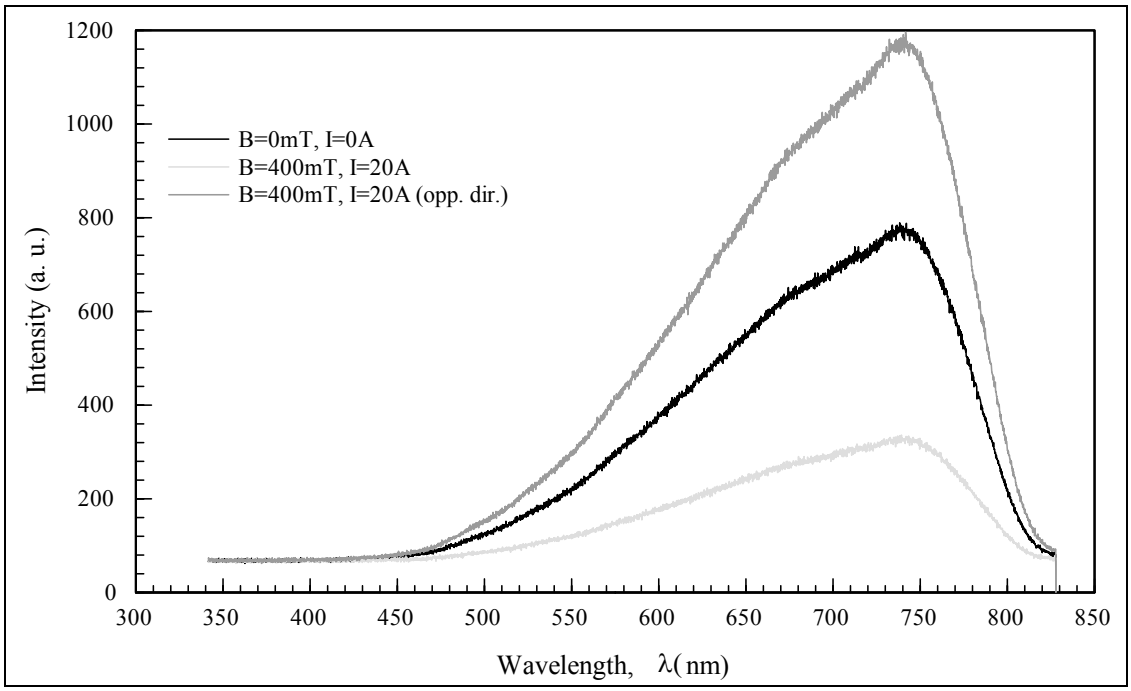

Figure 7.75. The reflectance versus wavelength graph for $B^{ext} = 400\,mT$ magnetic field and $20A$ current

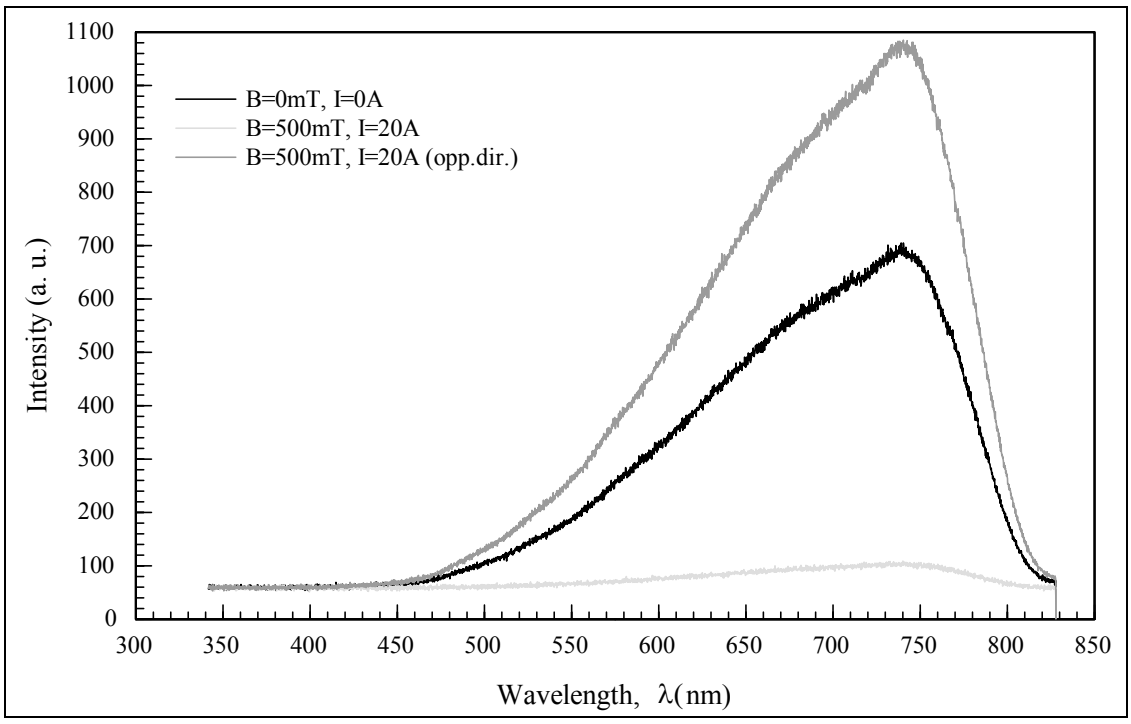

Figure 7.76.The reflectance versus wavelength graph for $B^{ext} = 500\,mT$ magnetic field and $20A$ current

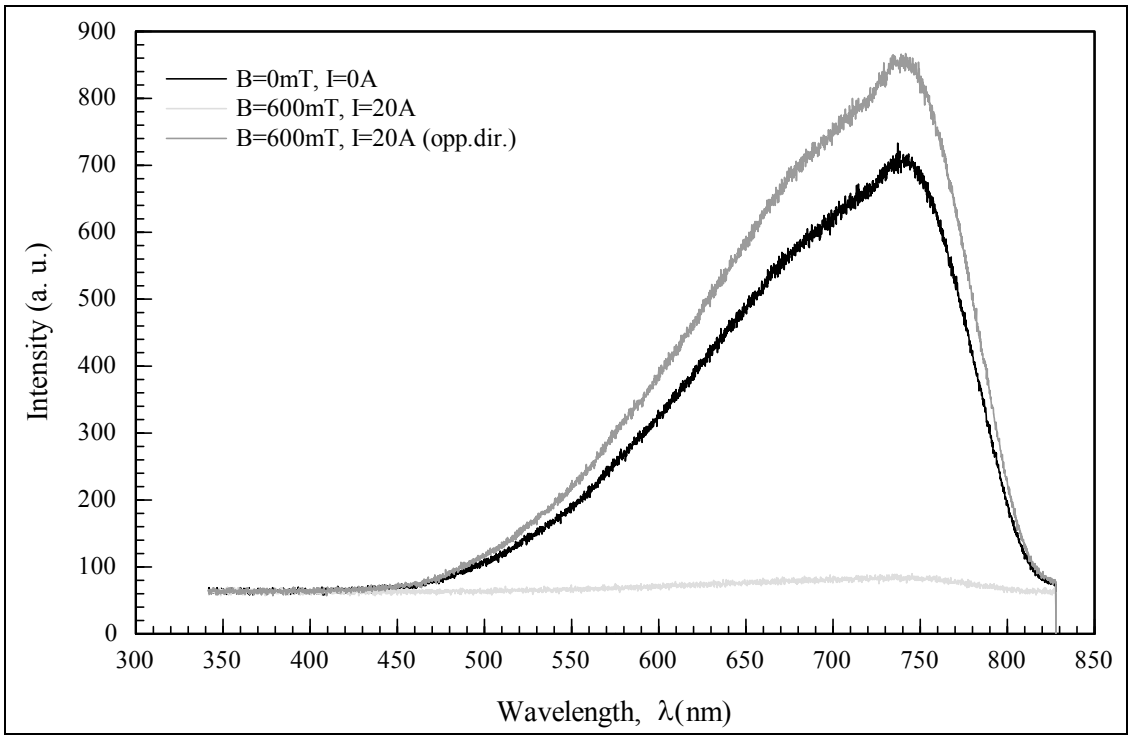

Figure 7.77. The reflectance versus wavelength graph for $B^{ext} = 600\ mT$ magnetic field and $20A$ current

As it is seen from the figures above there are three different spectra. Two of them represents case I and case II. The third spectrum was taken when the current and magnetic field were not applied. This spectrum is given as $B = 0mT, I = 0A$ at the legends of the graphs. In the figures above there is an expression given as 'opp. dir.' which means opposite direction and represents the current application direction given in case II.

Since the magnetic field change is strictly related to the geometry of the electromagnet it would be meaningful to normalize these data as given below. The geometry of electromagnet affects the measured intensities strongly. As an example when the magnetic field strength is wanted to be increased then the coils of electromagnet must be moved near each other and this can have an additional and significant effect. The light which is scattered from GaInSn surface can be reflected again from the coils which are placed near each other and this will change the data taken from the detector. However, for every different magnetic field the geometry is kept unchanged and the effect for three

spectra taken will be the same in amount. Therefore the rational change of reflectance can be more meaningful. The normalization is done in order to eliminate this additional effect.

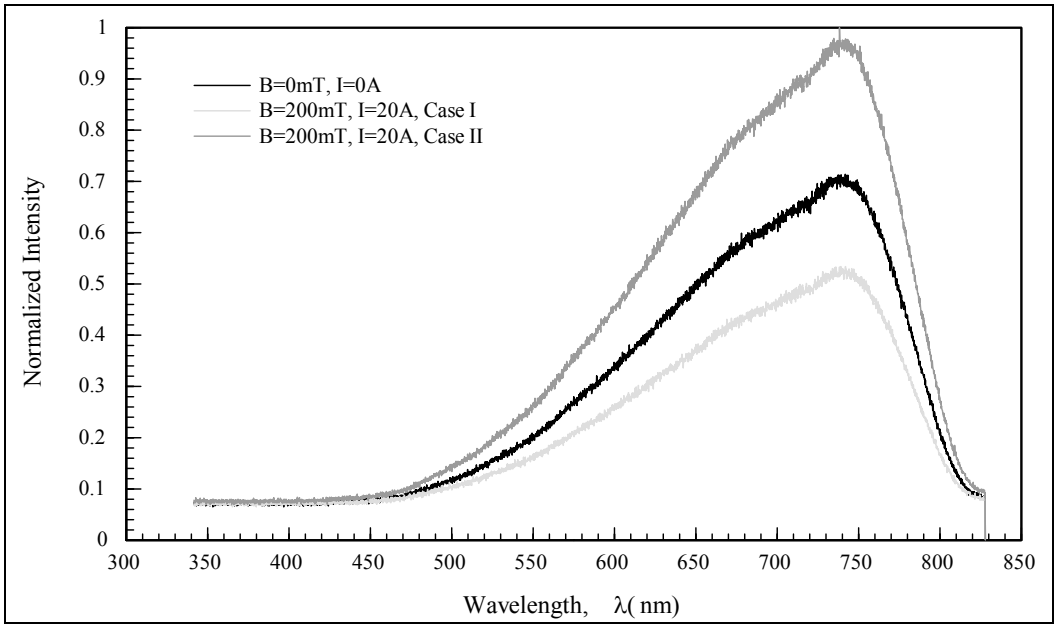

Figure 7.78. The normalized intensity versus wavelength graph for $B^{ext} = 200\ mT$ magnetic field and $20A$ current

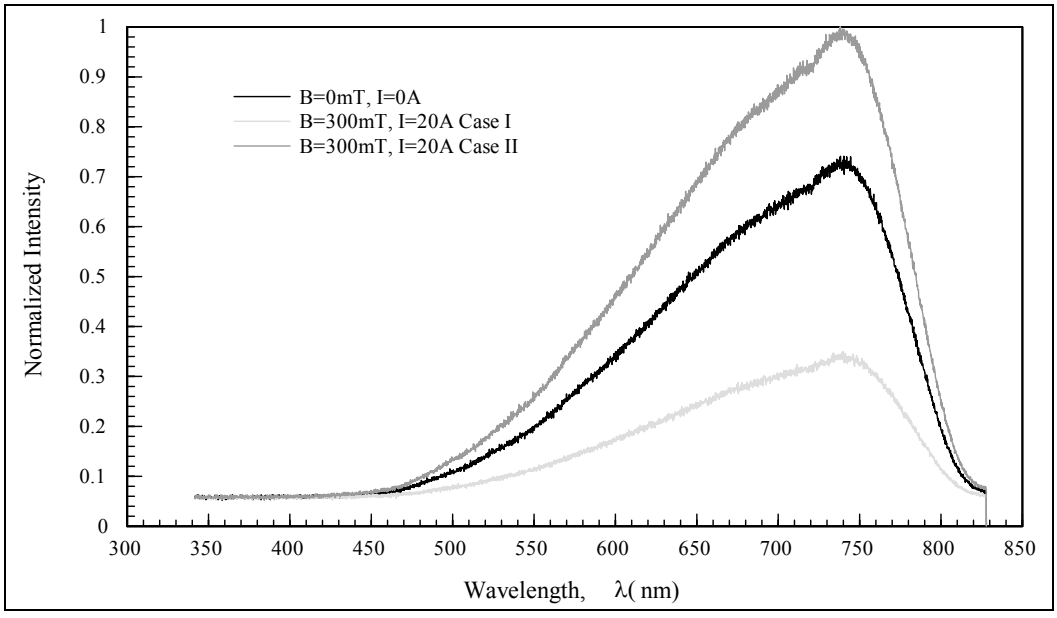

Figure 7.79. The normalized intensity versus wavelength graph for $B^{ext} = 300\ mT$ magnetic field and $20A$ current

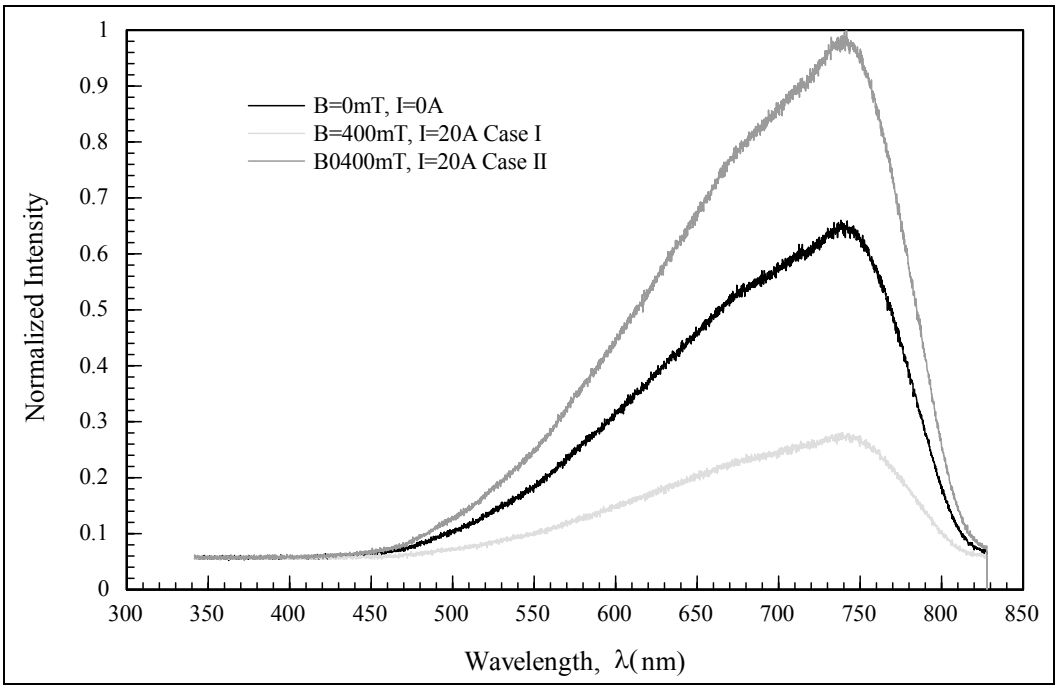

Figure 7.80. The normalized intensity versus wavelength graph for $B^{ext} = 400\ mT$ magnetic field and $20A$ current

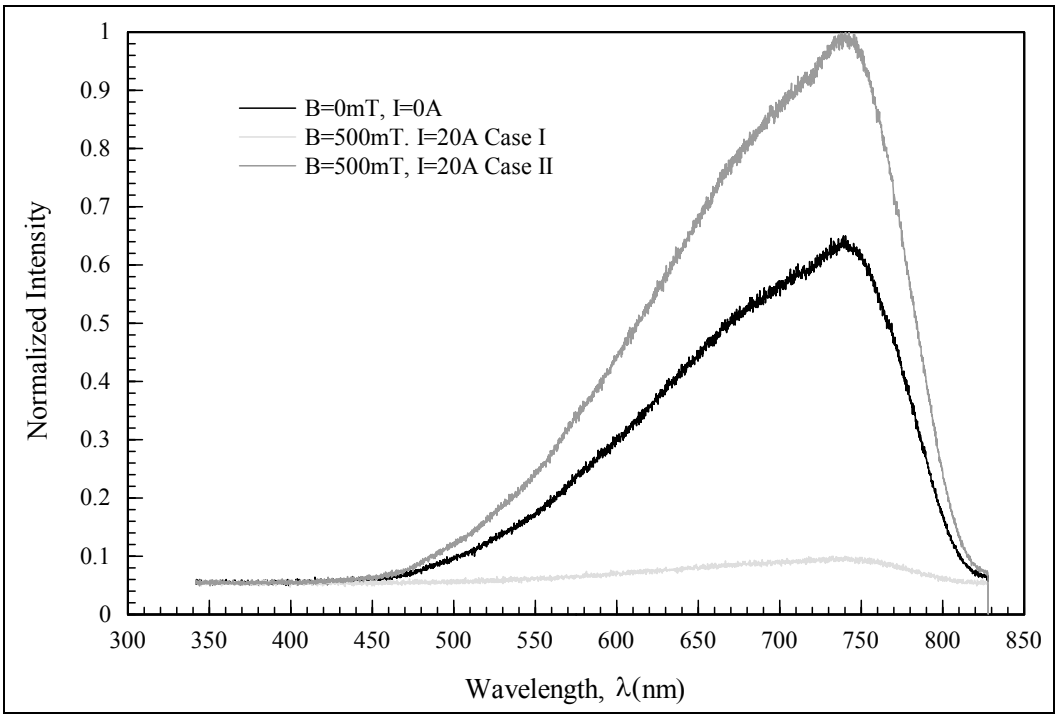

Figure 7.81. The normalized intensity versus wavelength graph for $B^{ext} = 500\ mT$ magnetic field and $20A$ current

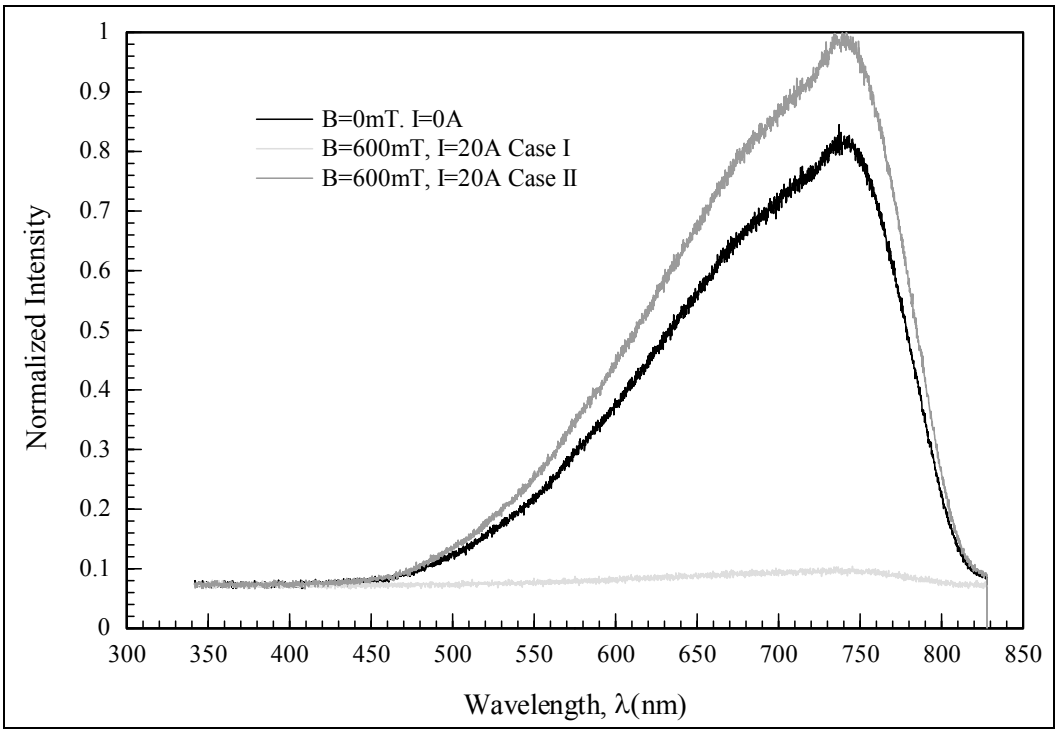

Figure 7.82. The normalized intensity versus wavelength graph for $B^{ext} = 600\ mT$ magnetic field and $20A$ current

In case I the mobile electrons were accumulated mostly at the top surface of GaInSn alloy. They were moving very fast in the opposite direction of externally applied current. The continuous disturbances occured in molecular level at liquid surface. When the Lorentz force is upward and is larger than gravity instabilities such as Rayleigh-Taylor instability starts to occure on the surface [65]. Evidently there were some magnetic fields also induced inside the alloy due to externally applied current but they can be neglected since the externally applied magnetic fields. The instabilities on the surface caused the decrease of intensity of reflected light which was falling on UV-Vis detector. The diffused reflection occured on the disturbed surface of GaInSn.

On the contrary in case II induced Lorentz force was in $-z$ direction which forced mobile electrons to move through the bulk of GaInSn alloy and accumulate at the bottom. This kind of application may smooth the surface. As a result the diffused reflection pattern can change to the reflection type more similar to specular one which occurs on smooth surfaces. During this experiment the data were collected in very small time intervals such

as ~ 15 seconds. Otherwise high valued direct current can heat up the GaInSn alloy and significant additional effect current can occur.

Since the current applied is constant ($20A$ DC) the only change in Lorentz force which is acting on the particles inside the GaInSn alloy is due to the change in externally applied magnetic field. The simplified expression for the Lorentz force is given as

$$\vec{F}_L = q(\vec{v} \times \vec{B}) \tag{7.18}$$

where q is the charge of the particle moving with the velocity v under the influence of magnetic field B. In both cases here (case I and case II) the applied current and magnetic fields are perpendicular to each other. Therefore the effect of Sin of the angle between current and magnetic field is unity. Since the number of moving charges inside GaInSn can be assumed to be constant and also the applied current which was driving the particles was constant the change of the magnetic field will dominate the Lorentz force magnitude. Under these conditions, Lorentz force will become as $F_L = qvB$ and not the exact numerical value for it but F_L for $200\,mT$ can be assumed to be F_{L1} where the same force for $300\,mT$, $400\,mT$, $500\,mT$ and $600\,mT$ will have the values $F_{L2} = 1.5F_{L1}$, $F_{L3} = 2F_{L1}$, $F_{L4} = 2.5F_{L1}$, and $F_{L5} = 3F_{L1}$ respectively. These values were collected in the Table 7. 7.

Table 7. 7. Externally applied magnetic field and the changes in Lorentz force comparing with the Lorentz force for $200\,mT$ magnetic field

Magnetic Field (mT)	Lorentz Force
200	F_{L1}
300	$1.5F_{L1}$
400	$2F_{L1}$
500	$2.5F_{L1}$
600	$3F_{L1}$

Since the graphs obtained from the results are similar in shape the differences between the peak values for every graph were calculated in order to see if there is a correlation depending on the Lorentz force acting. There were two different variables ΔI_{n1}, ΔI_{n2} defined here. This definition can be seen in the graph given as in Figure 7.83. ΔI_{n1} is the difference between maxima of normalized intensities for case II application and value taken without applying any current and magnetic field externally. Similarly ΔI_{n2} is the difference between maxima of normalized intensities for case I application and value taken without applying any current and magnetic field externally. Note that the magnitudes for the Lorentz forces for the same applied magnetic field will have the same value but different directions for case I and case II. The results for ΔI_{n1} and ΔI_{n2} are given in Table 7.8.

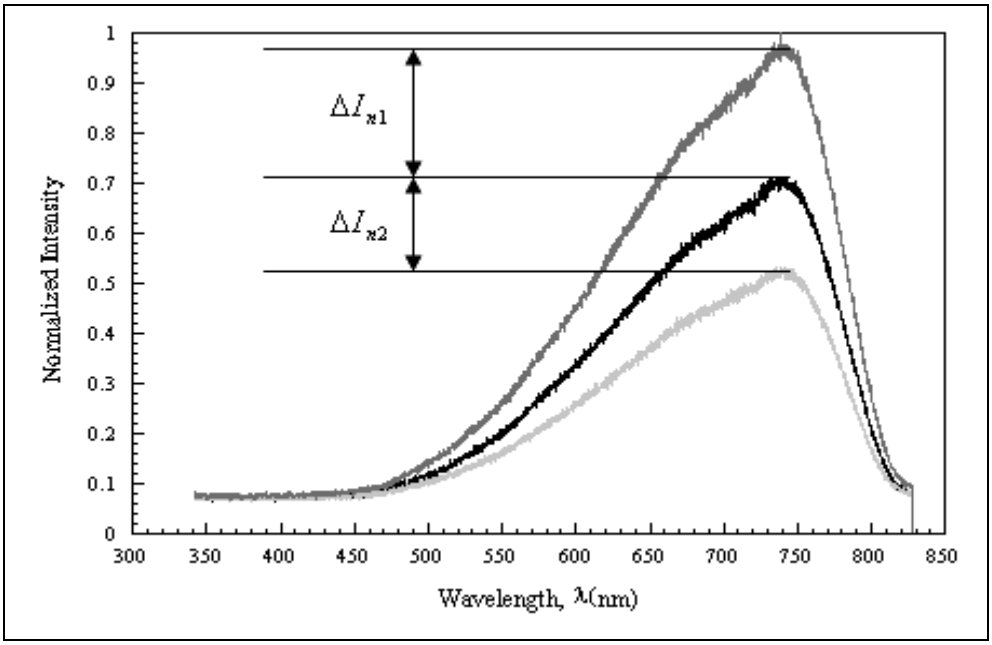

Figure 7.83. Normalized intensity differences for peak values of different spectra taken during the Lorentz force effect study

As it seen from Figure 7.84 a correlation between normalized intensity difference and Lorentz force can be investigated. By using more sensitive devices this correlation can be found and it can be represented as a constant number which can be found from the slope of these kinds of graphs. Actually the Lorentz force can have an effect also on the electric

resistance of the liquid metals [66]. This can be seen as an additional effect during the experiments related to liquid metals were conducted. This area deserves more and careful study.

Table 7.8. The Lorentz force and intensity differences table

Lorentz Force	ΔI_{n1}	ΔI_{n2}
F_{L1}	0.286	-0.180
$1.5F_{L1}$	0.259	-0.391
$2F_{L1}$	0.340	-0.409
$2.5F_{L1}$	0.350	-0.550
$3F_{L1}$	0.155	-0.741

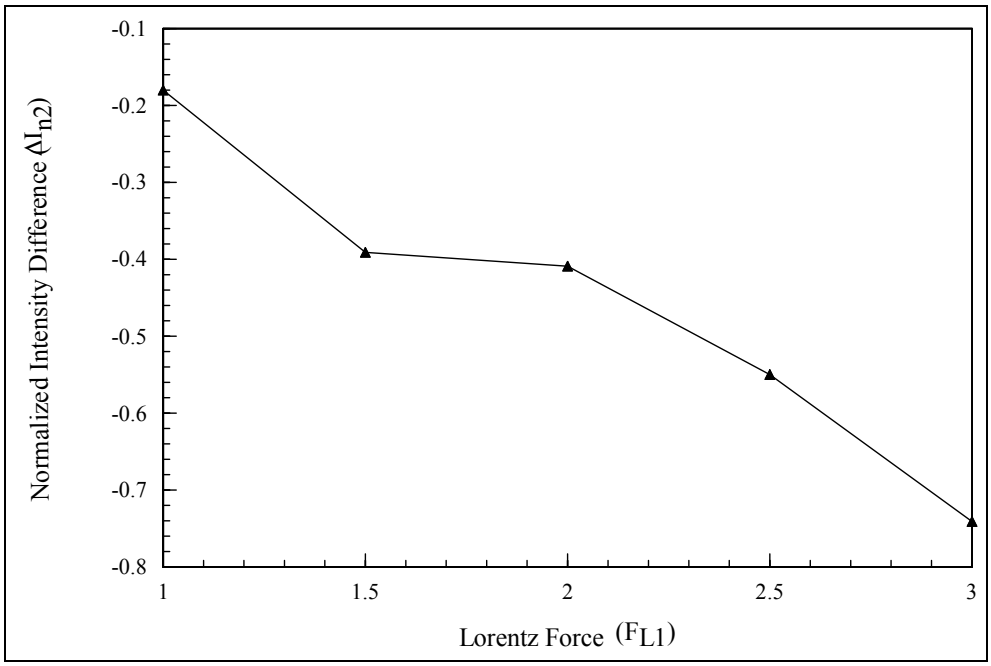

Figure 7.84. Normalized intensity difference versus Lorentz force graph

From the results obtained in this thesis it will not be an overstatement to say that there is an interesting physics hidden on the surface of liquid metals and alloys. The surfaces of liquids can have different structure from their bulks. The surface tension plays an important role in limiting the mobility of particles on the surface. However, the interatomic interactions are effective in microscopic structure of a bulk. These interatomic stuctures are strongly dependent on electronic structure [67].

Experimental investigations about the surfaces of liquid metals are an open area and is still largerly unexplored. The information about the surface is much more needed for the solution of reflection problems. Not only more experiments are needed but also a consistent fluid theory including ions and electrons should be investigated.

8. CONCLUSION

In this thesis, both theoretical and numerical studies with some experimental work were done. Firstly the very important physical phenomenon called as 'plasma' was studied in detail and connection between the plasma and Navier-Stokes equations (the governing equations for fluid dynamics) was studied. The terminology for plasma was given briefly. Under the title of 'From Plasma Definition to Magnetohydrodynamics Equations' the derivation of momentum equation was done by using a relatively different way from the derivations done in literature. This work is carried out under considerations of some assumptions which were mentioned in the thesis. The theoretical parts were given by using especially references [1-3].

Since the link between plasma and fluid was studied the properties of the fluid equations were also given in more detail by using especially reference [11]. The explanations for momentum and energy conservation equations were given in an explanatory way under the scope of reference [11].

Computational fluid dynamics and its properties were studied. Different space discretization methods were described in detail together with time discretizations. Matrix distribution scheme which was used as a space discretization method in the numerical simulation in this thesis was described together with dual time stepping procedure. Runge-Kutta method was also mentioned.

The two dimensional code which was used in numerical simulations was described in depth. The novel three dimensional mesh generation procedure was constructed and the original mesh generation programme was developed. This newly developed part of the programme will be embedded in the two diemensional original programme as a future work.

Numerical tests were done and the results for benchmark problems were compared with those of the references. The results were found in very good agreement with the results in references. Additionally to the benchmark problems originally designed

problems were also solved. Seven different test problems were discussed in detail in this thesis.

This thesis was not only about the theoretical studies in plasma physics and numerical studies in MHD but it also contains a very broad experimental part as was emphasized previously. The experimental part for this thesis is about the GaInSn alloy. The reflectance from the surface of GaInSn was especially studied in detail. Differently from the experiments in literature in which especially the x-ray wave is used as a reflecting electromagnetic wave, a halogen lamp which emits the light in the visible spectrum was used. The UV-Vis spectrometer was used as a main detector. However, in some experiments a luxmeter and a thermopile were also used as light detectors. The thermal expansion for GaInSn has checked firstly in order to be aware of the expansion of an alloy during the experiments in which high currents were used. Because of the fact that the currents will heat GaInSn alloy it can expand in volume and this can affect the intensity of reflected light detected. One of the most important environmental effects which is oxidation was also discussed since it can change the surface of the reflecting agent. The reflectance for GaInSn as a function of temperature, current application, magnetic field application, both current and magnetic field application were studied. It was seen that the reflectance of GaInSn alloy decreased with increasing temperature. These results were in good agreement with the results of literature in which for similar experiments the light source was x-ray. During the DC current applcation it was seen that the reflectance of an alloy also decreased. The polarization of light after reflection from the surface of GaInSn alloy was also studied and for small angles the possibility for polarization is seen however more sensitive experimental setup is needed. The DC magnetic field applications did not give big effect of the reflectance from the surface. The reflectance of GaInSn surface was so much affected when perpendicular current and magnetic field were applied at the same time. In this experiment the direction of magnetic field was kept constant during the change of direction of the current by 180°. Depending on the direction of Lorentz force induced after current and magnetic field are applied together the reflection from the surface of GaInSn was changed considerably. When the Lorentz force direction was in positive z direction the reflectance decreased on the contrary when Lorentz force is in negative z direction the reflectance increased. It was seen that the perpendicularly applied current and magnetic field affected the reflectance considerably. It was noticed that the direction of

Lorentz force had two different effects on reflection from GaInSn alloy surface depending on the direction of the force. These effects were explained by the movement of the electrons inside the alloy mentioned. The electrons freely moving in liquid metals are strongly affected by the induced Lorentz forces.

Actually the mechanical vibrations during the experiments were not eliminated totally. It had an additional effect in the experiments together with the geometrical orientation of the experimental setup and devices. They also caused some restrictions and additional effects during the experiments.

APPENDIX A: Computer Code

This algorithm is used in three dimensional mesh generation procedure. It can be run under Linux computer operating systems (such as Fedora) or it can be also run under Windows XP, Windows 7 by using 'c programming language' compilers such as Dev C++ 4.9.9.2. Firstly it is wanted from the user to define the maximum node numbers for x, y and z directions respectively when the code is run. In order to define the solution domain both minimum and maximum values (Xmin and Xmax) for each direction can be given from user and the step length sizes can be automatically calculated by the code. However, in this version of the code the step lengths are manually given by the user. The code creates a data file named as 'nodnokoor1.dat' in which the node number, x coordinate of the node , y coordinate of the node and z coordinate of the node are written. By using these coordinates the quantities such as the node numbers, which are calculated automatically by using the equation $jI+i+kIJ$ described intensively in 'Three Dimensional Mesh Generation Procedure' part of the thesis, the volume of each tetrahedron, four surface areas of each tetrahedron, the inward normal vectors for each surface. In order to check at least the volume calculations corrections the total volume of solution domain is compared by using the sum of the volumes of each tetrahedron in solution domain at the end of the code.

This code is planned to be adapted to the code which was used in the numerical simulations in this thesis (see 5. The Code and its Features part of the thesis). However, this adaptation is left as a postdoctoral study.

Since 3 dimensional mesh generating code developed in this thesis is relatively long only the part of it was given below. The whole code is in the compact disc given additionally together with the thesis.

Algorithm A.1: Computer code for three dimensional mesh generation

```
#include<stdio.h>
#include<math.h>
#define FILENAME "nodnokoor1.txt"
main()
{
float Nodx[22000],Nody[22000],Nodz[22000];
long Nodeno;
long k,j,i;
float dx,dy,dz,Vtotal,Vkontrol,Vfark,Vbirmolekul,V;
long IMAX,JMAX,KMAX,T,M,MOL,Tmax;
long Tetra_node0[20000],Tetra_node1[20000],Tetra_node2[20000],
Tetra_node3[20000];
float Tetra_hacim[10000],yuzey_norm0_X[40000],yuzey_norm0_Y[40000],
yuzey_norm0_Z[40000];
float yuzey_alan0[20000],yuzey_alan1[20000],yuzey_alan2[20000],
yuzey_alan3[20000];
long Tetra_yuzey0[20000],Tetra_yuzey1[20000],Tetra_yuzey2[20000],
Tetra_yuzey3[20000];
long yuzey_node0[21000],yuzey_node1[21000],yuzey_node2[21000],
yuzey_node3[21000];
float Ax,Bx,Ay,By,Az,Bz;
float adxcoord,adycoord,adzcoord;
float bdxcoord,bdycoord,bdzcoord;
float cdxcoord,cdycoord,cdzcoord;
float vekcarpx,vekcarpy,vekcarpz,scacarp;
FILE *nodnokoor1;
nodnokoor1=fopen(FILENAME,"w");
printf("Enter IMAX:\n");
scanf("%d",&IMAX);
printf("Enter dx:\n");
scanf("%f",&dx);
```

```
    printf("Enter JMAX:\n");
    scanf("%d",&JMAX);
    printf("Enter dy:\n");
    scanf("%f",&dy);
    printf("Enter KMAX:\n");
    scanf("%d",&KMAX);

    printf("Enter dz:\n");
    scanf("%f",&dz);
    for(k=0;k<KMAX;k++)
        for(j=0;j<JMAX;j++)
            for(i=0;i<IMAX;i++)
              {  Nodeno=j*IMAX+i+k*IMAX*JMAX;
                 Nodx[Nodeno]=dx*i;
                 Nody[Nodeno]=dy*j;
                 Nodz[Nodeno]=dz*k;
                 fprintf(nodnokoor1,"%d       %f %f %f
\n\n",Nodeno,Nodx[Nodeno],Nody[Nodeno],
    Nodz[Nodeno]);
              }
     fclose(nodnokoor1);
    nodnokoor1=fopen(FILENAME,"r");
    for(k=0;k<KMAX;k++)
        for(j=0;j<JMAX;j++)
            for(i=0;i<IMAX;i++)
              { Nodeno=j*IMAX+i+k*IMAX*JMAX;
                fscanf(nodnokoor1,"%d       %f %f %f
\n\n",&Nodeno,&Nodx[Nodeno],&Nody[Nodeno],&Nodz[Nodeno]);
              }
    Vtotal=0;
    Vkontrol=0;
    Vbirmolekul=0;
    Tmax=0;
```

```
    MOL=0;
    i=0;
    j=0;
    k=0;
    V=0;
    M=0;
    T=0;
    for(k=0;k<KMAX-1;k++)
       for(j=0;j<JMAX-1;j++)
           for(i=0;i<IMAX-1;i++)
    {
     printf("i=%d j=%d k=%d  \n\n ",i,j,k);
     printf("%d. Tetranin Hesaplamalari \n ",T);
     printf("--------------------------  \n");
                          Tetra_node0[T]=j*IMAX+i+k*IMAX*JMAX;
                          Tetra_node1[T]=j*IMAX+(i+1)+k*IMAX*JMAX;
                          Tetra_node2[T]=(j+1)*IMAX+i+k*IMAX*JMAX;
                          Tetra_node3[T]=j*IMAX+i+(k+1)*IMAX*JMAX;
printf("%d . tetranin node 0 i =%d nolu noddur\n",T,Tetra_node0[T]);
printf("%d . tetranin node 1 i =%d nolu noddur\n",T,Tetra_node1[T]);
printf("%d . tetranin node 2 si=%d nolu noddur\n",T,Tetra_node2[T]);
printf("%d . tetranin node 3 u =%d nolu noddur\n\n",T,Tetra_node3[T]);
    adxcoord=Nodx[Tetra_node0[T]]-Nodx[Tetra_node3[T]];
    adycoord=Nody[Tetra_node0[T]]-Nody[Tetra_node3[T]];
    adzcoord=Nodz[Tetra_node0[T]]-Nodz[Tetra_node3[T]];
    bdxcoord=Nodx[Tetra_node1[T]]-Nodx[Tetra_node3[T]];
    bdycoord=Nody[Tetra_node1[T]]-Nody[Tetra_node3[T]];
    bdzcoord=Nodz[Tetra_node1[T]]-Nodz[Tetra_node3[T]];
    cdxcoord=Nodx[Tetra_node2[T]]-Nodx[Tetra_node3[T]];
    cdycoord=Nody[Tetra_node2[T]]-Nody[Tetra_node3[T]];
    cdzcoord=Nodz[Tetra_node2[T]]-Nodz[Tetra_node3[T]];
    vekcarpx=bdycoord*cdzcoord-cdycoord*bdzcoord;
    vekcarpy=bdzcoord*cdxcoord-bdxcoord*cdzcoord;
```

```
    vekcarpz=bdxcoord*cdycoord-bdycoord*cdxcoord;
    scacarp=adxcoord*vekcarpx+adycoord*vekcarpy+adzcoord*vekcarpz;
    Tetra_hacim[T]=sqrt(scacarp*0.1666666667*scacarp*0.1666666667);
          printf("%d. tetranin hacmi = %f \n\n",T,Tetra_hacim[T]);
          Vbirmolekul=Tetra_hacim[T]+Vbirmolekul;
    Tetra_yuzey0[T]=0+M*18;
    printf("%d. tetranin ilk yuzeyi = %d numarali yuzeydir
\n",T,Tetra_yuzey0[T]);
    Tetra_yuzey1[T]=7+M*18;
    printf("%d. tetranin ikinci yuzeyi = %d numarali yuzeydir
\n",T,Tetra_yuzey1[T]);
    Tetra_yuzey2[T]=8+M*18;
    printf("%d. tetranin ucuncu yuzeyi = %d numarali yuzeydir
\n",T,Tetra_yuzey2[T]);
    Tetra_yuzey3[T]=12+M*18;
    printf("%d. tetranin dorduncu yuzeyi = %d numarali yuzeydir
\n\n",T,Tetra_yuzey3[T]);
          Nodeno=j*IMAX+i+k*IMAX*JMAX;
                yuzey_node0[Tetra_yuzey0[T]]=Nodeno;
                printf(" yuzey %d in 0. nodu=%d nolu
noddur\n",Tetra_yuzey0[T],yuzey_node0[Tetra_yuzey0[T]]);
          yuzey_node1[Tetra_yuzey0[T]]=j*IMAX+(i+1)+k*IMAX*JMAX;
                printf(" yuzey %d in 1. nodu=%d nolu
noddur\n",Tetra_yuzey0[T],yuzey_node1[Tetra_yuzey0[T]]);
          yuzey_node2[Tetra_yuzey0[T]]=j*IMAX+i+(k+1)*IMAX*JMAX;
                printf(" yuzey %d in 2. nodu=%d nolu noddur
\n\n",Tetra_yuzey0[T],yuzey_node2[Tetra_yuzey0[T]]);
                yuzey_node0[Tetra_yuzey1[T]]=Nodeno;
                printf(" yuzey %d in 0. nodu=%d nolu
noddur\n",Tetra_yuzey1[T],yuzey_node0[Tetra_yuzey1[T]]);
          yuzey_node1[Tetra_yuzey1[T]]=(j+1)*IMAX+i+k*IMAX*JMAX;
                printf(" yuzey %d in 1. nodu=%d nolu
noddur\n",Tetra_yuzey1[T],yuzey_node1[Tetra_yuzey1[T]]);
```

```
        yuzey_node2[Tetra_yuzey1[T]]=j*IMAX+i+(k+1)*IMAX*JMAX;
         printf(" yuzey %d in 2. nodu=%d nolu noddur
\n\n",Tetra_yuzey1[T],yuzey_node2[Tetra_yuzey1[T]]);
         yuzey_node0[Tetra_yuzey2[T]]=Nodeno;
        printf(" yuzey %d in 0. nodu=%d nolu noddur
\n",Tetra_yuzey2[T],yuzey_node0[Tetra_yuzey2[T]]);

        yuzey_node1[Tetra_yuzey2[T]]=j*IMAX+(i+1)+k*IMAX*JMAX;
                printf(" yuzey %d in 1. nodu=%d nolu noddur
\n",Tetra_yuzey2[T],yuzey_node1[Tetra_yuzey2[T]]);
           yuzey_node2[Tetra_yuzey2[T]]=(j+1)*IMAX+i+k*IMAX*JMAX;
         printf(" yuzey %d in 2. nodu=%d nolu noddur
\n\n",Tetra_yuzey2[T],yuzey_node2[Tetra_yuzey2[T]]);
        yuzey_node0[Tetra_yuzey3[T]]=j*IMAX+(i+1)+k*IMAX*JMAX;
                printf(" yuzey %d in 0. nodu=%d nolu noddur
\n",Tetra_yuzey3[T],yuzey_node0[Tetra_yuzey3[T]]);
        yuzey_node1[Tetra_yuzey3[T]]=(j+1)*IMAX+i+k*IMAX*JMAX;
                printf(" yuzey %d in 1. nodu=%d nolu noddur
\n",Tetra_yuzey3[T],yuzey_node1[Tetra_yuzey3[T]]);
        yuzey_node2[Tetra_yuzey3[T]]=j*IMAX+i+(k+1)*IMAX*JMAX;
         printf(" yuzey %d in 2. nodu=%d nolu noddur
\n\n",Tetra_yuzey3[T],yuzey_node2[Tetra_yuzey3[T]]);
   Ax=Nodx[yuzey_node2[Tetra_yuzey0[T]]]-
Nodx[yuzey_node0[Tetra_yuzey0[T]]];
   printf(" Yuzey %d nin A vektorunun  x coord=%f\n",Tetra_yuzey0[T],Ax);
   Ay=Nody[yuzey_node2[Tetra_yuzey0[T]]]-
Nody[yuzey_node0[Tetra_yuzey0[T]]];
   printf(" Yuzey %d nin A vektorunun  y coord=%f\n",Tetra_yuzey0[T],Ay);
   Az=Nodz[yuzey_node2[Tetra_yuzey0[T]]]-
Nodz[yuzey_node0[Tetra_yuzey0[T]]];
   printf(" Yuzey %d nin A vektorunun  z coord=%f\n\n",Tetra_yuzey0[T],Az);
   Bx=Nodx[yuzey_node1[Tetra_yuzey0[T]]]-
Nodx[yuzey_node0[Tetra_yuzey0[T]]];
```

```
    printf(" Yuzey %d nin B vektorunun  x coord=%f\n",Tetra_yuzey0[T],Bx);
    By=Nody[yuzey_node1[Tetra_yuzey0[T]]]-
Nody[yuzey_node0[Tetra_yuzey0[T]]];
    printf(" Yuzey %d nin B vektorunun  y coord=%f\n",Tetra_yuzey0[T],By);
    Bz=Nodz[yuzey_node1[Tetra_yuzey0[T]]]-
Nodz[yuzey_node0[Tetra_yuzey0[T]]];
    printf(" Yuzey %d nin B vektorunun  z coord=%f\n\n",Tetra_yuzey0[T],Bz);
    vekcarpx=0;
    vekcarpy=0;
    vekcarpz=0;
    vekcarpx=Ay*Bz-By*Az;
    vekcarpy=Az*Bx-Ax*Bz;
    vekcarpz=Ax*By-Ay*Bx;
    yuzey_norm0_X[Tetra_yuzey0[T]]=vekcarpx;
    printf(" Normal vektorun x coor =%f
\n",yuzey_norm0_X[Tetra_yuzey0[T]]);
    yuzey_norm0_Y[Tetra_yuzey0[T]]=vekcarpy;
    printf(" Normal vektorun y coor =%f
\n",yuzey_norm0_Y[Tetra_yuzey0[T]]);
    yuzey_norm0_Z[Tetra_yuzey0[T]]=vekcarpz;
    printf(" Normal vektorun z coor =%f
\n\n",yuzey_norm0_Z[Tetra_yuzey0[T]]);
    yuzey_alan0[Tetra_yuzey0[T]]=0.5*sqrt(vekcarpx*vekcarpx+
vekcarpy*vekcarpy+vekcarpz*vekcarpz);
    printf("%d ci yuzeyin alani
=%f\n\n",Tetra_yuzey0[T],yuzey_alan0[Tetra_yuzey0[T]]);
    Ax=Nodx[yuzey_node1[Tetra_yuzey1[T]]]-
Nodx[yuzey_node0[Tetra_yuzey1[T]]];
    printf(" Yuzey %d nin A vektorunun  x coord=%f\n",Tetra_yuzey1[T],Ax);
    Ay=Nody[yuzey_node1[Tetra_yuzey1[T]]]-
Nody[yuzey_node0[Tetra_yuzey1[T]]];
    printf(" Yuzey %d nin A vektorunun  y coord=%f\n",Tetra_yuzey1[T],Ay);
    Az=Nodz[yuzey_node1[Tetra_yuzey1[T]]]-
```

```
Nodz[yuzey_node0[Tetra_yuzey1[T]]];
   printf(" Yuzey %d nin A vektorunun  z coord=%f\n\n",Tetra_yuzey1[T],Az);
   Bx=Nodx[yuzey_node2[Tetra_yuzey1[T]]]-
Nodx[yuzey_node0[Tetra_yuzey1[T]]];
   printf(" Yuzey %d nin B vektorunun  x coord=%f\n",Tetra_yuzey1[T],Bx);
   By=Nody[yuzey_node2[Tetra_yuzey1[T]]]-
Nody[yuzey_node0[Tetra_yuzey1[T]]];
   printf(" Yuzey %d nin B vektorunun  y coord=%f\n",Tetra_yuzey1[T],By);
   Bz=Nodz[yuzey_node2[Tetra_yuzey1[T]]]-
Nodz[yuzey_node0[Tetra_yuzey1[T]]];
   printf(" Yuzey %d nin B vektorunun  z coord=%f\n\n",Tetra_yuzey1[T],Bz);
   vekcarpx=0;
   vekcarpy=0;
   vekcarpz=0;
   vekcarpx=Ay*Bz-By*Az;
   vekcarpy=Az*Bx-Ax*Bz;
   vekcarpz=Ax*By-Ay*Bx;
   yuzey_norm0_X[Tetra_yuzey1[T]]=vekcarpx;
   printf(" Normal vektorun x coor =%f
\n",yuzey_norm0_X[Tetra_yuzey1[T]]);
   yuzey_norm0_Y[Tetra_yuzey1[T]]=vekcarpy;
   printf(" Normal vektorun y coor =%f
\n",yuzey_norm0_Y[Tetra_yuzey1[T]]);
   yuzey_norm0_Z[Tetra_yuzey1[T]]=vekcarpz;
   printf(" Normal vektorun z coor =%f
\n\n",yuzey_norm0_Z[Tetra_yuzey1[T]]);
   yuzey_alan1[Tetra_yuzey1[T]]=0.5*sqrt(vekcarpx*vekcarpx+
vekcarpy*vekcarpy+vekcarpz*vekcarpz);
   printf("%d ci yuzeyin alani
=%f\n\n",Tetra_yuzey1[T],yuzey_alan1[Tetra_yuzey1[T]]);
   Ax=Nodx[yuzey_node1[Tetra_yuzey2[T]]]-
Nodx[yuzey_node0[Tetra_yuzey2[T]]];
   printf(" Yuzey %d nin A vektorunun  x coord=%f\n",Tetra_yuzey2[T],Ax);
```

```
    Ay=Nody[yuzey_node1[Tetra_yuzey2[T]]]-
Nody[yuzey_node0[Tetra_yuzey2[T]]];
    printf(" Yuzey %d nin A vektorunun  y coord=%f\n",Tetra_yuzey2[T],Ay);
    Az=Nodz[yuzey_node1[Tetra_yuzey2[T]]]-
Nodz[yuzey_node0[Tetra_yuzey2[T]]];
    printf(" Yuzey %d nin A vektorunun  z coord=%f\n\n",Tetra_yuzey2[T],Az);

    Bx=Nodx[yuzey_node2[Tetra_yuzey2[T]]]-
Nodx[yuzey_node0[Tetra_yuzey2[T]]];
    printf(" Yuzey %d nin B vektorunun  x coord=%f\n",Tetra_yuzey2[T],Bx);
    By=Nody[yuzey_node2[Tetra_yuzey2[T]]]-
Nody[yuzey_node0[Tetra_yuzey2[T]]];
    printf(" Yuzey %d nin B vektorunun  y coord=%f\n",Tetra_yuzey2[T],By);
    Bz=Nodz[yuzey_node2[Tetra_yuzey2[T]]]-
Nodz[yuzey_node0[Tetra_yuzey2[T]]];
    printf(" Yuzey %d nin B vektorunun  z coord=%f\n\n",Tetra_yuzey2[T],Bz);
    vekcarpx=0;
    vekcarpy=0;
    vekcarpz=0;
    vekcarpx=Ay*Bz-By*Az;
    vekcarpy=Az*Bx-Ax*Bz;
    vekcarpz=Ax*By-Ay*Bx;
    yuzey_norm0_X[Tetra_yuzey2[T]]=vekcarpx;
    printf(" Normal vektorun x coor =%f
\n",yuzey_norm0_X[Tetra_yuzey2[T]]);
    yuzey_norm0_Y[Tetra_yuzey2[T]]=vekcarpy;
    printf(" Normal vektorun y coor =%f
\n",yuzey_norm0_Y[Tetra_yuzey2[T]]);
    yuzey_norm0_Z[Tetra_yuzey2[T]]=vekcarpz;
    printf(" Normal vektorun z coor =%f
\n\n",yuzey_norm0_Z[Tetra_yuzey2[T]]);
    yuzey_alan2[Tetra_yuzey2[T]]=0.5*sqrt(vekcarpx*vekcarpx+
vekcarpy*vekcarpy+vekcarpz*vekcarpz);
```

```
   printf("%d ci yuzeyin alani
=%f\n\n",Tetra_yuzey2[T],yuzey_alan2[Tetra_yuzey2[T]]);
   Ax=Nodx[yuzey_node2[Tetra_yuzey3[T]]]-
Nodx[yuzey_node0[Tetra_yuzey3[T]]];
   printf(" Yuzey %d nin A vektorunun  x coord=%f\n",Tetra_yuzey3[T],Ax);
   Ay=Nody[yuzey_node2[Tetra_yuzey3[T]]]-
Nody[yuzey_node0[Tetra_yuzey3[T]]];
   printf(" Yuzey %d nin A vektorunun  y coord=%f\n",Tetra_yuzey3[T],Ay);
   Az=Nodz[yuzey_node2[Tetra_yuzey3[T]]]-
Nodz[yuzey_node0[Tetra_yuzey3[T]]];
   printf(" Yuzey %d nin A vektorunun  z coord=%f\n\n",Tetra_yuzey3[T],Az);
   Bx=Nodx[yuzey_node1[Tetra_yuzey3[T]]]-
Nodx[yuzey_node0[Tetra_yuzey3[T]]];
   printf(" Yuzey %d nin B vektorunun  x coord=%f\n",Tetra_yuzey3[T],Bx);
   By=Nody[yuzey_node1[Tetra_yuzey3[T]]]-
Nody[yuzey_node0[Tetra_yuzey3[T]]];
   printf(" Yuzey %d nin B vektorunun  y coord=%f\n",Tetra_yuzey3[T],By);
   Bz=Nodz[yuzey_node1[Tetra_yuzey3[T]]]-
Nodz[yuzey_node0[Tetra_yuzey3[T]]];
   printf(" Yuzey %d nin B vektorunun  z coord=%f\n\n",Tetra_yuzey3[T],Bz);
   vekcarpx=0;
   vekcarpy=0;
   vekcarpz=0;
   vekcarpx=Ay*Bz-By*Az;
   vekcarpy=Az*Bx-Ax*Bz;
   vekcarpz=Ax*By-Ay*Bx;
   yuzey_norm0_X[Tetra_yuzey3[T]]=vekcarpx;
   printf(" Normal vektorun x coor =%f
\n",yuzey_norm0_X[Tetra_yuzey3[T]]);
   yuzey_norm0_Y[Tetra_yuzey3[T]]=vekcarpy;
   printf(" Normal vektorun y coor =%f
\n",yuzey_norm0_Y[Tetra_yuzey3[T]]);
   yuzey_norm0_Z[Tetra_yuzey3[T]]=vekcarpz;
```

```
    printf(" Normal vektorun z coor =%f
\n\n",yuzey_norm0_Z[Tetra_yuzey3[T]]);
    yuzey_alan3[Tetra_yuzey3[T]]=0.5*sqrt(vekcarpx*vekcarpx+
vekcarpy*vekcarpy+vekcarpz*vekcarpz);
    printf("%d ci yuzeyin alani
=%f\n\n",Tetra_yuzey3[T],yuzey_alan3[Tetra_yuzey3[T]]);
    T=T+1;
    printf("%d. Tetranin Hesaplamalari \n ",T);
    printf("-------------------------  \n");
                Tetra_node0[T]=j*IMAX+(i+1)+k*IMAX*JMAX;
                Tetra_node1[T]=(j+1)*IMAX+i+k*IMAX*JMAX;
                Tetra_node2[T]=(j+1)*IMAX+(i+1)+k*IMAX*JMAX;
                Tetra_node3[T]=(j+1)*IMAX+(i+1)+(k+1)*IMAX*JMAX;
printf("%d . tetranin node 0 i =%d nolu noddur\n",T,Tetra_node0[T]);
printf("%d . tetranin node 1 i =%d nolu noddur\n",T,Tetra_node1[T]);
printf("%d . tetranin node 2 si=%d nolu noddur\n",T,Tetra_node2[T]);
printf("%d . tetranin node 3 u =%d nolu noddur\n\n",T,Tetra_node3[T]);
    adxcoord=Nodx[Tetra_node0[T]]-Nodx[Tetra_node3[T]];
    adycoord=Nody[Tetra_node0[T]]-Nody[Tetra_node3[T]];
    adzcoord=Nodz[Tetra_node0[T]]-Nodz[Tetra_node3[T]];
    bdxcoord=Nodx[Tetra_node1[T]]-Nodx[Tetra_node3[T]];
    bdycoord=Nody[Tetra_node1[T]]-Nody[Tetra_node3[T]];
    bdzcoord=Nodz[Tetra_node1[T]]-Nodz[Tetra_node3[T]];
    cdxcoord=Nodx[Tetra_node2[T]]-Nodx[Tetra_node3[T]];
    cdycoord=Nody[Tetra_node2[T]]-Nody[Tetra_node3[T]];
    cdzcoord=Nodz[Tetra_node2[T]]-Nodz[Tetra_node3[T]];
    vekcarpx=bdycoord*cdzcoord-cdycoord*bdzcoord;
    vekcarpy=bdzcoord*cdxcoord-bdxcoord*cdzcoord;
    vekcarpz=bdxcoord*cdycoord-bdycoord*cdxcoord;
    scacarp=adxcoord*vekcarpx+adycoord*vekcarpy+adzcoord*vekcarpz;
        Tetra_hacim[T]=sqrt(scacarp*0.1666666667*scacarp*0.1666666667);
                printf("%d. tetranin hacmi = %f \n\n",T,Tetra_hacim[T]);
          Vbirmolekul=Tetra_hacim[T]+Vbirmolekul;
```

```
    Tetra_yuzey0[T]=3+M*18;
    printf("%d. tetranin ilk yuzeyi = %d numarali yuzeydir
\n",T,Tetra_yuzey0[T]);
    Tetra_yuzey1[T]=4+M*18;
    printf("%d. tetranin ikinci yuzeyi = %d numarali yuzeydir
\n",T,Tetra_yuzey1[T]);
    Tetra_yuzey2[T]=9+M*18;
    printf("%d. tetranin ucuncu yuzeyi = %d numarali yuzeydir
\n",T,Tetra_yuzey2[T]);
    Tetra_yuzey3[T]=13+M*18;
    printf("%d. tetranin dorduncu yuzeyi = %d numarali yuzeydir
\n\n",T,Tetra_yuzey3[T]);

    printf("KONTROL HACMI =%f\n\n",Vbirmolekul);
    MOL=((IMAX-1)*(JMAX-1))*(KMAX-1);
    Tmax=MOL*6;
    Vtotal=(dx*(IMAX-1))*(dy*(JMAX-1))*(dz*(KMAX-1));
    printf("Meshin Toplam Hacmi=%f \n\n ",Vtotal);
    printf("Toplam Molekul sayisi=%d\n\n",MOL);
    printf("Toplam Tetrahedral sayisi=%d\n\n",Tmax);
    Vfark=Vtotal-Vbirmolekul;
    printf("Vfark=Vtotal-Vkontrol\n\n");
    printf("%f=%f-%f\n\n",Vfark,Vtotal,Vbirmolekul);
    printf("Vfark=%f",Vfark);
    fclose(nodnokoor1);

    }
```

REFERENCES

1. Chen, F. F., *Introduction to plasma physics and controlled fusion,* Volume1: Plasma Physics, Second Edition, Plenum Press.

2. Goldstone, R. J. and P. H. Rutherford, *Introduction to Plasma Physics,* Institute of Physics Publishing Ltd.

3. Krall, N. A. and A. W. Trivelpiece, Principles of Plasma Physics, San Francisco Press Inc.

4. Daily, J. W. and D. R. F.Harleman, *Fluid Dynamics,* Addison –Wesley Publishing Company.

5. Batchelor, G. K., *An Introduction to Fluid Dynamics*, Cambridge University Press.

6. Çoker, E. G., *Solutions of the Navier-Stokes Equations and Technological Applications Using Matrix-Distribution with N-Methods*, M. Sc. Thesis, 2005..

7. Middleman, S., *An Introduction to Fluid Dynamics Principles of Analysis and Design,* John Wiley & Sons, Inc.

8. Ansorge, R.., *Mathematical Models of Fluid Dynamics: Modelling, Theory, Basic Numerical Facts- An Introduction*, Wiley-VCH GmbH & Co. KGaA.

9. Meir, G. B., *Basics of Fluid Mechanics*, Orange Grove Texts Plus.

10. Nakayama, Y. and R. Boucher, *Introduction to Fluid Mechanics,* Butterworth-Heinemann.

11. Anderson, J. D. Jr., *Computational Fluid Dynamics-The Basics with Applications,* McGraw-Hill, Inc.

12. Ferziger, J. H. and M. Peric, *Computational Methods for Fluid Dynamics*, Springer 3rd Edition.

13. Van Der Weide, E., *Compressible Flow Simulation on Unstructured Grids Using Multi-Dimensional Upwind Schemes*.

14. Chung, T. J., *Computational Fluid Dynamics,* Cambridge University Press.

15. Johnson, C., *Numerical Solutions of Partial Differential Equations by Finite Element Method,* Cambridge University Press.

16. Eymard, R., T. Gallouet and R. Herbin, *Finite Volume Methods,* Updated preprint in Handbook of Numerical Analysis, Vol 7, pp 713-1020.

17. Şentürk, K., *Thermal-Hydraulic Analysis of Nuclear Systems by Using Boundary Element Method*, Ms. C. Thesis, 2003.

18. El Zafrany, A., *Techniques of the Boundary Element Method* , 1993, Computational Mechanics Group, Cranfield Institute of Technology, Bedford.

19. Rizzo, F. J., *An Integral Equation Approach to Boundary Value Problem of Classical Electrostatics*, 1967, , Q. Appl. Math, , 25, pp. 83-95.

20. Cruse, T. A., *Numerical Solutions in Three Dimensional Elastostaics, Int. J. Solids and Structures,* 5 pp, 1269-1274, 1969.

21. Becker, A. A., *The Boundary Element Method in Engineering A Complete Course* Department of Mechanical Engineering, University of Nottingham, 1992.

22. Street, R. L., G. Z. Watters and J. K. Vennard, *Elementary Fluid Mechanics,* John Wiley & Sons.

23. Paillere, H., *Multidimenisonla Upwinding Residual Distribution Schemes for the Euler and Navier-Stokes Equations on Unstructured Grids,* Ph. D. Thesis, June 1995.

24. Struijs, R., H. Deconinck and P. Roe, *Fluctuation Splitting Scheme for the 2D Euler Equations.* In VKI LS 1991-01, Computational Fluid Dynamics 1991.

25. Johnson, C., *Finite Element for Flow Problems In Unstructured Grid Methods for Advection Dominated Flows* , May 1992. AGARDR-787.

26. Aslan N., E. Onbasioglu and A.Erdogan, *Parallelization of visual magneto-hydrodynamics code based on fluctuation distribution scheme on triangular grids,* Computers and Fluids 2007; 36: 961-973.

27. Cash J. R. and A.H. Karp, *A variable order Runge-Kutta method for initial value problems with rapidly varying right hand sides.* ACM Transactions of Mathematical Software, Vol. 16, No. 3, September 1990.

28. Rogers S.E. and D. Kwak, *Upwind differncing scheme for the time accurate incompressible Navier-Stokes equations*, AIAA Journal 1990 ; 8(2):253-262.

29. Şentürk, K., M. Tessarotto and N. Aslan, *Numerical solutions of liquid metal flows by incompressible magneto-hydrodynamics with heat transfer,* Int. J. Numer. Meth. Fluids 2009; 60: 1200–1221.

30. Giancoli, D. C., *Physics for Scientists and Engineers with Modern Physics*:*Volume II* Prentice Hall, Third edition.

31. Stefani F., G. Gerbeth and T. Gundrum, *Contactless inductive flow tomography : Theory and experiment*, XXI ICTAM, 15-21 August 2004, Warsaw, Poland.

32. Chorin, A. J., *A Numerical Method for Solving Incompressible Viscous Flow Problems*, J. Comput. Phys., 1967, 2(1), 12-26.

33. Dailey L.D. and R.H. Pletcher , *Evaluation of multigrid acceleration for preconditioned time-accurate Navier–Stokes algorithms*. *Computers and Fluids* 1996; 25(8):791–811.

34. Granier B., A. Lerat and Wu Z-N., *An implicit centered scheme for steady and unsteady incompressible two-phase flows*, Computers and Fluids 1997; 26(4): 373–393.

35. de Vahl Davis G., *Natural convection of air in a square cavity: a bench mark numerical solution.* International Journal for Numerical Methods in Fluids 1983; 3:249–264.

36. Armero F. and J.C. Simo, *Long-term dissipativity of time stepping algorithms for an abstract evolution equation with applications to the incompressible MHD and Navier–Stokes equations.* Computer Methods in Applied Mechanics and Engineering 1996; 131:41–90.

37. Codutti A., A. Martinis, M. Pavlicevic, M. Tessarotto and D. Batic, *Mathematical modelling and experimental model validation for a DC electromagnetic valve for liquid steel.* Proceedings of EPM2000 3rd International Symposium on Electromagnetic Processing of Materials, Nagoya, Japan, published by The Iron and Steel Institute of Japan, 2000; 530.

38. Takamichi I. and I. L. G. Roderick, *The Physical Properties of Liquid Metals*, Oxford University Press.

39. Kaneda M., T. Tagawa and H. Ozoe, *Natural convection of liquid metal under a uniform magnetic field with an electric current supplied from outside*, Experimental Thermal and Fluid Science 30 (2006) 243-252.

40. Koha I., T. Mitsuo and T. Asoda, *Wave suppression of molten metal by imposing both stationary magnetic field and direct electric current*, Tetsu to Hagane Journal of the Iron and Steel Institule of Japan 80(8)(1994)617-622.

41. Fukuyama H., T. Yoshimura, H. Yasuda and H. Ohta, *Thermal Conductivity Measurements of Liquid Mercury and Gallium by a Transient Hot-Wire Method in a Static Magnetic Field,* International Journal of Thermophysics, Vol. 27, No. 6, November 2006.

42. *Revised Release on the IAPS Formulation 1985 for the Thermal Conductivity of Ordinary Water Substance* , The International Association for the Properties of Water and Steam, Berlin, Germany September 2008.

43. Thess A., A. Kolesnikov and T. Boeck, *A model for liquid metal electric current limiters,* ICTAM04 Proceedings, XXI ICTAM, 15-21 August 2004, Warsaw, Poland.

44. Liu X., L. Katehi and D. Peroulis, *Non-toxic Liquid Metal Microstrip Resonators*, Microwave conference, 2009, APMC 2009, Asia-Pacific, p 131-134.

45. Morley N. B., J. Burris, L. C. Cadwallader and M. D. Nornberg, *GaInSn usage in the research laboratory,* Review of Scientific Instruments 79, 056107 (2008).

46. Cadwallader L. C., *Gallium safety in the laboratory*, Energy Facility Contractors Group (EFCOG) Safety Analysis Working Group (SAWG) 2003 Annual Meeting, 21-27 June, 2003.

47. Kunquan M. and L. Jing, *Liquid metal cooling in thermal management of computer chips*, Front. Energy Power Eng. China 2007, 1(4): 384-402.

48. Karcher C. and Y. Kolesnikov, *Electromagnetic control of convective heat transfer during electron beam evaporation: model experiments*, Vacuum 77 (2005) 437-441.

49. Knoblauch M., J. M. Hibberd, J. C. Gray and A. J. E. van Bel, *A galinstan expansion femtosyringe for microinjection of eukaryotic organelles and prokaryotes*, Nature Biotechnology, Volume 17, September 1999, p. 906-909.

50. Scharmann F., G. Cherakashinin, V. Breternitz, C. Knedlik, G. Hartung, T. Weber and J. A Schaefer, *Viscosity effect on GaInSn studied by XPS*, Surface and Interface Analysis, (2004); 36: 981-985.

51. Van de Hulst H. C., *Light scattering by small particles,* Dover Publications, Inc..

52. Tostmann H., E. DiMasi, B. M. Ocko, M. Deutsch and P. S. Pershan, *X-ray studies of liquid metal surfaces,* Journal of Non-Crystalline Solids 250-252 (1999) 182-190.

53. Grigoriev A., O. Shpyrko, C. Steimer, P. S. Pershan, B. M. Ocko, M. Deutsch, B. Lin, M. Meron, T. Graber and J. Gebhardt, *Surface oxidation of liquid Sn,* Surface Science, Volume 575, Pages 223-232, 2005.

54. Dutchak Y. I., N. M. Klym and V. S. Frenchko V. S., *Structure of the ternary Gallium-Indium-Tin eutectic system in the liquid state*, Consultant Bureau, a division of Plenum Publishing Corporation, 227 West 17th Street, New York, N. Y. 10011, 1972.

55. Dadashev R. Kh., R. A. Kutuev, D. Z. Elimkhanov and Z. I. Bichueva, *Surface tension of Indium-Tin-Gallium Melts,* Russian Journal of Physical Chemistry A, Volume 81, Issue 11, pp.1734-1737.

56. Lin B., M. Meron, J. Gebhard, T. Graber, D. Li, B. Yang and S. A. Rice, *X-ray scattering study of height fluctuations at the liquid-vapor inreface of Gallium,* Physica B 357 (2005), 106-109.

57. Korotchenko A. I., A. A. Samokhin and A. B. Uspenskii, *Behaviour of the absorbitivity of metals under the action of laser radiation,* Kvantovaya Elektron. (Moscow) 6, 210-217, 1979.

58. Regan M. J., P. S. Pershan, O. M. Magnussen, B. M. Ocko, M. Deutsch and L. E. Berman, *Capillary-wave roughening of surface-induced layering in liquid Gallium,* Physical Review B, Volume 54, Number 14, 9730-9733, 1996.

59. Regan M. J., P. S. Pershan, O. M. Magnussen, B. M. Ocko, M. Deutsch and L. E. Berman, *X-ray reflectivity studies of liquid metal and alloy surfaces,* Physical Review B, Volume 55, Number 23, 15874-15884, 1997.

60. Keilmann F., *Instability of liquid metal surfaces under intense infrared irradiation,* Journal de Physique, Colloque C5, supplement au No 10, Tome 44, Octobre 1983, Page C5-77.

61. Pershan P. S., *Effect of thermal roughness on X-ray studies of liquid surfaces,* Colloids and Surfaces, A: Physicochemical and Engineering Aspects 171 , 149-157, 2000.

62. Schulze D., Ch. Karcher, V. Kocourek and J. U. Mohring, *Electrically induced instabilities of liquid metals free surfaces,* International Scientific Colloquium, Modelling for Material Processing, Riga, June 8-9, 2006.

63. Mohring J. U. and Ch. Karcher, *Stability of a liquid metal interface affected by a high-frequency magnetic field,* Proceedings of the Electromagnetic Processing of Materials International Conference, 2003.

64. Karcher Ch., V. Kocourek and D. Schulze, Experimental investigations of electromagnetic instabilities of free surfaces in a liquid metal drop, International Scientific Colloquium, Modelling for Electromagnetic Processing, Hannover, March 24-26, 2003.

65. Ji H., W. Fox, D. Pace and H. L. Rappaport, *Study of small-amplitude magnetohydrodynamic surface waves on liquid metal,* Phys. Plasmas 12, 012102, 2005.

66. Ogita M., T. Fujinami, Y. Nakanishi and Y. Hatanaka, *Surface reflection and nonlinearities in ac Hall measurements of liquid metals,* Applied Surface Science 113/114 777-782, 1997.

67. Di Masi E. and H. Tostmann, Surface induced order in liquid metals, Synchrotron Radiation News, Vol. 12, No.2 ,1999.